



HAL
open science

Macromolecular valorisation of humins, keratin and lignin through sustainable copolymers and composites

Roxana-Mihaela Dinu

► **To cite this version:**

Roxana-Mihaela Dinu. Macromolecular valorisation of humins, keratin and lignin through sustainable copolymers and composites. Other. Université Côte d'Azur, 2020. English. NNT : 2020COAZ4030 . tel-03505916

HAL Id: tel-03505916

<https://theses.hal.science/tel-03505916>

Submitted on 1 Jan 2022

HAL is a multi-disciplinary open access archive for the deposit and dissemination of scientific research documents, whether they are published or not. The documents may come from teaching and research institutions in France or abroad, or from public or private research centers.

L'archive ouverte pluridisciplinaire **HAL**, est destinée au dépôt et à la diffusion de documents scientifiques de niveau recherche, publiés ou non, émanant des établissements d'enseignement et de recherche français ou étrangers, des laboratoires publics ou privés.



THÈSE DE DOCTORAT

Valorisation macromoléculaire des humines, de la kératine et des lignines par copolymères et composites durables

Macromolecular valorisation of humins, keratin and lignin through sustainable copolymers and composites

Roxana DINU

Institut de Chimie de Nice

Présentée en vue de l'obtention
du grade de docteur en Chimie
d'Université Côte d'Azur

Dirigée par : Prof. Alice MIJA

Soutenue le : 09 Juillet 2020

Devant le jury, composé par :

Rapporteurs :

Prof. Irina VOLF, Univ. Gh. Asachi Iasi (Romania)
Prof. Marc ABADIE, Univ. Montpellier

Examineurs :

Prof. Veronica AMBROGI, Univ. of Naples (Italy)
Prof. Véronique MICHELET, Univ. Côte d'Azur
Prof. Alice MIJA, Univ. Côte d'Azur



Valorisation macromoléculaire des humines, de la kératine et des lignines par copolymères et composites durables

Macromolecular valorisation of humins, keratin and lignin through sustainable copolymers and composites

Jury:

Président du jury :

Prof. Véronique MICHELET, Univ. Côte d'Azur

Rapporteurs :

Prof. Irina VOLF, Univ. Gh. Asachi Iasi (Romania)

Prof. Marc ABADIE, Univ. Montpellier

Examineurs :

Prof. Veronica AMBROGI, Univ. of Naples (Italy)

Prof. Alice MIJA, Univ. Côte d'Azur

Abstract

Scientific and market researches are developed to replace the non-renewable fossil resources with renewable raw materials, and to reduce and valorise the industrial waste in order to develop new innovative green materials. Conversion of lignocellulose during acid-catalysed hydrolysis process leads to the valorisation of this biomass into value added chemical building blocks (HMF, FF, LA, etc.), but also provoke the formation of a dark-coloured by-product called humins. Feathers represent around 5–7% of the corporal mass of an adult chicken, being one of the main wastes generated by the poultry industry. Knowing that the chicken feathers consist of 91% keratin, this side-product can be an important renewable source used as alternative for fossil derivative materials. The main objective of this thesis was the valorisation of humins and of chicken feathers in order to develop eco-friendly materials. Firstly, humins-based resins have been designed with modulable properties from elastic to rigid. Then, these humins-based resins were used for composites production with chicken feathers and lignin as bio-fillers. Thereafter, to produce fully bio-based thermoset resins, humins were copolymerized with phloroglucinol diglycidyl ether, a green epoxy comonomer from algae. Moreover, recyclable bio-based composites were developed by reinforcing humins-based thermoset resins with various natural non-woven fibers such as chicken feathers and vegetable fibers in order to develop eco-friendly materials for automotive industry. Finally, bio-based thermoset materials based on resorcinol diglycidyl ether, an aromatic epoxy compound derived from wood, and chicken feathers or lignin were developed.

The studies developed in this thesis propose the synthesis, elaboration and characterization of several bio-resins and bio-composites fulfilling the criteria and requirements asked for an industrial valorisation.

Keywords: humins, keratin, chicken feathers, lignin, bio-based and sustainable polymers & composites, waste & by-products valorisation

Résumé

Des études scientifiques et industrielles sont axées pour remplacer les ressources fossiles par des matières premières renouvelables, pour réduire et valoriser les déchets industriels afin de développer de nouveaux matériaux verts et innovants. La conversion de la lignocellulose en bioraffineries par hydrolyse acide permet la valorisation de cette biomasse en produits plateforme à valeur ajoutée (HMF, FF, LA, etc.), mais provoque également la formation d'un sous-produit : les humines. Les plumes représentent de 5 à 7% de la masse corporelle d'un poulet adulte, étant l'un des principaux déchets générés par l'industrie de la volaille. Sachant que les plumes de poulet sont composées à 91% de kératine, ce déchet peut devenir une source renouvelable importante et utilisée comme alternative aux matières premières fossiles. L'objectif principal de cette thèse fut la valorisation des humines et des plumes de poulet afin de développer des matériaux « durables ». Tout d'abord, des résines à base d'humines ont été conçues, ayant des propriétés variant de flexibles au rigides. Ensuite, ces résines à base d'humines ont été utilisées comme matrice pour préparer de matériaux composites avec des plumes de poulet et de la lignine comme biocharges. Par la suite, des résines thermodurcissables entièrement biosourcées ont été synthétisées par la copolymérisation des humines avec le phloroglucinol diglycidyl éther, un monomère époxy obtenu à partir d'algues. De plus, des composites biosourcés recyclables ont été développés en renforçant les résines thermodurcissables à base d'humines avec diverses fibres non tissées comme les plumes de poulet ou les fibres végétales. Enfin, des matériaux thermodurcis biosourcés à base de diglycidyl éther de résorcinol et de plumes de poulet ou de lignine ont été élaborés.

Les études réalisées dans cette thèse proposent la synthèse, l'élaboration et la caractérisation de plusieurs bio-résines et bio-composites répondant aux critères et exigences demandés pour une valorisation industrielle.

Mots-clés: humins, kératine, plumes de poulet, lignine, polymères et composites et durables biosourcés, valorisation de déchets et de sous-produits

Acknowledgments

Firstly, I would like to express my deep and sincere gratitude to my PhD thesis Director, Prof. Alice Mija, for trusting me and guiding me step by step in the wonderful world of materials science. I still remember the first day when I arrived in front of the University Côte d'Azur. Everything seemed big and unknown to a young aspiring woman at the beginning of her journey, coming from a foreign country. I felt like I was lost in space, until a warm smile appeared in my way. Yes, it was her, Prof. Alice Mija, the wonderful person who guided and supported me throughout this entire period. Sincere thanks for the opportunity you offered to me and also for all the beneficial advice and teachings that you have given me. Many thanks for involving me in as many types of activities as possible, both scientific and administrative, thus taking part in the development with great effort and dedication of a new laboratory...our home. I am also deeply grateful for all the wonderful memories and experiences lived together in the many meetings and conferences in which you guided me. I would like also to sincerely thank you for learning me what science really means and for making me to fall in love with what I'm doing. In the 2 months of the pandemic, in which we had to work at home, I realized how much I miss the laboratory activities and the research, and this I owe only to you. Thank you for supporting me, teaching me and guiding me to become a true representative of materials science world.

I would like to thank to the previous director, Prof. Elisabet Duñach, and the current one, Prof. Uwe Meierhenrich, for the whole effort to make the Institute of Chemistry a friendly and conducive framework for scientific development.

I would like to kindly and deeply acknowledged to my rapporteurs, Prof. Irina Volf from University Gh. Asachi Iasi (Romania) and Prof. Marc Abadie from University Montpellier, for the honor of devoting part of their time to reading and analyzing my doctoral dissertation.

I would also like to address respectfully thanks to Prof. Veronica Ambrogi from University of Naples (Italy) and to Prof. Véronique Michelet from University Côte d'Azur, for agreeing to be part of my thesis jury, and I am deeply grateful that they will support me on one of the most important day of my career.

Acknowledgments to the European Commission for funding the most amazing and interesting European Project called KaRMA2020. I would like to express my sincere thanks to all the consortium partners who made this project possible. Thank you all for this wonderful experience, for all the meetings full of new information and knowledge, but also for the extraordinary events lived together. Thank you for warmly including me in the KaRMA2020

family. In particular, I would like to thank to the project coordinator, Dr. Sarah Montes from CIDETEC (San Sebastian, Spain), for all the help and support offered both during my internship within this company and throughout the entire collaboration. I am also deeply grateful and glad that I had the opportunity to collaborate with Dr. Krysztyna Wrześniewska-Tosik from Institute of Biopolymers and Chemical Fibers (IBWCh, Poland). I would like to thank her for all the energy and the scientific spirit that she instilled in me.

I would like also to bring my gratefulness to Dr. Francois Orange from Centre Commun de Microscopie Appliquée (CCMA) Nice and to Dr. Edith Peuvrel-Disdier and Dr. Romain Castellani from École des Mines de Paris-CEMEF Sophia Antipolis, for the opportunity to work together as well as for the advices and guidance offered for an appropriate analysis and interpretation for my thesis.

Many thanks to my colleagues Chiara, Pier, Cristina, Luna, Dima, Iuliana, Alan, Xavier, Erol et al. (apologize if I forgot someone) for all the nice experiences lived together. Special thanks to Chiara, with whom I spent most of this wonderful experience. Thank you all for all the amazing moments full of humor and happiness, for all the constructive disputes and for all the friendship offered. Thank you that with you this experience has become an unforgettable one and that every day of work was a day of joy for me.

I would like to thank to my parents and to my little sister Diana. I am deeply grateful for your full support and for all the kind words. I know that a part of your soul broke and left with me, but the evolution and fulfillment of your daughter and sister was more important than anything. I will be deeply grateful to you, and my whole life will not be enough to thank you for all the sacrifice and love that you offered to me.

In the end, I would like to thank to my best friend, confidant partner and husband, Andrei, the most important person in my life. Thank you for all the wonderful words and for all the support that you give me at any time and unconditionally. Thank you for always being the shoulder on which I can cry when it is difficult for me, because you rejoice with me for all my successes, because you listen to me every time I feel the need to speak. Thank you for being and for making me to be myself!

Index of Abbreviations

Chemicals

A	Acetone
AcN	Acetonitrile
BDMA	N,N-dimethylbenzylamine
CHCl ₃	Chloroform
DMF	Dimethylformamide
DMP-30	2,4,6-Tris(dimethylaminomethyl)phenol
DMSO	Dimethyl sulfoxide
GDE	Glycerol diglycidyl ether
MeOH	Methanol
PEGDE	Poly(ethylene glycol) diglycidyl ether
RDGE	Resorcinol diglycidyl ether
T	Toluene
TGPh	Triglycidyl ether of phloroglucinol
THF	Tetrahydrofuran
TMPTE	Trimethylolpropane triglycidyl ether

Characterization techniques

ATR-FTIR	Attenuated total reflection Fourier transform infrared spectroscopy
DMA	Dynamic mechanical analysis
DSC	Differential scanning calorimetry
FT-IR	Fourier transform infrared spectroscopy
SEM	Scanning electron microscopy
TGA	Thermogravimetric analysis
WA%	Water absorption percentage

Other abbreviations

B	brittleness
BCC	bio-based carbon content
CF	chicken feathers
E'	Young's modulus
E''	loss modulus

ESI	electronic supplementary information
G'	elastic modulus
G''	viscous modulus
Hu	humins
J	jute
K	keratin
L	lignin
LF	linseed flax
M_c	average molecular weight between crosslinks
Nu	nucleophilic group
R	Universal gas constant
SD	shore D scale of hardness test
SF	short flax
$\tan \delta$	damping factor
T	temperature
T_g	glass transition temperature
T_s	heat-resistance index
$T_{5\%}$	temperature at which the material loses 5 wt.%
wt.	weight
α	degree of conversion
$\Delta_r H$	reaction enthalpy
ρ	density
ν	crosslink density
ε_b	elongation at break

Table of contents

1 Industrial by-products from food industry and biorefinery as potential raw materials - State of the Art	
1.1. Keratin - a valuable renewable resource	2
1.1.1. Structure, physico-chemical and mechanical properties of chicken feathers	2
1.1.2. Keratin from chicken feathers	5
1.1.2.1. Characteristics and properties	5
1.1.2.2. Extraction of keratin protein from chicken feathers	7
1.1.2.3. Keratin modification	9
1.1.3. Purification and treatment methods of chicken feathers	9
1.1.4. Potential applications of chicken feathers	10
1.1.4.1. Feathers as biofertilizers and flame retardants	10
1.1.4.2. Micro and nanoparticles from feather keratin	11
1.1.4.3. Chicken feathers for thermoplastic resins and composites	12
1.1.4.4. Chicken feathers with elastomers and thermosets	17
1.2. Humins - valuable side-product of biorefineries	19
1.2.1. Biorefinery - the key concept of a renewable industry	20
1.2.2. Valorisation routes of humins by-products	22
1.3. Scope and outline of the thesis	23
Notes and references	24
2. Cross-linked polyfuran networks with elastomeric behaviour based on humins biorefinery by-products	
Abstract	34
2.1. Introduction	35
2.2. Results and discussion	38
2.2.1. DSC studies of reactivity	38
2.2.2. Evolution of the structure during copolymerization reactions	42
2.2.2.1. FT-IR investigations	42
2.2.2.2. Rheometry analysis	44
2.2.3. Physico-chemical characterization of humins-based copolymers	44
2.2.3.1. Glass and sub-glass transitions	44
2.2.3.2. Tensile properties	48
2.2.3.3. Thermal stability of the networks (TGA)	49
2.2.3.4. The bio-based content for humins-based copolymers	50
2.3. Conclusions	51
2.4. Experimental	51

Note and references	55
Electronic supplementary information (ESI)	59
3. Bio-based composites from industrial by-products and wastes as raw materials	
Abstract	64
3.1. Introduction	65
3.2. Results and discussion	68
3.2.1. Reactivity study of the humins-based resins in presence of chicken feathers powder or lignin bio-fillers	68
3.2.1.1. Differential scanning calorimetry	68
3.2.1.2. Rheometry analysis during crosslinking	70
3.2.2. Physico-chemical characterization of bio-composites	71
3.2.2.1. Thermogravimetric analysis (TGA)	71
3.2.2.2. Dynamic mechanical thermal analysis (DMA)	73
3.2.2.3. Tensile testing	76
3.2.2.4. Water absorption	78
3.2.2.5. Scanning electron microscopy (SEM)	78
3.3. Conclusions	79
3.4. Experimental	80
Notes and references	84
Electronic supplementary information (ESI)	89
4. Sustainable thermosets obtained by copolymerization of humins with triglycidyl ether of phloroglucinol	
Abstract	94
4.1. Introduction	95
4.2. Results and discussion	97
4.2.1. DSC study of the humins - TGPh copolymerization reactions	97
4.2.2. Physico-chemical and mechanical properties of bio-based thermosets	99
4.2.2.1. Thermal stability of thermosets	105
4.2.2.2. Water absorption analysis	107
4.2.2.3. Chemical resistance of the bio-based thermosets	108
4.2.2.4. Bio-based content of humins/TGPh copolymers	109
4.3. Conclusions	110
4.4. Experimental	111
Notes and references	114

5. Reprocessable Humins Thermosets and Composites for Sustainable Applications	
Abstract	120
5.1. Introduction	121
5.2. Results and discussions	123
5.2.1. Study of systems reactivity. Selection of optimal thermosetting matrices for the bio-composites development	123
5.2.2. Physico-chemical and mechanical characterization of the humins based resins and composites	125
5.2.2.1. Thermal stability studies	125
5.2.2.2. Glass transition and hardness of the bio-based materials	130
5.2.2.3. Tensile testing	131
5.2.2.4. Moisture absorption behavior	133
5.2.2.5. Fiber/matrix interface investigation by SEM analyses	135
5.2.3. Mechanical recycling of the humins-based composites	138
5.3. Conclusions	141
5.4. Experimental	142
Notes and references	145
Electronic supplementary information (ESI)	150
6. Design of sustainable materials by cross-linking a biobased epoxide with keratin and lignin	
Abstract	156
6.1. Introduction	157
6.2. Results and discussions	159
6.2.1. Reactivity study	159
6.2.2. Physico-chemical characterization of RDGE based composites	163
6.2.2.1. Thermal stability of obtained materials	163
6.2.2.2. Glass transition determined by DSC	165
6.2.2.3. Tensile testing	166
6.3. Conclusions	167
6.4. Experimental	168
Notes and references	171
Electronic supplementary information (ESI)	175
Concluding and perspectives	181

Chapter 1

Industrial By-products from Food Industry and Biorefinery as Potential Raw Materials - State of the Art

Context

The increasing amount of petroleum-based materials and products, as well as industrial waste discharged into nature, are among the most pressing factors that strongly affect the health of ecosystems in this last decade. To combat the environmental pollution problem, scientific researches place great emphasis on developing new environmentally friendly bio-based materials, and on waste and resources management by promoting the circular economy concept. The main purpose of this chapter is the bibliographic investigation on the use of two industrial by-products such as the chicken feathers from food industry and the humins from biorefinery. The formation processes of these industrial by-products but also different physical and mechanical characteristics were presented. Likewise, the potential valorisation routes of these industrial by-products have been reviewed in compliance with the research studies up to now.

1.1. Keratin - a valuable renewable resource

The need to significantly reduce environmental pollution has led to the investigation and development of new materials from renewable resources. Natural fibers come from biological origins and are found in plants, animals, and mineral-based sources. It is known that the animal fibers are mainly composed of proteins.¹ Proteins are biopolymers which can be used as alternative for materials derived from petroleum because are biodegradable, renewable, inexpensive and especially abundant. An important source of protein is represented by chicken feathers which are mainly obtained as by-product from the poultry industry.²

1.1.1. Structure, physico-chemical and mechanical properties of chicken feathers

Feathers represent around 5–7% of the corporal mass of an adult chicken,³ functioning as covering for poultry. For birds, feathers play an important role in functions such as flight, protection, heat retention or waterproofing. These large diversity of the feathers' functions has been generated over time by the permanent need for adaptability of the body to different times of their life.⁴ To archive all these functions, feathers are classified, according to their structural types as contour feather, semiplume, filoplume, chick down and bristle feather.^{4–6}

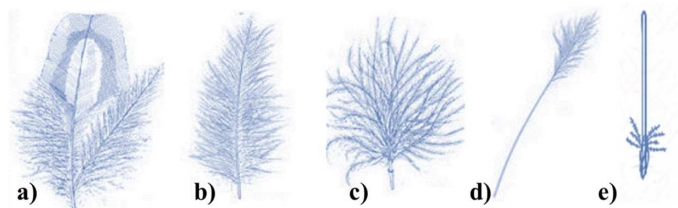


Figure 1. Types of feathers: a) contour feathers, b) semiplume, c) chick down, d) filoplume, e) bristle⁴⁻⁶

The most common of these feather structures are the “contour feathers” that cover the wings, tail and body. Contour feathers are the largest feathers which give the colour and round shape of the birds, providing also the first level of defence against collisions, sun, wind and rain. Chick down structures represents the finest layer of feathers being small, soft and fluffy downy feathers. This type of feathers provides most of the insulation against heat loss. The semiplume feathers are found between contour and chick down feathers, acting as extra insulation and providing shape to the bird. The filoplumes structures are situated at the base of each contour feather. These are very small, stiff and hair-like with a few soft barbs near the tip and without a very well understood function. It is assumed that the filoplumes present sensory functions, helping the birds to keep the optimal position of feathers for flight. Bristles feathers are found around the eyes and mouth of the birds being comparable to mammalian eyelashes.⁴

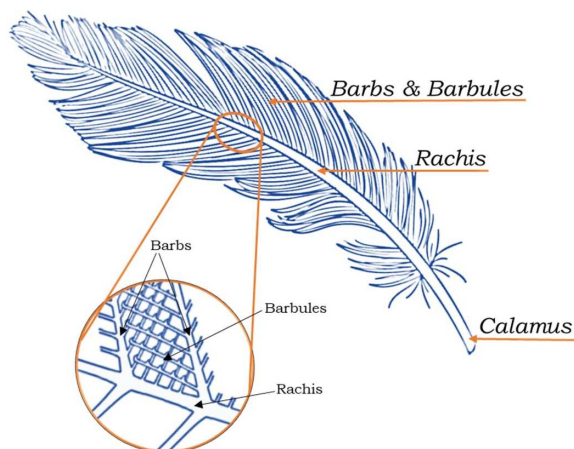


Figure 2. Structures of chicken feathers

Feathers present a complex hierarchical branched structure where rachis is the primary structure, barbs are the secondary and barbules the tertiary branches.⁷ The naked portion of the feather is named calamus and is implanted in bird's skin. The rachis represent the central axis of the feather and could be up to 17 cm in length.⁸ The widest part of the rachis may have a diameter around 3 mm.⁹ The barbs represent the secondary structure of the feathers and are attached on each side of the rachis, this portion of the feather being called vane. The barbs' length is from 1 to 4.5 cm depending on their location on rachis, such that the barbs present at the tip of the rachis are shorter than those at the base. The diameter of this filaments is between

40–400 μm , varying from the distal end to the proximal end.^{8–10} On the barbs are attached microfilaments called barbules which present structures like hook at their tips. The length of barbules is less than 1 mm (0.3–0.5mm) and their diameter ranges from 10 μm to 30 μm .^{8–11}

In the rachis and barbs cross-section it can be observed the presence of a honeycomb structure.^{7,10,12} The rachis consist of a hollow cylinder called cortex, inside of which is a supporting foam core called medulla.¹³ According to Reddy and Yang⁸ these honeycomb structures act as air and heat insulators, providing a high compressibility resistance and lightweight of the feathers. About 50% of the feathers weight is represented by barbs and the other 50% by rachis.¹⁴

According to theories^{15,16} it is assumed that the evolution process of feathers is divided in several stages like: elongation of scales, appearance of a central shaft, differentiation of vanes into barbs and appearance of barbules. In the first phase, feather originates as a hollow tube which than change into a series of barbs in the second phase. After this, the barbs self-organize along a central axis called rachis. In the last phase, the barbules appear attached by barbs and the feather develop their final organizational structure.⁷

The mechanical properties of chicken feathers make them unique fibers suitable for several applications. Reddy and Yang⁸ analysed the structure and properties of chicken feathers barbs and compared them with that of the wool and turkey feathers. The fineness and elongation of chicken feather barbs are similar to those of turkey feathers barbs but lower than those of the wool. The strength and the modulus of chicken feathers barbs are similar with that of wool. The modulus values indicate the softness and flexibility of a material, so a low modulus indicates a soft and flexible material.

Table 1. Properties of chicken feather, turkey feathers and wool fibers

Fiber	Fineness (denier)	Strength (g/den)	Elongation (%)	Modulus (g/den)	Moisture regain (%)	Reference
Chicken barbs	76	1.44	7.7	35.6	9.7	[8]
Turkey barbs-pennaceous	142	0.83	7.96	15.55	-	[17]
Turkey barbs-plumalaceous	55.2	0.36	16.43	4.47	-	[17]
Wool	11	1.2-1.8	30-40	30-45	16	[18]

Zhan and Wool⁹ report that both tensile modulus and tensile strength of different feathers are significantly different, so the tensile modulus of chicken feathers barbs is around 3.59 ± 1.09 GPa and the averages tensile strength is 203 ± 74 MPa. Sah *et al.*¹² found that chicken feather fibres have fineness of 36.48 denier, tensile strength of 1.32 g/den, elongation of 10.75% and modulus of 22.61 g/den. Through thermogravimetric analysis, they observed a decrease of 10% in feathers mass from 25°C to 80°C which is due to the loss of free water.

Around the temperature of 205°C appeared a second decline of weight in which feathers gradually started to decompose. Tesfaye *et al.*¹⁰ have examined the physical properties and morphological structure of chicken feathers in order to identify possible routes for the valorisation of these wastes. The authors report that the moisture content of the barbs is around 12.33%, for the whole feathers \approx 10.54%, while for the rachis \approx 8.75%, thus proving the hygroscopic character of the feathers. According with the reported studies,^{19,20} the glass transition temperature (T_g) of the chicken feathers fibers is ranged between 220 °C and 240 °C. Likewise, due to the complex chemical structure, the chicken feathers have both hydrophobic and hydrophilic character in a proportion of about 60:40%. The waterproof properties of the feathers are due to a thin layer composed of lipids covering their external part. The estimated value of the total fat content in the chicken feather is \approx 1.53%.²¹

1.1.2. Keratin from chicken feathers

1.1.2.1. Characteristics and properties

Chicken feathers are composed from approximately 91% proteins (keratin), 8% water and 1% lipids^{6,22}, so these are one of the main source of keratin. Keratin is considered one of the most important biopolymer.⁷ The term keratin is derived from the word "kera" which means horn in Greek. In the past, this term referred to all proteins extracted from horns, claws, hooves, nails or skin modifications.^{23,24} After several investigations, the term is currently redefined and refers to all filament-forming intermediate proteins with specific physico-chemical properties and produced in any vertebrate epithelia.²⁵ Keratin fibers present a hierarchical structure, with a highly-ordered conformation, product of a large evolution of animal species. Is the major component of hair, wool, nails, hooves, claws, scales, horn, beaks and feathers.²⁴

Based on X-ray diffraction, keratins can be classified into α -pattern, β -pattern, feather-pattern and amorphous pattern.²⁶⁻²⁹ The α -helix structure is characterized by intramolecular hydrogen bonds, while the β -sheet structure is characterized by inter-chains hydrogen bonds between amino and carbonyl groups.³⁰ Keratin is characterized by a high stability due to the intermolecular bonds between the polar and the non-polar amino acids and a low solubility caused by the presence of S-S cysteine bonds.^{30,31} The α -keratin proteins are organized as coiled coils. This conformation was first postulated independently by Pauling and Crick³². Shortly after, Pauling, Corey and Branson³³ identified the structure as consisting of two helically wound chains of polypeptides. The helical structure is stabilized by the hydrogen bonds inside the helix chain, causing the chain to twist and exhibit a helical shape. Also, this conformation consists of keratin microfibrils in a sulphur matrix, and the breaking strain of α -keratin fibers (*e.g.* hair and wool) is \approx 45%, while their Young's modulus is around 2000 MPa.²⁵ β -keratin looks like an pleated sheet, consisting of laterally packed β -strands which can be parallel or antiparallel, and the chains are held together by intermolecular hydrogen bonds.³⁴

The pleated sheet structure is stabilized by two factors such as the hydrogen bonds between beta strands which contribute to the formation of the sheet and the planarity of the peptide bond which forces the β -sheet to be pleated. Keratin can be considered as a polymer/polymer composite of crystalline filaments embedded in an amorphous matrix.³⁴ The amino acid chains of β -keratins are shorter than those of α -keratins, being characteristic for hard-keratinized and hard-cornified modified epidermis in reptiles and birds.²³

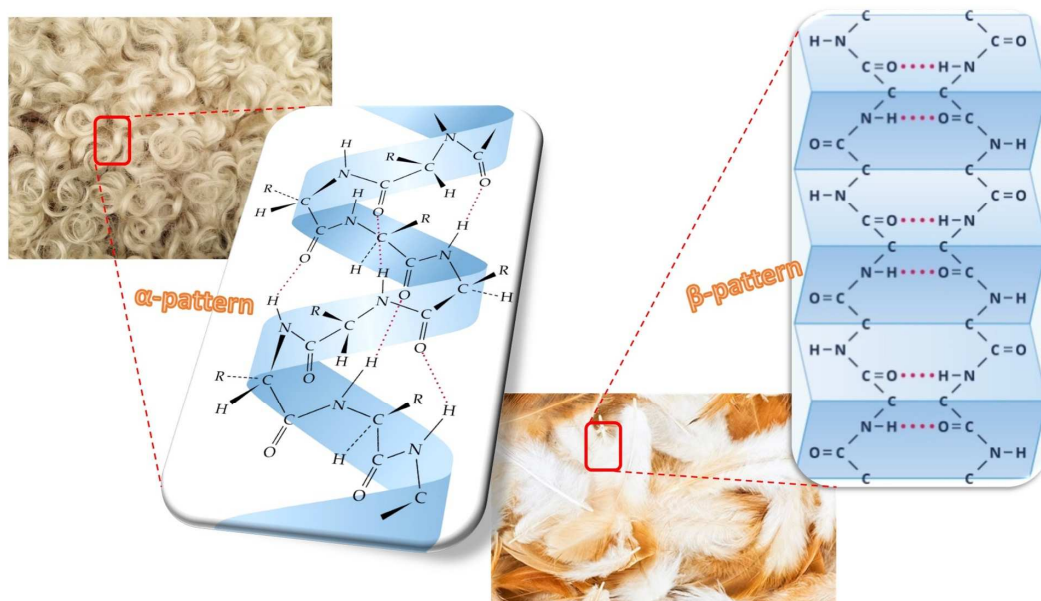


Figure 3. Molecular structure of α -helices and β -sheet keratin

Generally, proteins are composed of different amino acids joined in sequential chains. The fibril proteins consist of polypeptide chains by the condensation of different amino acids. The keratin shows an elevated content of the amino acid as glycine, alanine, serine, cysteine and valine, and lower amounts of lysine, methionine and tryptophane.^{24,35,36} Keratin feathers contains a range of noncovalent interactions (electrostatic forces, hydrogen bonds, hydrophobic forces) and covalent interactions (disulfide bonds).³⁷ Cysteine is a sulfur-containing amino acid which, by oxidation, forms inter- and intramolecular disulfide bonds and creates a crosslinked network.² The second largest quantity amino acid in chicken feathers is represented by serine who contains -OH groups. Hydrogen bonds are created by non-ionic polar amino acids and these can be found between amino and carbonyl groups. The energy of hydrogen bonds is lower than that of ionic or covalent bonds, but higher than the energy of hydrophobic interactions.²⁴

Keratin reactivity depends on several factors such as chemical composition, morphological structure, the character of intermolecular bonds and the presence of active functional groups, but can be also influenced by its solubility or water susceptibility.²⁴

Keratin is naturally insoluble due to inter- and intra-molecular disulfide linkages, and to interchain peptide linkages.^{34,36} The solubility of β -keratin was described by alkaline

thioglycolate and combination of a disulfide bond-breaking reagent and a protein denaturant.^{38,39} The keratin is highly stable in polar solvents like water, weak acids and bases. The presence of cysteine in ample amount made keratin susceptible for hydrolytic and oxidative reactions.^{35,37} Apparently, keratin is insoluble in water with very low chemical reactivity. However, its solubility in water increases at low pH, high temperature and in presence of some reducing agent (*i.e.* Na₂SO₃ or Na₂S). The reactive functional groups present in keratin protein, especially peptide backbone, such as disulfide (-S-S), amino (-NH₂) and carboxylic acid (-COOH), make it chemically reactive. On reduction, disulfide crosslinks are broken into free thiol (-SH) besides the protonation of some -NH₂ and other groups in keratin making its surface positive and thus its solubilization takes place.^{35,40} Thus, by protonation the keratin proteins acquire positive surface charge and become a pseudo-cationic biopolymer.

Keratinous materials exhibit exceptional mechanical functions depending on the host animal origin. Mineralization with calcium and other salts can contribute to the hardening of keratins. The alignment and volume fraction of filaments influence the mechanical properties of keratins, and humidity plays an important role in the mechanical behaviour of keratins.³⁴

1.1.2.2. Extraction of keratin protein from chicken feathers

Keratin proteins can be extracted by various routes such as acid, enzymatic or alkaline hydrolysis, reduction or oxidation of the disulfide bonds, thermal treatment in some organic solvents and various hydrothermal methods.^{40,41} The chemical hydrolysis leads to destruction of the native structure of keratin and the feather waste becomes more water-soluble. The acidic hydrolysis is highly efficient, but causes the loss of some amino acids, while the alkaline hydrolysis is slower and can be incomplete, but the loss of amino acids is lower.⁴²

David *et al.*³⁹ demonstrated that chicken feathers can be converted to natural proteins soluble in alkali or acid and digestible by trypsin and pepsin. This was accomplished by breaking the disulfide bonds of the keratin. By breaking the S-S bonds, the strength of the keratin can be reduced thus it become soluble and converted to natural protein. In another study, Gupta *et al.*⁴³ investigated the extraction of keratin from the chicken feathers by dissolving them using different reducing agents like potassium cyanide, thioglycolic acid and sodium sulfide. After feathers' dissolution the keratin was precipitated with ammonium sulphate solution and then was separated from chemicals. The percentage of keratin protein obtained was evaluated by biuret test and FTIR analysis. It was found that the extraction with sodium sulfide gives the highest efficiency in dissolving chicken feathers, the total mass of obtained protein being about 53%. Thereby, the products obtained after chicken feathers dissolution confirmed the presence of true keratin protein without any foreign materials. Bomou Ma *et al.*⁴⁴ extracted the keratin from chicken feathers by breaking the disulfide bond networks using l-cysteine as reducing agent. A mixture of urea and cysteine adjusted to pH 10.5 was used to

dissolve the feathers, and then the precipitate was extracted and washed. The water-keratin solution was freeze dried and pulverized to obtain the keratin powder, the yield being about 60%. Feather keratin was extracted also by Yin *et al.*⁴⁵ under reducing conditions with the so-called Shindai method. The process of extraction included three main steps such as ethanol pre-treatment, hydrochloric acid pre-treatment and 2-mercaptoethanol deoxidization. The yield of keratin obtained from chicken feathers was $\approx 93\%$, the molecular weight ≈ 20 kDa, with low dispersity, including 14–15% cysteine residues. Generally, various treatment conditions such as temperature, time, pH value and dosage of the reagents, have a significant influence on the yield and the molecular weight of the extracted keratin.

Sinkiewicz *et al.*⁴² determined the effect of thermo-chemical treatments with various reducing agents on the yield of keratin extracted from chicken feathers. To extract keratin, two processes were used, the reduction and the hydrolytic process. The results of the study demonstrate that the hydrolytic processes to obtain soluble keratin (yield about 94%) are more effective than its solubilization by reduction of the disulfide bonds (yield ≈ 82 –84%). Garrido *et al.*² obtained hydrolysed keratin, which has been used as a source of sulfur for protein-based films development. Commonly, alkaline hydrolysis is done using heating to increase the yield, but this heating increases also the amino acid destruction. In the reported study, hydrolysed keratin was obtained at room temperature to develop a simple, inexpensive and eco-friendly process. Keratin was extracted from chicken feather waste using alkaline hydrolysis obtaining a maximum protein yield around 70.23–80.2%.^{46,47} The extracted keratin particles were used to develop bioplastic films with potential applications in biomedical and pharmaceutical industries. In another work, Na Ayutthaya *et al.*⁴⁸ extracted keratin from chicken feathers *via* an environment-friendly method such as sulfitolysis method. To do this, the cleaned feathers were immersed in aqueous solution of sodium hydroxide, urea, sodium dodecyl sulphate and sodium meta-bisulfite in different proportions (0.0–0.5 M). Sodium meta-bisulfite was used to break covalent disulfide bonds from chicken feathers protein. The cysteine disulfide bonds were cleaved with sulfite and the cysteine thiol and cysteine-S-sulfonate were released. The highest yield of keratin (87.6%) was obtained when 0.2 M of sodium meta-bisulfite was used.

The use of ionic liquids (IL)^{37,49,50} and deep eutectic solvents (DES)⁵¹ as chemical treatments for keratin extraction has been intensively explored due to their capacity to keep the properties of the original polymer and due to their recyclability. The ILs are organic salts with ionocovalent structures and are often liquid at room temperature, while DES are low transition temperature mixtures consisting in an organic salt together with a H-bond donor.^{52,53} Ji *et al.*⁴⁹ dissolved poultry feathers using a common water-soluble imidazole IL such as 1-butyl-3-methylimidazolium chloride together with Na₂SO₃, succeeding to obtain a dissolution rate of feather $\approx 97\%$ and a yield of keratin about 75.1%. In order to produce an uniform keratin

feedstock, Nuutinen *et al.*⁵¹ processed the poultry feathers with an aqueous DES composed of non-toxic sodium acetate, urea, and a small amount of water. The processing conditions were optimized in terms of keratin yield and properties by varying different factors such as the dissolution time, the temperature, but also the molar ratio of sodium acetate–urea.

1.1.2.3. Keratin modification

Covalent modification of keratin is an effective way to modulate its macromolecular function.^{54–56} The chemical modifications of keratinous protein are selective for molecular residue of protein⁵⁷ and may be used to increase or modulate the reactivity of desired functional groups.

Alkylation of cysteine was accomplished using electrophiles such as iodoacetamide for the first time in 1935.⁵⁸ Chalker *et al.*⁵⁹ carried out chemical modifications of cysteine. Clark and Lowe⁶⁰ worked on conversion of the active-site cysteine residue of papain into dehydroserine, serine and glycine residues. They used bromoacetophenone derivatives to alkylate the cysteine of keratin and to convert it into formyl glycine photochemically. Many methods were adopted to form disulfide on keratinous cysteine, such as, air oxidation, mixing thiol in protein containing basic buffer, reaction of 5,5-dithiobis(2-nitrobenzoate) or Ellman's reagent with cysteine.^{61,62} Danishefsky and Wan⁶³ developed a mild radical based desulfurization, that is specific for cysteine. Such reactions regarding desulfurization have also been reported by Crich *et al.*^{64–66} on peptides. Holmes and Lawton⁶⁷ report about conversion of cysteine into dehydroalanine as a result of its oxidative elimination during desulfurization. In other studies, nickel and palladium are used to mediate the selective reduction of cysteine to alanine.⁴⁵

Keratin shows a high resistance to chemical and physical factors. This protein can be degraded using acids, bases, enzymes, increased temperature or UV radiation. Being exposed to mineral acids, the protein fibers undergo degradation, while under the influence of the bases, keratin first expands and then degrades.²⁴ The biodegradation process is also triggered by certain species of fungi (*e.g. Aspergillus fumigatus*), producing a keratinolytic enzyme that decomposes keratin. Enzymatic degradation is beneficial for the industry, since it occurs at room temperature, which reduces the costs of the process.

1.1.3. Purification and treatment methods of chicken feathers

After being removed from the chicken's body, feathers are contaminated with various impurities.⁶⁸ Therefore, feathers must first undergo a decontamination and pre-treatment process. The decontamination process refers to the removal of pathogens and microorganisms, while the pre-treatments represent the cleaning of feathers surface from impurities such as fats, sand, waste waters, *etc.*^{69,70} Tesfaye *et al.*^{69,70} tested various pre-treatments and decontamination processes of feathers in order to determine the most effective ones. The

authors used different surfactants, the obtained results being compared with the decontamination by high heat in autoclave unit.⁶⁹ It was found that the physico-chemical properties of the decontaminated and pre-treated chicken feathers with surfactants did not undergo significant changes and the microbial number decreased considerably, making them safe for handling and use in different applications.

Pourjavaheri *et al.*^{71,72} tested the effectiveness of various methods of chicken feathers purification correlated with their mechanical and microbiological properties. The purification techniques used were: a) Soxhlet extraction with ethanol (SEEt), b) ozonation, c) purification by ClO₂, d) purification with a non-ionic surfactant as poly(ethylene glycol) (PEG), e) purification with an anionic surfactant as sodium lauryl sulphate (SLS), f) purification with a cationic surfactant as cetyltrimethylammonium chloride (CTAC) and g) purification *via* a combination method (SLS–ClO₂–SEEt). Comparing the purification methods, it was found that the Soxhlet extraction with ethanol and purification *via* a combination method have reduced considerable the bacterial counts being the only treatments that destroyed Salmonella. Combined surfactant–oxidant–ethanol purification generated better mechanical and morphological properties compared to Soxhlet extraction with ethanol, providing superior tensile strength of fibers. However, the Soxhlet extraction with ethanol was chosen as the safest purification treatment.

For the degreasing of chicken feathers, one of the most used method is the treatment with petroleum ether in a Soxhlet device for a certain period of time (between 4 and 24h), then washed with distilled water and dried.^{42,46,47,73–75}

To improve the properties of chicken feathers and to increase their use, the researchers studied different methods of chemical modification to change their structure and morphology. Khosa, Wu et Ullah⁷⁶ analysed different chemical modifications of chicken feathers to further use them as raw materials for preparing arsenic removing biosorbents from water. The authors tried three types of chemical modifications: treatment with alkaline aqueous solution, sodium sulfite supported modifications and treatment with methyl alcohol. These chemical modifications focused on the following three functional groups from feather protein: a) sulfhydryl groups (SH), b) amino groups (-NH₂) and c) carboxylic groups (-COOH).⁷⁶ Flores-Hernandez *et al.*⁷⁴ treated the chicken feathers with sodium hydroxide, then used them as reinforcement material in chitosan–starch polymers. The authors report that this treatment modifies the surface of the fibers but does not affect the protein structure.

1.1.4. Potential applications of chicken feathers

1.1.4.1. Feathers as biofertilizers and flame retardants

The presence of high amounts of nitrogen in feathers makes them ideal for use as fertilizer. Gurav and Jadhav⁷⁷ demonstrated that hydrolysed feathers could be an inexpensive

and good fertilizer for banana plants. The chicken feathers were degraded with the help of *Chryseobacterium* species, being then used as fertilizer for banana plants. The inclusion of hydrolysed feathers as fertilizer led to an increase in chlorophyll content, the protein but also the amino acids content in banana fruits compared to the control plants. Gousterova *et al.*⁷⁸ treated the feather waste with thermophilic actinomycete strains and used them to restore contaminated soil and also as a fertilizer for rye grass cultivation. The authors demonstrated that the hydrolysed feathers could be used as biocontrol agents and as fertilizer. According to these studies was found that the availability of nitrogen from the feathers as fertilizer is considerably low because the feathers are highly crosslinked with cysteine linkages and are difficult to degrade.

The presence of high doses of nitrogen in the molecular structure of chicken feathers keratin led to the development of flame retardants by Wang *et al.*⁷⁹. In the first step, they hydrolysed the feathers using sodium hydroxide and urea. Next, the precipitate obtained was collected, dried and then was ground to powder. The P-N based flame retardant was prepared by mixing melamine, sodium pyrophosphate and chicken feather keratin powder in 1:8:5 mass ratio, then a certain amount of glyoxal was added to the mixture. In this manner the authors obtained a yellowish feather-based flame retardant. Then the flammability of different types of fabrics such as untreated cotton fabric, treated cotton fabrics with the chicken-feather protein-based flame retardant, treated cotton with borax and boric acid and treated cotton with the combination of the chicken-feather protein-based flame retardant and borax and boric acid were investigated by the vertical flammability test and limited oxygen index test. After tests, they concluded that the combination of the chicken-feather protein-based flame retardant and borax and boric acid had a good synergistic effect on enhancement of flame retardancy performance of the finished cotton fabric.

Wrześniewska-Tosik *et al.*⁸⁰ prepared composites based on elastic polyurethane with milled chicken feathers in order to produce foam materials. The flame-retardant effect of the chicken feathers on the developed composites was analysed. It was found that the addition of feathers decreased the density of materials, increased the limiting oxygen index and the maximum degradation rate of the resulting foams.

1.1.4.2. Micro and nanoparticles from feather keratin

Micro and nanoparticles made from organic and inorganic materials have been used in the food, agriculture, cosmetology, medicine and other areas. Dissolution and preparation of chicken feather particles present a high level of difficulty due to the high crosslinking by cysteine.⁷⁵

Researchers adopted various approaches to prepare micro- and nanoparticles using feather keratin. Sun *et al.*⁸¹ developed chicken feather based particles for potential removal of

chromium Cr(VI) using waste chicken feathers dissolved and regenerated in an ionic liquid of 1-butyl-3-methylimidazoliumchloride ([BMIM]Cl). The chicken feathers were solubilized in the ionic solution by heating, the particle formed being then added into chromium solution of a known concentration. The keratin particles regenerated from [BMIM]Cl showed an excellent efficiency (63.5–87.7%) for removing Cr(VI) ions in wastewater at the concentrations from 2 to 80 ppm, while the Freundlich constant (kF) for the adsorption of Cr(VI) ions by the particles of the regenerated chicken feathers was four times higher than that of the raw chicken feather. Xu *et al.*^{82,83} report the development of water-stable nanoparticles from feather keratin having the biocompatibility and stability required for medical applications such as controlled drug release systems. They obtained nanoparticles with diameters ranging between 5 and 130 nm, the keratin particles being stable in water, without the need for any crosslinking or other chemical modification.

The keratin powder can be obtained by many techniques like sonication, spray drying, rotary blades and through milling (ball, jet), but all these techniques generate powders with high particle size and nonuniform shape. Rad *et al.*⁸⁴ analysed the production of keratin nanopowder through electro-spraying a solution of recovered feather keratin. Using this technique, the authors produced keratin nano-powder with spherical shape particles and uniform size with an average particle size as low as 53nm.

Wang *et al.*⁸⁵ investigated the development of feathers keratin nanoparticles for haemostatic applications. Firstly, they pre-treated the chicken feathers with sodium dodecyl sulfate (SDS) to remove dust and then with ethanol and hydrochloric acid solution to degrease and break the hydrogen bonds in the chicken feathers. Keratin was extracted from pre-treated feathers using a solution of SDS, urea and Tris base. The chicken feathers keratin nanoparticles were prepared *via* an ultrasonic dispersion method. The obtained keratin nanoparticles were tested on rats and the results demonstrated that this feather keratin nanoparticles could have potential applications in haemorrhages healing.

1.1.4.3. Chicken feathers for thermoplastic resins and composites

Considerable efforts are made to utilize biopolymers to develop consumer products, especially disposable thermoplastics and packaging materials.⁸⁶ Poultry feathers have been used to develop thermoplastic films for food packaging and other applications. Since feathers are inherently non-thermoplastic and do not melt, several chemical modifications are done to make feathers thermoplastic. Chicken feathers were also used as reinforcement for biocomposites development.⁷⁵

Yin *et al.*⁴⁵ reported the fabrication of porous keratinous films developed with keratin extracted from chicken feathers using the so-called Shindai method. To produce films, the aqueous dispersion of the reduced keratin was mixed with a certain amount of glycerol. Tensile

strength of the obtained films varied from 4.5 to 7.5 MPa and modulus from 11 to 28 MPa depending on the amount of glycerol. Moreover, these films were pH responsive and showed controllable drug-release behaviour. Barone *et al.*⁸⁷ developed an environmentally friendly process to obtain cohesive films with good physical properties. In this study, the keratin feathers were modified with glycerol, acting as plasticizer and introducing free volume into the polymer. Thereafter, the samples were sandwiched between aluminium foils and pressed into film. After processing a clear amorphous film resulted, which was capable of being stretched by over 100%. The developed keratin films could have potential applications for food packaging or mulching films.

Soy protein isolate and hydrolysed keratin were used by Garrido *et al.*² to develop thermoplastic films. Hydrolysed keratin has been used as additive in the film forming process to increase the sulfur content of soy protein materials, thus leading to the improvement of the physicochemical properties of the resulting films. The films were obtained by compression molding, applying a pressure of 12 MPa for 2 minutes at 150 °C. The obtained films could be used in food and pharmaceutical industry as active and biodegradable films. Sharma *et al.*⁴⁶ used keratin extracted from chicken feather waste to develop a bioplastic film which can be used in biomedical and pharmaceutical industries. To synthesize a bioplastic film, the authors used keratin powder, glycerol (3.5%) and microcrystalline cellulose (0.2%) in NaOH for 48h at 60 °C. The Young's modulus and break elongation for resulted bioplastic film were about 1.52 MPa and 16%, respectively, while the calculated thickness was $\approx 1.12 \times 10^{-4}$ mm with a tensile strength of 3.62 MPa.

Song *et al.*⁸⁸ developed chicken feather protein/gelatine composite films with clove oil which could be used in active packaging. To prepare composite films, a solution made of chicken feathers, distilled water, gelatine and sorbitol was mixed and then heated at 75 °C. At the end, after clove oil addition, the film-forming solution was poured onto a flat Teflon-coated glass plate and dried at 25 °C for 24 h. The addition of clove oil in chicken feather/gelatine composite films increases the elongation, water vapor permeability and water solubility of the materials but decreased the tensile strength. The moisture content of the films was not visibly affected, but it was observed that it increased as the amount of clove oil increased. The prepared films can be considered as potential active packaging material for smoked salmon. Ramakrishnan *et al.*⁸⁹ studied the biodegradability and mechanical properties of films made from chicken feathers keratin and glycerol. As proved by SEM results, a good connection was observed between the components, the surface of the film appeared homogeneous, without holes or cavities. It has also found that increasing glycerol concentration produce a decrease in maximum tensile strength of films. The optimal thermomechanical properties were obtained in

keratin with 2% glycerol. Biodegradability tests showed that polymer films were completely degraded within 10 hours.

Das *et al.*⁹⁰ used the chicken feather proteins (CFP) and pomelo peel pectins (PPP) in the development of composite films. By increasing the pomelo peel pectins quantity was obtained a significant decrease to the water vapor permeability and moisture absorption, but also decreased the water solubility of the keratin/pectin-based films. The film prepared with 25:75 of CFP and PPP presented the adequate properties in order to be used for wrapping of fried fish fillets. The weight loss, hardness and microbial count of the unwrapped and wrapped fish samples were observed for a period of 5 days at every 24h. Wrapping of fried fish with chicken feather keratin and pomelo peel pectin based films reduces the weight loss by 3%, the hardness by 11% and microbial count was considerable reduce compared to unwrapped fried fish. Reddy *et al.*^{91,92} demonstrated that a simple alkaline hydrolysis of feather makes the feathers thermoplastic and suitable to develop films by compression molding. The chicken feathers were hydrolysed using various concentrations of alkali (0.05 to 0.75 wt.% NaOH) at 50 °C for 1 hour. Then the hydrolysed feathers were mixed with glycerol as plasticizer and crosslinked with citric acid to improve their water stability. The authors show that this method allows to develop inexpensive and biodegradable thermoplastics from inexpensive, renewable and sustainable poultry feathers.

Shi *et al.*⁹³ developed thermoplastics from chicken feathers by grafting them with different methacrylates (methyl, ethyl, butyl, and hexyl methacrylates), and the effects of graft polymerization conditions such as monomer concentrations, temperature, and time of reaction, were investigated. The samples were obtained by compression molding for 10 min at 180–200 °C. By addition of homopolymer, films with a better elongation, water stability and strength were obtained. It was found that the grafted feathers films present a lower strength but higher elongation with increasing the alkyl chain lengths. The developed films have good dry and wet tensile properties and are stable at high humidity. Jin *et al.*⁹⁴ developed inexpensive and biodegradable thermoplastics through graft polymerization of chicken feathers with methyl acrylate as a potential substitute for petroleum products. Patnam *et al.*⁹⁵ reported an efficient method for graft polymerization of chicken feathers with different vinyl monomers such as glycidyl methacrylate (GMA), styrene (S), and methyl methacrylate (MMA) without using any catalyst or initiator. The chicken feathers powder was mixed with water, sodium dodecyl sulphate and vinyl monomer at 70 °C, pH 2 and continuous flushing of nitrogen for 2 h. The obtained polymer particles were washed, dried, and then extracted with acetone in a Soxhlet installation in order to remove the homopolymers and unreacted monomers from the grafted polymers. The developed method has shown a good potential for using poultry feathers to produce thermoplastic materials for different industrial uses.

Similar to grafting, acetylation and etherification were found to make feathers thermoplastic and suitable to develop various products. Reddy *et al.*⁸⁶ showed that etherification using acrylonitrile (cyanoethylation) is a viable approach to develop thermoplastic films from chicken feathers by compression molding. Films with a strength ranging from 1.6 to 4.2 MPa and elongation at break about 5.8–14% depending on the extent of cyanoethylation were obtained. In another study,⁹⁶ acetylated and cyanoethylated chicken feathers were used to develop transparent thermoplastic films by compression molding. The obtained films showed good thermoplasticity being suitable for the development of inexpensive, biodegradable and environmentally friendly thermoplastic materials. Ullah *et al.*⁷³ investigated the effect of four different plasticizers such as ethylene glycol, propylene glycol, glycerol, and diethyl tartrate, on the thermoplastic properties of quill-based plastics. Blends of ground quill were prepared by mixing the feathers with the plasticizer and sodium sulfite. Sodium sulfite treatment was used as reducing agent. Extrusion was undertaken at temperatures of 90–120 °C and a screw speed of 50 rpm, then the films were prepared by compression molding. The authors noticed that all added plasticizers were able to reduce the melting temperature and the glass transition temperature of the materials, but the best mechanical properties, processability, transparency and flowability were obtained for the materials developed with ethylene glycol.

Flores-Hernández *et al.*⁹⁷ evaluated the performance as reinforcement of fibrillar keratin fiber over a biopolymeric matrix composed polysaccharides. Three kinds of keratin reinforcement such as short fibers, long fibers and rachis particles were used in composites development. The keratin fibers were added separately at 5, 10, 15 and 20 wt.% to the chitosan-starch matrix and the mixtures were poured into glass plates. The films were obtained after evaporation of the solvents. The thermal results indicate that the addition of keratin enhanced the thermal stability of the composites compared to that of neat matrix. The storage modulus of all composites was significantly higher than that of chitosan-starch matrix as result of keratin reinforcement. Also, the SEM micrographs indicated a uniform dispersion of keratin in the chitosan-starch matrix, result of good compatibility between these biopolymers. The obtained results demonstrate that chicken feathers can be useful to obtain novel keratin reinforcements and to develop new green composites. Barone *et al.*⁹⁸ prepared polyethylene-based composites using keratin feather fiber. Grounded keratin feathers were mixed with high-density polyethylene (HDPE) at 20 wt.%. The effects of compounding and molding process on the keratin-based composites properties were studied by tensile testing and scanning electron microscopy. It was found that the addition of keratin wool fibers increased the stiffness but decreases the tensile stress of the composites.

Martínez-Hernández *et al.*³ used keratin fibers from chicken feathers as short-fiber reinforcement for poly(methyl methacrylate) (PMMA) matrix. The physico-chemical and mechanical properties of the composites were characterized using different techniques. The thermal stability and transition temperature were found to be higher than standard PMMA. The storage modulus at room temperature increased for the composites reinforced with 1–2 wt.% keratin bio-fibers. Cheng *et al.*⁹⁹ investigated the feasibility of using chicken feather fibers as reinforcement for poly(lactic acid) (PLA) composites. The samples were prepared by extrusion and injection molding methods. The mechanical and thermal properties of the composites were analysed, the best results being obtained by the composites reinforced with 5 wt.% of chicken feather fibers. The authors observed that chicken feather fibers/PLA composites have the required thermo-mechanical properties for applications that do not require high load-bearing capability. Fully biodegradable bio-composite based on chicken feathers were developed also by Aranberri *et al.*¹⁰⁰ A torque rheometer was used to produce composites based on PLA, polybutyrate adipate terephthalate (PBAT) and a PLA/thermoplastic copolymer blend with high loadings of chicken feather fibers (50 and 60 wt.%). It was found that the formed composites have a low density, increased water adsorption and thermal insulating properties, while the thermal stability, tensile strength and elongation-at-break were negatively affected comparing with the neat resins. On the other hand, Cañavate *et al.*¹⁰¹ developed environmentally friendly PLA/poultry feather keratin bio-composites materials, and the effect of manufacturing conditions on the final properties of the composite and on the matrix–fiber compatibility was studied. They observed that the elastic modulus of PLA is not affected by the feather content, while the addition of 25% chicken feathers decreased the tensile strength by 58% and the elongation at break by 12%. However, the obtained chicken feathers/PLA composites present better tensile properties than medium-density fiberboards and organic resin-bonded particleboards.

Yang and Reddy¹⁰² reinforced the high-density polyethylene from plastic bags with chicken feathers to develop composites in an effort to reduce the amount of the plastics and feathers disposed in landfills. They created a sandwich structure with layers of plastic bags and feathers. Proportion (w/w) of the feathers to plastic was varied from 40/60 to 70/30. Incorporating feathers as reinforcement for HDPE provided much higher flexural strength, tensile modulus and sound absorption than 100% HDPE. Supri *et al.*¹⁰³ studied the effects of ϵ -caprolactam on morphology, thermal degradation and tensile test of composites made from chicken feather fibers and recycled high-density polyethylene (r-HDPE). They realized composites with ϵ -caprolactam and without ϵ -caprolactam to compare them. Following the tests, it was observed that composites with ϵ -caprolactam present a higher tensile strength and modulus of elasticity compared with the composites without ϵ -caprolactam, but instead,

presents a lower mass swell percentage and elongation at break. It was also found that the chicken feather fibers were better dispersed, and the thermal stability was better in composites with ϵ -caprolactam.

In order to replace non-renewable composite materials, Huda and Yang¹⁰⁴ proposed to develop composites from ground chicken quill and polypropylene. They investigated the mechanical and acoustical properties of this kind of composites and compared them with jute-polypropylene composites, concluding that the ground quill composites can be ideal candidates for acoustic panels or headliner substrates. Reddy and Yang¹⁰⁵ demonstrated that the composites reinforced with whole chicken feathers have better flexural, tensile and acoustic properties than the composites made from processed feathers. Pourjavaheri *et al.*¹⁰⁶ developed bio-composite materials from chicken feathers waste and thermoplastic polyurethanes via solvent-casting-evaporation method. Different amounts of thermoplastic polyether-polyurethane (TPU-polyether) and chicken feathers were mixed with 100 ml tetrahydrofuran (THF), then the mixture was left overnight to evaporate the solvent. The obtained films were sandwiched between two polytetrafluoroethylene sheets for compression molding/thermal pressing at 175 °C. Following the tests, it was found that the reinforcement of the polymer matrix with chicken feathers led to the improvement of the modulus of elasticity, storage modulus and thermal stability, but the glass transition temperature, recovery strain and mass loss of the composites decreased.

The association between feathers keratin and poly (urea-urethane)s (TPUU) was investigated by Aranberri *et al.*¹⁰⁷. The authors compared two analogous thermoplastic poly(urea-urethane) elastomers with two aromatic diamine chain extenders like bis(4-aminophenyl) disulfide (TPUU-SS) and the sulfur-free counterpart bis(4-aminophenyl) methane (TPUU). Bio-composites with high content of chicken feathers (40–75 wt.%) were developed in a torque rheometer and hot compression. Properties such as density, water absorption and relative thickness swelling were similar to both types of bio-composites. The TPUU-SS systems displayed the best interphase adhesion, consequently causing the improvement in mechanical properties, the tensile strength of 50/50 wt.% TPUU/feather fibers composite being up to 7.5-fold higher compared to neat polymer.

1.1.4.4. Chicken feathers with elastomer and thermosets

The thermoset materials are characterized by the fact that they irreversibly lead to a solid material during the curing step. Typical examples for thermosets resins are represented by phenolic and urea formaldehyde resins, unsaturated polyesters, and epoxy resins.¹⁰⁸ Due to proper physico-chemical and mechanical properties, the thermosetting resins present a real interest in their use as polymeric matrices for bio-composites development with keratin fibers.

Uzun *et al.*¹⁰⁹ manufactured vinyl ester and polyester thermoset composites reinforced with chicken feathers quill and fiber at different loadings (0%, 2.5%, 6% and 10%) using hand lay-up method. The matrix materials were prepared in a ratio of 73% of resin matrix and 23% of hardener by volume and then, the fibers were spread into mold and covered with the matrix. The mechanical properties of the composites were analysed and compared with that obtained for the neat resins. It was found that the impact properties of the composites were significantly improved due to feather addition, but their flexural properties decreased compared to the neat resins. Hong and Wool¹¹⁰ developed a novel bio-based composite material from soybean oils and keratin feather fibers. They used acrylated epoxidized soybean oil and soybean oil pentaerythritol glyceride maleates as liquid molding resins and two different types of non-woven keratin fiber mats. The physico-chemical and mechanical properties of the developed composites were investigated obtaining good performances. Alagarsamy *et al.*¹¹¹ obtained new composite materials using coconut coir fiber and chicken feathers as reinforcement for polyester resins. The composites samples were fabricated using the hand lay-up method. Zhan *et al.*¹¹² manufactured composites with epoxy resin, chicken feather fibers and glass fibers for potential applications, such as printed circuit boards.

Bassa *et al.*²⁰ evaluated the potential applications of chicken feathers as reinforcement for thermosetting materials. Chicken feathers were impregnated with a green epoxy resin, the materials being produced by compression molding process, using 2 tons' pressure at 120 °C for 6 min. The thermal and acoustic tests performed on the composite material samples showed that increasing the chicken feather fibers ratio, the thermal resistance increased and the noise decreased, making them potential materials for automotive and building applications.

Extensive work was done by Senoz *et al.*¹¹³ by incorporating pyrolyzed chicken feather fibers in acrylated epoxidized soybean oil and methacrylated lauric acid-based thermosetting resin to provide reinforcement in low density and rubbery polymer applications. The mechanical properties of the polymer composite, such as storage modulus, tensile modulus, tensile strength, and fracture energy were directly proportional to the fiber content. Varying the fiber content up to 32 wt.% a wide tuning of mechanical properties was obtained *i.e.* 20–300 MPa storage modulus and 10–150 MPa range at room temperature. The reinforcement with pyrolyzed or untreated chicken feather fibers did not give differences in the degree of reinforcement to the composites. Addition of pyrolyzed feathers significantly increased the tensile properties and facilitate using liquid molding techniques for composite fabrication without causing any degradation of the feathers. Winandy *et al.*¹¹⁴ made medium density fibreboard (MDF) panels with aspen fiber and chicken feather fiber (0–95%) using phenol formaldehyde resin (5%) as adhesive. The panels were made with a phenol formaldehyde resin which was applied to the wood fiber, chicken feather fiber, or to the combined MDF-chicken

feather fiber furnish in a rotating drum blender. Following mechanical and physical tests, the addition of feather fibers decreased the strength and stiffness but showed a significant improvement in the resistance to water-soak absorption of MDF-CFF composites compared with that of wood control panels.

Consequently, chicken feathers fibers are a major waste, generated in large quantities annually and which has a huge influence on environmental pollution. The production and consumption of chicken meat is in a constantly increasing, leading to the increase of the amount of feather waste and consequently to the increase of the pollution. The interest of researchers in the valorisation of chicken feathers increased considerably in the last years. Feathers, being composed from 91% keratin, represent a valuable waste with countless potential applications in cosmetics, tisular engineering, controlled drug release, biotechnology, thermoplastic, packaging, composites for different sectors of industry (construction, automobile, *etc.*), biofertilizers and coatings. Although the number of researches on the valorisation of this waste has increased, industrial valorisation is not yet sufficiently developed.

1.2. Humins - valuable side-product of biorefineries

One of the most used invention created by man which led to a significant evolution of the society is represented by the plastics or synthetic organic materials. The way in which the humanity managed this invention and transformed it into a single-use and disposable convenience, led to the transformation of this innovation into a factor of the environment imbalance and pollution.¹¹⁵

Humanity's first encounter with polymeric materials took place in 1600 BC when the ancient mesoamerican peoples harvested latex from *Castilla elastica*, processed it using liquid extracted from *Ipomoea alba* using the resulted material to develop rubber balls, hollow rubber figurines or other rubber artefacts.¹¹⁶ Although in 1839 Goodyear invented vulcanized rubber, and Eduard Simon discovered polystyrene,¹¹⁷ the first synthetic polymer, such as bakelite, appeared in 1907 in Belgium.¹¹⁸ The large-scale production and use of plastics dates back to 1950, and until now about 6.3 billion tons of plastic have been produced worldwide, of which 9% were recycled, 12% were incinerated and 79% were accumulated in landfills or the natural environment, leading to a pollution expansion.¹¹⁹ To combat this global pollution problem, intense research has been drawn to use the renewable resources to replace the fossil derivatives. The actual challenge is to find effective ways of converting the bioresources into fuels and chemicals and to develop new innovative green and environmentally friendly products.

1.2.1. Biorefinery - the key concept of a renewable industry

The continuous population growth, but especially of its needs, has led to an increased focus on the conservation and management of resources used in industrial production. A future-oriented approach can be represented by the conversion of the global economy into a sustainable economy in which the bioenergy, biofuels, and bio-based products are the main components. Applying and growing the sustainable economy requires reliable and sustainable resources for industrial production but is already known that the fossil resources are not considered sustainable, and their availability is more than questionable in the long term. Therefore, the need to establish solutions that reduce the consumption of non-renewable fossil products and the increasing concern for the environment, have led to the production of chemicals on the platform *via* biochemical processes using renewable biomass sources.¹²⁰

The biorefinery concept represents the industry solution of creating a wide range of products from renewable resources, while the biomass term refers to the renewable organic matters, such as agricultural crops, trees, algae and various residues or waste.¹²¹ Based on feedstock type used to produce biofuels and bio-based products, biorefineries are divided into three different generations such as: i) first-generation biorefineries which use traditional forms of agriculture biomass (e.g. corn, sugarcane, maize, soybean, etc.), ii) second-generation biorefineries which use lignocellulosic biomass, and iii) third-generation biorefineries which use agricultural residues, forestry, petroleum and urban waste, or microalgae as biomass.^{121–123}

Lignocellulose is one of the most abundant sources of biomass, their availability being unaffected by land use. This biomass is generally found in structural material of the plant cells wall. Lignocellulosic biomass is constituted of three major components such as 40-50% cellulose, 25-30% hemicellulose and 15-20% lignin.¹²⁴ The structure and the quantity of this three components vary according to species, tissues and maturity of the plant cell wall. The major constituent of lignocellulosic biomass is the cellulose $(C_6H_{10}O_6)_n$, a β -1-4-glucan that is a linear syndiotactic polymer. Its structure consists of extensive intramolecular and intermolecular hydrogen bonding networks, which tightly binds the glucose units. These hydrogen bonding determines 'straightness' of the chain but interchain hydrogen bonding introduce the crystalline character into the cellulose structure. The degree of polymerization of cellulose chains in nature ranges from 10,000 glucopyranose units in wood to 15,000 in native cotton.¹²⁵ The cellulosic chains are grouped into microfibrils, which are also grouped in cellulose fibers. The second most abundant polymer in lignocellulosic biomass is represented by hemicellulose. Hemicellulose $(C_5H_8O_5)_n$ is a branched polymer consisting of a mixture of different carbon monosaccharide units such as pentoses (xylose, arabinose), hexoses (mannose, glucose, galactose) and acetylated sugars. This polymer has a random and amorphous structure and is found between the cellulose microfibrils and lignin giving cohesion to the whole

cellulose–hemicellulose–lignin network.¹²⁶ Hemicelluloses differ in composition in function of the nature of feedstock. Hemicelluloses in agricultural biomass like straw and grasses or hardwood hemicelluloses are composed mainly of xylans while softwood hemicelluloses contain mostly glucomannans.¹²⁷ The third constituent of lignocellulosic biomass, the lignin ($C_9H_{10}O_2(OCH_3)_n$), is a three-dimensional amorphous phenolic polymer whose structure is formed by three phenylpropanes building blocks such as p-coumaryl alcohol, coniferyl alcohol, and sinapyl alcohol.¹²⁸ Its functions as cellular glue provides overall rigidity to the structure of plants and trees and resistance against insects and pathogens. Generally, softwoods contain more lignin than the hardwoods, and lignin from softwoods contain mainly coniferyl alcohol, while those from hardwoods and grass contain mainly coniferyl and sinapyl alcohols.¹²⁷

Valorisation of lignocellulosic biomass in fuels and valuable chemicals in an economical, ethical and ecological way, represent the main purpose of the biorefinery concept. Transforming biomass raw materials into valuable products within a biorefining process requires several technological treatments such as thermochemical, biochemical, mechanical/physical and chemical processes.¹²⁹ Thermochemical process is divided in two different pathways such as gasification and pyrolysis, and is used for converting biomass into energy and chemical products. Biochemical processes occur at lower temperatures with low reaction rates the most common being the fermentation and anaerobic digestion. In the mechanical processes the state or composition of the biomass is not changed, but only a reduction in size or a separation of the components of the raw material takes place, while the chemical processes change the structure of the molecules by reacting them with other substances. The most common chemical processes in biomass conversion are hydrolysis and transesterification.¹²⁹ Lignocellulosic biomass is generally resistant to hydrolysis in water due to the presence of cellulose as main component, thus its hydrolysis require the use of strong liquid acids as catalysts. During acid-catalysed hydrolysis process the cellulose is depolymerized forming glucose, this one being then converted into value added chemical building blocks, namely, 5-hydroxymethyl furfural (HMF), furfural (FF), and levulinic acid (LA). Besides obtaining these valuable chemical building blocks, the acid-catalysed hydrolysis of sugars provoke the formation of a dark-coloured insoluble polymeric side-product called “humins”.^{130–132} The yield of humins is influenced by various process parameters such as the type of substrate, time, temperature, and type of acid catalyst.^{133,134} Although considerable efforts have been made to suppress the formation of humins, the yield of this side-product is still about 14–30 wt.%, representing a major fraction during sugar conversion.^{134,135} Despite intense investigations the understanding of the pathway for the humins formation is weak, and its chemical structure has not yet been accurately determined.^{136–138} Generally, humins are described as heterogenous macromolecules, composed from polycondensed furanic structures

($\approx 60\%$) with aliphatic linkers ($\approx 20\%$).¹³³ The elemental composition of humins prepared by the acid-catalysed dehydration of sugars was reported to be about 50–66 wt.% C, 29–46 wt.% O, the rest being H.^{139–141} To improve the economic feasibility of biorefineries, humins require intense investigations for the development of new valorisation routes.

1.2.2. Valorisation routes of humins by-products

Currently, the commercial valorisation of the humins takes place in biorefineries where this by-product is burnt being used for its heating qualities similar to coal-like fuel.¹²⁰ Another possible valorisation routes is represented by the production of syngas and higher value chemicals *via* gasification and pyrolysis of humins products. In order to obtain syngas, Hoang *et al.*¹³⁴ studied the gasification and steam reforming of the humins over a variety of alkali- and alkaline-earth based catalysts, obtaining a complete conversion of the by-product and a yield of H₂ of approximately 82%. Rasrendra *et al.*¹³⁵ developed laboratory made humins by acid-catalysed dehydration of D-glucose and D-fructose in aqueous systems. The obtained humins samples were fast pyrolyzed using GC-MS pyrolysis (300–600 °C, 10 s, He atmosphere) and micro-pyrolysis (500 °C, 12 s, N₂ atmosphere). It was found that the major components in the liquid pyrolysates are low molecular weight furanics such as furfural and 2,5-dimethylfuran, the product thus having potential as biofuel, while the isolated individual components can serve as building blocks for renewable polymers.

Humins were also used in the preparation of porous carbon materials with variable industrial applications such as substrates for plant growth, absorbents for wastewater treatment, insulation materials, support for solid catalysts, *etc.*^{142–148} For example, Tosi *et al.*¹⁴⁴ developed new rigid microporous foams by auto-crosslinking of industrial humins. The rigid foams were obtained through an usual heating process without a prior treatment, resulting foams with a high control of the morphology, porosity and carbon content. Recently, humins revealed also a real interest in the development of polymeric resins and composites, being still in the incipient phase of research.^{115,149–151} Pin *et al.*¹⁴⁹ combined large amounts of industrial humins with polyfurfuryl alcohol to develop new fully bio-based thermoset resins via acid-induced polymerizations. Then, the furanic resins were used as matrix for the development of composites in which the cellulose filter papers acted as reinforcement. The PFA/humins/cellulose composite properties were analysed and compared with those of neat PFA and PFA/lignin/cellulose composites. Furthermore, Licsandru *et al.*¹⁵¹ has copolymerized an industrial by-product such as humins, with a vegetable resource comonomer such as epoxidized linseed oil (ELO), in order to develop new bio-resins. Following the analyses, it was observed that the mechanical properties of the bio-based materials vary depending on the amount of humins, making them a feasible candidate for a wide range of industrial applications.

1.3. Scope and outline of the thesis

The main objective of this thesis is to investigate and explore possible routes for the valorisation of the two industrial by-products such as humins and chicken feathers.

This manuscript is organized as follows:

The **Chapter 1** introduces the thesis context, the problematic and the presentation of materials used for valorisation in this thesis work.

The **Chapter 2** focus on the study of new polymeric materials based on humins copolymerization. The investigation of the humins-based copolymers structure, behaviour but also of the properties of the materials were performed via different characterization techniques. The development of polyfuranic materials based on humins, with modulable properties having from a rigid to an elastomeric character was demonstrated.

In **Chapter 3** the humins-based resins previously developed were studied as polymeric matrices for the design of new green bio-composites. The humins-based bio-composites were manufactured using as reinforcing material different side-products such as chicken feathers and lignin. In the first part of the study, the influence of the filler on the matrix' crosslinking reaction was investigated, then the physico-chemical and mechanical properties of the cured humins-based composites were analysed.

Chapter 4 presents the investigation of the development of environmentally friendly bio-based materials by copolymerization of humins with phloroglucinol triglycidyl ether, a green epoxy monomer. The obtained materials with a high bio-based carbon content (BCC) about 94% were characterized by thermomechanical analysis and solvents stability.

The **Chapter 5** presents of using the humins as raw material together with various environmentally friendly epoxy compounds to design recyclable thermoset resins with various properties. The humins/epoxy-based resins are then used as matrices to produce bio-composites, using untreated chicken feathers and vegetable fibers (flax and jute) non-woven as reinforcement. The characterizations on the properties of the bio-composites and of the thermo-mechanically recycled materials are presented.

Chapter 6 describes the study the copolymerization of resorcinol diglycidyl ether, an aromatic epoxy compound derived from wood biomass. The obtained resins were combined with chicken feathers and lignin. The copolymerization reactions were studied together with the properties of the final materials. The results shown that both keratin and lignin play a dual role, acting as co-reactant and reinforcing materials.

Finally, some general conclusions and perspectives are proposed.

Notes and references

- (1) Gholampour, A.; Ozbakkaloglu, T. A Review of Natural Fiber Composites: Properties, Modification and Processing Techniques, Characterization, Applications. *J. Mater. Sci.* **2020**, *55* (3), 829–892. <https://doi.org/10.1007/s10853-019-03990-y>.
- (2) Garrido, T.; Peñalba, M.; de la Caba, K.; Guerrero, P. A More Efficient Process to Develop Protein Films Derived from Agro-Industrial by-Products. *Food Hydrocoll.* **2019**, *86*, 11–17. <https://doi.org/10.1016/j.foodhyd.2017.11.023>.
- (3) Martínez-Hernández, A. L.; Velasco-Santos, C.; De-Icaza, M.; Castaño, V. M. Dynamical-Mechanical and Thermal Analysis of Polymeric Composites Reinforced with Keratin Biofibers from Chicken Feathers. *Compos. Part B Eng.* **2007**, *38* (3), 405–410. <https://doi.org/10.1016/j.compositesb.2006.06.013>.
- (4) Ng, C. S.; Wu, P.; Fan, W. L.; Yan, J.; Chen, C. K.; Lai, Y. T.; Wu, S. M.; Mao, C. T.; Chen, J. J.; Lu, M. Y. J.; Ho, M. R.; Widelitz, R. B.; Chen, C. F.; Chuong, C. M.; Li, W. H. Genomic Organization, Transcriptomic Analysis, and Functional Characterization of Avian α - and β -Keratins in Diverse Feather Forms. *Genome Biol. Evol.* **2014**, *6* (9), 2258–2273. <https://doi.org/10.1093/gbe/evu181>.
- (5) Seawright Alonso, R.; Sanches, R.; Marcicano, J. P. P. Chicken Feather - Study of Physical Properties of Textile Fibers for Commercial Use. *Int. J. Text. Fash. Technol.* **2013**, *3* (2), 29–38.
- (6) Bansal, G.; Singh, V. K. Review on Chicken Feather Fiber (CFF) a Livestock Waste in Composite Material Development. *Int. J. Waste Resour.* **2016**, *6* (4), 4–7. <https://doi.org/10.4172/2252-5211.1000254>.
- (7) Martínez-Hernández, A. L.; Velasco-Santos, C. Keratin Fibers from Chicken Feathers: Structure and Advances in Polymer Composites. In *Keratin: Structure, Properties and Applications*; Renke Dullaart and João Mousquès, Ed.; 2011; pp 149–211.
- (8) Reddy, N.; Yang, Y. Structure and Properties of Chicken Feather Barbs as Natural Protein Fibers. *J. Polym. Environ.* **2007**, *15* (2), 81–87. <https://doi.org/10.1007/s10924-007-0054-7>.
- (9) Zhan, M.; Wool, R. P. Mechanical Properties of Chicken Feather Fibers. *Polym. Compos.* **2011**, *32* (6), 937–944. <https://doi.org/10.1002/pc.21112>.
- (10) Tesfaye, T.; Sithole, B.; Ramjugernath, D.; Chunilall, V. Valorisation of Chicken Feathers: Characterisation of Physical Properties and Morphological Structure. *J. Clean. Prod.* **2017**, *149*, 349–365. <https://doi.org/10.1016/j.jclepro.2017.02.112>.
- (11) Belarmino, D. D.; Ladchumananandasivam, R.; Belarmino, L. D.; Pimentel, J. R. de M.; da Rocha, B. G.; Galvão, A. O.; de Andrade, S. M. B. Physical and Morphological Structure of Chicken Feathers (Keratin Biofiber) in Natural, Chemically and Thermally Modified Forms. *Mater. Sci. Appl.* **2012**, *03* (12), 887–893. <https://doi.org/10.4236/msa.2012.312129>.
- (12) Sah, N.; Goel, A.; Omre, P. K. Characterization of Chicken Feather Fibre as Novel Protein Fiber for Commercial Applications. *Int. J. Trop. Agric.* **2015**, *33* (4), 3373–3378.
- (13) Myers, M. A.; Chen, P.; Albert, Y. L.; Seki, Y. Biological Materials: Structure and Mechanical Properties. *Prog. Mater. Sci.* **2008**, *53*, 1–206. <https://doi.org/10.1016/j.pmatsci.2007.05.002>.
- (14) Barone, J. R.; Schmidt, W. F. Polyethylene Reinforced with Keratin Fibers Obtained from Chicken Feathers. *Compos. Sci. Technol.* **2005**, *65* (2), 173–181. <https://doi.org/10.1016/j.compscitech.2004.06.011>.
- (15) Zhang, F.; Zhou, Z. A Primitive Enantiornithine Bird and the Origin of Feathers. *Science* (80-.). **2000**, *290* (5498), 1955–1959. <https://doi.org/10.1126/science.290.5498.1955>.
- (16) Perrichot, V.; Marion, L.; Néraudeau, D.; Vullo, R.; Tafforeau, P. The Early Evolution of Feathers: Fossil Evidence from Cretaceous Amber of France. *Proc. R. Soc. B Biol. Sci.* **2008**, *275* (1639), 1197–1202. <https://doi.org/10.1098/rspb.2008.0003>.

- (17) George, B. R.; Bockarie, A.; McBride, H.; Hoppy, D.; Scutti, A. Utilization of Turkey Feather Fibers in Nonwoven Erosion Control Fabrics. *Int. Nonwovens J.* **2003**, *os-12* (2), 1558925003os-12. <https://doi.org/10.1177/1558925003os-1200212>.
- (18) Lewin, M. *Handbook of Fiber Chemistry*, 3rd ed.; CRC Press Taylor & Francis Group: New York, 2007.
- (19) Cheung, H. Y.; Ho, M. P.; Lau, K. T.; Cardona, F.; Hui, D. Natural Fibre-Reinforced Composites for Bioengineering and Environmental Engineering Applications. *Compos. Part B Eng.* **2009**, *40* (7), 655–663. <https://doi.org/10.1016/j.compositesb.2009.04.014>.
- (20) Bessa, J.; Souza, J.; Lopes, J. B.; Sampaio, J.; Mota, C.; Cunha, F.; Figueiro, R. Characterization of Thermal and Acoustic Insulation of Chicken Feather Reinforced Composites. *Procedia Eng.* **2017**, *200*, 472–479. <https://doi.org/10.1016/j.proeng.2017.07.066>.
- (21) Saravanan, K.; Dhurai, B. Exploration on Amino Acid Content and Morphological Structure in Chicken Feather Fiber. *J. Text. Apparel, Technol. Manag.* **2012**, *7* (3), 1–6.
- (22) Ho, M.; Wang, H.; Lee, J.; Ho, C.; Lau, K.; Leng, J.; Hui, D. Critical Factors on Manufacturing Processes of Natural Fibre Composites. *Compos. Part B Eng.* **2012**, *43* (8), 3549–3562. <https://doi.org/10.1016/j.compositesb.2011.10.001>.
- (23) Donato, R. K.; Mija, A. Keratin Associations with Synthetic, Biosynthetic and Natural Polymers: An Extensive Review. *Polymers (Basel)*. **2019**, *12* (1), 32. <https://doi.org/10.3390/polym12010032>.
- (24) Staron, P.; Banach, M.; Kowalski, Z. Keratin – Origins, Properties, Application. *Chemik* **2011**, *65* (10), 1019–1026.
- (25) Bragulla, H. H.; Homberger, D. G. Structure and Functions of Keratin Proteins in Simple, Stratified, Keratinized and Cornified Epithelia. *J. Anat.* **2009**, *214* (4), 516–559. <https://doi.org/10.1111/j.1469-7580.2009.01066.x>.
- (26) Astbury, W. T.; Street, A. X-Ray Studies of the Structure of Hair, Wool, and Related Fibres. I. General. *R. Soc.* **1932**, *230* (681–693), 75–101.
- (27) Astbury, W. T.; H. J. Woods. X-Ray Studies of the Structure of Hair, Wool, and Related Fibres II. The Molecular Structure and Elastic Properties of Hair Keratin. *Philos. Trans. R. Soc.* **1934**, *232*, 333–394.
- (28) Fraser, R. D. B.; MacRae, T. P. The Structure of α -Keratin. *Polymer (Guildf)*. **1973**, *14* (2), 61–67.
- (29) Fraser, R. D. B.; MacRae, T. P.; Parry, D. A. D.; Suzuki, E. The Structure of β -Keratin. *Polymer (Guildf)*. **1969**, *10*, 810–826. [https://doi.org/10.1016/0032-3861\(69\)90110-4](https://doi.org/10.1016/0032-3861(69)90110-4).
- (30) Barone, J. R.; Schmidt, W. F. Effect of Formic Acid Exposure on Keratin Fiber Derived from Poultry Feather Biomass. *Bioresour. Technol.* **2006**, *97* (2), 233–242. <https://doi.org/10.1016/j.biortech.2005.02.039>.
- (31) Cardamone, J. M. Investigating the Microstructure of Keratin Extracted from Wool: Peptide Sequence (MALDI-TOF/TOF) and Protein Conformation (FTIR). *J. Mol. Struct.* **2010**, *969* (1–3), 97–105. <https://doi.org/10.1016/j.molstruc.2010.01.048>.
- (32) Crick, F. H. C. The Packing of α -Helices: Simple Coiled-Coils. *Acta Crystallogr.* **1953**, *6*, 689–697. <https://doi.org/10.1107/S0365110X53001964>.
- (33) Pauling, L.; Corey, R. B.; Branson, H. R. The Structure of Proteins: Two Hydrogen-Bonded Helical Configurations of the Polypeptide Chain. *Proc. Natl. Acad. Sci. U. S. A.* **1951**, *37* (4), 205–211.
- (34) Wang, B.; Yang, W.; McKittrick, J.; Meyers, M. A. Keratin: Structure, Mechanical Properties, Occurrence in Biological Organisms, and Efforts at Bioinspiration. *Prog. Mater. Sci.* **2016**, *76*, 229–318. <https://doi.org/10.1016/j.pmatsci.2015.06.001>.
- (35) Sharma, S.; Gupta, A. Sustainable Management of Keratin Waste Biomass: Applications and Future Perspectives. *Brazilian Arch. Biol. Technol.* **2016**, *59* (December), 1–14.

- <https://doi.org/10.1590/1678-4324-2016150684>.
- (36) Harding, H. W. J.; Rogers, G. E. ϵ -(γ -Glutamyl)Lysine Cross-Linkage in Citrulline-Containing Protein Fractions From Hair. *Biochemistry* **1971**, *10* (4), 624–630.
 - (37) Wang, Y. X.; Cao, X. J. Extracting Keratin from Chicken Feathers by Using a Hydrophobic Ionic Liquid. *Process Biochem.* **2012**, *47* (5), 896–899. <https://doi.org/10.1016/j.procbio.2012.02.013>.
 - (38) Harrap, B. S.; Woods, E. F. Soluble Derivatives of Feather Keratin I. Isolation, Fractionation and Amino Acid Composition. *Biochem. J.* **1964**, *92* (8), 8–18.
 - (39) Goddard, D. R.; Michaelis, L. A Study on Keratin. *J. Biol. Chem.* **1934**, *106*, 605–614.
 - (40) Khosa, M. A.; Ullah, A. A Sustainable Role of Keratin Biopolymer in Green Chemistry : A Review. *J. Food Process. Beverages* **2013**, *1* (1), 1–8.
 - (41) Pourjavaheri, F.; Pour, S. O.; Jones, O. A. H.; Smooker, P. M.; Brkljača, R.; Sherkat, F.; Blanch, E. W.; Gupta, A.; Shanks, R. A. Extraction of Keratin from Waste Chicken Feathers Using Sodium Sulfide and L-Cysteine. *Process Biochem.* **2019**, *82*, 205–214. <https://doi.org/10.1016/j.procbio.2019.04.010>.
 - (42) Sinkiewicz, I.; Śliwińska, A.; Staroszczyk, H.; Kołodziejska, I. Alternative Methods of Preparation of Soluble Keratin from Chicken Feathers. *Waste and Biomass Valorization* **2017**, *8* (4), 1043–1048. <https://doi.org/10.1007/s12649-016-9678-y>.
 - (43) Gupta, A.; Perumal, R.; Bin, R.; Yunus, M.; Kamarudin, N. B. Extraction of Keratin Protein from Chicken Feather. *J. Chem. Chem. Eng.* **2012**, *6*, 732–737.
 - (44) Ma, B.; Qiao, X.; Hou, X.; Yang, Y. Pure Keratin Membrane and Fibers from Chicken Feather. *Int. J. Biol. Macromol.* **2016**, *89*, 614–621. <https://doi.org/10.1016/j.ijbiomac.2016.04.039>.
 - (45) Yin, X.; Li, F.; He, Y.; Wang, Y.; Wang, R. Study on Effective Extraction of Chicken Feather Keratins and Their Films for Controlling Drug Release. *Biomater. Sci.* **2013**, *1* (5), 528. <https://doi.org/10.1039/c3bm00158j>.
 - (46) Sharma, S.; Gupta, A.; Kumar, A.; Kee, C. G.; Kamyab, H.; Saufi, S. M. An Efficient Conversion of Waste Feather Keratin into Ecofriendly Bioplastic Film. *Clean Technol. Environ. Policy* **2018**, *20* (10), 2157–2167. <https://doi.org/10.1007/s10098-018-1498-2>.
 - (47) Sharma, S.; Gupta, A.; Chik, S. M. S. T.; Kee, C. G.; Mistry, B. M.; Kim, D. H.; Sharma, G. Characterization of Keratin Microparticles from Feather Biomass with Potent Antioxidant and Anticancer Activities. *Int. J. Biol. Macromol.* **2017**, *104*, 189–196. <https://doi.org/10.1016/j.ijbiomac.2017.06.015>.
 - (48) Na Ayutthaya, S. I.; Tanpichai, S.; Wootthikanokkhan, J. Keratin Extracted from Chicken Feather Waste: Extraction, Preparation, and Structural Characterization of the Keratin and Keratin/Biopolymer Films and Electrospuns. *J. Polym. Environ.* **2015**, *23* (4), 506–516. <https://doi.org/10.1007/s10924-015-0725-8>.
 - (49) Ji, Y.; Chen, J.; Lv, J.; Li, Z.; Xing, L.; Ding, S. Extraction of Keratin with Ionic Liquids from Poultry Feather. *Sep. Purif. Technol.* **2014**, *132*, 577–583. <https://doi.org/10.1016/j.seppur.2014.05.049>.
 - (50) Sun, P.; Liu, Z. T.; Liu, Z. W. Particles from Bird Feather: A Novel Application of an Ionic Liquid and Waste Resource. *J. Hazard. Mater.* **2009**, *170* (2–3), 786–790. <https://doi.org/10.1016/j.jhazmat.2009.05.034>.
 - (51) Nuutinen, E. M.; Willberg-Keyriläinen, P.; Virtanen, T.; Mija, A.; Kuutti, L.; Lantto, R.; Jääskeläinen, A. S. Green Process to Regenerate Keratin from Feathers with an Aqueous Deep Eutectic Solvent. *RSC Adv.* **2019**, *9* (34), 19720–19728. <https://doi.org/10.1039/C9RA03305J>.
 - (52) Mahmood, H.; Moniruzzaman, M.; Yusup, S.; Welton, T. Ionic Liquids Assisted Processing of Renewable Resources for the Fabrication of Biodegradable Composite Materials. *Green Chem.* **2017**, *19* (9), 2051–2075. <https://doi.org/10.1039/C7GC00318H>.
 - (53) Smith, E. L.; Abbott, A. P.; Ryder, K. S. Deep Eutectic Solvents (DESs) and Their Applications.

- Chem. Rev.* **2014**, *114* (21), 11060–11082. <https://doi.org/10.1021/cr300162p>.
- (54) Carrico, I. S. Chemoselective Modification of Proteins: Hitting the Target. *Chem. Soc. Rev.* **2008**, *37* (7), 1423. <https://doi.org/10.1039/b703364h>.
- (55) Foley, T. L.; Burkart, M. D. Site-Specific Protein Modification: Advances and Applications. *Curr. Opin. Chem. Biol.* **2007**, *11* (1), 12–19. <https://doi.org/10.1016/j.cbpa.2006.11.036>.
- (56) Qi, D.; Tann, C.; Haring, D.; Distefano, M. D. Generation of New Enzymes via Covalent Modification of Existing Proteins. *Chem. Rev.* **2001**, *101* (10), 3081–3112. <https://doi.org/10.1021/cr000059o>.
- (57) Davis, B. G. Mimicking Posttranslational Modifications of Proteins. *Science (80-.)*. **2004**, *303*, 480–482.
- (58) Moore, G. R. P.; Martelli, S. M.; Gandolfo, C.; Sobral, P. J. do A.; Laurindo, J. B. Influence of the Glycerol Concentration on Some Physical Properties of Feather Keratin Films. *Food Hydrocoll.* **2006**, *20* (7), 975–982. <https://doi.org/10.1016/j.foodhyd.2005.11.001>.
- (59) Chalker, J. M.; Bernardes, G. J. L.; Lin, Y. A.; Davis, B. G. Chemical Modification of Proteins at Cysteine: Opportunities in Chemistry and Biology. *Chem. - An Asian J.* **2009**, *4* (5), 630–640. <https://doi.org/10.1002/asia.200800427>.
- (60) Clark, P. I.; Lowe, G. Conversion of the Active-Site Cysteine Residue of Papain into a Dehydro-Serine, a Serine and a Glycine Residue. *Eur. J. Biochem.* **1978**, *84*, 293–299.
- (61) Ellman, G. L. Tissue Sulfhydryl Groups. *Arch. Biochem. Biophys.* **1959**, *82*, 70–77.
- (62) Weerapana, E.; Simon, G. M.; Cravatt, B. F. Disparate Proteome Reactivity Profiles of Carbon Electrophiles. *Nat. Chem. Biol.* **2008**, *4* (7), 405–407. <https://doi.org/10.1038/nchembio.91>.
- (63) Wan, Q.; Danishefsky, S. J. Free-Radical-Based, Specific Desulfurization of Cysteine: A Powerful Advance in the Synthesis of Polypeptides and Glycopolypeptides. *Angew. Chemie Int. Ed.* **2007**, *46* (48), 9248–9252. <https://doi.org/10.1002/anie.200704195>.
- (64) Crich, D.; Yang, F. Synthesis of Neoglycoconjugates by the Desulfurative Rearrangement of Allylic Disulfides. *J. Org. Chem.* **2008**, *73* (18), 7017–7027. <https://doi.org/10.1021/jo8015314>.
- (65) Crich, D.; Brebion, F.; Krishnamurthy, V. Allylic Disulfide Rearrangement and Desulfurization: Mild, Electrophile-Free Thioether Formation from Thiols. *Org. Lett.* **2006**, *8* (16), 3593–3596. <https://doi.org/10.1021/ol061381+CCC>.
- (66) Crich, D.; Krishnamurthy, V.; Hutton, T. K. Allylic Selenosulfide Rearrangement: A Method for Chemical Ligation to Cysteine and Other Thiols. *J. Am. Chem. Soc.* **2006**, *128* (8), 2544–2545. <https://doi.org/10.1021/ja057521c>.
- (67) Holmes, T. J.; Lawton, R. G. Cysteine Modification and Cleavage of Proteins with 2-Methyl-N-Benzenesulfonyl-N-Bromoacetylquinonediimide. *J. Am. Chem. Soc.* **1977**, *99* (6), 1984–1986. <https://doi.org/10.1017/CBO9781107415324.004>.
- (68) Rouger, A.; Tresse, O.; Zagorec, M. Bacterial Contaminants of Poultry Meat: Sources, Species, and Dynamics. *Microorganisms* **2017**, *5* (3), 50. <https://doi.org/10.3390/microorganisms5030050>.
- (69) Tesfaye, T.; Sithole, B.; Ramjugernath, D.; Ndlela, L. Optimisation of Surfactant Decontamination and Pre-Treatment of Waste Chicken Feathers by Using Response Surface Methodology. *Waste Manag.* **2018**, *72*, 371–388. <https://doi.org/10.1016/j.wasman.2017.11.013>.
- (70) Tesfaye, T.; Sithole, B.; Ramjugernath, D. Valorisation of Waste Chicken Feathers: Optimisation of Decontamination and Pre-Treatment with Bleaching Agents Using Response Surface Methodology. *Sustain. Chem. Pharm.* **2018**, *8*, 21–37. <https://doi.org/10.1016/j.scp.2018.02.003>.
- (71) Pourjavaheri, F.; Mohaddes, F.; Shanks, R. A.; Czajka, M.; Gupta, A. Effects of Different Purification Methods on Chicken Feather Keratin. *Adv. Mater. Res.* **2014**, *941–944*, 1184–1187. <https://doi.org/10.4028/www.scientific.net/AMR.941-944.1184>.

- (72) Pourjavaheri, F.; Mohaddes, F.; Bramwell, P.; Sherkat, F.; Shanks, R. A. Purification of Avian Biological Material to Refined Keratin Fibres. *RSC Adv.* **2015**, *5* (86), 69899–69906. <https://doi.org/10.1039/C5RA08947F>.
- (73) Ullah, A.; Vasanthan, T.; Bressler, D.; Elias, A. L.; Wu, J. Bioplastics from Feather Quill. *Biomacromolecules* **2011**, *12* (10), 3826–3832. <https://doi.org/10.1021/bm201112n>.
- (74) Flores-Hernández, C. G.; Colín-Cruz, A.; Velasco-Santos, C.; Castaño, V. M.; Almendarez-Camarillo, A.; Olivas-Armendariz, I.; Martínez-Hernández, A. L. Chitosan–Starch–Keratin Composites: Improving Thermo-Mechanical and Degradation Properties Through Chemical Modification. *J. Polym. Environ.* **2018**, *26* (5), 2182–2191. <https://doi.org/10.1007/s10924-017-1115-1>.
- (75) Reddy, N. Non-Food Industrial Applications of Poultry Feathers. *Waste Manag.* **2015**, *45*, 91–107. <https://doi.org/10.1016/j.wasman.2015.05.023>.
- (76) Khosa, M. A.; Wu, J.; Ullah, A. Chemical Modification, Characterization, and Application of Chicken Feathers as Novel Biosorbents. *RSC Adv.* **2013**, *3*, 20800–20810. <https://doi.org/10.1039/c3ra43787f>.
- (77) Hadas, A.; Kautsky, L. Feather Meal, a Semi-Slow-Release Nitrogen Fertilizer for Organic Farming. *Fertil. Res.* **1994**, *38* (2), 165–170. <https://doi.org/10.1007/BF00748776>.
- (78) Gousterova, A.; Nustorova, M.; Paskaleva, D.; Naydenov, M.; G.Neshev; Vasileva-Tonkova, E. Assessment of Feather Hydrolysate from Thermophilic Actinomycetes for Soil Amendment and Biological Control Application. *Int. J. Environ. Res.* **2012**, *6* (2), 467–474.
- (79) Wang, X.; Lu, C.; Chen, C. Effect of Chicken-Feather Protein-Based Flame Retardant on Flame Retarding Performance of Cotton Fabric. *J. Appl. Polym. Sci.* **2014**, *131* (15), n/a-n/a. <https://doi.org/10.1002/app.40584>.
- (80) Wrześniewska-Tosik, K.; Zajchowski, S.; Bryskiewicz, A.; Ryszkowska, J. Feathers as a Flame-Retardant in Elastic Polyurethane Foam. *Fibres and Textiles in Eastern Europe*. 2014, pp 119–128.
- (81) Sun, P.; Liu, Z. T.; Liu, Z. W. Particles from Bird Feather: A Novel Application of an Ionic Liquid and Waste Resource. *J. Hazard. Mater.* **2009**, *170* (2–3), 786–790. <https://doi.org/10.1016/j.jhazmat.2009.05.034>.
- (82) Xu, H.; Cai, S.; Xu, L.; Yang, Y. Water-Stable Three-Dimensional Ultrafine Fibrous Scaffolds from Keratin for Cartilage Tissue Engineering. *Langmuir* **2014**, *30* (28), 8461–8470. <https://doi.org/10.1021/la500768b>.
- (83) Xu, H.; Shi, Z.; Reddy, N.; Yang, Y. Intrinsically Water-Stable Keratin Nanoparticles and Their in Vivo Biodistribution for Targeted Delivery. *J. Agric. Food Chem.* **2014**, *62* (37), 9145–9150. <https://doi.org/10.1021/jf502242h>.
- (84) Pedram Rad, Z.; Tavanai, H.; Moradi, A. R. Production of Feather Keratin Nanopowder through Electrospraying. *J. Aerosol Sci.* **2012**, *51*, 49–56. <https://doi.org/10.1016/j.jaerosci.2012.04.007>.
- (85) Wang, J.; Hao, S.; Luo, T.; Yang, Q.; Wang, B. Development of Feather Keratin Nanoparticles and Investigation of Their Hemostatic Efficacy. *Mater. Sci. Eng. C* **2016**, *68*, 768–773. <https://doi.org/10.1016/j.msec.2016.07.035>.
- (86) Reddy, N.; Hu, C.; Yan, K.; Yang, Y. Thermoplastic Films from Cyanoethylated Chicken Feathers. *Mater. Sci. Eng. C* **2011**, *31* (8), 1706–1710. <https://doi.org/10.1016/j.msec.2011.07.022>.
- (87) Barone, J. R.; Schmidt, W. F.; Liebner, C. F. E. Thermally Processed Keratin Films. *J. Appl. Polym. Sci.* **2005**, *97* (4), 1644–1651. <https://doi.org/10.1002/app.21901>.
- (88) Song, N. B.; Lee, J. H.; Al Mijan, M.; Song, K. Bin. Development of a Chicken Feather Protein Film Containing Clove Oil and Its Application in Smoked Salmon Packaging. *LWT - Food Sci. Technol.* **2014**, *57* (2), 453–460. <https://doi.org/10.1016/j.lwt.2014.02.009>.
- (89) Ramakrishnan, N.; Sharma, S.; Gupta, A.; Alashwal, B. Y. Keratin Based Bioplastic Film from

- Chicken Feathers and Its Characterization. *Int. J. Biol. Macromol.* **2018**, *111*, 352–358. <https://doi.org/10.1016/j.ijbiomac.2018.01.037>.
- (90) Das, P.; Borah, P. P.; Badwaik, L. S. Transformation of Chicken Feather Keratin and Pomelo Peel Pectin into Biodegradable Composite Film. *J. Polym. Environ.* **2018**, *26* (5), 2120–2129. <https://doi.org/10.1007/s10924-017-1109-z>.
- (91) Reddy, N.; Chen, L.; Yang, Y. Biothermoplastics from Hydrolyzed and Citric Acid Crosslinked Chicken Feathers. *Mater. Sci. Eng. C* **2013**, *33* (3), 1203–1208. <https://doi.org/10.1016/j.msec.2012.12.011>.
- (92) Reddy, N.; Jiang, Q.; Jin, E.; Shi, Z.; Hou, X.; Yang, Y. Bio-Thermoplastics from Grafted Chicken Feathers for Potential Biomedical Applications. *Colloids Surfaces B Biointerfaces* **2013**, *110*, 51–58. <https://doi.org/10.1016/j.colsurfb.2013.04.019>.
- (93) Shi, Z.; Reddy, N.; Hou, X.; Yang, Y. Tensile Properties of Thermoplastic Feather Films Grafted with Different Methacrylates. *ACS Sustainable Chem. Eng.* **2014**, *2*, 1849–1856. <https://doi.org/10.1021/sc500201q>.
- (94) Jin, E.; Reddy, N.; Zhu, Z.; Yang, Y. Graft Polymerization of Native Chicken Feathers for Thermoplastic Applications. *J. Agric. Food Chem.* **2011**, *59* (5), 1729–1738. <https://doi.org/10.1021/jf1039519>.
- (95) Patnam, P. L.; Ray, S. S.; Chatterjee, A. K.; Jain, S. L. Self-Driven Graft Polymerization of Vinyl Monomers on Poultry Chicken Feathers in the Absence of Initiator/Catalyst. *J. Appl. Polym. Sci.* **2017**, *134* (13), 1–9. <https://doi.org/10.1002/app.44645>.
- (96) Hu, C.; Reddy, N.; Yan, K.; Yang, Y. Acetylation of Chicken Feathers for Thermoplastic Applications. *J. Agric. Food Chem.* **2011**, *59* (19), 10517–10523. <https://doi.org/10.1021/jf2023676>.
- (97) Flores-Hernández, C.; Colín-Cruz, A.; Velasco-Santos, C.; Castaño, V.; Rivera-Armenta, J.; Almendarez-Camarillo, A.; García-Casillas, P.; Martínez-Hernández, A. All Green Composites from Fully Renewable Biopolymers: Chitosan-Starch Reinforced with Keratin from Feathers. *Polymers (Basel)*. **2014**, *6* (3), 686–705. <https://doi.org/10.3390/polym6030686>.
- (98) Barone, J. R.; Schmidt, W. F.; Liebner, C. F. E. Compounding and Molding of Polyethylene Composites Reinforced with Keratin Feather Fiber. *Compos. Sci. Technol.* **2005**, *65* (3–4), 683–692. <https://doi.org/10.1016/j.compscitech.2004.09.030>.
- (99) Cheng, S.; Lau, K.; Liu, T.; Zhao, Y.; Lam, P.; Yin, Y. Mechanical and Thermal Properties of Chicken Feather Fiber/PLA Green Composites. *Compos. Part B Eng.* **2009**, *40* (7), 650–654. <https://doi.org/10.1016/j.compositesb.2009.04.011>.
- (100) Aranberri, I.; Montes, S.; Azcune, I.; Rekondo, A.; Grande, H. J. Fully Biodegradable Biocomposites with High Chicken Feather Content. *Polymers (Basel)*. **2017**, *9* (11). <https://doi.org/10.3390/polym9110593>.
- (101) Cañavate, J.; Aymerich, J.; Garrido, N.; Colom, X.; Macanás, J.; Molins, G.; Álvarez, M.; Carrillo, F. Properties and Optimal Manufacturing Conditions of Chicken Feathers/Poly(Lactic Acid) Biocomposites. *J. Compos. Mater.* **2016**, *50* (12), 1671–1683. <https://doi.org/10.1177/0021998315595534>.
- (102) Yang, Y.; Reddy, N. Utilizing Discarded Plastic Bags as Matrix Material for Composites Reinforced with Chicken Feathers. *J. Appl. Polym. Sci.* **2013**, *130* (1), 307–312. <https://doi.org/10.1002/app.39173>.
- (103) Supri, A. G.; Aizat, A. E.; Yazid, M. I. M.; Masturina, M. Chicken Feather Fibers-Recycled High-Density Polyethylene Composites: The Effect of ϵ -Caprolactam. *J. Thermoplast. Compos. Mater.* **2015**, *28* (3), 327–339. <https://doi.org/10.1177/0892705713484746>.
- (104) Huda, S.; Yang, Y. Composites from Ground Chicken Quill and Polypropylene. *Compos. Sci. Technol.* **2008**, *68* (3–4), 790–798. <https://doi.org/10.1016/j.compscitech.2007.08.015>.
- (105) Reddy, N.; Yang, Y. Light-Weight Polypropylene Composites Reinforced with Whole Chicken Feathers. *J. Appl. Polym. Sci.* **2010**, *116*, NA-NA. <https://doi.org/10.1002/app.31931>.

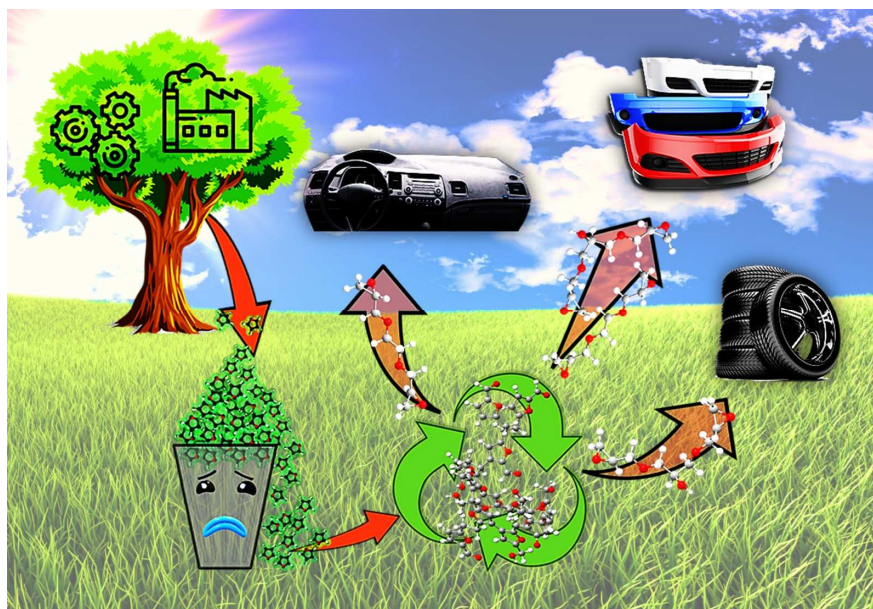
- (106) Pourjavaheri, F.; Jones, O. A. H.; Czajka, M.; Martinez-Pardo, I.; Blanch, E. W.; Shanks, R. A. Design and Characterization of Sustainable Bio-Composites from Waste Chicken Feather Keratin and Thermoplastic Polyurethane. *Polym. Compos.* **2018**, *39*, E620–E632. <https://doi.org/10.1002/pc.24794>.
- (107) Aranberri, I.; Montes, S.; Azcune, I.; Rekondo, A.; Grande, H. J. Flexible Biocomposites with Enhanced Interfacial Compatibility Based on Keratin Fibers and Sulfur-Containing Poly(Urea-Urethane)S. *Polymers (Basel)*. **2018**, *10* (10), 1056. <https://doi.org/10.3390/polym10101056>.
- (108) Auvergne, R.; Caillol, S.; David, G.; Boutevin, B.; Pascault, J. P. Biobased Thermosetting Epoxy: Present and Future. *Chem. Rev.* **2014**, *114* (2), 1082–1115. <https://doi.org/10.1021/cr3001274>.
- (109) Uzun, M.; Sancak, E.; Patel, I.; Usta, I.; Akalın, M.; Yuksek, M. Mechanical Behaviour of Chicken Quills and Chicken Feather Fibres Reinforced Polymeric Composites. *Arch. Mater. Sci. Eng.* **2011**, *52* (2), 82–86.
- (110) Hong, C. K.; Wool, R. P. Development of a Bio-Based Composite Material from Soybean Oil and Keratin Fibers. *J. Appl. Polym. Sci.* **2005**, *95* (6), 1524–1538. <https://doi.org/10.1002/app.21044>.
- (111) Alagarsamy, S. V.; Sagayaraj, S. A. V.; Vignesh, S. Investigating the Mechanical Behaviour of Coconut Coir – Chicken Feather Reinforced Hybrid Composite. *Int. J. Sci. Eng. Technol. Res.* **2015**, *4* (12), 4215–4221.
- (112) Zhan, M.; Wool, R. P.; Xiao, J. Q. Electrical Properties of Chicken Feather Fiber Reinforced Epoxy Composites. *Compos. Part A Appl. Sci. Manuf.* **2011**, *42* (3), 229–233. <https://doi.org/10.1016/j.compositesa.2010.11.007>.
- (113) Senoz, E.; Stanzione, J. F.; Reno, K. H.; Wool, R. P.; Miller, M. E. N. Pyrolyzed Chicken Feather Fibers for Biobased Composite Reinforcement. *J. Appl. Polym. Sci.* **2013**, *128* (2), 983–989. <https://doi.org/10.1002/app.38163>.
- (114) Winandy, J. E.; Muehl, J. H.; Glaeser, J. A.; Schmidt, W. Chicken Feather Fiber as an Additive in MDF Composites. *J. Nat. Fibers* **2007**, *4* (1), 35–48. https://doi.org/10.1300/J395v04n01_04.
- (115) Filiciotto, L.; Balu, A. M.; Romero, A. A.; Rodríguez-Castellón, E.; Van der Waal, J. C.; Luque, R. Benign-by-Design Preparation of Humin-Based Iron Oxide Catalytic Nanocomposites. *Green Chem.* **2017**, *19* (18), 4423–4434. <https://doi.org/10.1039/C7GC01405H>.
- (116) Hosler, D. Prehistoric Polymers: Rubber Processing in Ancient Mesoamerica. *Science (80-.)*. **1999**, *284* (5422), 1988–1991. <https://doi.org/10.1126/science.284.5422.1988>.
- (117) Andrady, A. L.; Neal, M. A. Applications and Societal Benefits of Plastics. *Philos. Trans. R. Soc. B Biol. Sci.* **2009**, *364* (1526), 1977–1984. <https://doi.org/10.1098/rstb.2008.0304>.
- (118) Geyer, R.; Jambeck, J. R.; Law, K. L. Production, Use, and Fate of All Plastics Ever Made. *Sci. Adv.* **2017**, *3* (7), e1700782. <https://doi.org/10.1126/sciadv.1700782>.
- (119) Okunola A, A.; Kehinde I, O.; Oluwaseun, A.; Olufiropo E, A. Public and Environmental Health Effects of Plastic Wastes Disposal: A Review. *J. Toxicol. Risk Assess.* **2019**, *5* (2). <https://doi.org/10.23937/2572-4061.1510021>.
- (120) Kamm, B.; Gruber, P. R.; Kamm, M. *Biorefineries-Industrial Processes and Products. Status Quo and Future Directions*; WILEY-VCH Verlag GmbH & Co. KGaA: Weinheim, 2006; Vol. 1. <https://doi.org/10.1002/9783527619849.ch22>.
- (121) Julio, R.; Albet, J.; Vialle, C.; Vaca-Garcia, C.; Sablayrolles, C. Sustainable Design of Biorefinery Processes: Existing Practices and New Methodology. *Biofuels, Bioprod. Biorefining* **2017**, *11* (2), 373–395. <https://doi.org/10.1002/bbb.1749>.
- (122) Fernando, S.; Adhikari, S.; Chandrapal, C.; Murali, N. Biorefineries: Current Status, Challenges, and Future Direction. *Energy & Fuels* **2006**, *20* (4), 1727–1737. <https://doi.org/10.1021/ef060097w>.
- (123) Azapagic, A. Sustainability Considerations for Integrated Biorefineries. *Trends Biotechnol.*

- 2014, 32 (1), 1–4. <https://doi.org/10.1016/j.tibtech.2013.10.009>.
- (124) Menon, V.; Rao, M. Trends in Bioconversion of Lignocellulose: Biofuels, Platform Chemicals & Biorefinery Concept. *Prog. Energy Combust. Sci.* **2012**, 38 (4), 522–550. <https://doi.org/10.1016/j.pecs.2012.02.002>.
- (125) Agbor, V. B.; Cicek, N.; Sparling, R.; Berlin, A.; Levin, D. B. Biomass Pretreatment: Fundamentals toward Application. *Biotechnol. Adv.* **2011**, 29 (6), 675–685. <https://doi.org/10.1016/j.biotechadv.2011.05.005>.
- (126) Isikgor, F. H.; Becer, C. R. Lignocellulosic Biomass: A Sustainable Platform for the Production of Bio-Based Chemicals and Polymers. *Polym. Chem.* **2015**, 6 (25), 4497–4559. <https://doi.org/10.1039/c5py00263j>.
- (127) Taherzadeh, M.; Karimi, K. Pretreatment of Lignocellulosic Wastes to Improve Ethanol and Biogas Production: A Review. *Int. J. Mol. Sci.* **2008**, 9 (9), 1621–1651. <https://doi.org/10.3390/ijms9091621>.
- (128) Barakat, A.; de Vries, H.; Rouau, X. Dry Fractionation Process as an Important Step in Current and Future Lignocellulose Biorefineries: A Review. *Bioresour. Technol.* **2013**, 134, 362–373. <https://doi.org/10.1016/j.biortech.2013.01.169>.
- (129) Cherubini, F. The Biorefinery Concept: Using Biomass Instead of Oil for Producing Energy and Chemicals. *Energy Convers. Manag.* **2010**, 51 (7), 1412–1421. <https://doi.org/10.1016/j.enconman.2010.01.015>.
- (130) Patil, S. K. R.; Lund, C. R. F. Formation and Growth of Humins via Aldol Addition and Condensation during Acid-Catalyzed Conversion of 5-Hydroxymethylfurfural. *Energy and Fuels* **2011**, 25 (10), 4745–4755. <https://doi.org/10.1021/ef2010157>.
- (131) Patil, S. K. R.; Heltzel, J.; Lund, C. R. F. Comparison of Structural Features of Humins Formed Catalytically from Glucose, Fructose, and 5-Hydroxymethylfurfuraldehyde. *Energy Fuels* **2012**, 26, 5281–5293.
- (132) Signoretto, M.; Taghavi, S.; Ghedini, E.; Menegazzo, F. Catalytic Production of Levulinic Acid (LA) from Actual Biomass. *Molecules* **2019**, 24 (15), 2760. <https://doi.org/10.3390/molecules24152760>.
- (133) Van Zandvoort, I.; Wang, Y.; Rasrendra, C. B.; Van Eck, E. R. H.; Bruijninx, P. C. A.; Heeres, H. J.; Weckhuysen, B. M. Formation, Molecular Structure, and Morphology of Humins in Biomass Conversion: Influence of Feedstock and Processing Conditions. *ChemSusChem* **2013**, 6 (9), 1745–1758. <https://doi.org/10.1002/cssc.201300332>.
- (134) Hoang, T. M. C.; Lefferts, L.; Seshan, K. Valorization of Humin-Based Byproducts from Biomass Processing - A Route to Sustainable Hydrogen. *ChemSusChem* **2013**, 6 (9), 1651–1658. <https://doi.org/10.1002/cssc.201300446>.
- (135) Rasrendra, C. B.; Windt, M.; Wang, Y.; Adisasmito, S.; Makertihartha, I. G. B. N.; Van Eck, E. R. H.; Meier, D.; Heeres, H. J. Experimental Studies on the Pyrolysis of Humins from the Acid-Catalysed Dehydration of C6-Sugars. *J. Anal. Appl. Pyrolysis* **2013**, 104, 299–307. <https://doi.org/10.1016/j.jaap.2013.07.003>.
- (136) Constant, S.; Lancefield, C. S.; Weckhuysen, B. M.; Bruijninx, P. C. A. Quantification and Classification of Carbonyls in Industrial Humins and Lignins by ¹⁹F NMR. *ACS Sustain. Chem. Eng.* **2017**, 5 (1), 965–972. <https://doi.org/10.1021/acssuschemeng.6b02292>.
- (137) Shi, N.; Liu, Q.; Ju, R.; He, X.; Zhang, Y.; Tang, S.; Ma, L. Condensation of α -Carbonyl Aldehydes Leads to the Formation of Solid Humins during the Hydrothermal Degradation of Carbohydrates. *ACS Omega* **2019**, 4, 7330–7343. <https://doi.org/10.1021/acsomega.9b0050>.
- (138) Portillo Perez, G.; Mukherjee, A.; Dumont, M. J. Insights into HMF Catalysis. *J. Ind. Eng. Chem.* **2019**, 70, 1–34. <https://doi.org/10.1016/j.jiec.2018.10.002>.
- (139) Schweizer, A. Caramel and Humin. A Contribution to the Knowledge of the Decomposition Products of Sugars. *Recl. des Trav. Chim. des Pays-Bas* **2010**, 57 (4), 345–382. <https://doi.org/10.1002/recl.19380570402>.

- (140) A. Schweizer. The Composition of the Humins Produced by the Action of Sulphuric Acid on Some Organic Substances. *Recl. des Trav. Chim. des Pays-Bas* **1940**, 59 (8), 781–784. <https://doi.org/10.1002/recl.19400590814>.
- (141) Girisuta, B.; Janssen, L. P. B. M.; Heeres, H. J. A Kinetic Study on the Decomposition of 5-Hydroxymethylfurfural into Levulinic Acid. *Green Chem.* **2006**, 8 (8), 701–709. <https://doi.org/10.1039/b518176c>.
- (142) Mija, A.; Jong, E. De; Waal, J. C. Van der; Klink, G. P. M. Van. Humins-Containing Foam. WO 2017/074183 A1, 2017.
- (143) Mija, A.; Waal, J. C. Van der; Jong, E. De; Klink, G. P. M. Van. Process for the Modification Humins. WO 2018/062995 A1, 2018.
- (144) Tosi, P.; Van Klink, G. P. M.; Celzard, A.; Fierro, V.; Vincent, L.; De Jong, E.; Mija, A. Auto-Crosslinked Rigid Foams Derived from Biorefinery Byproducts. *ChemSusChem* **2018**, 11 (16), 2797–2809. <https://doi.org/10.1002/cssc.201800778>.
- (145) Kang, S.; Fu, J.; Deng, Z.; Jiang, S.; Zhong, G.; Xu, Y.; Guo, J.; Zhou, J. Valorization of Biomass Hydrolysis Waste: Activated Carbon from Humins as Exceptional Sorbent for Wastewater Treatment. *Sustainability* **2018**, 10 (6), 1795. <https://doi.org/10.3390/su10061795>.
- (146) Merle, J.; Birot, M.; Deleuze, H.; Mitterer, C.; Carré, H.; Bouhtoury, F. C. E. New Biobased Foams from Wood Byproducts. *Mater. Des.* **2016**, 91 (January 2016), 186–192. <https://doi.org/10.1016/j.matdes.2015.11.076>.
- (147) Hao, W.; Björnerbäck, F.; Trushkina, Y.; Oregui Bengoechea, M.; Salazar-Alvarez, G.; Barth, T.; Hedin, N. High-Performance Magnetic Activated Carbon from Solid Waste from Lignin Conversion Processes. 1. Their Use As Adsorbents for CO₂. *ACS Sustain. Chem. Eng.* **2017**, 5 (4), 3087–3095. <https://doi.org/10.1021/acssuschemeng.6b02795>.
- (148) Chernysheva, D. V.; Chus, Y. A.; Klushin, V. A.; Lastovina, T. A.; Pudova, L. S.; Smirnova, N. V.; Kravchenko, O. A.; Chernyshev, V. M.; Ananikov, V. P. Sustainable Utilization of Biomass Refinery Wastes for Accessing Activated Carbons and Supercapacitor Electrode Materials. *ChemSusChem* **2018**, 11 (20), 3599–3608. <https://doi.org/10.1002/cssc.201801757>.
- (149) Pin, J. M.; Guigo, N.; Mija, A.; Vincent, L.; Sbirrazzuoli, N.; Van Der Waal, J. C.; De Jong, E. Valorization of Biorefinery Side-Stream Products: Combination of Humins with Polyfurfuryl Alcohol for Composite Elaboration. *ACS Sustain. Chem. Eng.* **2014**, 2 (9), 2182–2190. <https://doi.org/10.1021/sc5003769>.
- (150) Kang, S.; Fu, J.; Zhang, G.; Zhang, W.; Yin, H.; Xu, Y. Synthesis of Humin-Phenol-Formaldehyde Adhesive. *Polymers (Basel)*. **2017**, 9 (12), 373. <https://doi.org/10.3390/polym9080373>.
- (151) Licsandru, E.; Mija, A. From Biorefinery By-Product to Bioresins. Thermosets Based on Humins and Epoxidized Linseed Oil. *Cellul. Chem. Technol.* **2019**, 53 (9–10), 963–969. <https://doi.org/10.35812/CelluloseChemTechnol.2019.53.94>.

Chapter 2

Cross-linked Polyfuran Networks With Elastomeric Behaviour Based On Humins Biorefinery By-products



This chapter is based on Roxana Dinu and Alice Mija, “*Cross-linked polyfuran networks with elastomeric behaviour based on Humins biorefinery by-products*”, *Green Chemistry*, 2019, 21, 6277-6289, doi: 10.1039/c9gc01813a (invited cover page).

Abstract

Biorefinery by-products have received much attention in the last few years. Humins are one of these candidates. Nevertheless, one common feature of humins, as a polyfuranic thermoset material, is their inherent brittleness which is a direct consequence of the network's structure. Auto-crosslinked humins networks exhibit only minor deformation and break very easily. Consequently, this behavior limits their use in many industrial applications. For this reason, we used in this work the copolymerization strategy, by combining humins with epoxide based aliphatic ethers, as a toughening approach. To gain a fundamental understanding of the humins based copolymers we thoroughly investigated their structure, behavior and properties by FT-IR, rheology, DSC, TGA, DMA and tensile tests. These investigations show one of the most important results: the humins copolymers have a ductile and elastomeric character. The tensile strain at break of the copolymers reaches $\approx 60\%$ which is a significant advantage in terms of applications of humins as structural materials. To our knowledge, these are the first data reported on the synthesis of elastomeric humins based copolymers paving the way for the utilization of these emergent materials in industrial applications.

2.1. Introduction

In the last few years, particular attention has been paid to the use of renewable resources in order to replace fossil derivatives, which increasingly affect the environment. A continuous challenge for the researchers is to find effective ways of conversion of abundant or cheap bioresources into fuels, chemicals or materials. Lignocellulosic biomass is a renewable resource composed mainly of three principal constituents *e.g.* lignin, cellulose, and hemicellulose, each of them having different compositions and reactivities. Lignin is an amorphous, branched polymer of aromatic alcohols while cellulose and hemicelluloses are polysaccharides consisting of hexoses and pentoses.¹ Generally, 35–50% from lignocellulosic biomass is represented by cellulose, 20–35% by hemicellulose, and 10–25% by lignins and the remaining fraction is composed of oils, ash and proteins.²

Under acid-catalyzed hydrolysis, the cellulosic biomass can be converted into various platform molecules such as 5-hydroxymethylfurfural (HMF), levulinic acid or formic acid in biorefineries but the processing is sometimes accompanied by the formation of a dark-colored by-product.^{3,4} It has been revealed that this by-product, called humins, is formed more rapidly from fructose than from glucose.⁵ The formation of this by-product has been reported in almost all the papers linked to the synthesis of levulinic acid, HMF or furfural. The yield of humins depends much on process parameters (catalysts, temperature, duration, *etc.*).⁶ Although many efforts have been focused on reducing the amount of this side-product from biorefineries, the yield of humins still remains high, between 14 and 30 wt.%.^{7,8} Considering these factors, the valorization of humins is the optimal method for improving the economic value of a biorefinery chain, but above all, it is the best way to improve the environmental impact of the entire technological process. Another environmentally friendly process in which this side-product is formed, is represented by the hydrothermal conversion of different biomass and derivatives.^{9–11}

Since the 90's, the production and the composition of the caramelization of sugars have been a subject of great interest to the scientists.^{12–15} Caramel is produced by heating sucrose and, from the compositional point of view, appears as a mixture of humins and iso-saccharosan in various proportions.^{5,16,17} Despite numerous investigations regarding caramel formation, the compositions of caramel and humins are not yet fully understood.⁵ Following the investigations, humins have been found to consist of about 50–65% C, 29–46% O and 4–5.5% H and contain in their structure aromatic rings, mostly of them furanics.^{5–7} The structure of humins is known to depend on the reaction time, temperature, feedstock and solvent (water and alcohol).^{10,18–20}

Van Zandvoort *et al.*¹⁸ have analyzed in detail the formation, morphology and molecular structure of laboratory made humins samples, prepared from different feedstocks using various processing parameters (Figure 1). Also, Hoang *et al.*^{21,22} have investigated the chemical structure of humins prepared in laboratory by dehydration of D-glucose in order to produce levulinic acid. Based on these studies, the authors revealed that humins present a variable furanic structure formed by a dehydration pathway and contain alcohol, acid, ketone, and aldehyde functional groups. In their study, Constant *et al.*²³ have quantified and classified the ketone and aldehyde carbonyl functional groups contained in industrial humins and lignins by ¹⁹F NMR. Following these investigations, they found that the industrial humins contains 6.6 wt.% carbonyl functions. The abundance of such functional groups provides opportunities for the use of these humins by-products in various domains of applications.

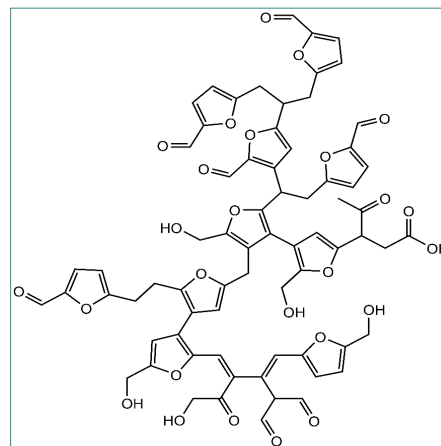


Figure 1. Proposed molecular structure of a glucose-derived humins fragment¹⁸

Recently, researchers started to explore possible routes to valorize this by-product derived from biomass conversion processes in order to turn them into high-value products. Kang *et al.*²⁴ have completely degraded humins by alkaline-catalytic hydrothermal treatment followed by wet oxidation. By this technology, the authors managed to convert humins into acetic acid obtaining a yield of 25.6% and a purity of 46.2%. Hoang *et al.*⁶ studied the gasification and steam reforming of the humins at 750 °C over a variety of alkali- and alkaline-earth based catalysts in order to obtain syngas (a mixture of hydrogen and CO_x). The authors found that the Na₂CO₃ was the most effective catalyst enabling complete conversion of humins (81% of H₂ yield). The liquefaction of humins has been reported by Rasrendra *et al.*⁸ through fast pyrolysis resulting in low molecular furanics such as furfural and 2,5 dimethylfuran.

The potential of humins to generate materials has also been tested. Pin *et al.*²⁵ combined the furfuryl alcohol (FA) with humins to produce a fully bio-based furanic resin tested in the development of thermoset furanic composites where cellulose fibers act as reinforcement. An original way to valorize the humins was their transformation into polymeric foams with potential applications in substrates for plant growth, absorbents for wastewater treatment, insulation materials, support for solid catalysts, *etc.*^{26–30} In our previous studies^{26,27} we succeeded in developing macroporous foam materials based on an auto-crosslinking reaction of the industrial humins. By adjusting the parameters of the humins-foam preparation process, we achieved a good control of the morphology and cell dimensions. The obtained foams show

open and/or closed cells with cell diameters between 0.2 and 3.5 mm making possible the use of these materials in different application sectors. Humins were used by Kang *et al.*²⁸ in the production of activated carbons as sorbent for wastewater treatment. These activated carbons were developed through KOH activation in a temperature range of 500–900 °C to investigate the optimal adsorption of methylene blue (MB) and phenol in aqueous solutions. The authors obtained very good results; the methylene blue adsorption capacity was about 40% while the phenol adsorption was around 39.7%. These results show the capacity of humins to produce porous materials with potential use as membranes for water purification, for the building sector or for use in green houses.

Following our previous work, the objective of this study is not only the valorization of industrial humins by-products obtained in biorefineries but also the development of emergent materials for different application sectors using non-toxic, low cost and environmentally friendly co-monomers. To do this, we had to decrease the inherent brittleness of the reticulated humins, as it limits their use in many industrial applications. Auto-crosslinked humins networks allow only minor deformation and break very easily. To toughen brittle polyfuranic humins resins the strategy used in this work was chemical modifications of their backbone structure. The idea was to include more flexible moieties by copolymerizing humins with more flexible chains such as aliphatic diglycidyl ethers. Moreover, this pathway will possibly also result in lowering the crosslinking density intrinsic to humins. To produce a toughened network there are some requirements. Firstly, good compatibility between the humins matrix and the diglycidyls must exist, meaning the two components need to be totally miscible prior to curing. Subsequently, the humins should react with the diglycidyls in order to form chemical linkages between the modifier and the matrix.

To chemically modify the humins backbone we chose to copolymerize it with two aliphatic diglycidyl ethers: the polyethylene glycol diglycidyl ether (PEGDE) and the glycerol-1,3-diglycidyl ether (GDE). Polyethylene glycol (PEG) is a synthetic polyether which can be easily synthesized with a wide range of molecular weights. This polymer is soluble in water and also in many organic solvents.³¹ PEG has been found to be nontoxic and is approved by the U.S. Food and Drug Administration; therefore it is used in many different applications such as biomedical research, drug deliveries, tissue engineering scaffolds, surface functionalization, etc.^{31–34} For example, Kono³⁵ crosslinked a carboxymethyl cellulose sodium salt with PEGDE obtaining new hydrogels which could be used as carriers of drug delivery systems for protein-based drugs.

Glycerol, a by-product obtained by biodiesel refining, can be used as a monomer in the synthesis of polymers and materials in its original form or after chemical modifications.³⁶ Zhao *et al.*³⁷ developed a biodegradable microgel system based on glycerol-1,3-diglycidyl ether

crosslinked with oxidized potato starch for controlled uptake and release of proteins. In another study, ur Rehman *et al.*³⁸ reported the preparation of a new microgel from tris(2-aminoethyl)amine and glycerol diglycidyl ether by using L- α lecithin as a surfactant and gasoline as the organic phase. The prepared microgels were found to be biocompatible against L929 Fibroblast cells, showing antibacterial characteristics against common bacteria and possessing great potential in the biomedical fields.

In consequence, the two chosen chemical modifiers for the humins structure, the PEGDE and GDE, are non-toxic, have biomedical applications, and have good potential to produce materials by crosslinking in copolymerization with targeted structures. Together with their low viscosity and relatively low molar mass, they were ideal candidates for humins modification. The reactivity study of these novel formulations was realized by differential scanning calorimetry (DSC), chemo-rheology and *in situ* Fourier Transform Infrared Spectroscopy (FTIR). The physical and thermo-mechanical properties of the obtained thermoset materials were analyzed by thermogravimetric analysis (TGA), dynamic mechanical analysis (DMA), Shore hardness test and tensile tests.

2.2. Results and Discussion

A first series of studies were carried out to determine the optimal formulations for the development of humins based thermosets by its copolymerization with the PEGDE and GDE in the presence of BDMA as the initiator. The formulations were analyzed using differential scanning calorimetry (DSC), rheology analysis and FTIR to determine the temperature range and the reactivity of the mixtures. We studied at the beginning eight formulations by increasing from 20 to 50% the weight ratio of each comonomer in the humins mix in order to determine the optimum amounts of compounds required for the development of each system humins/PEGDE and humins/GDE. Thereafter, we complexified the system by combining the humins with both GDE and PEGDE. Again, these formulations were analyzed, and the optimal formulations retained. So, in total, we decided to select three formulations: humins/PEGDE, humins/GDE, and humins/PEGDE/GDE.

2.2.1. DSC studies of reactivity

Humins are materials with peculiar compositions and reactivities. To gain insights into their reactivity with the selected diglycidyl structures, dynamic DSC was conducted during thermally induced crosslinking *via* copolymerization. To select the optimum ratios of humins/PEGDE and humins/GDE copolymerization mixtures the reactivity between the humins and the comonomers without an initiator was analysed first by DSC. The collected

results are gathered in Figure 2. As can be seen from the DSC analysis, the curing mixtures with low PEGDE content (20% and 30 wt.%) have a complex and wide temperature interval of reactivity, ranging between 115 °C and 260 °C. On increasing the PEGDE content (40% and 50 wt.%), an evident double reaction can be observed, with the first exotherm taking place between 120 °C and 180 °C followed by a second one between 190 °C and 250 °C.

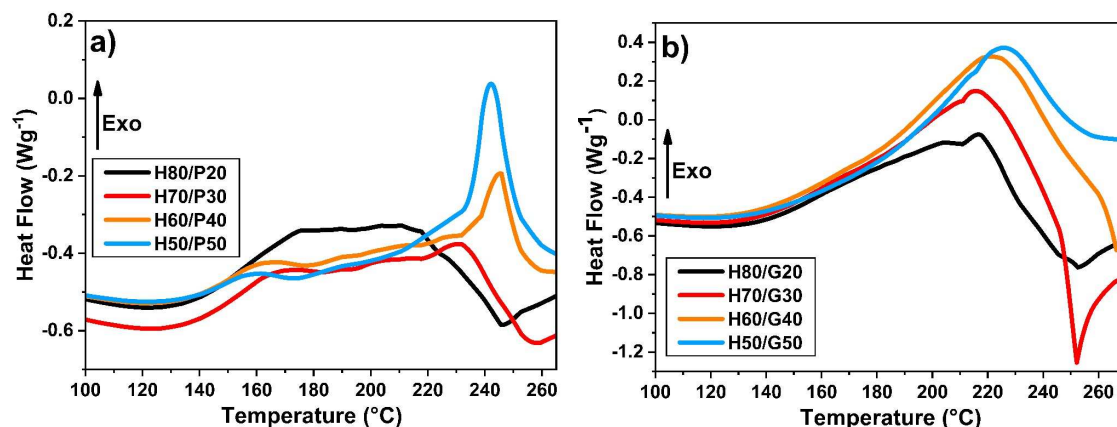


Figure 2. DSC analysis of curing mixtures without an initiator at 10 °C min⁻¹ between (a) humins and different amounts of PEGDE; and (b) humins and different amounts of GDE

With the increase in the amount of PEGDE, a decrease in the enthalpy of reaction can be observed which could be a sign that the PEGDE interrupts the auto-crosslinking of humins and that the copolymerization needs the activation by an initiator. In case of humins/GDE mixtures, the double reaction peak is no longer observed, there being present a single, long temperature range, reaction.

Regardless of the amount of GDE, the maximum reactivity of the mixtures is observed around a temperature of 220 °C, the temperature range of reactivity ranging between 110 °C and 260 °C. With the increase in amount of GDE, the total heat release of reaction rises from $\approx 240 \text{ J g}^{-1}$ to $\approx 300 \text{ J g}^{-1}$, except for the mixture with 50% comonomer, where the enthalpy of the reaction decreased considerably.

Following this study, these formulations were developed and cured in an oven to analyze if the amounts of compounds influence the physicochemical and mechanical properties of the materials. Practically, the thermosets obtained with less than 20 wt.% PEGDE or GDE were rigid, brittle and thermally unstable, starting to foam at 130 °C, while the materials obtained with more than 30 wt.% PEGDE or GDE were elastic and thermally stable when heated for curing at 150 °C. Then, the resins with 50 wt.% comonomers ratios were not selected because the aim of the study is valorization of the industrial humins by-product which should be the major part of the formulations composition. Following these rationales, the

optimal amount of comonomers was determined to 40 wt.%. Therefore, three formulations were selected: HP40B5, HG40B5 and the combination HP20G20B5.

To analyze properly the copolymerization reactions between humins and PGDE or GDE, the reactivity of selected formulations in the presence of BDMA (5 wt.%) as the initiator was studied. Normalized dynamic DSC thermograms of humins-based resins polymerizations are shown in Figure 3 and data summarized in Table 1.

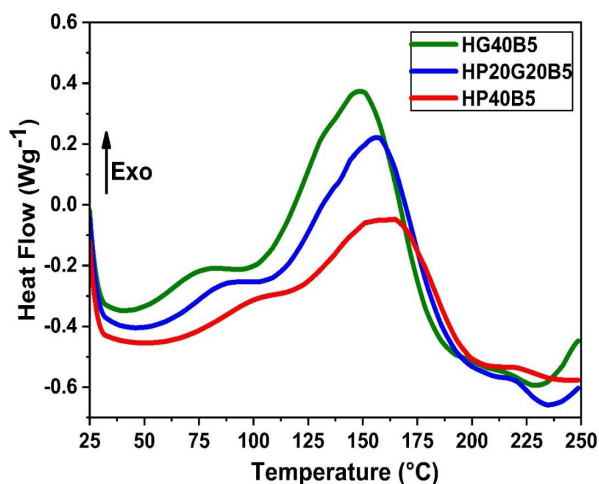


Figure 3. Comparison between humins copolymerization reactions by dynamic DSC at $10\text{ }^{\circ}\text{C min}^{-1}$

When BDMA is used as initiator a strong decrease in the starting reactions temperature occurs, whatever the type of the diglycidyl type comonomer. If the systems without an initiator start to react at temperatures superior to $\approx 100\text{ }^{\circ}\text{C}$, the presence of BDMA allow reactions to start at around $40\text{ }^{\circ}\text{C}$. Then, the reactivities remain complex, with overlapped thermal events translating the multiple reactions that could occur between the functional groups present in humins and the diglycidyls. The three thermograms follow the same trend, with a first small exotherm with a peak at $\approx 80\text{--}100\text{ }^{\circ}\text{C}$ followed by the main exotherm of the reaction with the maximum at $150\text{--}160\text{ }^{\circ}\text{C}$. At around $230\text{ }^{\circ}\text{C}$ the DSC heat flows return to a quasi-linear response which represents the completion of curing.

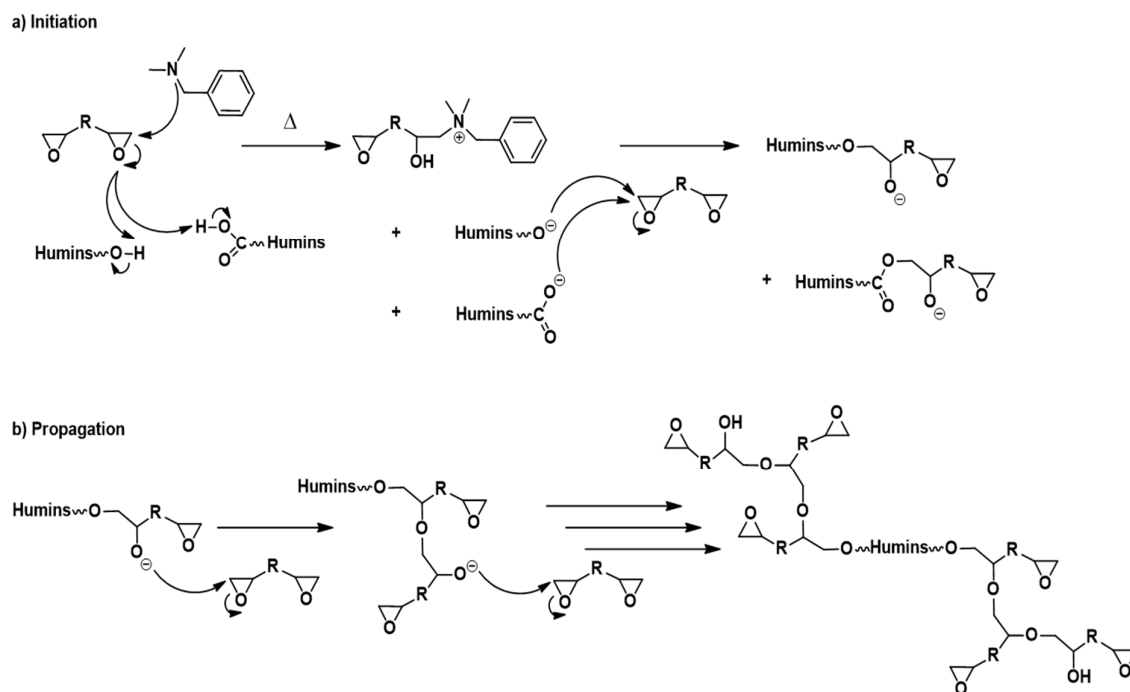
The areas under the exothermal peaks were integrated to obtain the heat of copolymerization. The greatest reaction enthalpy from these three formulations is given by the mixture in which it has been used GDE and it is around 333 J g^{-1} . Secondary DSC scans to $250\text{ }^{\circ}\text{C}$ reveal that no residual reactions occur.

Table 1. DSC analysis of humins/PEGDE, humins/GDE and humins/(PEGDE + GDE) copolymerization initiated by BDMA

	HP40B5	HP20G20B5	HG40B5
$T_{peak}\text{ (}^{\circ}\text{C)}$	164 ± 1	157 ± 1	149 ± 1
(reaction interval)	(42–215)	(40–230)	(38–228)
$\Delta_r H\text{ (J g}^{-1}\text{)}$	212 ± 4	319 ± 4	333 ± 4

As presented in Scheme 1 the copolymerization reactions of the humins with the diglycidyls could occur *via* an anionic mechanism. The first step is the initiation reaction with

the participation of the tertiary amine to the ring opening of epoxy groups and formation of the zwitterions and then of the alkoxides which are the active species in anionic propagation reactions. We can suppose that this reaction of initiation appears in the three DSC thermograms as the small exotherms in the 80–100 °C temperature range. Then, once the alkoxides are formed, the propagation reactions occur faster, with a high enthalpy of reaction. The propagation reactions of humins-diglycidyls copolymerization are the main exothermic phenomena appearing in the DSC thermograms (Figure 3) in the ≈ 100 –200 °C interval. By comparing the reactions of humins with PEGDE and GDE, it is found that the copolymerization with the glycerol diglycidyl ether is more exothermic, with a higher reaction rate as shown by the higher slope of the peak. This higher reactivity could be explained by the presence of -OH in the GDE structure. The hydroxyl group of GDE could have a dual contribution: (i) *via* the interaction with the -COOH functions of the humins, and/or (ii) *via* the formation of ternary systems in the initiation steps. GDE's contribution also appears in terms of enthalpy and reaction rate in the HP20G20B5 copolymerization system.



Scheme 1. Summary of possible interactions among humins, aliphatic diepoxides and BDMA

2.2.2. Evolution of the structure during copolymerization reactions

2.2.2.1. FT-IR investigations

To highlight the copolymerization of humins with the diglycidyl comonomers, FT-IR spectra of the initial components of formulations, of their mixture at $t = 0$ and of the cured systems were compared (Figure 4). The industrial humins used in this study present similar IR spectra to those reported in the literature.^{18,22,25,39} The significant assignments for all the initial components of the mixtures are presented in the Table 2. In the humins spectra we can observe an important peak at 1666 cm^{-1} which can be assigned to the C=O stretching vibrations of the aldehyde groups of HMF and MMF, while the C=O asymmetric stretching vibrations are presented at 1702 cm^{-1} . FT-IR absorption signals that can be ascribed to the substituted furan rings are at 1617 cm^{-1} a C=C stretching vibration, at 1018 cm^{-1} a C-O stretching vibrations or furan ring deformation, and also the signals from C-H out-of-plane deformation vibrations at 804 cm^{-1} , 768 cm^{-1} and 756 cm^{-1} . In the case of PEGDE and GDE spectra, the most important signals are CH₂-O-CH₂ asymmetric stretching vibrations of the ether groups at 1092 cm^{-1} for PEGDE and at 1089 cm^{-1} for GDE, and also the asymmetric stretching vibrations for the epoxy ring which appear at 994 , 946 , 910 and 840 cm^{-1} for PEGDE and at 984 , 906 and 837 cm^{-1} for GDE. After analyzing the spectra of precursors, the three crosslinked resins were examined.

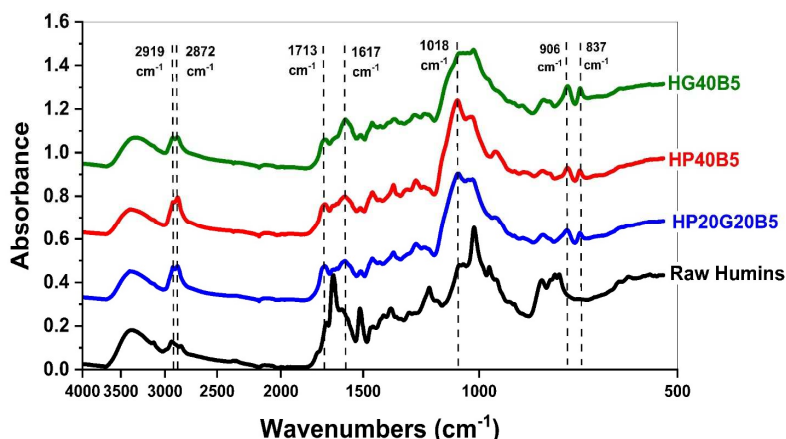


Figure 4. FT-IR spectra of cured humins-based resins

For example, in the HG40B5 resin case we can observe that the peaks corresponding to -OH of humins and -OH present in the GDE structure are still present in the thermoset, meaning that the main reactions are not the etherification through epoxy ring additions to these groups (Figure ESI2). Then at 2919 and 2872 cm^{-1} a well-defined doublet corresponding to the sp^3 C-H stretching could indicate that during the copolymerization the alkyl connections were formed insight the network. The C=O asymmetric stretching vibration

at 1702 cm^{-1} in the humins spectrum is shifted slightly to the left (1713 cm^{-1}) and the shape is wider in the thermoset spectrum. This peak is not observed for GDE. The C=C stretching peak for the disubstituted furans is no longer visible in the resin spectrum, and the peak of the polysubstituted furans shifts from 1517 cm^{-1} to 1596 cm^{-1} , this being larger and lower in intensity. The C-O-C bonding of the humins are present as a multiplet with a maximum at 1018 cm^{-1} , and in the case of GDE there is an intense and well-defined peak at 1090 cm^{-1} . In the resin spectrum, the peak is located at 1020 cm^{-1} , being larger compared to those of the other two compounds, and its absorbance is lower.

The disappearance of the peak of oxirane ring stretching which absorbs in GDE at 980–840 cm^{-1} confirms the consumption of epoxy functions during humins/GDE copolymerization (Table 2).

Table 2. Assignment of bands in FT-IR spectra of the initial components of humins systems of copolymerization

Sample	Wavenumber (cm^{-1})	Assignments	Sample	Wavenumber (cm^{-1})	Assignments
Humins	3369	O–H stretching	GDE	3482	O–H stretching
	2930, 2837	Alkyl C–H stretching		3000, 2872	C–H stretching
	1702	C=O stretching		1457, 1432	CH ₂ δ-deformation vibration, coincides with CH ₃ δ asymmetric
	1666	C=O stretching in furan		1339	O–H δ-deformation, in plane
	1617, 1517	C=C stretching		1253	C–O stretching
	1396, 1360	O–H δ-deformation, in plane		1089	CH ₂ –O–CH ₂ asymmetric stretching (ether group)
	1277, 1190, 1058, 1018	C–O stretching C–O stretching in furan		984, 906, 837	asymmetric stretching vibration for epoxy ring
	965	=C–H δ deformation		755, 702	CH ₂ γ-skeletal
804, 768, 756	C–H out-of-plane deformation				
PEGDE			BDMA	3086, 3063, 3027, 2973, 2941, 2854, 2814, 2763	C–H stretching
	2865	C–H stretching vibration		1601	C=C stretching vibration (benzene ring)
	1456	CH ₂ δ-deformation, coincides with CH ₃ δ asymmetric		1495, 1452	CH ₂ δ -deformation, coincides with CH ₃ δ asymmetric
	1349, 1295, 1251	C–O stretching		1363, 1317	CH ₃ δ-symmetric deformation (from-N(CH ₃) ₂)
	1092	CH ₂ -O-CH ₂ asymmetric stretching (ether group)		1259, 1174, 1146, 1097, 1075, 1025	C–N stretching
	994, 946, 910, 840	asymmetric stretching for epoxy ring		975	=C–H deformation
758	CH ₂ γ-skeletal	908, 850, 734, 696, 608	=C–H out-of-plane deformation (benzene ring)		

2.2.2.2. Rheometry analysis

To study the copolymerization reactions of viscoelastic liquids such as humins-based resins, a parallel plate geometry was used, and the evolutions of G' , G'' moduli and viscosity were recorded (Figure 5).

According with the rheology analyses it can be observed that the systems start to react, when heated at $0.2\text{ }^{\circ}\text{C min}^{-1}$, in the interval $65\text{--}75\text{ }^{\circ}\text{C}$ depending on the composition. The onset of reaction for the three formulations takes place at different temperatures, decreasing from $75\text{ }^{\circ}\text{C}$ for the formulation with PEGDE till $65\text{ }^{\circ}\text{C}$ for the system with humins and GDE. These results are in good agreement with the DSC analyses results (Figure 3) which show a higher reactivity for the system with GDE. The hardening of resin is given by the gel point of the system, taken as crossover between G' and G'' . For the resin formulation composed of humins and PEGDE the gelation process takes place at around $98\text{ }^{\circ}\text{C}$, while for the humins/GDE resin the gelling point is at around $86\text{ }^{\circ}\text{C}$. It can also be seen that the viscosity at $25\text{ }^{\circ}\text{C}$ of the formulation which contains PEGDE is low, around $\approx 0.35\text{ Pa s}$, around ten times lower compared with the viscosity of the formulation with GDE with an approximate value of 2.5 Pa s .

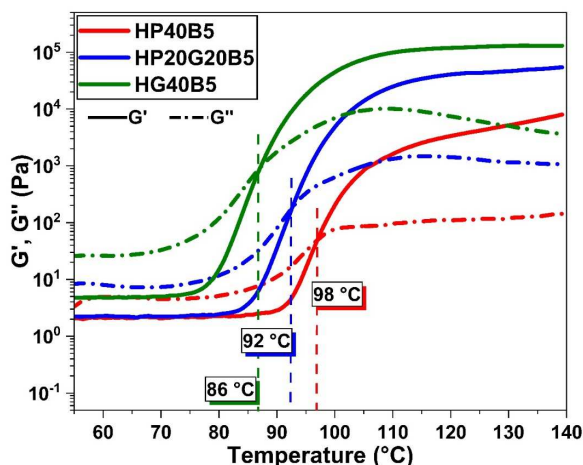


Figure 5. Rheology study of the humins-based systems for copolymerization. Evolution of moduli and viscosity during heating at $50\text{--}200\text{ }^{\circ}\text{C}$ at $0.2\text{ }^{\circ}\text{C min}^{-1}$. Comparison between formulations.

2.2.3. Physico-chemical characterization of humins-based copolymers

2.2.3.1. Glass and sub-glass transitions

Dynamic mechanical analysis (DMA) was used to determine the evolution of the viscoelastic properties of the prepared humins/diglycidyl thermosets. Furthermore, the copolymer molecular motions which depend on the time-temperature scale were also studied by DMA. These polymer's chains motions have been classified according to their nature in α , β and γ transitions. At low temperature (short time), the so-called secondary relaxations are related to local motions such as rotation of lateral groups (γ relaxation) or motions of the main chain segment (β relaxation). At higher temperature (*i.e.* longer time), the so-called α relaxation relates to cooperative motions of main chains.⁴⁰ The damping factor and the different transition temperatures of the materials were evaluated according to ASTM 1-0003 and ASTM D7028-07.⁴¹

The DMA results obtained over the interval temperature range -150 to 150 °C are given in Figure 6 and the main parameters are listed in Table 3. The values of maximum of $\tan \delta$ are assigned to the α relaxation (T_α) phenomenon related to cooperative chain motions and associated with the macroscopic T_g . Figure 6 shows the evolution of the storage and loss moduli of the three humins-based resins as a function of temperature.

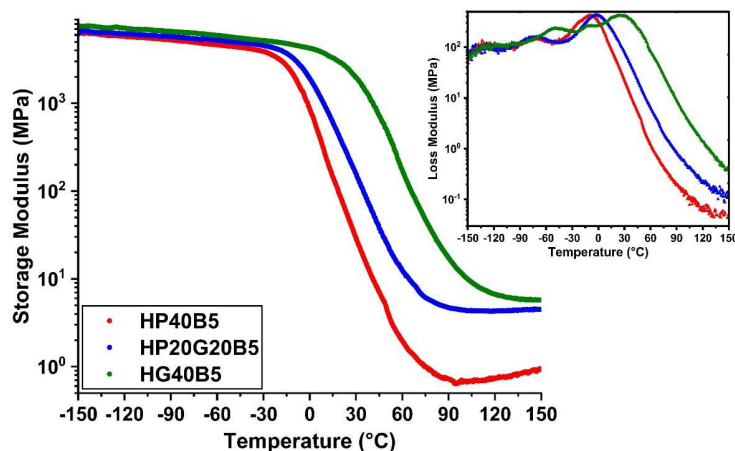


Figure 6. Evolution of the storage modulus and loss modulus vs. temperature for humins-based copolymers

At temperatures below the glass transition, in the glassy region of the materials, high storage modulus values were measured, of about 5400–6700 MPa. We can notice that the humins/PEGDE copolymer presents the smallest value of the E' modulus (≈ 5500 MPa), emphasizing the contribution of aliphatic flexible chains insight the copolymer network, giving an elastic resin. A higher value of modulus (≈ 6800 MPa) was measured in the humins/GDE copolymer showing a stiffer network, which was initially intended to achieve by the choice of a shorter aliphatic ether chain. Obviously, the copolymer with mixed glycidyls has an intermediate behavior.

With the increase of temperature, in the transition zone, we can observe a substantial decrease in the E' values. A clear shift of the E' drop between the three resins can be observed. The temperature at which E' of the flexible humins-based resin starts to decrease is about -26 °C while for the GDE based resin this drop starts at around 10 °C.

The domain above the glass transition has a width dependent on the molecular weight of the chains between entanglements or crosslinks.^{42,43} By increasing the molecular weight of chain segments the transition to the rubbery plateau appears at higher temperatures. In the prepared humins/diglycidyls copolymers the zone appears in the order HP40B5 < HP20G20B5 < HG40B5.

In the rubbery plateau, the storage modulus value is directly correlated with the crosslinking density of the networks (Flory's theory).⁴⁴ The bigger the crosslinking density of the polymer, the smaller the drop of the storage modulus value.^{45,46} The crosslinking densities for the three humins-based copolymers were calculated and given in Table 3.

Table 3. Mechanical properties of the humins-based resins according to the DMA analysis

System	Tan δ			Storage Modulus, E' (MPa)			U (mmol·cm ⁻³)
	Peak (°C)	Interval of Tan δ (°C)	Peak height	In glassy plateau (at -100 °C)	At Tan δ	In rubbery plateau (at 150 °C)	
HP40B5	30	100	0.76	5473	27	1	0.07
HP20G20B5	49	123	0.5	5916	25	4.5	0.43
HG40B5	71	142	0.4	6777	96	6.6	0.56

Moreover, the α , β and γ transitions of copolymers were also investigated by DMA. Figure 7 shows the evolution of tan δ for the three humins based copolymers networks. In our previous work²⁷ we have shown by dynamic DSC that the crude humins have a T_g at -15 °C, while humins auto-crosslinked at 250 °C have a T_g around 66 °C. Compared with the humins thermoset we can observe that the copolymerization with tailored diglycidyl aliphatic ethers allowed the tailoring of the mechanical properties. The shorter aliphatic ether chains from GDE gave a more rigid network, with a $T_\alpha \approx 71$ °C and a less ample intensity of tan δ peak. In contrast, by increasing the length of the aliphatic ether chains, copolymers with PEGDE, the T_α decreases to ≈ 30 °C. The copolymer prepared with the combination of diglycidyls (PEGDE + GDE) and humins has an intermediate trend, with a $T_\alpha \approx 49$ °C and a peak intensity more determined by the GDE contribution.

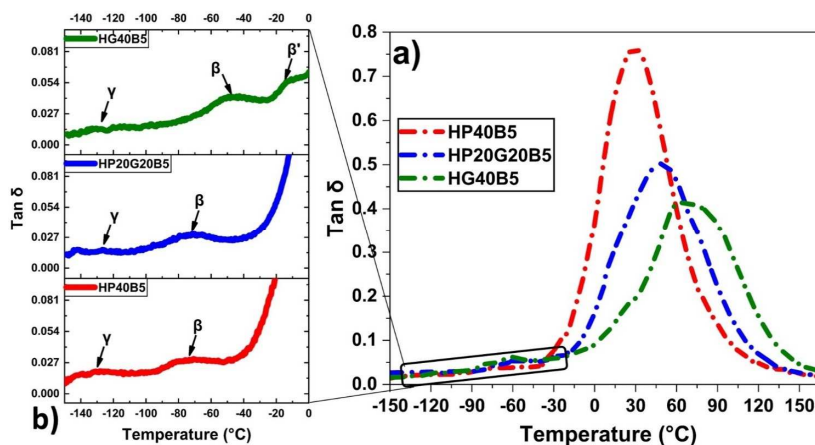


Figure 7. Evolution of relaxation processes with temperature on the humins-based copolymers: a) tan δ ; and b) β and γ transitions

Interestingly, all the three copolymer networks have similar range of the α relaxation peaks which are very large (between 100 and 140 °C) indicating a large distribution of relaxation times, characteristic of long polymeric chains. The amplitude of $\tan \delta$ provides information on the crosslinking density of the materials. For the HG40B5 resin, the small amplitude of the $\tan \delta$ peak indicates a low damping capacity of the material and consequently indicates that HG40B5 is a less elastic thermoset. This observation is in accord with the fact that the HG40B5 resin present the highest crosslinking density. In contrast, HP40B5 shows a relaxation at lower temperature, because of a much more flexible network due to the PEGDE aliphatic ether contribution. The corresponding $\tan \delta$ peak exhibits an intensity that indicates higher damping capacity through energy dissipation, and consequently a flexible network, in good accord with its low value of crosslinking density. As illustrated in Figure 7b, all the three copolymers present a small γ relaxation at around $T_\gamma \approx -130$ °C which could be associated with the rotation of hydroxyl or other functional groups from humins or from diglycidyls. Then, at ≈ -73 °C for HP40B5 and at ≈ -71 °C for HP20G20B5 occur the beta relaxations corresponding to local motions of copolymers. For the HG40B5 system two beta transitions emerge at $T_{\beta} \approx -47$ °C and $T_{\beta'} \approx -12$ °C.

The free moving dangling of segments chains present in the network after crosslinking and the local breathing of furanic entities could be the origin and could explain these relaxations.⁴⁷ The glass transition phenomenon was also studied with the help of the DSC. The T_g of cured materials were analyzed using 2 heating/cooling cycles at temperature range of -50 to 220 °C and 10 °C min⁻¹ heating rate.

The obtained results (Figure ESI4) corroborate very well with those measured by DMA (T_{g-loss}) and are summarized in Table 4. In perfect accord with previously reported DMA results, the DSC results indicate the difference between the three humins based copolymers in terms of T_g . Accordingly, the presence of PEGDE in the copolymer network has a strong effect on its thermomechanical properties. The copolymer with a higher content on PEGDE – HP40B5 – has negative T_g values ≈ -10 to -8 °C.

Its combination with a shorter aliphatic ether (GDE) gives a less elastic material, with a higher T_g at around 10°C, $T_g \approx -2$ to -1 °C. In contrast, the resin with GDE was considered a more rigid material, having a T_g of ≈ 27 °C. These results were corroborated with the hardness test results where the hardness of the materials follow the same trend as the T_g values. Using the Shore hardness tests, the resistance of the humins-based resins was measured at the penetration of a spring-loaded needle-like indenter. Hardness of hard elastomers and most polymer materials such as thermoplastics and thermosets is measured with a Shore D scale. The Shore hardness test of the three copolymers revealed values from 44SD to 72SD.

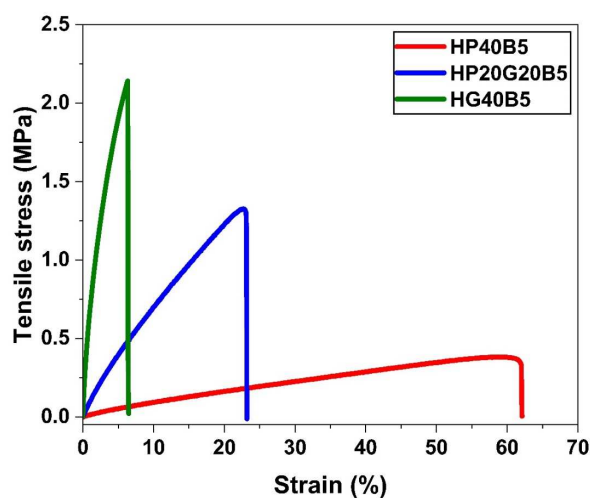
Table 4. Comparison of glass transition temperatures (T_g) of materials by DSC and DMA; and Shore hardness values

	HP40B5	HP20G20B5	HG40B5
T_g from DSC / °C	- 8	1	27
T_{g-loss} / °C (DMA)	- 10	- 2	26
$T_{g-onset}$ / °C (DMA)	- 11	- 4	27
Shore hardness / SD	44	59	72

According to the Shore hardness scale, the first formulation corresponds to a medium hard material which can be compared with shoe heel, door seal, or automotive tire tread, while the hardness of the other two resins can be compared with ebonite rubber, solid truck tires, hard wheels of roller skates and skateboard, computer casing, *etc.*

2.2.3.2. Tensile properties

With the help of tensile tests measurements on the three humins-based copolymers we analyzed their mechanical properties as Young's modulus and elongation at break. In particular, the tensile strength, Young's modulus, and yield stress are of primary importance for technical applications. The Young's modulus indicates the stiffness of materials and is defined by the relationship between stress and strain in a material in the linear elasticity regime of a uniaxial deformation. Figure

**Figure 8.** Tensile profiles for the three humins-based resins

8 shows the tensile tests results with stress-strain curves of the three humins based copolymers investigated in this work. We can notice that the combination of humins–diglycidyls gave copolymers with different mechanical responses which vary coherently with the values obtained by DMA, DSC and hardness tests. A significant increase in the maximum strength of the resins with the GDE content can be noticed. In agreement with the DMA results, the HP40B5 copolymer presents low T_g and high ductility, the tensile strength for this resin being around 0.4 MPa, while for the rigid copolymer (HG40B5) the strength reaches around 2.2

MPa. The elastic character of the HP40B5 resin is also shown by its elongation at break, the maximum strain being at around 60%.

As the HG40B5 resin matrix is crosslinked more densely, its capability to undergo plastic deformation is reduced. The HG40B5 resin presents a low elongation at break ($\approx 7\%$) which means that this resin is more rigid and brittle than the HP40B5 resin (Table 5). Comparing with the commercial resins it appears that the HP40B5 resin could be included in the category of elastomers having a tensile strength value close to that of butyl rubber (0.001–0.002 GPa), or of silicone elastomers (0.005–0.2 GPa).⁴⁸

Table 5. Tensile properties for the humins-based resins

	Young's Modulus (MPa)	Tensile Stress (MPa)	Strain (%)
HP40B5	1.01 ± 0.08	0.38 ± 0.12	62.4 ± 6.18
HP20G20B5	8.29 ± 0.61	1.33 ± 0.19	23.2 ± 6.76
HG40B5	106.1 ± 39	2.14 ± 0.55	6.4 ± 5.23

2.2.3.3. Thermal stability of the networks (TGA)

Thermogravimetric analyses were carried out to determine the thermal stability of fully cured materials under inert (N₂) or oxidant (Air) flows. TGA thermograms of the studied humins-based copolymers are reported in Figure 9. The temperature of degradation was considered at 5% weight loss, $T_{5\%}$. Under air, the thermal degradation is quite complex, with at least three stages of degradation which starts above the temperatures of 200 °C (Table 6).

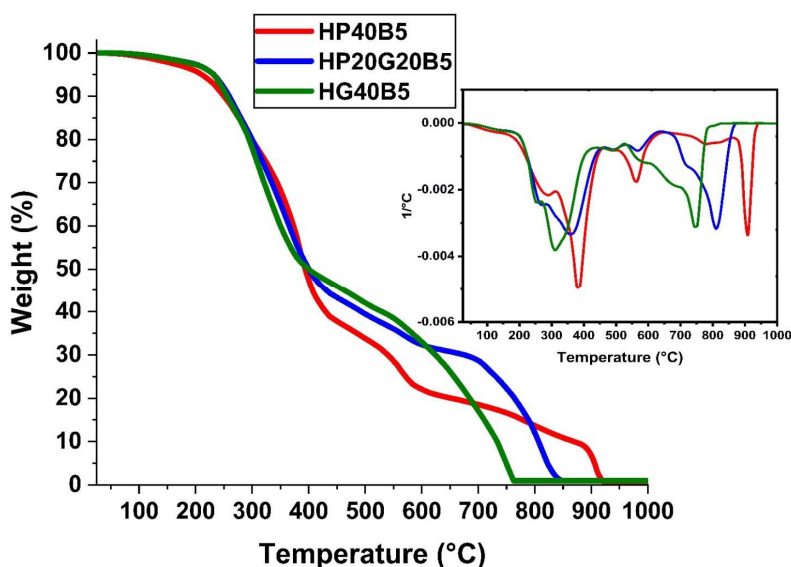


Figure 9. Thermogravimetric analysis of humins based copolymers at $10\text{ }^{\circ}\text{C min}^{-1}$ under air flow.

Inset: weight loss of the derivative.

The first degradation step shows the same shape under air and nitrogen atmosphere (Figure ESI5), indicating that at this stage mainly non-oxidative degradation reactions of thermolysis occur. This first degradation step presents the largest mass loss of resins $\approx 55\text{--}63\%$. The mass loss decreases in this stage from 63% (formulation with PEGDE) to $\approx 55\%$ (formulation with GDE). Above 450 °C a second mass loss follows for the three systems under air flow, with a lower mass loss (13–20%). Finally, starting with 600 °C thermo-oxidations and carbonization reactions degrade the thermosets completely. As summarized in Table 6, the inert atmosphere slows down the initial degradation of the materials, the $T_{5\%}$ temperatures increasing with 20 °C. It can also be observed that the degradation at $T > 500$ °C is completely absent in the TGA analysis under nitrogen flow, this step being characteristic of the oxidative degradation.

Table 6. Thermal stability of humins copolymers under Air and Nitrogen

	Temperature (°C)		
	HP40B5	HP20G20B5	HG40B5
$T_{5\%}$ under Air	212	232	233
$T_{5\%}$ under N ₂	244	251	246

2.2.3.4. The Bio-based Content for humins-based copolymers

In January 2005, the US Department of Agriculture defined the bio-based content of a product as the amount of bio-based carbon in the material or product as a percent of the weight (mass) of the total organic carbon in the product.⁴⁹ Currently, the minimum acceptable percentage of biomass plastics is ≈ 25 wt.% of the total weight of the product.^{50,51} According to Pan *et al.*⁵² we calculated the bio-based carbon content for each humins-based system. Humins are made of renewable raw materials and hence are 100% bio-based, while PEGDE, GDE and BDMA are still petrochemical-based products, even if ethylene glycol and glycerol are nowadays produced *via* bio-resources.

According to previous studies performed on industrial humins produced by Avantium^{29,53}, the carbon content of the crude humins is around 54%. Based on weight, the %C in PEGDE is = 51.69%, in GDE it is = 52.88% and in BDMA it is = 79.88%. The HP40B5 and HG40B5 systems contain 55 g humins, 40 g PEGDE or GDE and 5 g BDMA. The HP20G20B5 system contains 55 g humins, 20 g PEGDE, 20g GDE and 5 g BDMA. Theoretically, when only carbon is considered, the bio-based carbon content in each formulation is: $\approx 54.63\%$ for HP40B5, $\approx 54.14\%$ for HG40B5 and $\approx 54.39\%$ for HP20G20B5. Hence, the prepared formulations are biomass materials satisfying the criteria for bio-based carbon content.

2.3. Conclusions

In conclusion three thermoset resins with a bio-based carbon content $> 54\%$ were obtained from humins and aliphatic diglycidyl ethers. The effect of formulations composition on the reactivity of the systems were studied by various methods, DSC, FT-IR and rheometry. All systems showed good reactivity during the copolymerization between the humins and the diglycidyls. The properties of the obtained materials were analyzed by DMA, tensile and Shore tests. These analyses proven the macroscopic homogeneity of the three copolymers materials and their ductile character. Resins with longer aliphatic chains, HP40B5, reached $\approx 60\%$ elongation at break. All these properties together with the low curing time and temperature, and also the reduced numbers of components make these results feasible for the industry. To our knowledge, these are the first data reported on the synthesis of elastomeric humins based copolymers opening their utilization for example as matrix for composites for industrial applications.

2.4. Experimental

2.4.1. Materials

The main component of formulations is represented by humins, which are an industrial polymeric by-product produced by Avantium Chemicals at their Pilot Plant in Geleen, The Netherlands, formed during acid-catalyzed processing of carbohydrates. As already reported, the humins are carbonaceous, heterogeneous, polydisperse structures whose molecular structure remain largely unknown. To obtain thermoset materials, the humins were copolymerized with diglycidyl comonomers such as the poly(ethylene glycol) diglycidyl ether (PEGDE) and glycerol diglycidyl ether (GDE), with *N,N*-dimethylbenzylamine (BDMA) being used as an initiator. The comonomers and the initiator were purchased from Sigma-Aldrich and used as received.

2.4.1.1. Humins-based formulations and thermoset samples preparation

To design and develop different kinds of humins-based materials we tested different humins/comonomer formulations as presented in Table 7. The formulations were studied in terms of their reactivity, the temperature interval of the reaction and aspect of the synthesized material (homogeneity, foaming during curing, fragility of the final material, *etc.*). In all the formulations the BDMA initiator was used at 5 wt.%. To produce the reaction mixtures, the required amount of humins was mechanically mixed with necessary amounts of the comonomers and initiator until homogenization. The obtained formulations were poured into

silicone molds and the thermosets were obtained by applying a curing and post-curing temperature program.

Table 7. General properties of the compounds used for humins copolymerization

Compound Name	Molecular weight (g mol⁻¹)	Density at 25°C (g cm⁻³)
N, N-Dimethylbenzylamine (BDMA)	135.21	0.9
Glycerol diglycidyl ether (GDE)	204.22	1.23
Poly (ethylene glycol) diglycidyl ether (PEGDE)	average M _n 500–650	1.14

Reactions were conducted for 4 h at 80 °C followed by post-curing for 1.5 h at 130 °C. To study the reactivity of humins with the diglycidyls, three types of humins mixture systems were prepared with PEGDE, GDE and (PEGDE + GDE), in different ratios. BDMA was used as initiator, at 5 wt.%. The acronyms for the mixtures are reported based on their composition: “HPB” – for the system humins/PEGDE/BDMA; “HGB” – for the system humins/GDE/BDMA; “HPGB” – for the system humins/(PEGDE + GDE)/BDMA. Knowing that 5% represents the quantity of the initiator in all the formulations, *e.g.* HP40B5 is the formulation with 40% PEGDE, 5% BDMA and 55% humins. After the first screen of reactivity optimization, the best three formulations (one of each system) were selected and characterized.

2.4.2. Experimental techniques

2.4.2.1. Differential Scanning Calorimetry

DSC measurements were carried out on a Mettler-Toledo DSC 3 apparatus controlled by STARe Software developed by Mettler-Toledo. The heat flow and temperature of the instrument were calibrated in 3 points using water, indium and zinc standards. The humins–diglycidyl ethers copolymerization reactions were directly performed in DSC pans, by simple heating. Samples of 10–15 mg were placed into 100 μL aluminum crucibles. The different mixtures were reacted under non-isothermal conditions at a heating rate β of 10 °C min⁻¹ under air (100 mL min⁻¹) over a temperature range 25–250 °C. This thermal analysis technique was also used to study the second-order phase transitions on the resins. Samples of humins-based thermosets with masses between 9 and 12 mg were scanned at 10 °C min⁻¹ from -50 °C to 140 °C.

2.4.2.2. FT-Infrared Spectroscopy

FT-IR technique was used to investigate the evolution of structures before, during and after the copolymerization of each formulation. The Fourier transform infrared (FT-IR) spectra were recorded using a Nicolet iS50 FT-IR spectrometer equipped with a GladiATR (PIKE

Technologies, Inc.) single diamond attenuated total reflectance system. The spectrum of air was recorded as a background before each sample. All spectra were acquired with a spectral resolution of 4 cm^{-1} and 32 scans in the range of $4000\text{--}500\text{ cm}^{-1}$.

2.4.2.3. Rheometry

Chemorheological measurements were conducted under nitrogen in an Anton Paar MCR-302 rheometer using disposable plate-plate geometries (25 mm diameter and 1 mm gap). The measurements were carried out at a scan rate of $0.2\text{ }^{\circ}\text{C min}^{-1}$ over a temperature range $50\text{ }^{\circ}\text{C}$ to $200\text{ }^{\circ}\text{C}$. The complex viscosity, storage modulus (G') and loss modulus (G'') were measured by oscillatory shear experiments with an angular frequency of 10 rad s^{-1} and a deformation of 0.2%. The temperature of crossover of the values of storage (G') and loss (G'') moduli was considered as the temperature of gelation (T_{gel}).

2.4.2.4. Dynamic Mechanical Analysis

DMA measurements were performed using a Mettler-Toledo DMA 1 equipped with a three-point bending assembly at an oscillatory frequency of 1.0 Hz and an amplitude of $20\text{ }\mu\text{m}$. The analyzed samples had rectangular dimensions of $48 \times 8 \times 4\text{ mm}^3$ (length \times width \times thickness). Each resin formulation was analyzed three times and the values averaged. The DMA was performed in the temperature-scanning mode with a constant displacement amplitude and frequency. The temperature ramp covered a range from -150 to $180\text{ }^{\circ}\text{C}$ at a heating rate of $3\text{ }^{\circ}\text{C min}^{-1}$ under a nitrogen atmosphere. The loss (E''), storage (E') Young moduli and damping factor ($\tan \delta = E''/E'$) were determined.

Three different T_g values can be determined by the measurement according to AITM 1-0003 and ASTM D7028-07⁴¹. The three different T_g values are (i) $T_{g-onset}$, defined as the temperature of extrapolated tangents drawn from points on the storage modulus curve before and after the start of the glass transition; (ii) T_{g-loss} , defined as the maximum temperature on the loss modulus *versus* temperature curve; (iii) T_{g-peak} , defined as the maximum of $\tan \delta$ (damping). The T_{g-peak} value is generally higher than T_{g-loss} value and corresponds more closely to the transition midpoint while the $T_{g-onset}$ value more closely signifies the initial drop from the glassy state into the transition state. To unify the notation, the T_{g-peak} will be noted as $\tan \delta$ assigned to the temperature of the maximum of the loss factor peak and attributed to the α transitions.

The crosslinking densities for the humins-based copolymers were calculated using Flory's theory.⁴⁴ According to Flory the value of the storage modulus at the rubber plateau allows the calculation of the cross-linking density of the resins:

$$\nu = \frac{E'}{3RT} \quad (1)$$

where ν is the crosslinking density (mol cm^{-3}), T represents the temperature ($^{\circ}\text{K}$), E' is the storage modulus at the rubbery plateau at T (MPa) and R is the perfect gas constant. To calculate the crosslinking density for the three humins-based resins, the values were taken at the rubber plateau where the values of the modulus and $\tan \delta$ are constant, namely at $T_g + 80$ $^{\circ}\text{C}$.

2.4.2.5. Shore Hardness Test

A Zwick Roell 3116 hardness tester was used for determining the hardness according to ISO 7619-1, ASTM D2240 and ISO 868. The Shore D hardness tester was released smoothly with a load force of $50 \text{ N} \pm 0.5 \text{ N}$ until the presser foot was firmly seated on the specimens. To avoid the errors, three samples of each resin formulation were tested, and three measurements were performed for each sample.

2.4.2.6. Tensile Tests

The tensile strength and the Young's modulus of the humins/diglycidyl based thermosets were determined by tensile tests according to standard ISO 527-1⁵⁴ and ASTM D638-08⁵⁵ on a mechanical universal testing machine Instron, model 3365, controlled by BlueHill Lite software developed by Instron (Norwood, MA, USA). For the tests, a crosshead speed of 10 mm min^{-1} was used on samples of dimension $75 \times 10 \times 2 \text{ mm}^3$ (length \times width \times thickness). Five samples for each formulation were tested to evaluate the average calculations of mechanical properties (Young's modulus, tensile strength, and elongation at break).

2.4.2.7. Thermogravimetric Analysis

Thermal stabilities of copolymerization formulations and the obtained thermosets were analyzed using thermogravimetric analysis (TGA). The thermal degradations, mass loss and its derivative as a function of temperature were evaluated using a TGA 2 Mettler-Toledo between 25 $^{\circ}\text{C}$ and 1000 $^{\circ}\text{C}$ under oxidative (Air) and nitrogen flows (150 mL min^{-1}) at a heating rate of 10 $^{\circ}\text{C min}^{-1}$. Samples of about 4 – 7 mg of were placed into 70 μL alumina pans and tested.

Acknowledgements

This work was supported by KaRMA2020 project. This project has received funding from the European Union's Horizon 2020 Research and Innovation program under Grant Agreement no. 723268.

Notes and references

- (1) Delidovich, I.; Hausoul, P. J. C.; Deng, L.; Pfützenreuter, R.; Rose, M.; Palkovits, R. Alternative Monomers Based on Lignocellulose and Their Use for Polymer Production. *Chem. Rev.* **2016**, *116* (3), 1540–1599. <https://doi.org/10.1021/acs.chemrev.5b00354>.
- (2) Isikgor, F. H.; Becer, C. R. Lignocellulosic Biomass: A Sustainable Platform for the Production of Bio-Based Chemicals and Polymers. *Polym. Chem.* **2015**, *6* (25), 4497–4559. <https://doi.org/10.1039/c5py00263j>.
- (3) Patil, S. K. R.; Lund, C. R. F. Formation and Growth of Humins via Aldol Addition and Condensation during Acid-Catalyzed Conversion of 5-Hydroxymethylfurfural. *Energy and Fuels* **2011**, *25* (10), 4745–4755. <https://doi.org/10.1021/ef2010157>.
- (4) Patil, S. K. R.; Heltzel, J.; Lund, C. R. F. Comparison of Structural Features of Humins Formed Catalytically from Glucose, Fructose, and 5-Hydroxymethylfurfuraldehyde. *Energy Fuels* **2012**, *26*, 5281–5293.
- (5) Schweizer, A. Caramel and Humin. A Contribution to the Knowledge of the Decomposition Products of Sugars. *Recl. des Trav. Chim. des Pays-Bas* **2010**, *57* (4), 345–382. <https://doi.org/10.1002/recl.19380570402>.
- (6) Hoang, T. M. C.; Lefferts, L.; Seshan, K. Valorization of Humin-Based Byproducts from Biomass Processing - A Route to Sustainable Hydrogen. *ChemSusChem* **2013**, *6* (9), 1651–1658. <https://doi.org/10.1002/cssc.201300446>.
- (7) Hu, X.; Lievens, C.; Larcher, A.; Li, C. Z. Reaction Pathways of Glucose during Esterification: Effects of Reaction Parameters on the Formation of Humin Type Polymers. *Bioresour. Technol.* **2011**, *102* (21), 10104–10113. <https://doi.org/10.1016/j.biortech.2011.08.040>.
- (8) Rasrendra, C. B.; Windt, M.; Wang, Y.; Adisasmito, S.; Makertihartha, I. G. B. N.; Van Eck, E. R. H.; Meier, D.; Heeres, H. J. Experimental Studies on the Pyrolysis of Humins from the Acid-Catalysed Dehydration of C6-Sugars. *J. Anal. Appl. Pyrolysis* **2013**, *104*, 299–307. <https://doi.org/10.1016/j.jaap.2013.07.003>.
- (9) Titirici, M. M.; Antonietti, M.; Baccile, N. Hydrothermal Carbon from Biomass: A Comparison of the Local Structure from Poly- to Monosaccharides and Pentoses/Hexoses. *Green Chem.* **2008**, *10* (11), 1204–1212. <https://doi.org/10.1039/b807009a>.
- (10) Sevilla, M.; Fuertes, A. B. The Production of Carbon Materials by Hydrothermal Carbonization of Cellulose. *Carbon N. Y.* **2009**, *47* (9), 2281–2289. <https://doi.org/10.1016/j.carbon.2009.04.026>.
- (11) Zheng, M.; Liu, Y.; Jiang, K.; Xiao, Y.; Yuan, D. Alcohol-Assisted Hydrothermal Carbonization to Fabricate Spheroidal Carbons with a Tunable Shape and Aspect Ratio. *Carbon N. Y.* **2010**, *48* (4), 1224–1233. <https://doi.org/10.1016/j.carbon.2009.11.045>.
- (12) Buera, M. D. P.; Chirife, J.; Resnik, S. L.; Wetzler, G. Nonenzymatic Browning in Liquid Model Systems of High Water Activity: Kinetics of Color Changes Due to Maillard's Reaction Between Different Single Sugars and Glycine and Comparison with Caramelization Browning. *J. Food Sci.* **1987**, *52* (4), 1063–1067. <https://doi.org/10.1111/j.1365-2621.1987.tb14276.x>.
- (13) Kroh, L. W. Caramelisation in Food and Beverages. *Food Chem.* **1994**, *51* (4), 373–379. [https://doi.org/10.1016/0308-8146\(94\)90188-0](https://doi.org/10.1016/0308-8146(94)90188-0).
- (14) Cämmerer, B.; Wedzicha, B. L.; Kroh, L. W. Nonenzymatic Browning Reactions of Retro-Aldol Degradation Products of Carbohydrates. *Eur. Food Res. Technol.* **1999**, *209* (3–4), 261–265. <https://doi.org/10.1007/s002170050490>.
- (15) Quintas, M. A. C.; Brandão, T. R. S.; Silva, C. L. M. Modelling Colour Changes during the Caramelisation Reaction. *J. Food Eng.* **2007**, *83* (4), 483–491. <https://doi.org/10.1016/j.jfoodeng.2007.03.036>.
- (16) Buera, M. D. P.; Chirife, J.; Resnik, S. L.; Lozano, R. D. Nonenzymatic Browning in Liquid

- Model Systems of High Water Activity: Kinetics of Color Changes Due to Caramelization of Various Single Sugars. *J. Food Sci.* **1987**, 52 (4), 1059–1062. <https://doi.org/10.1111/j.1365-2621.1987.tb14275.x>.
- (17) Campanella, A.; Zhan, M.; Watt, P.; Grous, A. T.; Shen, C.; Wool, R. P. Triglyceride-Based Thermosetting Resins with Different Reactive Diluents and Fiber Reinforced Composite Applications. *Compos. Part A Appl. Sci. Manuf.* **2015**, 72, 192–199. <https://doi.org/10.1016/j.compositesa.2015.02.009>.
- (18) Van Zandvoort, I.; Wang, Y.; Rasrendra, C. B.; Van Eck, E. R. H.; Bruijninx, P. C. A.; Heeres, H. J.; Weckhuysen, B. M. Formation, Molecular Structure, and Morphology of Humins in Biomass Conversion: Influence of Feedstock and Processing Conditions. *ChemSusChem* **2013**, 6 (9), 1745–1758. <https://doi.org/10.1002/cssc.201300332>.
- (19) Sevilla, M.; Fuertes, A. B. Chemical and Structural Properties of Carbonaceous Products Obtained by Hydrothermal Carbonization of Saccharides. *Chem. - A Eur. J.* **2009**, 15 (16), 4195–4203. <https://doi.org/10.1002/chem.200802097>.
- (20) Filiciotto, L.; Balu, A. M.; Van der Waal, J. C.; Luque, R. Catalytic Insights into the Production of Biomass-Derived Side Products Methyl Levulinate, Furfural and Humins. *Catal. Today* **2018**, 302, 2–15. <https://doi.org/10.1016/j.cattod.2017.03.008>.
- (21) Châu, H. T. M. Catalytic Gasification of Humin Based By-Product from Biomass Processing - a Sustainable Route for Hydrogen, 2014.
- (22) Hoang, T. M. C.; Van Eck, E. R. H.; Gardeniers, J. G. E.; Lefferts, L.; Seshan, K. Humin Based By-Products from Bioprocessing as Potential Carbonaceous Source for Synthesis Gas Production. *Green Chem.* **2015**, 17, 959–972. <https://doi.org/10.1039/x0xx00000x>.
- (23) Constant, S.; Lancefield, C. S.; Weckhuysen, B. M.; Bruijninx, P. C. A. Quantification and Classification of Carbonyls in Industrial Humins and Lignins by ¹⁹F NMR. *ACS Sustain. Chem. Eng.* **2017**, 5 (1), 965–972. <https://doi.org/10.1021/acssuschemeng.6b02292>.
- (24) Kang, S.; Zhang, G.; Yang, Q.; Tu, J.; Guo, X.; Qin, F. G. F.; Xu, Y. A New Technology for Utilization of Biomass Hydrolysis Residual Humins for Acetic Acid Production. *BioResources* **2017**, 11 (4), 9496–9505. <https://doi.org/10.15376/biores.11.4.9496-9505>.
- (25) Pin, J. M.; Guigo, N.; Mija, A.; Vincent, L.; Sbirrazzuoli, N.; Van Der Waal, J. C.; De Jong, E. Valorization of Biorefinery Side-Stream Products: Combination of Humins with Polyfurfuryl Alcohol for Composite Elaboration. *ACS Sustain. Chem. Eng.* **2014**, 2 (9), 2182–2190. <https://doi.org/10.1021/sc5003769>.
- (26) Mija, A.; Jong, E. De; Waal, J. C. Van der; Klink, G. P. M. Van. Humins-Containing Foam. WO 2017/074183 A1, 2017.
- (27) Tosi, P.; Van Klink, G. P. M.; Celzard, A.; Fierro, V.; Vincent, L.; De Jong, E.; Mija, A. Auto-Crosslinked Rigid Foams Derived from Biorefinery Byproducts. *ChemSusChem* **2018**, 11 (16), 2797–2809. <https://doi.org/10.1002/cssc.201800778>.
- (28) Kang, S.; Fu, J.; Deng, Z.; Jiang, S.; Zhong, G.; Xu, Y.; Guo, J.; Zhou, J. Valorization of Biomass Hydrolysis Waste: Activated Carbon from Humins as Exceptional Sorbent for Wastewater Treatment. *Sustainability* **2018**, 10 (6), 1795. <https://doi.org/10.3390/su10061795>.
- (29) Muralidhara, A.; Tosi, P.; Mija, A.; Sbirrazzuoli, N.; Len, C.; Engelen, V.; De Jong, E.; Marlair, G. Insights on Thermal and Fire Hazards of Humins in Support of Their Sustainable Use in Advanced Biorefineries. *ACS Sustain. Chem. Eng.* **2018**, 6 (12), 16692–16701. <https://doi.org/10.1021/acssuschemeng.8b03971>.
- (30) Mija, A.; Waal, J. C. Van der; Jong, E. De; Klink, G. P. M. Van. Process for the Modification Humins. WO 2018/062995 A1, 2018.
- (31) Capanema, N. S. V.; Mansur, A. A. P.; De Jesus, A. C.; Carvalho, S. M.; De Oliveira, L. C.; Mansur, H. S. Superabsorbent Crosslinked Carboxymethyl Cellulose-PEG Hydrogels for Potential Wound Dressing Applications. *Int. J. Biol. Macromol.* **2018**, 106, 1218–1234. <https://doi.org/10.1016/j.ijbiomac.2017.08.124>.

- (32) Ghorpade, V. S.; Yadav, A. V.; Dias, R. J.; Mali, K. K.; Pargaonkar, S. S.; Shinde, P. V.; Dhane, N. S. Citric Acid Crosslinked Carboxymethylcellulose-Poly(Ethylene Glycol) Hydrogel Films for Delivery of Poorly Soluble Drugs. *Int. J. Biol. Macromol.* **2018**, *118*, 783–791. <https://doi.org/10.1016/j.ijbiomac.2018.06.142>.
- (33) Van Wagner, E. M.; Sagle, A. C.; Sharma, M. M.; La, Y. H.; Freeman, B. D. Surface Modification of Commercial Polyamide Desalination Membranes Using Poly(Ethylene Glycol) Diglycidyl Ether to Enhance Membrane Fouling Resistance. *J. Memb. Sci.* **2011**, *367* (1–2), 273–287. <https://doi.org/10.1016/j.memsci.2010.11.001>.
- (34) Vasylieva, N.; Barnych, B.; Meiller, A.; Maucler, C.; Pollegioni, L.; Lin, J. S.; Barbier, D.; Marinesco, S. Covalent Enzyme Immobilization by Poly(Ethylene Glycol) Diglycidyl Ether (PEGDE) for Microelectrode Biosensor Preparation. *Biosens. Bioelectron.* **2011**, *26* (10), 3993–4000. <https://doi.org/10.1016/j.bios.2011.03.012>.
- (35) Kono, H. Characterization and Properties of Carboxymethyl Cellulose Hydrogels Crosslinked by Polyethylene Glycol. *Carbohydr. Polym.* **2014**, *106* (1), 84–93. <https://doi.org/10.1016/j.carbpol.2014.02.020>.
- (36) Kasetaitė, S.; Ostrauskaitė, J.; Grazulevičienė, V.; Svedienė, J.; Bridziuvienė, D. Photocross-Linking of Glycerol Diglycidyl Ether with Reactive Diluents. *Polym. Bull.* **2015**, *72* (12), 3191–3208. <https://doi.org/10.1007/s00289-015-1461-x>.
- (37) Zhao, L.; Chen, Y.; Li, W.; Lu, M.; Wang, S.; Chen, X.; Shi, M.; Wu, J.; Yuan, Q.; Li, Y. Controlled Uptake and Release of Lysozyme from Glycerol Diglycidyl Ether Cross-Linked Oxidized Starch Microgel. *Carbohydr. Polym.* **2015**, *121*, 276–283. <https://doi.org/10.1016/j.carbpol.2015.01.002>.
- (38) urRehman, S.; Sahiner, M.; Sel, K.; Siddiq, M.; Sahiner, N. Synthesis and Characterization of New Microgel from Tris(2-Aminoethyl)Amine and Glycerol Diglycidyl Ether as Poly(TAEA-Co-GDE). *Colloids Surfaces B Biointerfaces* **2015**, *136*, 1156–1165. <https://doi.org/10.1016/j.colsurfb.2015.11.014>.
- (39) Tsilomelekis, G.; Orella, M. J.; Lin, Z.; Cheng, Z.; Zheng, W.; Nikolakis, V.; Vlachos, D. G. Molecular Structure, Morphology and Growth Mechanisms and Rates of 5-Hydroxymethyl Furfural (HMF) Derived Humins. *Green Chem.* **2016**, *18* (7), 1983–1993. <https://doi.org/10.1039/c5gc01938a>.
- (40) Menard, K. P. *Dynamic Mechanical Analysis - A Practical Introduction*, 2nd ed.; CRC Press LLC, 2008.
- (41) ASTM-D7028. Standard Test Method for Glass Transition Temperature (DMA Tg) of Polymer Matrix Composites by Dynamic Mechanical Analysis (DMA). 2008. <https://doi.org/10.1520/D7028-07E01.2>.
- (42) Carvalho, M. S.; Padmanabhan, M.; Macosko, C. W. Single-point Correction for Parallel Disks Rheometry. *J. Rheol. (N. Y. N. Y.)* **2002**, *38* (6), 1925–1936. <https://doi.org/10.1122/1.550532>.
- (43) Pascault, J.; Sautereau, H.; Verdu, J.; Williams, R. J. J. *Thermosetting Polymers*; MarcelDekker, Inc., 2002.
- (44) Flory, P. J. *Principles of Polymer Chemistry*; Cornell University Press: Ithaca, New York, 1953.
- (45) Gupta, V. B.; Drzal, L. T.; Lee, C. Y. C. The Temperature-dependence of Some Mechanical Properties of a Cured Epoxy Resin System. *Polym. Eng. Sci.* **1985**, *25* (13), 812–823. <https://doi.org/10.1002/pen.760251305>.
- (46) Ullah, A.; Wu, J. Feather Fiber-Based Thermoplastics: Effects of Different Plasticizers on Material Properties. *Macromol. Mater. Eng.* **2013**, *298* (2), 153–162. <https://doi.org/10.1002/mame.201200010>.
- (47) Pin, J. M.; Guigo, N.; Vincent, L.; Sbirrazzuoli, N.; Mija, A. Copolymerization as a Strategy to Combine Epoxidized Linseed Oil and Furfuryl Alcohol: The Design of a Fully Bio-Based Thermoset. *ChemSusChem* **2015**, *8* (24), 4149–4161. <https://doi.org/10.1002/cssc.201501259>.
- (48) Cambridge University Engineering Department. *Materials Data Book*; 2003.

- (49) Norton, G. A.; Devlin, S. L. Determining the Modern Carbon Content of Biobased Products Using Radiocarbon Analysis. *Bioresour. Technol.* **2006**, *97* (16), 2084–2090. <https://doi.org/10.1016/j.biortech.2005.08.017>.
- (50) Kunioka, M. Measurement Methods of Biobase Carbon Content for Biomass-Based Chemicals and Plastics. *Radioisotopes* **2013**, *62*, 901–925.
- (51) NCS-16785. *Bio-Based Content Certification Scheme*; 2016.
- (52) Pan, X.; Sengupta, P.; Webster, D. C. High Biobased Content Epoxy-Anhydride Thermosets from Epoxidized Sucrose Esters of Fatty Acids. *Biomacromolecules* **2011**, *12* (6), 2416–2428. <https://doi.org/10.1021/bm200549c>.
- (53) Muralidhara, A.; Bado-Nilles, A.; Marlair, G.; Engelen, V.; Len, C.; Pandard, P. Humins in the Environment: Early Stage Insights on Ecotoxicological Aspects. *Biofuels, Bioprod. Biorefining* **2018**, 1–7. <https://doi.org/10.1002/bbb.1964>.
- (54) ISO-527-1. *Plastics-Determination of Tensile Properties-Part 1: General Principles*. 1996.
- (55) ASTM-D638. *Standard Test Method for Tensile Properties of Plastics*. **2014**. <https://doi.org/10.1520/D0638-14.1>.

Electronic Supplementary Information (ESI)

Table ESI 1. Results of DSC analysis for humins/PEGDE and humins/GDE polymerization

	H80/P20	H70/P30	H60/P40	H50/P50	H80/G20	H70/G30	H60/G40	H50/G50
T_{peak} (°C)	203 ± 1	225 ± 1	160 ± 1	157 ± 1	215 ± 1	215 ± 1	221 ± 1	225 ± 1
(reaction interval)	(115–247)	(120–257)	(135–173)	(122–178)	(95–255)	(116–268)	(115–267)	(118–266)
			244	242				
			(215–262)	(190–262)				
$\Delta_r H$ (J g ⁻¹)	112 ± 2	111 ± 2	8 ± 1	6 ± 1	239 ± 4	301 ± 4	300 ± 4	145 ± 4
			28 ± 1	50 ± 1				

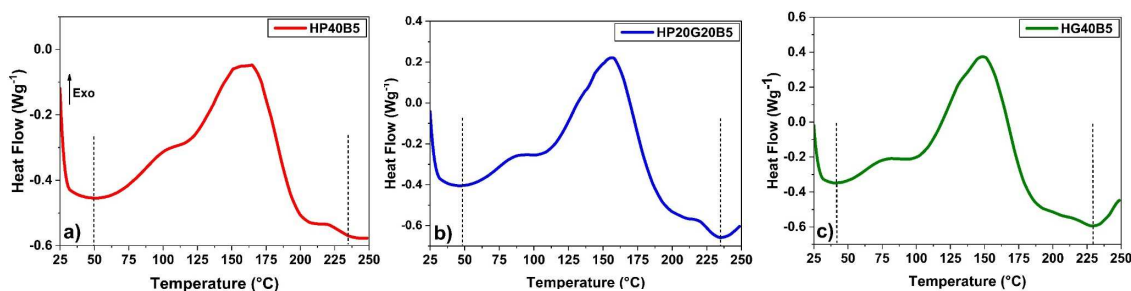


Figure ESI 1. DSC analysis for uncured mixtures: a) 55% H – 40% PEGDE – 5% BDMA, b) 55% H – 20% PEGDE – 20% GDE – 5% BDMA, c) 55% H – 40% GDE – 5% BDMA

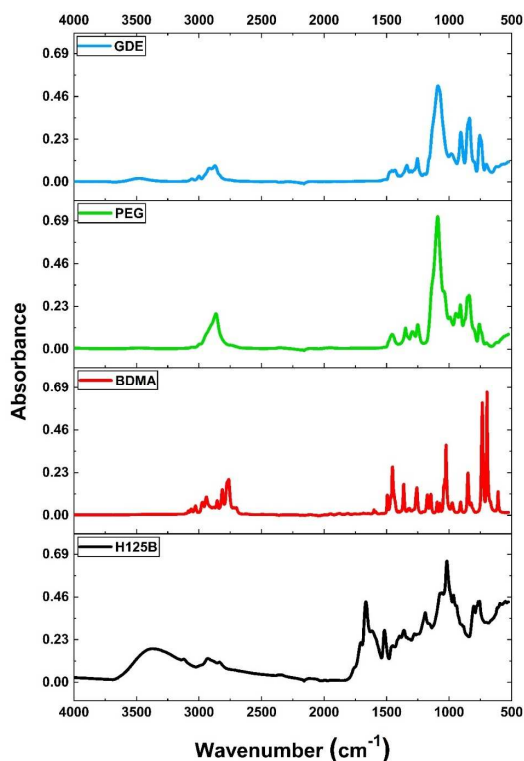


Figure ESI 2. FT-IR spectra of raw materials

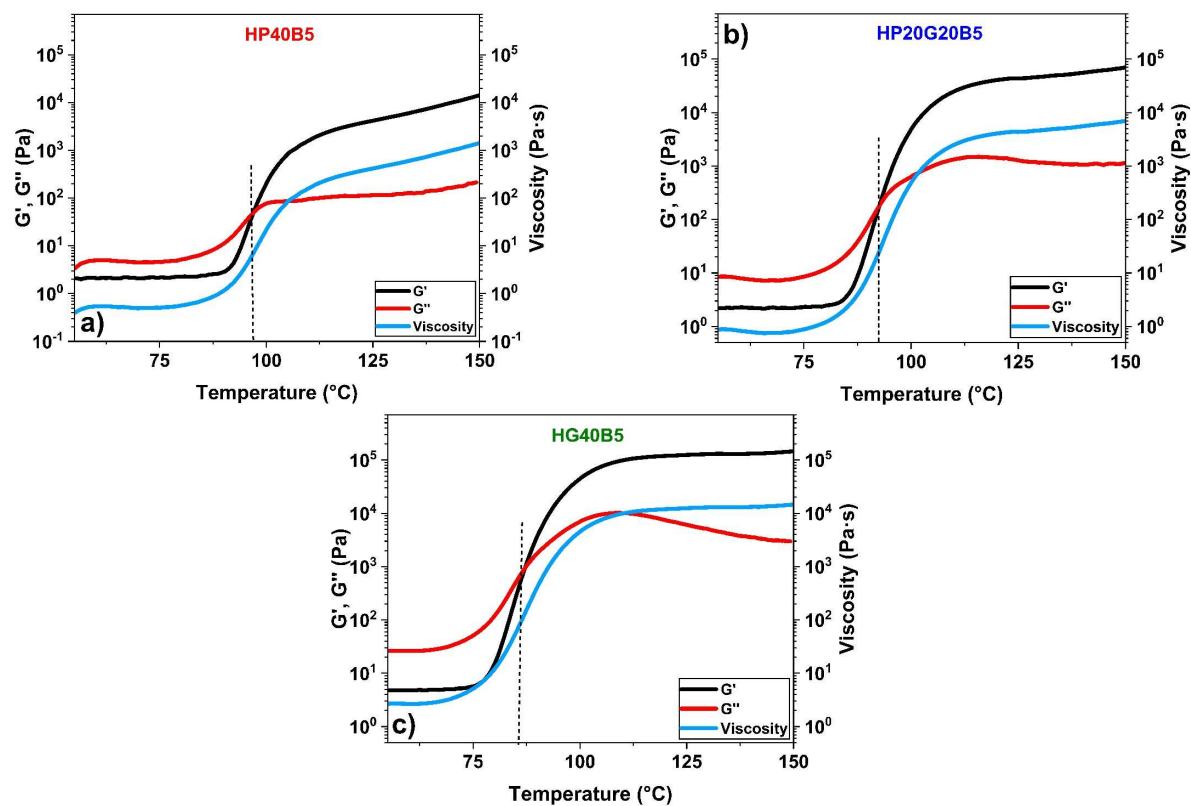


Figure ESI 3. Rheometry study of the humins-based resins: a) 55% H – 40% PEGDE – 5% BDMA, b) 55% H – 20% PEGDE – 20% GDE – 5% BDMA, c) 55% H – 40% GDE – 5% BDMA

Table ESI 2. Rheological data for humins-based resins

Resins	Gelling point (°C)	Start of reaction (°C)	End of reaction (°C)
HP40B5	98	75	125
HP20G20B5	92	73	120
HG40B5	86	65	115

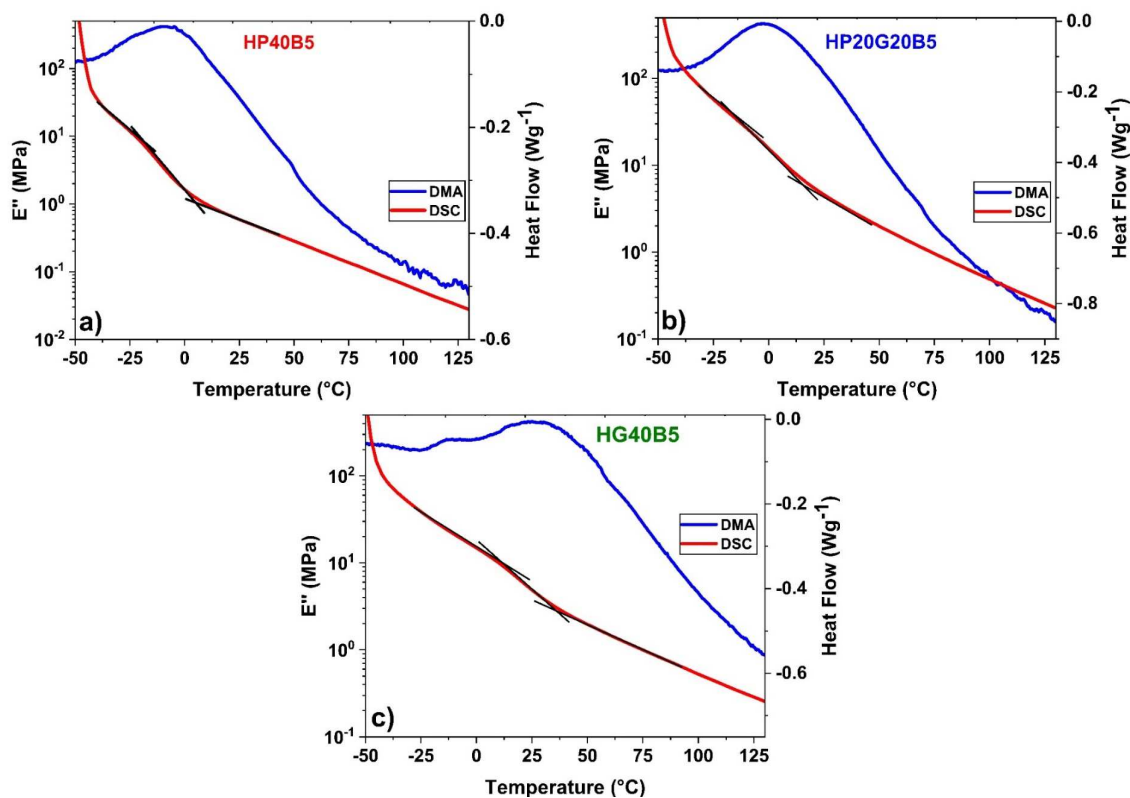


Figure ESI 4. Mechanical response of materials as compared to DSC scans showing the glass transition temperature for the humins-based resins

Table ESI 3. Temperatures and related storage modules for cross-link density determination of humins-based resins

	Tan δ + 80 °C (°C)	E' at Tan δ + 80 °C (MPa)	ν (mmol·cm ⁻³)
HP40B5	110	0.7	0.07
HP20G20B5	130	4.36	0.43
HG40B5	146	5.81	0.56

Table ESI 4. Sub-glass transitions of the humins-based copolymers

Sample	T_{γ} (°C) max / peak height	T_{β} (°C) max / peak height
HP40B5	-131 / 0.019	-73 / 0.03
HP20G20B5	-130 / 0.014	-71 / 0.03
HG40B5	-133 / 0.019	β -47 / 0.03 β' -2 / 0.17

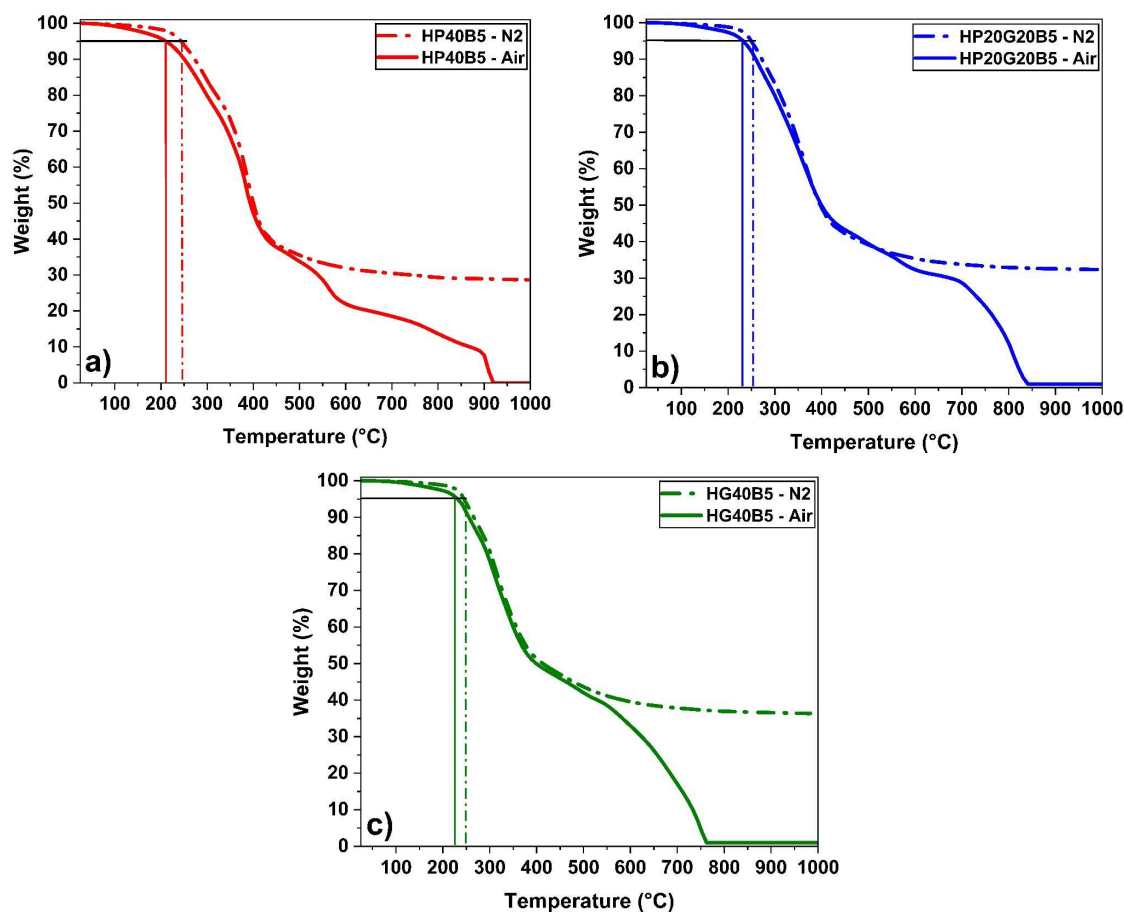


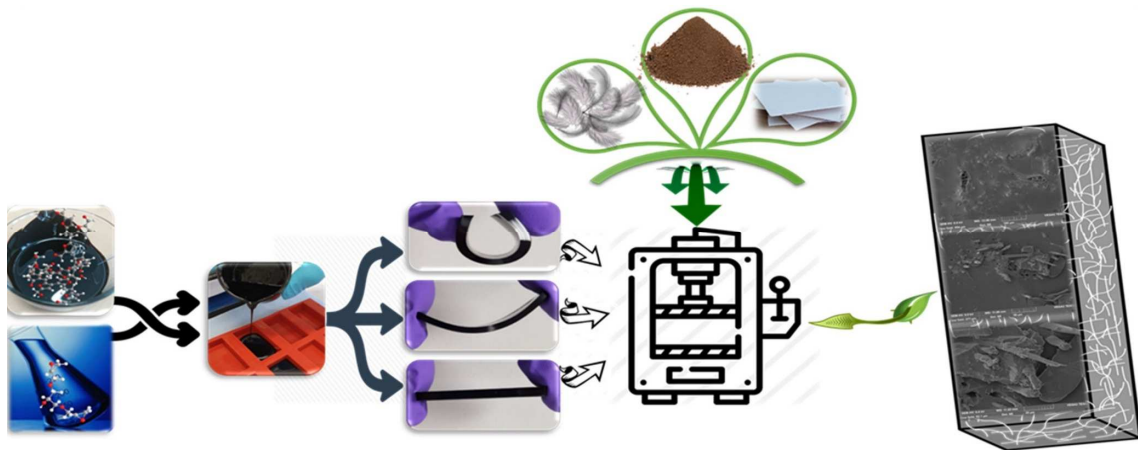
Figure ESI 5. Weight ratio vs temperature for the non-isothermal degradation of humins based resins conducted under inert (dash line) and oxidative atmosphere (solid line)

Table ESI 5. TGA degradation steps of the materials

Resins	1st degradation		2nd degradation		3rd degradation	
	T_{max} peak (°C)	Mass loss (%)	T_{max} peak (°C)	Mass loss (%)	T_{max} peak (°C)	Mass loss (%)
HP40B5	379	63	566	20	910	17
HP20G20B5	359	57	566	13	812	30
HG40B5	310	55	498	14	753	31

Chapter 3

Bio-Based Composites from Industrial By-products and Wastes as Raw Materials



This chapter is based on Roxana Dinu and Alice Mija, "Bio-based Composites from Industrial By-products and Wastes as Raw Materials", *Journal of Materials Science Research*, 2020, 9 (2), 29-45, <https://doi.org/10.5539/jmsr.v9n2p29>

Abstract

Innovative bio-based composites combining humins as biorefinery by-product with keratin or lignin as wastes or industrial side-products were developed. The bio-composites were prepared using three types of matrix formulations allowing the synthesis of elastic to rigid thermosets. These matrices were combined with chicken feathers powder, non-woven chicken feathers mat or lignin to produce bio-composites. A maximum quantity of bio-fillers was used, around 10 wt.%. The effect of the bio-fillers on the matrix's crosslinking was studied by rheology and DSC. Then, the obtained materials were analyzed by TGA, DMA, tensile tests, water absorption and SEM. The results show a very good compatibility of the humins matrix with the bio-fillers, without any preliminary modification of the matrix, that is exceptional for the point of view of a composite. The overall performances of the neat matrix were maintained or improved through the composites. Therefore, bio-composites with potentially interesting thermal and mechanical properties have been synthesized. In the case of the elastic ductile matrix the Young's modulus value was improved from 1 to 22 MPa, while for the rigid matrix the increase was from 106 to 443 or 667 MPa, in the case of composites with non-woven chicken feathers mat or lignin. To our knowledge this is the first study combining humins matrix with keratin. The obtained bio-composites are sustainable materials linked *via* the used raw materials to the circular economy and biomass valorization.

3.1. Introduction

One of the main problems faced by humanity currently and in the future is the intense pollution of the environment due to the production and use of materials based on fossil derivatives but also due to the increasing amount of industrial wastes.¹ The need to significantly reduce the environmental pollution has led to the investigation and development of new materials from renewable resources. Proteins are biopolymers with a big potential to develop materials since they are biodegradable, renewable, inexpensive and especially abundant.² An important source of protein is the chicken feathers, a by-product from the poultry industry.³

Since ancient times, people have been using birds for food, falconry, in ritual, for aviary specimens and pets. Historical sources prove that bird feathers were used for preparing arrows, while the archaeological data present evidence for the use of wild birds (*e.g.*, hooded crow) in funeral ceremonies.⁴ According to the biannual report on global food markets made by Food and Agriculture Organization of the United Nations, the global production of poultry meat was estimated at 128.4 million tons in 2019.⁵ Given that feathers represent about 5–7% of the body weight of an adult chicken^{6,7}, about 9 million tons of feathers are annually produced worldwide. The chicken feathers are composed of 91% keratin, 8% water and 1% fats.^{8–11} Only a small part of chicken feathers is converted in low nutritional animal feed. The largest amount of feathers is deposited in landfills or burned, leading to environmental pollution, and moreover to the loss of a very rich resource of high protein raw material.

For birds, feathers play an important role in flight, protection, heat retention, waterproofing, *etc.* All of these functions are performed with the help of some types of feathers such as contour feather, semiplume, filoplume, chick down and bristle feather, which are found in different parts of the body and have distinct role and structures.^{8,12} Feathers present a complex hierarchical branched structure where rachis is the primary structure, barbs are the secondary and barbules the tertiary branches structure.⁹ In the cross-section of the rachis and the barb one can see the presence of a honeycomb structure.^{9,10,13} According to Reddy and Yang¹¹ this honeycomb structure act as an air and heat insulator, providing high resistance to compressibility and making the fibers very light in weight, having a very low-density (0.8 g cm^{-3}) compared with the wool (1.3 g cm^{-3}) and cellulose fibers (1.5 g cm^{-3}).^{14,15}

Chicken feathers being composed from 91% protein (keratin), represent one of the main sources of keratin. Keratin is a natural and small protein, uniform in size with a molecular weight around 10 kDa (10500 Da)¹⁶, consisting of polypeptide chains obtained by the condensation of different amino acids, their content on feathers depending on the environment, food and breed.⁹ One of the most important keratin's polypeptide is the cysteine which is

present in a large quantity.¹⁷ The cysteine contains thiol groups which interact to form disulfide bonds therefore contributing to the semi-crystalline structure of feather keratin and it is hydrophobic. The second largest amino acid in chicken feathers is the serine which contains the -OH groups making the feathers hydrophilic. Chicken feather fibers have both hydrophobic and hydrophilic character and approximately the ratio is 60:40 percentages.¹⁷⁻²⁰ Based on X-ray diffraction, keratins can be classified into α -pattern, β -pattern, feather-pattern and amorphous pattern.²¹⁻²³ The feather pattern has been considered as β -pattern since both patterns show the same characteristic reflections.²⁴ Usually, keratin classification are used the two regular secondary structures α -helix and β -sheet. The α -keratins are found in the soft tissues such as sheep wool, skin and hair while β -keratins are present in hard tissues proteins of bird feathers, fish scales, nails and others.²⁵ The most representative α -keratin material is the wool while the feathers are typical for β -keratin materials.²⁶

Considering the large amount of keratin present in chicken feathers, these represent a valuable resource with countless potential applications in cosmetics, biomedical applications^{27,28}, thermoplastics and packaging materials²⁹⁻³¹, thermosets, composites for different sectors of industry (construction, automobile, *etc.*), biofertilizers^{32,33}, coatings, *etc.* The good properties but also the abundance of the chicken feathers made them more and more interesting and used by the researchers in the development of new green materials able to replace those based on fossil derivatives.³⁴ For example, Yin *et al.*³⁵ reported the fabrication of porous keratin films using keratin from chicken feathers for controlled drug delivery systems. Firstly, a stable and homogeneous keratin was extracted from chicken feathers using Shindai method, with a yield of 93% and a molecular weight of around 20 kDa. Thereafter, the obtained chicken feather keratin was mixed with glycerol developing films with controlled thickness (by varying the volume of the keratin dispersion) and good mechanical properties. These keratin-based films were pH-responsive, showing a controllable drug-releasing behavior making them an attractive candidate for application in the biomedical field. Song *et al.*³⁶ have developed chicken/gelatin composite protein films with clove oil, with potential application in the active packaging for smoked salmon. The mechanical properties of the prepared composite films were investigated showing that the tensile strength and elongation at break significantly increased with the increase of the gelatin content. Also, the incorporation of 1.5% clove oil into the film improved the antimicrobial properties of the composite film and its mechanical properties were not affected, being considered a potential active packaging material for smoked salmon preservation Yang and Reddy³⁷ reinforced the high-density polyethylene (HDPE) from plastic bags with chicken feathers to develop composites in an effort to add value and to reduce the amount of the plastics and feathers disposed in landfills. The authors created sandwich structures with layers of plastic and feathers varying the proportions (w/w) from

40/60 to 70/30. The effect of the ratio of feathers in the composite and the influence of the manufacturing parameters on the mechanical properties of the final materials have been studied. It was found that incorporating feathers as reinforcement for HDPE at the optimum conditions (182 °C and 2 min) substantially improved the flexural strength, tensile modulus and sound absorption than 100% HDPE. The authors showed by this research that discarded plastic bags and chicken feathers can be used as valuable products in the composites production for different industrial sectors. In order to replace the non-renewable composite materials, Huda and Yang³⁸ proposed to develop composites from ground chicken quill and polypropylene. They investigated the mechanical and acoustical properties of this kind of composites and compared them with jute-polypropylene composites, concluding that the ground quill composites can be an ideal candidate for acoustic panels or headliner substrates. Hong and Wool³⁹ developed a novel bio-based composite material from soybean oils and keratin feather fibers. The authors used acrylated epoxidized soybean oil and soybean oil pentaerythritol glyceride maleates as liquid molding resins and two different types of non-woven keratin fiber mats, obtaining environmentally friendly, low-cost composites, suitable for electronic as well as automotive and aeronautical applications. Following the studies, it was observed that the literature deals with applications of other chicken products also, not only of chicken feathers. For instance, Rivera *et al.*⁴⁰ used the eggshells in a phosphate solution at an elevated temperature, developing a new procedure for the synthesis of porous hydroxyapatite.

Another abundant renewable resource in nature is the lignocellulosic biomass composed mainly from three principal components *i.e.* cellulose (35–50%), hemicellulose (20–35%) and lignin (10–25%).⁴¹ Lignin is a phenolic complex macromolecule with an irregular structure affected by various factors like biomass sources, fractionation's methods, and fractionation's severity.^{42,43} Lignin is a three-dimensional network composed mainly of three types of phenylpropanoid units as coniferyl, sinapyl, and p-coumaryl alcohols.⁴⁴ This heterogeneous biopolymer is a by-product of biorefineries that process plant biomass to produce fuels and chemicals, but also a waste of the pulp and paper industries. Generally, most of the lignins are burned to generate heat and electricity, but has also gained increased attention in other application areas such as pharmacology⁴⁵, as lignin nanostructure for possible applications in UV protection and biomedical applications⁴⁶, or bioplastic and biocomposites.⁴⁷ For example, Diop *et al.*⁴⁸ reported the development of the composites with around 20% lignin used as filler in a low-density polyethylene matrix, obtaining an increment of the mechanical properties of the materials. Composites were developed by Yin *et al.*⁴⁹ by blending the lignin with an epoxy-polyamine resin and using a hot press molding process. They studied the effect of molding's temperature and pressure on the mechanical properties

and microstructure of the lignin/epoxy resin composites. After these studies, the authors noticed that the properties of the materials initially increased, then decreased, the excessively high applied temperature causing the degradation of the composite that become brittle, the optimal temperature being around 130 °C. Therefore, according to literature studies, the lignin begun to show great interest, being extensively researched as an possible alternative to petrochemical-based reinforcements.^{50,51}

Another industrial side-product generated by the processing and valorization of lignocellulose is a black and viscous compound called humins. Humins are polyaromatic condensed structures derived from sugar conversion processes with a molecular structure unknown, which is influenced by the type of feedstock and the processing parameters.^{52,53} These carbon-rich agglomerate particles contain acid, ketone, alcohol, aldehyde groups and are composed of approximately 50–66 wt.% C and 29–46 wt.% O, the rest being H.⁵⁴ In recent years, the valorization of this by-product derived from biorefinery into high value products has shown a growing interest for researchers. The humins' potential to generate materials has been tested, thus obtaining thermosets furanic resins and composites^{55,56} or porous materials^{57–59}, but this by-product is not yet sufficiently valued and exploited.

In this study, humins-based resins were combined for the first time with bio-fillers like chicken feathers powder, non-woven chicken feathers mat or lignin in order to develop sustainable bio-composites with potential industrial applicability. The influence of these natural fillers on humins-based resins reactivity was analyzed by differential scanning calorimetry (DSC) and rheometry. The morphology of the bio-composites was investigated by scanning electronic microscopy (SEM). Then, the thermomechanical properties were analyzed by thermogravimetric analysis (TGA), dynamic mechanical analysis (DMA), Shore hardness test and tensile tests. The materials' water absorption was also investigated.

3.2. Results and Discussion

3.2.1. Reactivity study of the humins-based resins in presence of chicken feathers powder or lignin bio-fillers

3.2.1.1. Differential scanning calorimetry

To identify the influence of the two bio-fillers on the thermal crosslinking of the humins based resins, the DSC analyses for reactive humins formulations and their mixtures with chicken feathers powder and lignin were made and compared. Figure 1 highlights the changes taking place during crosslinking reactions.

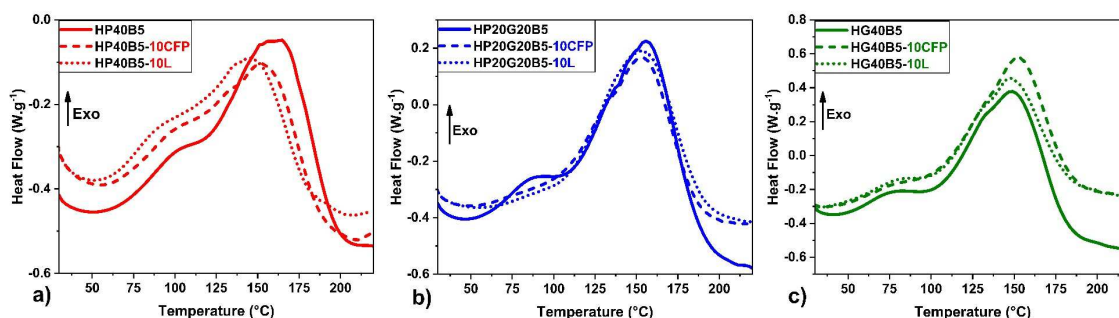


Figure 1. DSC analysis for uncured resins and their mixtures with 10 wt.% chicken feathers powder (10CFP) or 10 wt.% lignin (10L): a) HP40B5, b) HP20G20B5, c) HG40B5

The curing of all the samples is observed as a large exothermic peak, sign of a complex reactivity, characteristic for the humins resin. We can observe also from Figure 1 that the onset of crosslinking is around 35–45 °C and this value is more or less the same, whatever the system composition. This result could already translate that the presence of the bio-fillers didn't affect the curing initiation. The two bio-fillers could be considered, at this point, inert *vis-à-vis* of generation of active species that initiate the crosslinking. According to the data summarized in Table 1, it can be observed that for the HP40B5 formulation, the maximum temperatures of reaction of mixtures with chicken feathers powder or lignin decrease compared to that of the neat resins.

In the HP20G20B5 system, we can observe that the T_{max} of curing is not affected by the filler and the T_{max} values between the resin and the mixture resin-filler are almost the same. The area under the exothermic crosslinking peak was integrated in order to obtain the heat of cure ($\Delta_r H_{cure}$, J g⁻¹) of each formulation. In all the cases we can notice a decrease in the value of the reaction enthalpy when the filler is added. For HP40B5 and HG40B5 systems, the enthalpy of crosslinking in presence of CFP shows a relatively small decrease (≈ 20 J g⁻¹) compared to that of the neat resin, while the difference between the reactivity of resins and that of the mixtures with lignin is much higher (≈ 90 J g⁻¹). This result translates that nor the CFP nor the lignin enter in reactions with the resins and they play the role of inert fillers. The decrease in enthalpy is higher in the presence of the lignin, perhaps due to the morphology of lignin powder that is formed by bigger particles than the CFP's one. For the HP20G20B5 formulations with the two bio-fillers the heat of cure is similar (≈ 230 J g⁻¹). However, it is very difficult here to give a clear interpretation on the curing behavior since the humins crosslinking process is a very complex one, due to the complex composition of the neat humins. Moreover, this DSC study clearly shows that no chemical interaction between the CFP or L could be found with the humins resins. The allure of the DSC thermograms are very similar inside the same system. Nor the reaction onset, nor the end of reaction are affected by the presence of

the bio-fillers. The T_{max} suffers some changes together with the reaction enthalpy that is the most affected by the presence of the fillers.

Table 1. DSC analyses for curing of three reactive systems and their mixtures with chicken feathers powder or lignin

Sample	Reaction T_{max} (interval) (°C)			Enthalpy of reaction (J g ⁻¹)		
	Neat Resin	Mix Resin–10CFP	Mix Resin–10L	Neat Resin	Mix Resin–10CFP	Mix Resin–10L
HP40B5	164 ± 1 (42–215)	157 ± 2 (40–210)	146 ± 1 (45–206)	212 ± 3	192 ± 4	160 ± 4
HP20G20B5	157 ± 2 (40–230)	156 ± 1 (40–215)	153 ± 1 (48–217)	319 ± 2	228 ± 3	230 ± 3
HG40B5	154 ± 1 (38–228)	152 ± 1 (36–215)	149 ± 1 (33–208)	333 ± 4	313 ± 4	253 ± 3

3.2.1.2. Rheometry analysis during crosslinking

Rheometry analysis was used to study the evolution of viscosity and of the viscoelastic properties during the crosslinking reaction of the three humins-based systems and of their mixtures with the bio-fillers. Figure 2 give the results of the evolution of moduli (G' , G'') during curing of a selected system resins: the HG40B5 and its mixtures with the two bio-fillers, the influence of the filler amount being analysed. From the shape of the viscosity curves it can be seen the changes of the samples from a low-melting solid to a low viscosity liquid, thereafter to a gel, and at the end of the curing to a stiff solid.

According with the data displayed in Figure 2 and Table ES11, we can notice that the fillers' nature and ratio influence the rheological behavior of the systems during the curing. Firstly, we can notice that the resin mixture has almost the same viscosity that the resin with 10 wt.% L, both in the initial (unreacted) or final (crosslinked) state. This result is correlated with that of moduli, that are also very close for the resin and its mixture with the lignin. What we can observe is that the presence of the lignin provokes a small decrease, with some degrees, in the gelling point of the mixture. In contrast, the mixture with 10 wt.% CFP show a strong increase in the unreacted system's viscosity, with around a decade. This increase on viscosity could be correlated with the particle-particle interactions of CFP or by the interactions of the CFP particles with the resin, like hydrogen bonding between amino groups from keratin with oxygen based functional groups of the humins resins. The fact that the viscosity of the systems increases by the amount of the CFP (Figure ES11) could reinforce the first hypothesis by the thickening of the suspensions by particle-particle interactions. This behavior is also reflected in the increased values of the 10 wt.% CFP system moduli compared with that of the neat resin.

The sol-gel transition occurs at lower temperatures in this system that conduct to thermosets with higher stiffness.

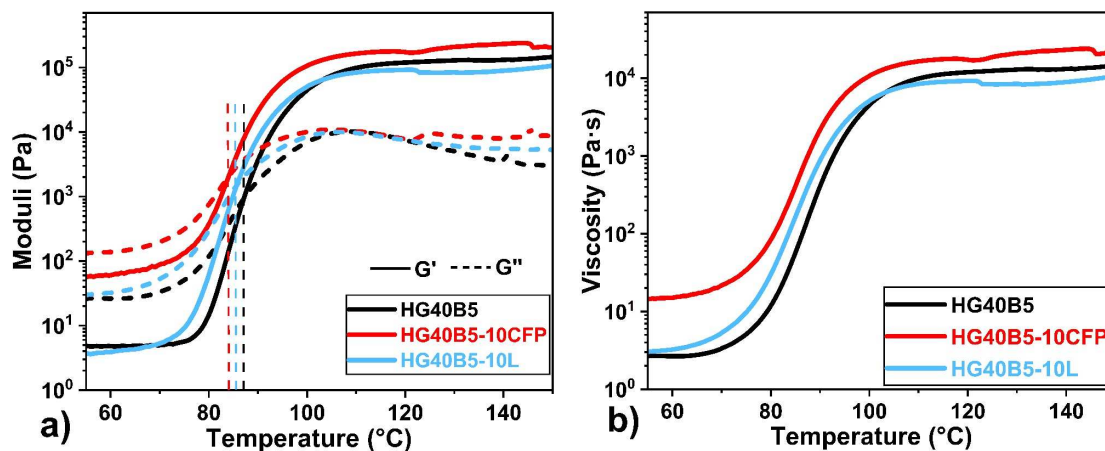


Figure 2. Rheology study of the unfilled HG40B5 curing system and their mixture with CFP and Lignin. Evolution of a) moduli and b) viscosity during heating from 50 °C to 200 °C at 0.2 °C min⁻¹. Comparison between unfilled, 10CFP and 10L filled resins.

If we corroborate the DSC and rheometry results, is somehow difficult to understand why the system with CFP has a higher reactivity, considering that the viscosity of this system is much higher than the neat resin. According with the literature, the filler effects on the chemorheology of thermosetting resins has not been studied extensively.⁶⁰ Chirayil *et al.*⁶¹ studied the rheological changes during the crosslinking of an unsaturated polyester system and the influence of nanocellulose filler which was extracted from *Helicteres isora* plant using steam explosion technique. They found that the presence of nanocellulose filler influences the rheological behavior of the systems during the curing process and the gelation process is shifted to smaller values seeing it a clear tendency of cure acceleration in the presence of the filler.

A comparison of rheological behavior between the HG40B5 curing system and its mixtures with different amounts of CFP or lignin is represented in Figure ESI1. It can be noticed that the viscosity and G' and G'' moduli are significantly higher in the case of systems with CFP while for the materials with lignin the values remain similar to that of the unfilled resin.

3.2.2. Physico-chemical characterization of bio-composites

3.2.2.1. Thermogravimetric analysis (TGA)

Thermogravimetric analyses (TGA) were carried out to determine the influence of the bio-fillers on the thermal stabilities of the cured materials as a function of temperature under oxidative atmosphere. The thermal stability of each resin is compared in Figure ESI3 with

three types of composites: i) composites with 10 wt.% CFP, ii) composites with 10 wt.% Lignin and iii) composites with 12 wt.% CFM. The temperature of degradation was considered at 5% of the weight loss of materials, the $T_{5\%}$ values being tabulated in Table 2. The thermal stability stipulated in the literature for the chicken feathers fibers is between 220 °C and 240 °C.^{62,63}

Table 2. Thermal characterization of the resins and bio-composites

	$T_{5\%}$ (°C)			
	Neat	Resin-10CFP	Resin-12CFM	Resin-10L
CFP	239			
CFM	236			
Lignin	202			
HP40B5	212	240	241	240
HP20G20B5	232	235	240	245
HG40B5	232	232	235	250

According to reported results^{64–67} it has been observed that the addition of chicken feathers as filler in a polymeric matrix decreases the thermal stability of the composites compared to the neat resin. Pourjavaheri *et al.*⁶⁵ developed by solvent-casting method new bio-composites using thermoplastic poly(ether urethane) as matrix and chicken feather fibers (CFF) as reinforcement. The thermal stability of the composites developed with 30 and 60 % w/w CFF was analyzed and compared with the neat resins, thus observing that the addition of the chicken feathers decreases the thermal stability of the final materials. If the $T_{5\%}$ of the neat resins is about 313 °C, the addition of 30% CFF decreased the thermal stability of the final material with around 40 °C, while the $T_{5\%}$ of the bio-composite with 60% CFF was \approx 249 °C. There are also studies in which the feathers improve the thermal stability of resins,^{7,68} as in our case. It can be seen that the nature of the polymer matrix does not affect the thermal behavior trend of the composites. The presence of the CFP or CFM in the three humins formulations improve the thermal stability ($T_{5\%}$) of the composites in a similar manner, while the addition of lignin in the polymer matrix provides a greater improvement in thermal stability compared to the composites with feathers. Following the thermogravimetric analyses it can be observed that the thermal stability of the bio-composites with CFP (230–240 °C, depending of the resin nature) is similar with that of the materials with CFM (235–243 °C), and for the composites with lignin the thermal stability is \approx 240–250 °C. These values indicate a good stability of the composites, being comparable to those already stipulated in the literature. For example, the thermal stability of the poly(urea-urethane)/chicken feathers bio-composites developed by Aranberri *et al.*⁶⁷ is between 205–240 °C depending on the polymer/CF ratio.

The shape of thermogram curve of the polymer matrix is similar with that with 10 wt.% lignin composites, presenting three main steps of degradation. The first degradation step of

pyrolysis presents the largest mass loss of lignin composites, being around 50–60%. Between 450–700 °C a second mass loss occur for systems under the air flow, with a lower mass loss compared to the first stage. Over 700 °C begins the complete degradation of the systems that takes place through the thermo-oxidation and carbonization reactions. The mechanism of thermal degradation of the composites with chicken feathers (10 wt.% CFP/ 12 wt.% CFM) it also consists of three main degradation steps, but these materials present also an additional very small degradation step ($\approx 1.5\%$ mass loss) between 40–170 °C which can be ascribe with the evaporation of absorbed water by the hydrophilic groups of the chicken feathers. The main step of thermal decomposition for composites with chicken feathers occurs between 200 °C and 450 °C where the material loss around 60% from its mass. From 450 °C to 650 °C take place the oxidative thermal degradation of $\approx 25\text{--}30\%$ of the CF composite weight mass. For the material with CFP or CFM the third step of thermal degradation arises faster than that of the neat matrix or of the composite with lignin.

3.2.2.2. Dynamic mechanical thermal analysis (DMA)

Dynamic mechanical analyses (DMA) were used to analyse the mechanical properties of the humins-based resins and their bio-composites. A sinusoidal stress was applied to determine the storage and loss moduli but also the damping factor of these materials. The effect of temperature and of the bio-fillers presence in the thermoset matrices on the storage modulus (E') and loss modulus (E'') of the samples at a frequency of 1.0 Hz are given in Figure 3 and Table ESI2.

According with the obtained data the filler influences both moduli of the materials. The storage modulus value in the glassy region (at around -70 °C) drops considerably in presence of the bio-filler in the polymer matrix. The order in which the E' decreases for all three resins and composites materials is as follows: Resins > Composites with 10L > Composites with 10CFP > Composites with 12CFM. Nevertheless, it is important to emphasize the composite behavior at higher temperatures, in the rubbery region. Is already know from literature^{69,70} that in the rubbery plateau, the storage modulus depends highly on the density of the material's crosslinks such that the bigger the crosslinking density of the materials, the smaller the drop of the storage modulus value. In the case of composites with lignin, the loss modulus values in the glassy region are similar to that of neat resins, meanwhile a significant increase occurs in the case of composites with feathers, the highest being for the materials with CFM. We can observe that for HP40B5 system, the addition of 12 wt.% CFM increases with four times the E'' modulus value in glassy plateau (from 1 to 5 MPa), while for the HG40B5 the increase is up to eight higher compared to the neat matrix (from 6 to 42 MPa).). Also, the DMA tests can generate important information about a mechanical parameter important in the design and production of materials, namely their brittleness (B). Following the studies developed by W.

Brostow *et al.*^{71–73} it has been shown that the brittleness (B) of the materials is inversely proportional to the storage modulus (E') at a frequency of 1.0 Hz.

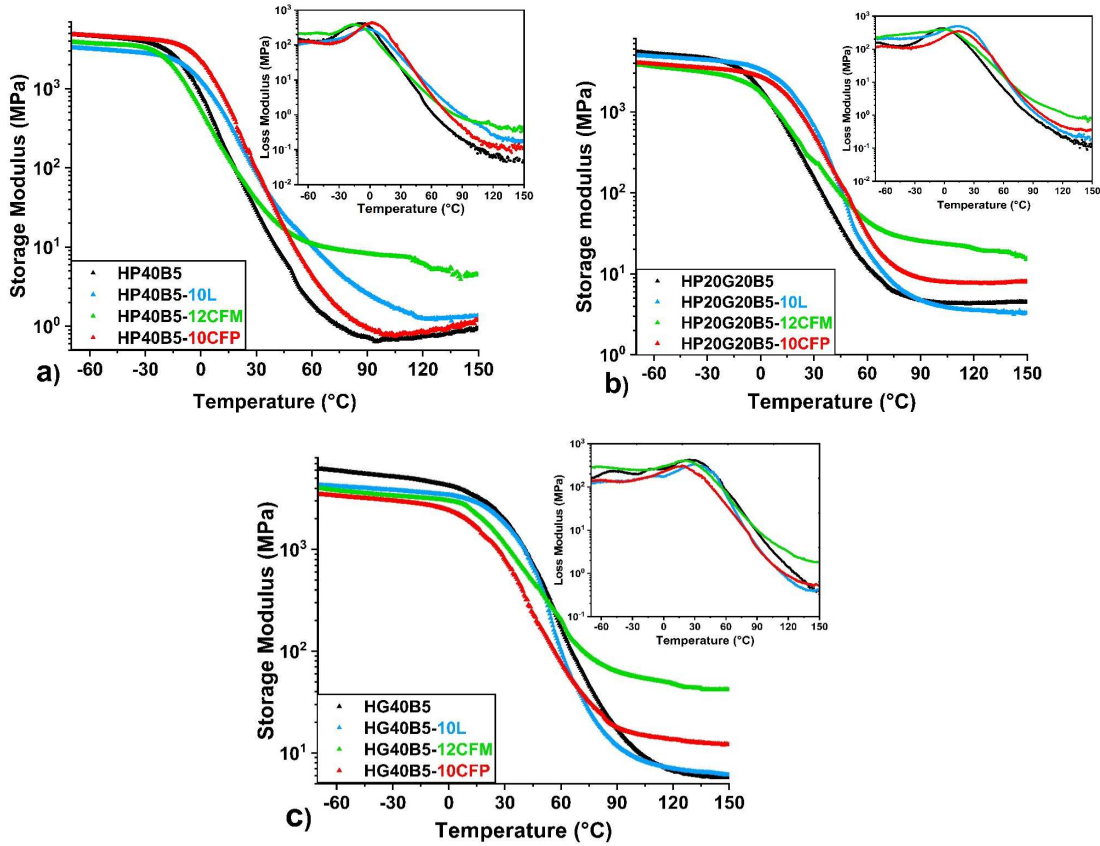


Figure 3. Comparison of the evolution of storage and loss moduli vs. temperature for the three humins-based resins (black line) and their bio-composites with: Resin-10L (blue line), Resin-10CFP (red line), Resin-12CFM (green line)

The crosslinking density of the materials was also calculated (Table ESI2) using the Flory's theory⁷⁴ and compared with the values obtained for the neat resins. In the Figure 4 is represented the evolution with temperature of the damping factor of the resin's materials and their bio-composites. The damping factor was determined by the ratio between the loss and the storage moduli (E''/E') and showing the width of the glass transition regions of the materials.⁷⁵ For the composites with 12CFM it can be observed a decrease of the intensity of $\tan \delta$ peak and also a shift of its maximum to lower temperatures compared with the neat resins which means that the reinforcement improves the elasticity of the materials. According to the maximum values of $\tan \delta$ peak, CFP act differently on the polymer resin depending on its nature. From Figure 4a we can observe that the damping factor curves for the HP40B5 elastic matrix and for the composite with CFP are similar, showing the same height of the peak but the maximum of $\tan \delta$ of the resin is higher with 5 °C compared with the composite. This

similarity between the two curves may show that the chicken feathers powder is fully compatible and integrated in the elastic matrix composition, the crosslinking density being almost the same ($0.7\text{--}0.8\text{ mmol cm}^{-3}$). In the case of the rigid resin, HG40B5, the maximum value of $\tan \delta$ is shifted to a lower temperature which means that the CFP filler acts like a plasticizer for the matrix.

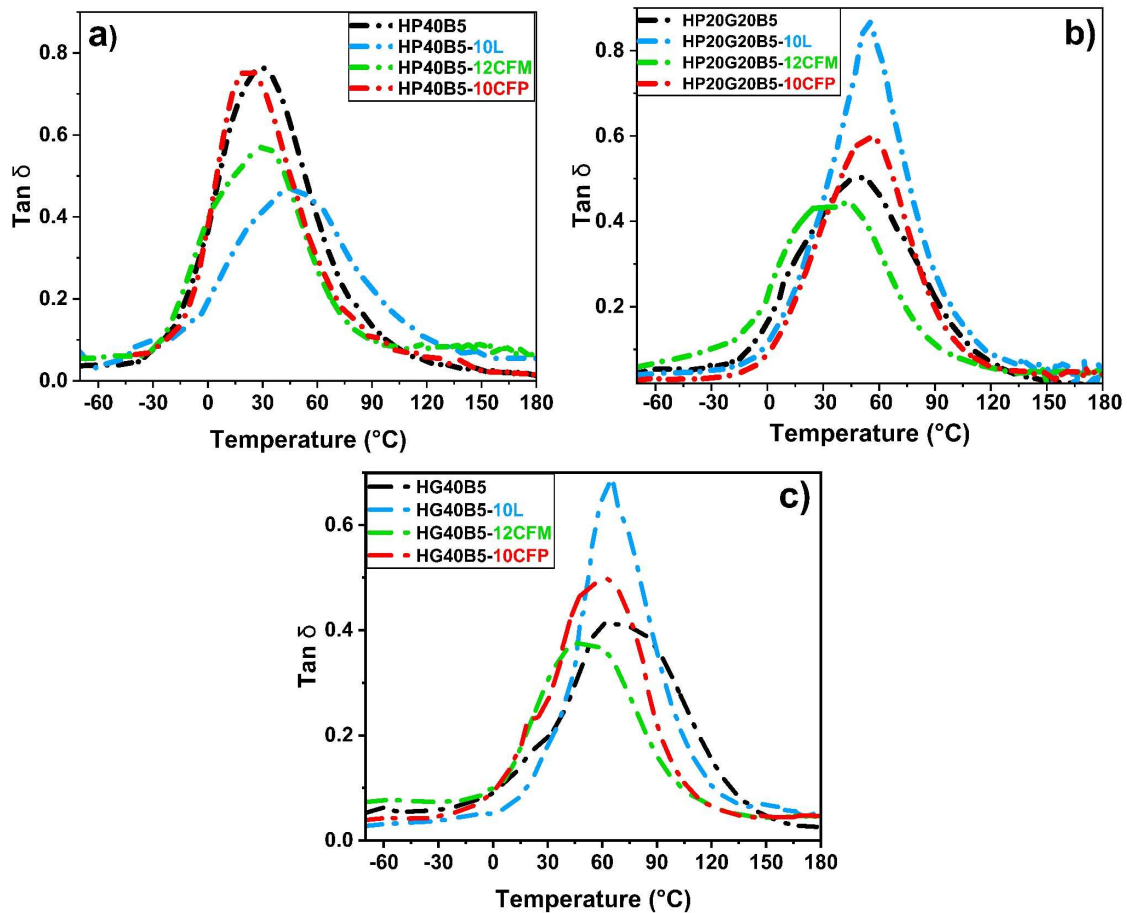


Figure 4. Evolution with temperature of $\tan \delta$ of the three resins and their bio-composites

The thermal properties of the materials measured by DMA according with ASTM D7028-07⁷⁶ were in accordance with the results obtained by DSC and are presented in Table ESI3. The density of materials is an important concept in terms of their use, representing the degree of compactness of materials; mathematically it is defined as mass divided by volume ($\rho = m/v$). So, two materials with the same weight can have different density, the lower dense material occupying more volume than higher dense material. Therefore, the resins and composites densities (Table 3) were determined and compared in order to analyze the influence of the bio-filler.

Table 3. Density of the three resins and their related composites

Sample	Density (g cm ⁻³)		
	HP40B5	HP20G20B5	HG40B5
Neat Resin	1.23	1.22	1.25
Resin- 10L	1.25	1.28	1.29
Resin- 12CFM	1.11	1.10	1.11
Resin- 10CFP	1.10	1.11	1.01

According with the literature, it was already reported^{10,11} that the properties of chicken feathers make them preferable for several applications due to their low-density (0.8 g cm⁻³) compared with that of the wool (1.3 g cm⁻³) or cellulose fibers (1.5 g cm⁻³). The density values determined for the HP40B5, HP20G20B5 and HG40B5 resins are 1.23, 1.22 and 1.25 g cm⁻³, respectively. As can be seen in Table 3, the addition of lignin to the polymeric matrix increases the density of the composites with approximately 0.02–0.06 g cm⁻³ compared to the neat resins. For the composites developed with CFP or CFM, the low density of the chicken feathers decreased the density of the composites, thus obtaining values between 1.01 and 1.11 g cm⁻³.

3.2.2.3. Tensile testing

The mechanical properties of the materials are essential parameters determining the industrial area of their use. The Young's modulus, tensile strength and the elongation at break of each type of humins-based resin were compared with the values obtained for the composites made with lignin, chicken feathers powder or mat and are presented in Figure 5 and Table 4. According with the reported results^{64,77,78}, the reinforcement of polymeric matrix with chicken feathers decreases more or less the elongation at break or the tensile strength of the composites.

Fully biodegradable bio-composite were developed by Aranberri *et al.*⁶⁶ using three biodegradable matrices (polylactic acid (PLA), polybutyrate adipate terephthalate (PBAT) and a PLA/thermoplastic copolyester blend) and a high loadings of chicken feathers (50–60 wt.%) as reinforcement. The authors investigated and compared the mechanical properties of the three matrices with those obtained for bio-composites with CF. It was observed that the addition of feathers affects the mechanical properties of the composites in comparison with the neat matrix (*e.g.* elongation at break from 570% for PBAT resin decreased to 2.5% for PBAT 50% /CF 50% bio-composite), but on the other way improved the lightweight and thermal-insulating of the materials converting them as a good alternative to wood-plastic composites. In another study⁶⁷, were developed composites with poly(urea-urethane)/chicken feather fibers (different ratios) with similar mechanical properties to those presented in this study. The Young's modulus of the composites developed by Aranberri *et al.*⁶⁷ is range 1.2–410 MPa in function of the polymer/CF ratio, while for the bio-materials developed in this study is from 1 MPa to 800 MPa depending on the resin or filler nature.

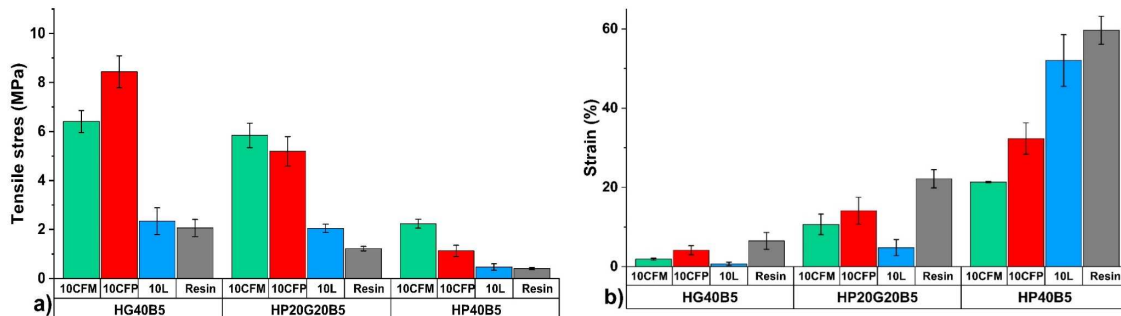


Figure 5. Comparison between tensile properties of the neat resins and composites: a) tensile stress; b) strain of the materials

From figure 5 we can highlight that the tensile stress values of all bio-composites were considerably improved compared to that of resins, but this improvement depends on the nature of the filler but also of the resin formulation. Considering the nature of the bio-filler, it can be observed that the tensile strength of the composites increases in the following bio-filler order: $L < CFP < CFM$, apart from the HG40B5 resin where the bio-composites with chicken feathers powder show the highest increase in tensile strength. In the case of HP40B5 ductile matrix, the tensile strength of the composite with lignin was improved with 13% compared with the neat resin. For the same matrix, the composite with 10CFP has a tensile modulus with 64% higher while the composite with 12CFM has a tensile value increased with 82% compared to that of the matrix. For the HG40B5 rigid matrix, the addition of lignin improved the tensile modulus with 12%, while the addition of 10 CFP enhanced the tensile strength with 76% and the addition of 12CFM with 68% compared with the neat resin. Such results could be the effect from a better stress transfer between the matrix and the bio-fillers. The elongation at break of the bio-composites decreases (depending on the nature of the filler) which shows that the fillers increased the materials' rigidity. The stiffness of the obtained materials, defined by the relationship between stress and strain in the linear elasticity regime of a uniaxial deformation, are presented in Table 4 as Young's modulus values. As in the case of strain results, the values of the Young's modulus were considerably improved for all three types of bio-composites, but the highest values were obtained for the composites with 12 wt.% CFM. For example, in the case of the HP40B5 elastic resin the Young's modulus value was improved from 1 to 22 MPa, while for the HG40B5 (rigid resin) the increase was from 106 to 443 MPa. Consulting the MatWeb online database (<http://www.matweb.com/index.aspx>), the mechanical properties of the materials developed in this study have been compared with the commercial ones showing that have comparable performances for *e.g.* with Silicone Rubber/Fiberglass, Epoxy/Carbon Fiber Composites.

Table 4. Tensile properties of the three neat resins and composites materials

		Young's Modulus (MPa)	Maximum Stress (MPa)	Maximum Strain (%)
HP40B5	Neat Resin	1.01 ± 0.08	0.41 ± 0.04	59.66 ± 3.53
	Resin-10L	1.60 ± 0.40	0.47 ± 0.13	52.02 ± 18.25
	Resin-10CFP	5.05 ± 1.18	1.13 ± 0.23	32.33 ± 3.94
	Resin-12CFM	22.36 ± 4.96	2.24 ± 0.18	21.37 ± 1.49
HP20G20B5	Neat Resin	8.29 ± 0.61	1.22 ± 0.09	22.16 ± 2.3
	Resin-10L	105.85 ± 22.65	2.05 ± 0.17	4.82 ± 2.04
	Resin-10CFP	112.81 ± 27.84	5.19 ± 2.22	14.12 ± 6.41
	Resin-12CFM	134.02 ± 39.10	5.84 ± 0.90	10.66 ± 2.58
HG40B5	Neat Resin	106.1 ± 39.82	2.06 ± 0.55	6.49 ± 2.11
	Resin-10L	667.18 ± 260.91	2.34 ± 1.16	0.71 ± 0.42
	Resin-10CFP	346.30 ± 57.13	8.44 ± 1.25	4.17 ± 1.14
	Resin-12CFM	442.76 ± 17.92	6.41 ± 0.70	1.90 ± 0.26

3.2.2.4. Water absorption

The water absorptions of the neat resins and their bio-composites with 10 wt.% CFP, 12 wt.% CFM and 10 wt.% L are represented in Figure ESI4. The samples were immersed in distilled water at 25 °C and have been maintained until they have reached a steady state. Both resins and composites were kept in the water for 11 days, their weight being measured daily. It can be observed that the water absorption (average value) of the neat resins increases with the increasing of the elasticity of the materials: HG40B5 (10.1% WA%) < HP20G20B5 (11.3% WA%) < HP40B5 (13.4% WA%). For the composites with 10 wt.% L was observed an increasing of water absorption with around 2–4% compared with the neat resins. In the case of bio-composites with 10 wt.% CFP and with 12 wt.% CFM the water gain is similar. By comparing the percentage of water absorbed by neat resins with that absorbed by the bio-composites with CFP and CFM (\approx 24–26% WA%), one can observe that the water absorption increases two times for the last one. According to the literature^{9,11,19,79}, the high water gain of the composites with feathers compared with that of resins is mainly attributed to the high hygroscopic character of keratin from feathers. The results obtained are in agreement with the results already published^{39,66,67,80}, in which the addition of CFP's increases significantly the water absorption in a composite irrespective of the nature of the polymeric matrix.

3.2.2.5. Scanning electron microscopy (SEM)

To study the compatibility and the adhesion between the bio-fillers and the resins, the obtained composites were analyzed by SEM. In the Figure 6 are revealed the SEM results at different resolutions as 100 μ m, 50 μ m and 10 μ m for the composites developed with 10 wt.% CFP.

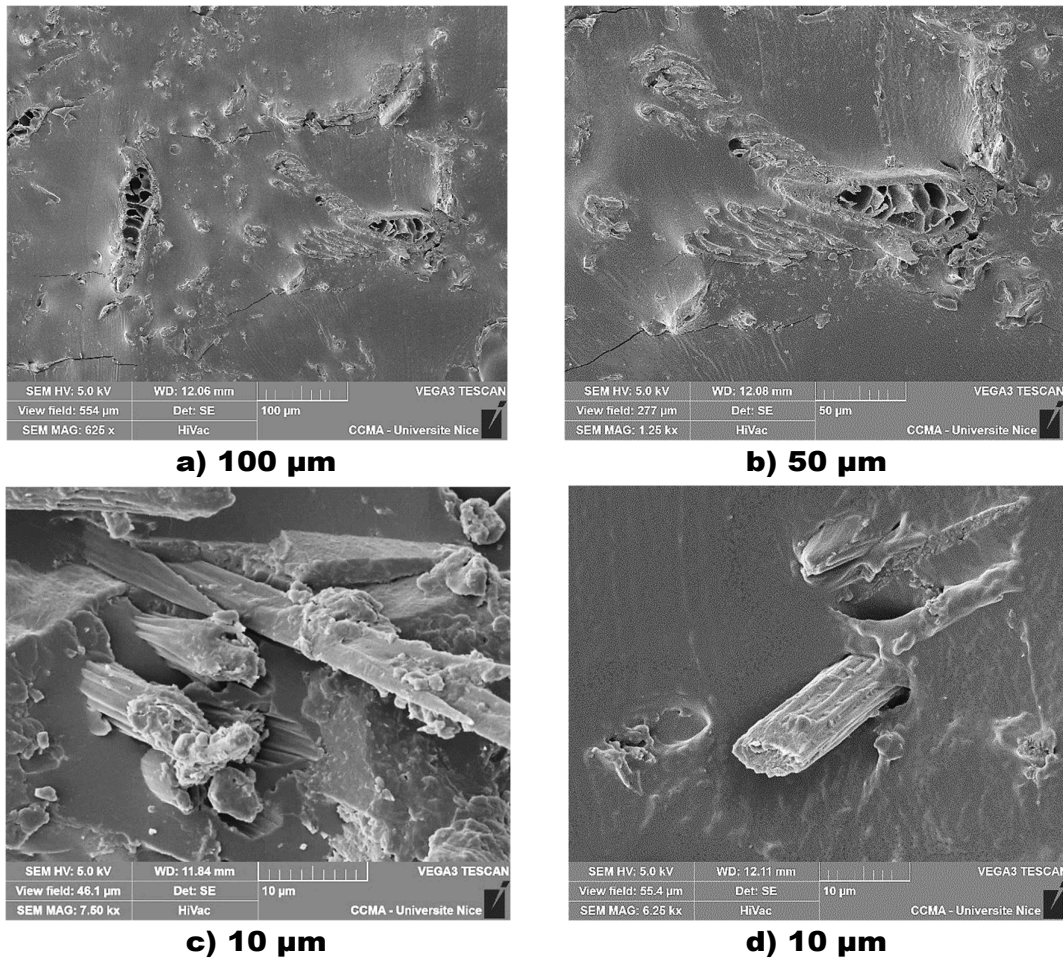


Figure 6. SEM images for HG40B5 composites with 10 wt.% CFP

The surface's fracture of the composites was analyzed to evaluate the adhesion of the matrix on the chicken feathers but also the appearance of the resin. It can be observed that the compatibility between chicken feathers and humins-based matrix is very good, we cannot observe spaces or voids between the humins polymeric matrix and the CF fibers. It can also be seen that the humins matrix remains attached to the fibers after the sample fracture. In the same time, the surface of the humins-matrix shows a smooth and homogeneous appearance.

3.3. Conclusions

In this study, bio-composites were developed using three types of humins-based resins and chicken feathers powder, chicken feathers non-woven mat or lignin. The influence of nature and amount of filler on the crosslinking reactions were studied by DSC analyses and rheology and compared with the corresponding neat resins. Therefore, the thermomechanical properties of the obtained bio-composites were investigated. The thermal stability of the

composites was maintained or improved with around 20–30 °C compared with the resins. The DMA analyses show that the filler influences the storage modulus of the bio-composites. In the glassy region (-70 °C) this modulus significantly decreases for all bio-composite materials. In the rubbery plateau, the E' values of the composites with lignin are similar with that of neat resins, while that of the bio-composites with chicken feathers increased considerably. It has to be noticed that not only the nature of the filler influences the mechanical properties of the materials, but also its form, the composites with chicken feathers powder having a lower value of the storage modulus compared to the materials developed with chicken feathers mats.

The mechanical tensile properties of the bio-composites were considerably improved compared with that of the resins. In the case of the ductile matrix the tensile modulus increased by 82%, in presence of 12CFM, while for the rigid matrix the increase was till 76% with 10CFP. Then, for the ductile matrix the Young's modulus value was improved from 1 to 22 MPa, while for the rigid matrix the increase was from 106 to 443 or 667 MPa, in the case of composites with chicken feathers non-woven mat or lignin.

The addition of the bio-fillers in the humins matrix affect the water absorption behavior. The bio-composites with lignin show an increase in water stability of about 2–4% compared to the neat resins, while that with feathers increased twice times. The compatibility between humins-based resins and the chicken feathers is excellent, a very good adhesion between the polymer matrix and the reinforcing material was observed by SEM.

In conclusion, humins-based resins were successfully reinforced with natural and valuable bio-fillers obtained by industrial wastes, thus obtaining eco-friendly composite materials with properties that could recommend them for various industrial applications.

3.4. Experimental

3.4.1. Materials

The main component of the elaborated resins is represented by the humins, an industrial by-product, produced and supplied by Avantium Chemicals at their Pilot Plant in Geleen, The Netherlands. To obtain thermoset resins, humins were mixed with comonomers like poly(ethylene glycol) diglycidyl ether (PEGDE) and glycerol diglycidyl ether (GDE). As crosslinking initiator was used the N,N-Dimethylbenzylamine (BDMA). Except the humins, all the chemicals were purchased from Sigma-Aldrich and used as received. The protocol of resins' preparation was described elsewhere.⁸¹ To develop composites, the humins-based mixtures were combined with different industrial wastes like chicken feathers (from food industry) or lignin (from biorefineries) which were used as structural elements for reinforcing the humins polymeric matrix. The fractioned Kraft lignin used in this work is a brown powder with a weak odour, a pH ranged between 2.5–7 and sulfur content 1–3%. This product is not

soluble under acidic condition, but is soluble under alkaline condition, in DMSO, and was supplied by VTT Technical Research centre of Finland. The chicken feathers were firstly cleaned at 95 °C for 2h with a neutral cleaning solution, bleached with hydrogen peroxide (4%) for 14h and then were sterilized by Grupo SADA p.a.S.A from Spain. The sanitised chicken feathers were then grinded and supplied by Institute of Biopolymers and Chemical Fibres (IBWCh) from Poland. In order to produce the humins/chicken composites, two different types of chicken feathers were tested like powder- and non-woven fibres. Chicken feather powder (CFP) were obtained using a Planetary Ball Mill (Type: XQM-16 A) and an industrial shredder with a smooth adjustment (Type: MK 15-200 B-S) in order to achieve a high degree of fragmentation (10-250 µm). The non-woven chicken feathers mat (CFM) were produced by IBWCh by combining 90 wt.% chicken feathers fibres with 10 wt.% bicomponent synthetic fibres, core PET, Type T25 Biko flat 2.2 dtex, semi-matte, used in the production of wet-laid non-woven.⁸²

3.4.1.1. Samples preparation

The humins-based resins were developed as previously described⁸¹ by mixing the required amount of humins with the comonomers (PEGDE and GDE) and the initiator (BDMA), thus obtaining three different kind of resins with mechanical properties ranging from elastic to the rigid. For an easier identification of the resins, acronyms have been used, depending on the composition, to name the mixtures as follows: Humins55% /PEGDE40% /BDMA5% = HP40B5 for the flexible resin, Humins55% /PEGDE20% /GDE20% /BDMA5% = HP20G20B5 for the semi-elastic matrix and Humins55% /GDE40% /BDMA5% = HG40B5 for the rigid one. The bio-composites in which 10 wt.% of chicken feathers powder (CFP) or 10 wt.% lignin (L) act as bio-filler components were made by combining the fresh resins mixtures with the required amounts of filler by mechanically mixing, continuously, until the mixture was completely homogenized. The mixtures of resin/chicken feather powder or resin/lignin were poured in a rectangular metallic mould (150 × 150 × 4 mm³) and cured using a heated press (Bench Top Manually Heated Mini CH 5420 Model Press, Carver Inc.) for 4 hours at 130 °C and 2 metric tons pressure. The composites with chicken feathers mat were developed using a hand lay-up technique in order to obtain a humins/chicken feathers prepreg. Composite panels with non-woven chicken feathers fibres were consolidated from three plies of mats; the number of plies was selected to achieve a thickness of approximately 0.4 cm. In the rectangular metallic mould covered with Kapton film to facilitate an easy removal of the laminate, a layer of resin was poured. Thereafter, the first non-woven mat was laid in the mould being covered with a second layer of resin. The composites were placed between the platens of the Carver press and cured during 4 hours at 130 °C and 2 metric tons pressure. After curing under compression, the samples were cooled and removed from the metallic moulds.

Following the calculation, it was determined that the 2 plies of mats represent 12 wt.% of the total weight of the CF mat in the composite. The acronyms of the composites were reported as the “resin name” then complementing with the initials of the filling present in the composite. The chicken feather powder was abbreviated with “CFP”, the lignin with “L” and the chicken feathers mat with “CFM”. So, if the material was developed combining the HG40B5 resin with 10 wt.% CFP, the final composite was called HG40B5–10CFP.

3.4.2. Experimental techniques

3.4.2.1. Density of the composites

The ISO 9427 standard was used to experimentally determine the density of the humins-based resins and composites. Five rectangular samples ($50 \times 8 \times 4 \text{ mm}^3$) of each specimen with a known volume were weighed. The density of the samples was then calculated as the ratio of the mass to volume.

3.4.2.2. Differential Scanning Calorimetry (DSC)

A DSC 3 Mettler-Toledo apparatus controlled by STARe Software developed by Mettler-Toledo was used. The calibration of the instrument heat flow and temperature was done using water, indium and zinc standards. Samples of 10–15 mg were placed into 100 μL aluminum crucibles. The crosslinking reaction were studied under non-isothermal conditions, at a heating rate of $10 \text{ }^\circ\text{C min}^{-1}$ under air flow (150 mL min^{-1}), over a temperature range of 25–250 $^\circ\text{C}$. The reactions’ enthalpies of humins-resins and fillers mixtures were normalized to the mass of resin in the analyzed compositions. After the curing of the materials, the DSC was also used to determine the first-order transitions like eventual residual exothermy or the second-order transitions like the glass transitions of the obtained materials and composites. Samples of crosslinked humins-based composites with the mass between 9–12 mg were scanned at $10 \text{ }^\circ\text{C min}^{-1}$ under air flow (150 mL min^{-1}) from $-50 \text{ }^\circ\text{C}$ to $180 \text{ }^\circ\text{C}$.

3.4.2.3. Rheometry

To determine the influence of the bio-fillers on the cross-linking process different amounts of chicken feathers powder or lignin were added to the reactive resins mixtures and then analysed by rheometry. Rheological measurements were conducted under nitrogen atmosphere in an Anton Paar MCR-302 rheometer using disposable plate-plate geometries (25 mm diameter and 1 mm gap). The measurements were made at a scan rate of $0.2 \text{ }^\circ\text{C min}^{-1}$ from $50 \text{ }^\circ\text{C}$ to $200 \text{ }^\circ\text{C}$. To determine the storage modulus (G') and loss modulus (G'') but also the complex viscosity of the samples, the measurements were conducted by oscillatory shear experiments with an angular frequency of 10 rad s^{-1} and a deformation of 0.2%.

3.4.2.4. Thermogravimetric analysis (TGA)

Thermal stability of humins-based composites was studied using thermogravimetric analysis (TGA). The mass loss and its derivative as a function of temperature for the cured samples were evaluated using a TGA 2 Mettler-Toledo over a temperature range of 25 °C–1000 °C under oxidative atmosphere (150 mL min⁻¹) and a heating rate of 10 °C min⁻¹. Samples with the mass between 10–15 mg of each formulation were placed into 70 µL alumina pans and analysed three times for average calculation.

3.4.2.5. Dynamic mechanical analysis (DMA)

Mechanical properties of the composites (storage modulus E' , loss modulus E'' and damping factor $\tan \delta = E''/E'$) were analysed in a DMA 1 by Mettler-Toledo using a three-point bending fixture at an oscillatory frequency of 1.0 Hz and an amplitude of 20 µm. The rectangular samples with the dimensions of 48 × 8 × 4 mm³ (length × width × thickness) were analysed three times and the values averaged. The temperature ramp was selected from -150 to 180 °C at a heating rate of 3 °C min⁻¹ under nitrogen atmosphere.

3.4.2.6. Tensile testing

The tensile properties of the materials were determined by a universal testing machine Instron, Norwood, MA, USA model 3365, controlled by BlueHill Lite software developed by Instron (Norwood, MA, USA). For the test, a crosshead speed of 10 mm min⁻¹ was used on samples of dimension 75 × 10 × 4 mm³ (length × width × thickness).

Ten samples for each formulation were tested in order to evaluate the average calculations of mechanical properties like Young's modulus, tensile strength, and elongation at break.

3.4.2.7. Water absorption

Water absorption of the humins-based resins and composites were determined by immersion of the samples in distilled water at 25 °C in accordance with the ASTM D570 standard test method.⁸³ In the first step, the rectangular test specimens (50 × 8 × 4 mm³) were dried in an oven at 50 °C for 24h, after cooled in a desiccator and immediately weighed. Then, the specimens were immersed in distilled water and maintained at room temperature for 24 hours. At the end of the 24h, the samples were removed from water and all the surface water wiped off with a dry cloth. Thereafter, the so prepared specimens were weighed and immediately immersed again in distilled water and then the percentage of absorbed water (%WA) was calculated.

3.4.2.8. Scanning electron microscopy (SEM)

The morphology of fracture surfaces of the bio-composites but also the compatibility between the humins based matrix and the filler were investigated by scanning electron

microscopy (SEM). The sample were analyzed using a Tescan Vega XMU SEM at an accelerating voltage of 5 kV. All samples were coated with platinum prior to observations.

Acknowledgements

Funding for this work was received from the European Union's Horizon 2020 Research and Innovation program under Grant Agreement 723268 on a project KaRMA2020.

Also, the authors acknowledge M. Francois Orange for his help and assistance with SEM observations performed at CCMA Common Centre of Applied Electronic Microscopy of University Côte d'Azur. CCMA electron microscopy equipment has been funded by the Region Sud - Provence-Alpes-Côte d'Azur, the Conseil General des Alpes Maritimes, and the GIS-IBiSA.

Notes and references

- (1) Brostow, W.; Hagg Lobland, H. E. *Materials: Introduction and Applications*; John Wiley and Sons, 2017.
- (2) Poole, A. J.; Church, J. S.; Huson, M. G. Environmentally Sustainable Fibers from Regenerated Protein. *Biomacromolecules* **2009**, *10* (1), 1–8. <https://doi.org/10.1021/bm8010648>.
- (3) Garrido, T.; Peñalba, M.; De la Caba, K.; Guerrero, P. A More Efficient Process to Develop Protein Films Derived from Agro-Industrial by-Products. *Food Hydrocoll.* **2019**, *86*, 11–17. <https://doi.org/10.1016/j.foodhyd.2017.11.023>.
- (4) Gorobets, L.; Kovalchuk, O. Birds in the Medieval Culture and Economy of the East Slavs in the 10–13th Centuries AD. *Environ. Archaeol.* **2017**, *22* (2), 147–165. <https://doi.org/10.1080/14614103.2016.1141088>.
- (5) FAO. *Food Outlook - Biannual Report on Global Food Markets*; 2019.
- (6) McLelland, J. *A Colour Atlas of Avian Anatomy*; Wolfe Publishing Ltd: London, 1990.
- (7) Martínez-Hernández, A. L.; Velasco-Santos, C.; De-Icaza, M.; Castaño, V. M. Dynamical–Mechanical and Thermal Analysis of Polymeric Composites Reinforced with Keratin Biofibers from Chicken Feathers. *Compos. Part B Eng.* **2007**, *38* (3), 405–410. <https://doi.org/10.1016/j.compositesb.2006.06.013>.
- (8) Bansal, G.; Singh, V. K. Review on Chicken Feather Fiber (CFF) a Livestock Waste in Composite Material Development. *Int. J. Waste Resour.* **2016**, *6* (4), 4–7. <https://doi.org/10.4172/2252-5211.1000254>.
- (9) Martínez-Hernández, A. L.; Velasco-Santos, C. Keratine Fibers from Chicken Feathers: Structure and Advances in Polymer Composites. In *Keratin: Structure, Properties and Applications*; Dullaart, R., Ed.; 2012; pp 149–211.
- (10) Tesfaye, T.; Sithole, B.; Ramjugernath, D.; Chunilall, V. Valorisation of Chicken Feathers: Characterisation of Physical Properties and Morphological Structure. *J. Clean. Prod.* **2017**, *149*, 349–365. <https://doi.org/10.1016/j.jclepro.2017.02.112>.
- (11) Reddy, N.; Yang, Y. Structure and Properties of Chicken Feather Barbs as Natural Protein Fibers. *J. Polym. Environ.* **2007**, *15* (2), 81–87. <https://doi.org/10.1007/s10924-007-0054-7>.
- (12) Seawright, R. A.; Marcicano, J. P. P.; Navarrete, F. C. Study of Physical Properties of Chicken Feathers for Commercial Use. **2013**, *3* (2), 1–7.

- (13) Sah, N.; Goel, A.; Omre, P. K. Characterization of Chicken Feather Fibre as Novel Protein Fiber for Commercial Applications. *Int. J. Trop. Agric.* **2015**, *33* (4), 3373–3378.
- (14) Barone, J. R.; Schmidt, W. F. Polyethylene Reinforced with Keratin Fibers Obtained from Chicken Feathers. *Compos. Sci. Technol.* **2005**, *65* (2), 173–181. <https://doi.org/10.1016/j.compscitech.2004.06.011>.
- (15) Lewin, M. *Handbook of Fiber Chemistry*, 3rd ed.; CRC Press Taylor & Francis Group: New York, 2007.
- (16) Khosa, M. A.; Ullah, A. A Sustainable Role of Keratin Biopolymer in Green Chemistry : A Review. *J. Food Process. Beverages* **2013**, *1* (1), 1–8.
- (17) Wallenberger, F. T.; Weston, N. E. *Natural Fibers, Plastics and Composites*; Springer Science+Business Media: New York, 2004. <https://doi.org/10.1007/978-1-4419-9050-1>.
- (18) Saravanan, K.; Dhurai, B. Exploration on Amino Acid Content and Morphological Structure in Chicken Feather Fiber. *J. Text. Apparel, Technol. Manag.* **2012**, *7* (3), 1–6.
- (19) Staron, P.; Banach, M.; Kowalski, Z. Keratin – Origins, Properties, Application. *Chemik* **2011**, *65* (10), 1019–1026.
- (20) Pauling, L.; Corey, R. B.; Branson, H. R. The Structure of Proteins: Two Hydrogen-Bonded Helical Configurations of the Polypeptide Chain. *Proc. Natl. Acad. Sci. U. S. A.* **1951**, *37* (4), 205–211.
- (21) Astbury, W. T.; Street, A. X-Ray Studies of the Structure of Hair, Wool, and Related Fibres.- I. General. *Philos. Trans. R. Soc. A* **1931**, *230*, 681–693.
- (22) Fraser, R. D. B.; MacRae, T. P. The Structure of α -Keratin. *Polymer (Guildf)*. **1973**, *14* (February), 61–67.
- (23) Fraser, R. D. B.; Macrae, T. P.; Parry, D. A. D.; Suzuki, E. The Structure of β -Keratin. *Polymer (Guildf)*. **1969**, *10*, 810–826. [https://doi.org/10.1016/0032-3861\(69\)90110-4](https://doi.org/10.1016/0032-3861(69)90110-4).
- (24) Fraser, R. D. B.; Parry, D. A. D. The Structural Basis of the Filament-Matrix Texture in the Avian/Reptilian Group of Hard β -Keratins. *J. Struct. Biol.* **2011**, *173* (2), 391–405. <https://doi.org/10.1016/j.jsb.2010.09.020>.
- (25) Sharma, S.; Gupta, A. Sustainable Management of Keratin Waste Biomass: Applications and Future Perspectives. *Brazilian Arch. Biol. Technol.* **2016**, *59* (December), 1–14. <https://doi.org/10.1590/1678-4324-2016150684>.
- (26) Wang, B.; Yang, W.; McKittrick, J.; Meyers, M. A. Keratin: Structure, Mechanical Properties, Occurrence in Biological Organisms, and Efforts at Bioinspiration. *Prog. Mater. Sci.* **2016**, *76*, 229–318. <https://doi.org/10.1016/j.pmatsci.2015.06.001>.
- (27) Xu, H.; Cai, S.; Xu, L.; Yang, Y. Water-Stable Three-Dimensional Ultrafine Fibrous Scaffolds from Keratin for Cartilage Tissue Engineering. *Langmuir* **2014**, *30* (28), 8461–8470. <https://doi.org/10.1021/la500768b>.
- (28) Wang, J.; Hao, S.; Luo, T.; Yang, Q.; Wang, B. Development of Feather Keratin Nanoparticles and Investigation of Their Hemostatic Efficacy. *Mater. Sci. Eng. C* **2016**, *68*, 768–773. <https://doi.org/10.1016/j.msec.2016.07.035>.
- (29) Reddy, N. Non-Food Industrial Applications of Poultry Feathers. *Waste Manag.* **2015**, *45*, 91–107. <https://doi.org/10.1016/j.wasman.2015.05.023>.
- (30) Reddy, N.; Chen, L.; Yang, Y. Biothermoplastics from Hydrolyzed and Citric Acid Crosslinked Chicken Feathers. *Mater. Sci. Eng. C* **2013**, *33* (3), 1203–1208. <https://doi.org/10.1016/j.msec.2012.12.011>.
- (31) Shi, Z.; Reddy, N.; Hou, X.; Yang, Y. Tensile Properties of Thermoplastic Feather Films Grafted with Different Methacrylates. *ACS Sustain. Chem. Eng.* **2014**, *2*, 1849–1856.
- (32) Gurav, R. G.; Jadhav, J. P. A Novel Source of Biofertilizer from Feather Biomass for Banana Cultivation. *Env. Sci Pollut Res* **2013**, 4532–4539. <https://doi.org/10.1007/s11356-012-1405-z>.

- (33) Hadas, A.; Kautsky, L. Feather Meal, a Semi-Slow-Release Nitrogen Fertilizer for Organic Farming. *Fertil. Res.* **1994**, *38* (2), 165–170. <https://doi.org/10.1007/BF00748776>.
- (34) Donato, R. K.; Mija, A. Keratin Associations with Synthetic, Biosynthetic and Natural Polymers: An Extensive Review. *Polymers (Basel)*. **2019**, *12* (1), 32. <https://doi.org/10.3390/polym12010032>.
- (35) Yin, X.; Li, F.; He, Y.; Wang, Y.; Wang, R. Study on Effective Extraction of Chicken Feather Keratins and Their Films for Controlling Drug Release. *Biomater. Sci.* **2013**, *1* (5), 528. <https://doi.org/10.1039/c3bm00158j>.
- (36) Song, N. B.; Lee, J. H.; Al Mijan, M.; Song, K. B. Development of a Chicken Feather Protein Film Containing Clove Oil and Its Application in Smoked Salmon Packaging. *LWT - Food Sci. Technol.* **2014**, *57* (2), 453–460. <https://doi.org/10.1016/j.lwt.2014.02.009>.
- (37) Yang, Y.; Reddy, N. Utilizing Discarded Plastic Bags as Matrix Material for Composites Reinforced with Chicken Feathers. *J. Appl. Polym. Sci.* **2013**, *130* (1), 307–312. <https://doi.org/10.1002/app.39173>.
- (38) Huda, S.; Yang, Y. Composites from Ground Chicken Quill and Polypropylene. *Compos. Sci. Technol.* **2008**, *68* (3–4), 790–798. <https://doi.org/10.1016/j.compscitech.2007.08.015>.
- (39) Hong, C. K.; Wool, R. P. Development of a Bio-Based Composite Material from Soybean Oil and Keratin Fibers. *J. Appl. Polym. Sci.* **2005**, *95* (6), 1524–1538. <https://doi.org/10.1002/app.21044>.
- (40) Rivera, E. M.; Araiza, M.; Brostow, W.; Castaño, V. M.; Díaz-Estrada, J. ; Hernández, R.; Rodríguez, J. R. Synthesis of Hydroxyapatite from Eggshells. *Mater. Lett.* **1999**, *41* (3), 128–134. [https://doi.org/10.1016/S0167-577X\(99\)00118-4](https://doi.org/10.1016/S0167-577X(99)00118-4).
- (41) Delidovich, I.; Hausoul, P. J. C.; Deng, L.; Pfützenreuter, R.; Rose, M.; Palkovits, R. Alternative Monomers Based on Lignocellulose and Their Use for Polymer Production. *Chem. Rev.* **2016**, *116* (3), 1540–1599. <https://doi.org/10.1021/acs.chemrev.5b00354>.
- (42) Wang, H.; Pu, Y.; Ragauskas, A.; Yang, B. From Lignin to Valuable Products—Strategies, Challenges, and Prospects. *Bioresour. Technol.* **2019**, *271* (September 2018), 449–461. <https://doi.org/10.1016/j.biortech.2018.09.072>.
- (43) Ponnusamy, V. K.; Nguyen, D. D.; Dharmaraja, J.; Shobana, S.; Banu, J. R.; Saratale, R. G.; Chang, S. W.; Kumar, G. A Review on Lignin Structure, Pretreatments, Fermentation Reactions and Biorefinery Potential. *Bioresour. Technol.* **2019**, *271*, 462–472. <https://doi.org/10.1016/j.biortech.2018.09.070>.
- (44) Abreu, H. D. S.; Nascimento, A. M. Do; Maria, M. A. Lignin Structure and Wood Properties. *Wood Fiber Sci.* **1999**, *31* (4), 426–433.
- (45) Spiridon, I. Biological and Pharmaceutical Applications of Lignin and Its Derivatives: A Mini-Review. *Cellul. Chem. Technol* **2018**, *52* (8), 543–550.
- (46) Mishra, P. K.; Ekielski, A. The Self-Assembly of Lignin and Its Application in Nanoparticle Synthesis: A Short Review. *Nanomaterials* **2019**, *9* (2), 243. <https://doi.org/10.3390/nano9020243>.
- (47) Yang, J.; Ching, Y. C.; Chuah, C. H. Applications of Lignocellulosic Fibers and Lignin in Bioplastics: A Review. *Polymers (Basel)*. **2019**, *11* (5), 751. <https://doi.org/10.3390/polym11050751>.
- (48) Diop, A.; Mijiyawa, F.; Koffi, D.; Kokta, B. V.; Montplaisir, D. Study of Lignin Dispersion in Low-Density Polyethylene. *J. Thermoplast. Compos. Mater.* **2015**, *28* (12), 1662–1674. <https://doi.org/10.1177/0892705714556829>.
- (49) Yin, Q.; Yang, W.; Sun, C.; Di, M. Preparation and Properties of Lignin-Epoxy Resin Composite. *BioResources* **2012**, *7* (4), 5737–5748. <https://doi.org/10.15376/biores.7.4.5737-5748>.
- (50) Thakur, V. K.; Thakur, M. K.; Raghavan, P.; Kessler, M. R. Progress in Green Polymer

- Composites from Lignin for Multifunctional Applications: A Review. *ACS Sustain. Chem. Eng.* **2014**, 2 (5), 1072–1092. <https://doi.org/10.1021/sc500087z>.
- (51) Feghali, E.; Torr, K. M.; Van de Pas, D. J.; Ortiz, P.; Vanbroekhoven, K.; Eevers, W.; Vendamme, R. Thermosetting Polymers from Lignin Model Compounds and Depolymerized Lignins. *Top. Curr. Chem.* **2018**, 376 (32). <https://doi.org/10.1007/s41061-018-0211-6>.
- (52) Hu, X.; Lievens, C.; Li, C. Z. Acid-Catalyzed Conversion of Xylose in Methanol-Rich Medium as Part of Biorefinery. *ChemSusChem* **2012**, 5 (8), 1427–1434. <https://doi.org/10.1002/cssc.201100745>.
- (53) Van Zandvoort, I.; Wang, Y.; Rasrendra, C. B.; Van Eck, E. R. H.; Bruijninx, P. C. A.; Heeres, H. J.; Weckhuysen, B. M. Formation, Molecular Structure, and Morphology of Humins in Biomass Conversion: Influence of Feedstock and Processing Conditions. *ChemSusChem* **2013**, 6 (9), 1745–1758. <https://doi.org/10.1002/cssc.201300332>.
- (54) Hu, X.; Lievens, C.; Larcher, A.; Li, C. Z. Reaction Pathways of Glucose during Esterification: Effects of Reaction Parameters on the Formation of Humin Type Polymers. *Bioresour. Technol.* **2011**, 102 (21), 10104–10113. <https://doi.org/10.1016/j.biortech.2011.08.040>.
- (55) Pin, J. M.; Guigo, N.; Vincent, L.; Sbirrazzuoli, N.; Mija, A. Copolymerization as a Strategy to Combine Epoxidized Linseed Oil and Furfuryl Alcohol: The Design of a Fully Bio-Based Thermoset. *ChemSusChem* **2015**, 8 (24), 4149–4161. <https://doi.org/10.1002/cssc.201501259>.
- (56) Pin, J. M.; Guigo, N.; Mija, A.; Vincent, L.; Sbirrazzuoli, N.; Van Der Waal, J. C.; De Jong, E. Valorization of Biorefinery Side-Stream Products: Combination of Humins with Polyfurfuryl Alcohol for Composite Elaboration. *ACS Sustain. Chem. Eng.* **2014**, 2 (9), 2182–2190. <https://doi.org/10.1021/sc5003769>.
- (57) Kang, S.; Fu, J.; Deng, Z.; Jiang, S.; Zhong, G.; Xu, Y.; Guo, J.; Zhou, J. Valorization of Biomass Hydrolysis Waste: Activated Carbon from Humins as Exceptional Sorbent for Wastewater Treatment. *Sustainability* **2018**, 10 (6), 1795. <https://doi.org/10.3390/su10061795>.
- (58) Tosi, P.; Van Klink, G. P. M.; Celzard, A.; Fierro, V.; Vincent, L.; De Jong, E.; Mija, A. Auto-Crosslinked Rigid Foams Derived from Biorefinery Byproducts. *ChemSusChem* **2018**, 11 (16), 2797–2809. <https://doi.org/10.1002/cssc.201800778>.
- (59) Mija, A.; Jong, E. De; Waal, J. C. Van der; Klink, G. P. M. Van. Humins-Containing Foam. WO 2017/074183 A1, 2017.
- (60) Halley, P. J.; Mackay, M. E. Chemorheology of Thermosets-An Overview. *Polym. Eng. Sci.* **1996**, 36 (5), 593–609. <https://doi.org/10.1002/pen.10447>.
- (61) Chirayil, C. J.; Mathew, L.; Hassan, P. A.; Mozetic, M.; Thomas, S. Rheological Behaviour of Nanocellulose Reinforced Unsaturated Polyester Nanocomposites. *Int. J. Biol. Macromol.* **2014**, 69, 274–281. <https://doi.org/10.1016/j.ijbiomac.2014.05.055>.
- (62) Cheung, H. Y.; Ho, M. P.; Lau, K. T.; Cardona, F.; Hui, D. Natural Fibre-Reinforced Composites for Bioengineering and Environmental Engineering Applications. *Compos. Part B Eng.* **2009**, 40 (7), 655–663. <https://doi.org/10.1016/j.compositesb.2009.04.014>.
- (63) Bessa, J.; Souza, J.; Lopes, J. B.; Sampaio, J.; Mota, C.; Cunha, F.; Figueiro, R. Characterization of Thermal and Acoustic Insulation of Chicken Feather Reinforced Composites. *Procedia Eng.* **2017**, 200, 472–479. <https://doi.org/10.1016/j.proeng.2017.07.066>.
- (64) Flores-Hernández, C.; Colín-Cruz, A.; Velasco-Santos, C.; Castaño, V.; Rivera-Armenta, J.; Almendarez-Camarillo, A.; García-Casillas, P.; Martínez-Hernández, A. All Green Composites from Fully Renewable Biopolymers: Chitosan-Starch Reinforced with Keratin from Feathers. *Polymers (Basel)*. **2014**, 6 (3), 686–705. <https://doi.org/10.3390/polym6030686>.
- (65) Pourjavaheri, F.; Mohades, F.; Jones, O.; Sherkat, F.; Kong, I.; Gupta, A.; Shanks, R. A. Avian Keratin Fibre-Based Bio-Composites. *World J. Eng.* **2017**, 14 (3), 183–187. <https://doi.org/10.1108/WJE-08-2016-0061>.
- (66) Aranberri, I.; Montes, S.; Azcune, I.; Rekondo, A.; Grande, H. J. Fully Biodegradable Biocomposites with High Chicken Feather Content. *Polymers (Basel)*. **2017**, 9 (11).

- <https://doi.org/10.3390/polym9110593>.
- (67) Aranberri, I.; Montes, S.; Azcune, I.; Rekondo, A.; Grande, H. J. Flexible Biocomposites with Enhanced Interfacial Compatibility Based on Keratin Fibers and Sulfur-Containing Poly(Urea-Urethane)S. *Polymers (Basel)*. **2018**, *10* (10), 1056. <https://doi.org/10.3390/polym10101056>.
 - (68) Amieva, E. J. C.; Velasco-Santos, C.; Martínez-Hernández, A.; Rivera-Armenta, J.; Mendoza-Martínez, A.; Castaño, V. Composites from Chicken Feathers Quill and Recycled Polypropylene. *J. Compos. Mater.* **2015**, *49* (3), 275–283. <https://doi.org/10.1177/0021998313518359>.
 - (69) Gupta, V. B.; Drzal, L. T.; Lee, C. Y. C.; Rich, M. J. The Temperature-dependence of Some Mechanical Properties of a Cured Epoxy Resin System. *Polym. Eng. Sci.* **1985**, *25* (13), 812–823. <https://doi.org/10.1002/pen.760251305>.
 - (70) Ullah, A.; Wu, J. Feather Fiber-Based Thermoplastics: Effects of Different Plasticizers on Material Properties. *Macromol. Mater. Eng.* **2013**, *298* (2), 153–162. <https://doi.org/10.1002/mame.201200010>.
 - (71) Brostow, W.; Hagg Lobland, H. E.; Narkis, M. Sliding Wear, Viscoelasticity, and Brittleness of Polymers. *J. Mater. Res.* **2006**, *21* (9), 2422–2428. <https://doi.org/10.1557/jmr.2006.0300>.
 - (72) Brostow, W.; Hagg Lobland, H. E. Brittleness of Materials: Implications for Composites and a Relation to Impact Strength. *J. Mater. Sci.* **2010**, *45* (1), 242–250. <https://doi.org/10.1007/s10853-009-3926-5>.
 - (73) Brostow, W.; Hagg Lobland, H. E.; Narkis, M. The Concept of Materials Brittleness and Its Applications. *Polym. Bull.* **2011**, *67* (8), 1697–1707. <https://doi.org/10.1007/s00289-011-0573-1>.
 - (74) Flory, P. J. *Principles of Polymer Chemistry*; Cornell University Press: Ithaca, New York, 1953.
 - (75) Kalogeras, I. M.; Hagg Lobland, H. E. The Nature of the Glassy State: Structure and Glass Transitions. *J. Mater. Educ.* **2012**, *34* (3–4), 69–94.
 - (76) ASTM-D7028. Standard Test Method for Glass Transition Temperature (DMA T_g) of Polymer Matrix Composites by Dynamic Mechanical Analysis (DMA). 2008. <https://doi.org/10.1520/D7028-07E01.2>.
 - (77) Cheng, S.; Lau, K.; Liu, T.; Zhao, Y.; Lam, P.; Yin, Y. Mechanical and Thermal Properties of Chicken Feather Fiber/PLA Green Composites. *Compos. Part B Eng.* **2009**, *40* (7), 650–654. <https://doi.org/10.1016/j.compositesb.2009.04.011>.
 - (78) Zhan, M.; Wool, R. P. Mechanical Properties of Composites with Chicken Feather and Glass Fibers. *J. Appl. Polym. Sci.* **2016**, *133* (45). <https://doi.org/10.1002/app.44013>.
 - (79) Belarmino, D. D.; Ladchumanandasivam, R.; Belarmino, L. D.; Pimentel, J. R. de M.; da Rocha, B. G.; Galvão, A. O.; de Andrade, S. M. B. Physical and Morphological Structure of Chicken Feathers (Keratin Biofiber) in Natural, Chemically and Thermally Modified Forms. *Mater. Sci. Appl.* **2012**, *03* (12), 887–893. <https://doi.org/10.4236/msa.2012.312129>.
 - (80) Colom, X.; Rahalli, A.; Cañavate, J.; Carrillo, F. Properties and Optimal Manufacturing Conditions of Chicken Feathers Thermoplastic Biocomposites. *J. Compos. Mater.* **2015**, *49* (3). <https://doi.org/10.1177/0021998313518569>.
 - (81) Dinu, R.; Mija, A. Cross-Linked Polyfuran Networks with Elastomeric Behaviour Based on Humins Biorefinery by-Products. *Green Chem.* **2019**, *21*, 6277–6289. <https://doi.org/10.1039/c9gc01813a>.
 - (82) Wrześniewska-Tosik, K.; Szadkowski, M.; Marcinkowska, M.; Pałczyńska, M. Chicken Feather-Containing Composite Non-Wovens with Barrier Properties. *Fibres and Textiles in Eastern Europe*. 2012, pp 96–100.
 - (83) ASTM-D570. Water Absorption of Plastics. 1998. <https://doi.org/10.1520/D0570-98>.

Electronic Supplementary Information (ESI)

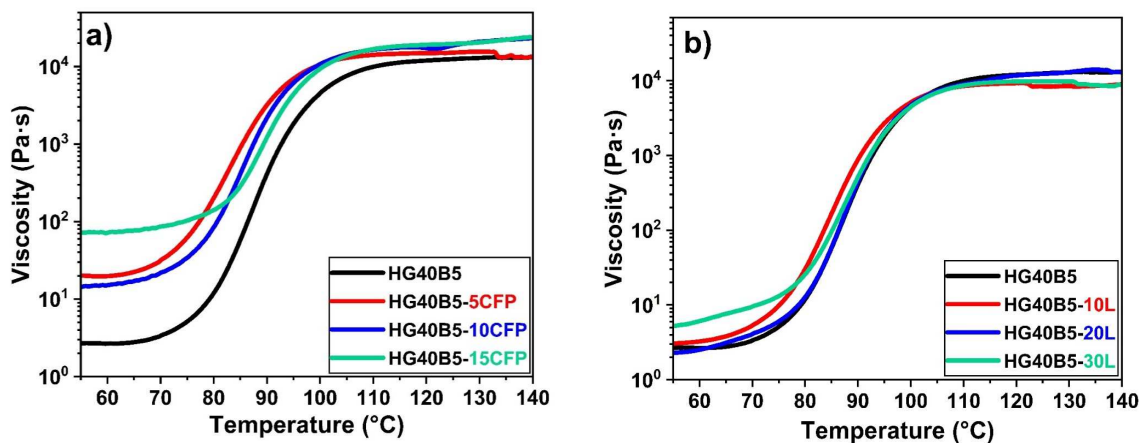


Figure ESI 1. Rheology study on the influence of the CFP amount in the HG40B5 curing system.

Evolution of viscosity with temperature during curing

Table ESI 1. Rheology data for the HG40B5 resin and the mixtures with different amount of filler

System	Gelling point (reaction interval) (°C)	G' (at Start & End) (Pa)	G'' (at Start & End) (Pa)	Viscosity (at Start & End) (Pa s)
Neat Resin	86 (65–115)	5–290 $\times 10^3$	24–16 $\times 10^3$	3–15 $\times 10^3$
Mix with CFP	5% CFP 83 (60–105)	27–150 $\times 10^3$	200–12 $\times 10^3$	20–15 $\times 10^3$
	10% CFP 84 (60–105)	57–220 $\times 10^3$	126–17 $\times 10^3$	14–21 $\times 10^3$
	15% CFP 83 (60–105)	560–410 $\times 10^3$	458–11 $\times 10^3$	76–22.5 $\times 10^3$
Mix with Lignin	10% L 85 (60–115)	4–600 $\times 10^3$	29–13 $\times 10^3$	3–11 $\times 10^3$
	20% L 87 (60–115)	5–300 $\times 10^3$	22–20 $\times 10^3$	2–13 $\times 10^3$
	30% L 88 (60–115)	9–400 $\times 10^3$	50–15 $\times 10^3$	5–10 $\times 10^3$

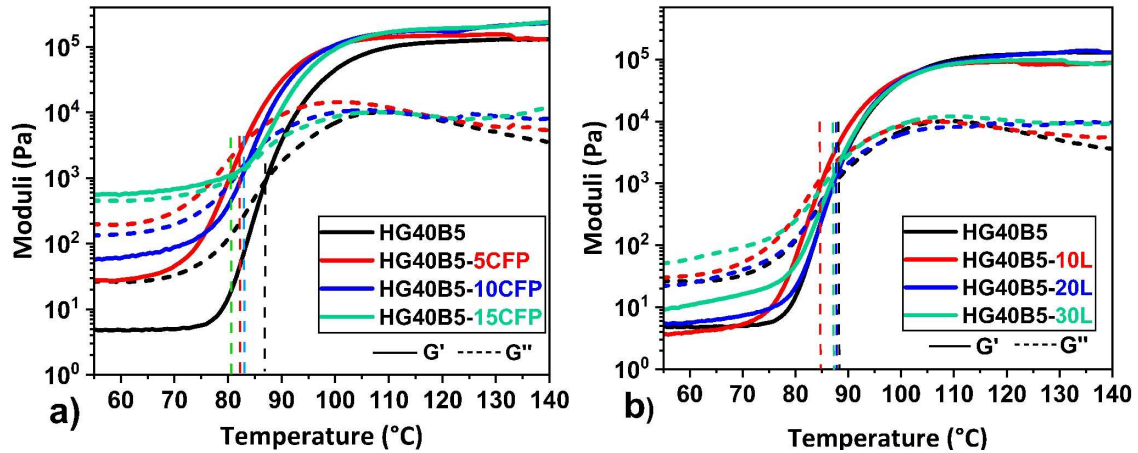


Figure ESI 2. Rheology study of the influence of the bio-fillers amount in HG40B5 humins-based resins curing systems

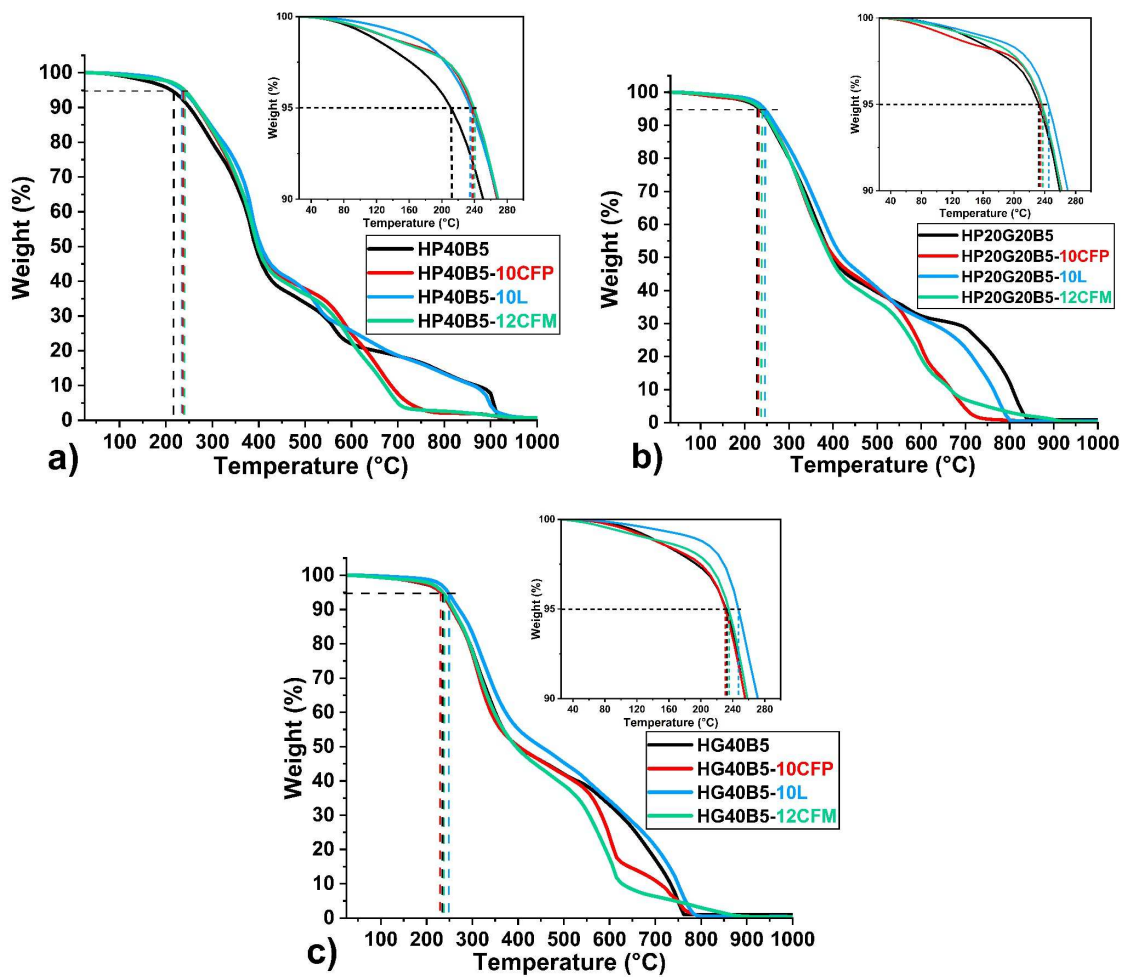


Figure ESI 3. Thermogravimetric analyses of humins based materials at $10\text{ }^{\circ}\text{C min}^{-1}$ under air flow. Comparison between resins and composites

Table ESI 2. Mechanical properties of the humins-based resins and composites according with the DMA analysis

Sample	Tan δ ($^{\circ}\text{C}$) (peak $^{\circ}\text{C}$ range)	Peak height (Tan δ max)	E' at Glassy Plateau (-70 $^{\circ}\text{C}$) (MPa)	E' at Rubbery Plateau (150 $^{\circ}\text{C}$) (MPa)	u (mmol cm^{-3})	
HP40B5	Neat Resin	30 (-50–150)	0.76	4840	1	0.07
	Resin-10L	44 (-53–147)	0.47	3288	1.4	0.12
	Resin-12CFM	30 (-40–115)	0.57	3865	4.5	–
	Resin-10CFP	25 (-55–155)	0.76	4835	1.2	0.08
HP20G20B5	Neat Resin	49 (-35–158)	0.5	5304	4.5	0.43
	Resin-10L	54 (-30–145)	0.87	4985	3.2	0.33
	Resin-12CFM	42 (-65–135)	0.44	3794	15.7	–
	Resin-10CFP	55 (-30–140)	0.6	4030	8	0.76
HG40B5	Neat Resin	71 (-25–167)	0.4	6191	5.7	0.56
	Resin-10L	66 (-22–150)	0.68	4278	6.1	0.65
	Resin-12CFM	52 (-23–144)	0.35	3940	41.8	–
	Resin-10CFP	61 (-40–144)	0.5	3498	12.1	1.20

Table ESI 3. Comparison of glass transition (T_g) of materials by DSC and DMA; Shore hardness result

	HP40B5				HP20G20B5				HG40B5			
	Neat Resin	Resin-10L	Resin-12CFM	Resin-10CFP	Neat Resin	Resin-10L	Resin-12CFM	Resin-10CFP	Neat Resin	Resin-10L	Resin-12CFM	Resin-10CFP
T_g ($^{\circ}\text{C}$) (DSC)	-8	-2	-13	-9	1	16	2	3	27	27	20	13
T_{g-loss} ($^{\circ}\text{C}$) (DMA)	-10	-3	-15	3	-2	13	2	15	26	30	20	18
$T_{g-onset}$ ($^{\circ}\text{C}$) (DMA)	-11	-4	-18	-1	-4	16	0	11	27	37	17	19
Shore hardness SD	44	40	37	37	59	75	66	72	72	85	86	77

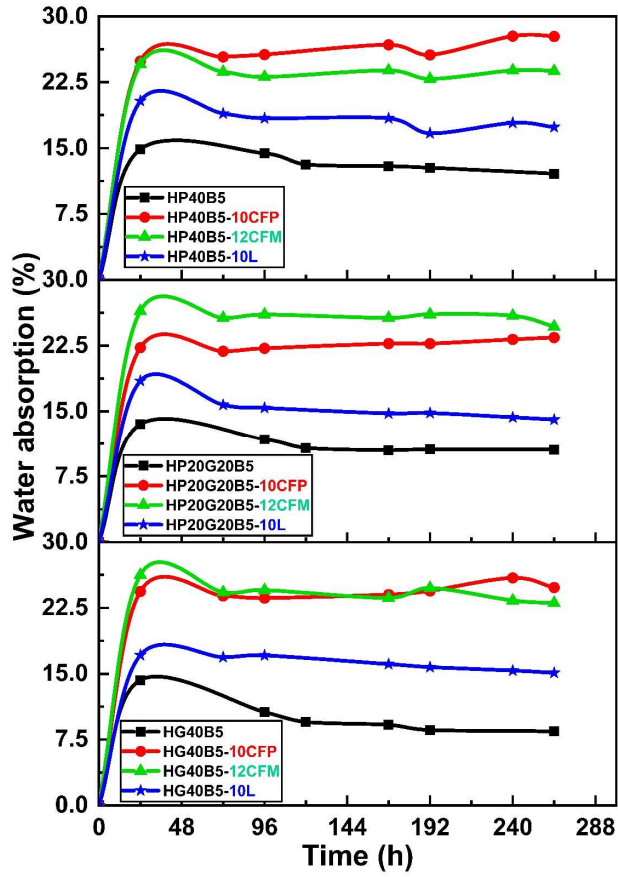


Figure ESI 4. Water absorption in function of time. Comparison between resins and composites

Chapter 4

Sustainable Thermosets Obtained by Copolymerization of Humins with Triglycidyl Ether of Phloroglucinol

This chapter is based on Roxana Dinu and Alice Mija, “Sustainable Thermosets Obtained by Copolymerization of Humins with Triglycidyl Ether of Phloroglucinol”, *Journal of Materials Science Research*, 2020, 9 (2),1-17, doi: 10.5539/jmsr.v9n1p1

Abstract

The environmental pollution is growing continuously being a worldwide problem. Production and use of petroleum-based materials but also huge quantities of industrial wastes are important factors that affect the well-being of the environment. New scientific researches place great emphasis on waste valorization, and also on developing new environmentally friendly bio-based materials. In this work we focus on the valorization of humins, a biorefinery side product, by its copolymerization with a bio-based triepoxide. In this manner we produce materials with a bio-based carbon content (BCC) $\approx 94\%$. The physico-chemical and mechanical properties of the cured bio-based resins were investigated using different technics as TGA, DMA, Shore hardness test, water absorption and solvents resistance. It was revealed that the obtained materials present very good mechanical properties with values of E' in glassy region $\approx 3.7\text{--}5$ GPa. The $\tan \delta$ – maxima of the three humins-based resins are ranging from 122 to 154 °C. The thermosets' hardness values $\approx 82\text{--}85$ SD confirm the stiffness of these materials.

4.1. Introduction

Plastics or synthetic organic polymers are extremely highly used materials, their production and employment increasing significantly and exceeding almost all others human-developed materials. Most plastics materials use in their production fossil derivatives as raw materials, and commonly these used plastics are non-biodegradable, which leads to ecological disaster by the huge quantities of waste generation. The use of fossil derivatives and the production of non-biodegradable waste are some of the biggest problematics of the 21st century, namely the pollution of the environment.^{1,2} According to statistics, in 2015 were generated 6300 Mt of plastic waste, of which 9% were recycled, 12% incinerated and 79% were deposited in landfills or in nature.^{3,4} In order to combat these major problems, intense research has begun on the development of materials from bio-resources and industrial waste. This work proposes to develop new green thermoset materials based on biorefineries side-products like the humins and a bio-based monomer as triglycidyl ether of phloroglucinol (TGPh).

The epoxy resins represent an one of the most important class of thermosetting materials that are used in many sectors of applications, such as automobiles and transports, constructions and civil constructions, electrical and electronic energy, packaging, *etc.*^{5,6} The epoxy group can undergo a myriad of chemical reactions by following a wide variety of mechanisms so to produce materials with a wide range of properties. In this work we propose the study of a green epoxy monomer in order to develop sustainable thermoset materials: *i.e.* the triglycidyl ether of phloroglucinol. Phlorotannins are polyphenol compounds found in marine brown algae or in the bark of fruit. These compounds are present in non-vascular plant tannins, being composed of phloroglucinol (1,3,5-trihydroxybenzene) units with different degrees of polymerization.^{7,8} Due to the abundance in the aquatic environment of this polyphenols as well as its bioactivity and its beneficial effects on health (antioxidant, anti-allergic, anti-carcinogenic, anti-inflammatory activity, *etc.*), researches on their potential uses in the medical field has increased considerably.⁹⁻¹¹ Also, intensive researches are being carried out on the use of phloroglucinol as a renewable resource in the development of various monomers in order to limit the environmental impact of the production of polymers. In order to develop fully bio-based flame-retardant epoxy resins, Menard *et al.*⁶ functionalized the phloroglucinol by glycidylation and/or phosphorylation, the obtained monomers being cross-linked with a bio-based diamine. In the first step, these bio-based flame-retardant epoxy resins were analyzed in order to identify the influence of the chemical structure of monomers and hardeners on the thermal and fire properties of the thermosets. After, the obtained resins have been compared to a conventional DGEBA-IPDA control to determine their overall thermal and

fire behavior. In another study, Ng *et al.*¹² developed novel food contact low-toxic epoxy coatings based on bio-based epoxy compounds as epoxidized cardanol, diglycidyl ether of vanillin or triglycidyl ether of phloroglucinol and dicyandiamide. This green monomer was involved also in the development of other categories of materials such as porous carbonaceous materials used as adsorbents in chemical and environmental fields^{13,14} or electrode materials for high-performance supercapacitors.^{15,16} Due to its versatility, but also its abundance in nature, phloroglucinol represents a potential alternative to fossil compounds in the materials industry.

Humanity evolution and the standard of living has led to a significant increase in the consumption of chemicals, energy and fuels, these compounds being generally obtained from non-renewable and exhaustible fossil raw materials. A valuable and abundant alternative sustainable feedstock for the conversion into chemical-platform molecules is represented by lignocellulosic biomass. The largest constituents of lignocellulose are the carbohydrates such as cellulose and hemicellulose, representing about 70–80 wt.% of this biomass.¹⁷ Conversion of these carbohydrates into valuable chemical-platform molecules as 5-hydroxymethyl furfural (HMF), furfural (FF) and levulinic acid (LA), taking place under acid-catalyzed hydrolysis, represent an important part of the biorefinery concept. Besides the production of valuable chemical building blocks, the dehydration of sugar generates also the formation of dark-colored viscous by-product.¹⁸ This polymeric side-product called humins, is a complex and heterogenous product, lacking a well-defined molecular structure. In order to streamline the biomass conversion through biorefineries processing, a good knowledge and understanding of physico-chemical properties and potential of application of the humins by-product are required. To elucidate the molecular structure and morphology of this by-product, Van Zandvoort *et al.*¹⁹ studied different laboratory humins products as a function of feedstock and processing parameters. The reaction conditions were established with the purpose of an ideal simulation of the typical biorefinery operations. Following the investigation of the laboratory humins developed by dehydration of D-glucose, Hoang²⁰ observed that this by-product has a variable furan structure that contains a variety of functional groups such as alcohol, acid, ketone and aldehyde. Based on the studies so far, humins are carbon-rich agglomerate particles, composed of approximately 50–65 wt.% C, 29–46% wt.% O, and 4–5.5 wt.% H, depending on the process parameters and feedstock.^{21–23} Until recently, due to the variation of the degree of branching and the molecular mass of humins oligomers depending on the production process, the industrial uses of this by-product were limited only to the conversion of energy and power by gasification or combustion.^{24,25} Furthermore, the complex structure and the abundance of different functional groups convert the humins into a promising renewable material for new innovative end-products such as absorbents for wastewater treatment, insulation materials,

support for solid catalysts or furanic resins and composites for different industrial sector applications.^{26–29} In our previous studies,^{30–32} the industrial humins were intensely studied and converted into valuable bio-materials. For example, industrial humins were copolymerized with aliphatic diglycidyl ethers obtaining different thermoset resins.³¹ By tailoring both the composition and the process parameters of the resins, their physico-chemical and mechanical properties have been modulated, thus obtaining a variety of materials, from elastic to rigid for a large industrial applications area. In another study, Pin *et al.*³⁰ developed fully bio-based furanic resins by combining the industrial humins with polyfurfuryl alcohol (PFA). Thereafter, PFA/humins thermoset resins were used as matrices in the development of composites, where cellulose acted as reinforcing materials.

Given that the need to replace fossil materials with renewable ones is increasing, the purpose of this study is the development of sustainable materials. The copolymerization study of the humins with triglycidyl ether of phloroglucinol, initiated and/or accelerated by various compounds and the reactivities of the obtained systems were already explained in detail in our previous work.³³ The physico-chemical and mechanical properties of the humins-based thermoset resins were analyzed in this study using different techniques and methods such as differential scanning calorimetry (DSC), thermogravimetric analysis (TGA), dynamic mechanical analysis (DMA), Shore hardness test, water absorption or chemical resistance test in order to determine their potential uses at industrial level.

4.2. Results and Discussion

4.2.1. DSC study of the humins - TGPh copolymerization reactions

The first objective of this work focused on establishing the thermodynamical parameters of copolymerization reactions and crosslinking but also on the elaboration of the optimal compositions for the development of the humins-based sustainable materials. The proof of the copolymerization, the chemical connectivity between the two comonomers, their molecular structure and their reactivity were elucidated by ATR-FTIR and NMR spectroscopies in our previous study.³³ In order to study the thermodynamic processes of the copolymerization, different formulations, in different ratios of humins, TGPh and BDMA/DMP-30 were studied by DSC. Firstly, mixtures between humins and TGPh in different ratios were analyzed to select the optimal ratios for the development of new resins. In Figure 1 are revealed the DSC thermograms during heating of humins/TGPh reactive mixtures without catalyst or accelerator.

An important objective in this study is the valorization in large quantities of the humins, the biorefineries' side-product. Considering this aspect, four different ratios, in which humins

represents the major compound of the mixture, were tested. In Figure 1 we can observe that all four mixtures have a good humins vs. epoxy reactivity even if in these systems we didn't used any catalyst. Although the reactivity between the two compounds is present, in the case of mixtures with 10–30 wt.% TGPh, the appearance of an endothermic peak between 200–230 °C can be observed in Figure 1 thermograms. These peak displays that the amount of epoxy compound is insufficient for the complete crosslinking of humins, so the unreacted humins begins to degrade at around 200 °C. This behavior was confirmed by TGA analysis, not presented here. As can be seen in Figure 1, the mixture with 60 wt.% humins and 40 wt.% TGPh (purple line) reveal a good reactivity and the degradation of humins is not anymore present. To optimize the crosslinking process, *i.e.* to decrease the reaction temperature interval so also the maximum crosslinking temperature, different catalyst/accelerator ratios were tested. The DSC thermograms of the evolution of different mixtures in function of temperature are presented in Figure 2, and the values of the copolymerization's enthalpies and temperatures of reaction are summarized in Table 1.

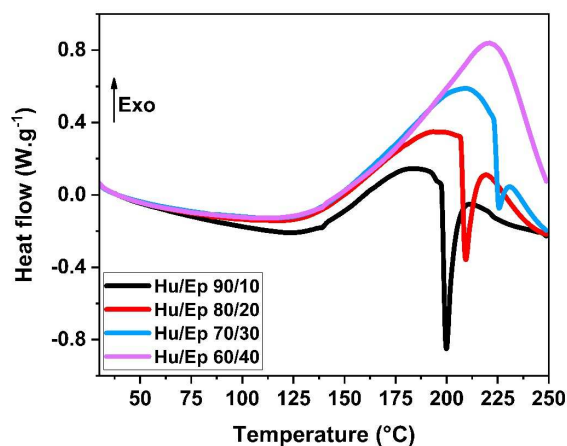


Figure 1. DSC thermograms obtained during heating at 10 °C min^{-1} of humins/epoxide reactive mixtures at different ratios (w/w %), without catalyst or accelerator

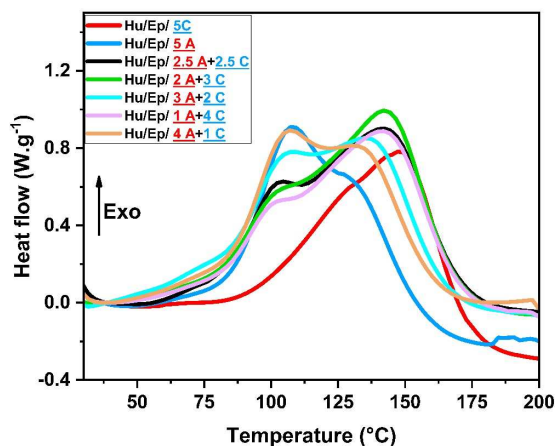


Figure 2. DSC thermograms during heating at 10 °C min^{-1} of humins-TGPh copolymerization systems at different % ratios accelerator (A) and catalyst (C)

It can be observed that the addition of the catalyst and accelerator improves the copolymerization reactivity and decreases considerably the onset of thermal reactions and the T_{max} of the reactions. In the presence of the activating species, *i.e.* the catalyst and/or the accelerator, a complex reactivity is exhibited in all the formulations since two exothermic peaks can be observed in Figure 2. A first exothermal reaction occurs at around 100 °C. This reaction occurs very fast, with a rapid increase of the curve's slope and could be mainly attributed to the accelerator's contribution on the crosslinking. In the presence of the accelerator the TGPh

ring opening occurs very fast promoting both TGPh homopolymerization and crosslinking *via* -OH functions from the humins.³³ The second reaction occurs at around 140–148 °C (depending on the system) and is mainly the result of the catalyst contribution on the copolymerization. In our previous study of chemical mechanism of this copolymerization, an anionic mechanism of polymerization is involved. In the presence of the catalyst the initiation is the determinant step with the nucleophilic attack of the BDMA to the epoxy ring from TGPh. Then, the propagation occurs *via* a transfer proton between the TGPh adduct and the -OH from the humins. The copolymerization reactions is accompanied by humins structural rearrangements γ -keto acid cyclization, γ -keto esterification, favored at high temperatures (> 130 °C).³³ We can notice that in the systems containing both activating species we can identify an additional contribution of each species.

Three different formulations were selected to be developed and analyzed: like the mix with 5 wt.% catalyst (BDMA), that with 5 wt.% accelerator (DMP-30) and the equal combination between the two (2.5/2.5 wt.%). The obtained DSC results show that the addition of 5 wt.% BDMA or 5 wt.% DMP-30 produce reactions with similar enthalpy values ($\approx 290 \text{ J.g}^{-1}$) and intervals of temperature between 45 °C to 190 °C. The difference appears in the T_{max} of the reactions that is around 106 °C for the system with accelerator, HuEpA, but much higher 148 °C for the system with catalyst, HuEpC. The third selected formulation containing the 2.5/2.5 wt.% of BDMA/DMP-30 combination reveals the highest enthalpy of reaction $\approx 365 \text{ J.g}^{-1}$. The onset of crosslinking for HuEpAC is at 40 °C, reaching the maximum rate at 142 °C. It can also be seen for this formulation that the crosslinking's completion is similar with that of HuEpC and HuEpA systems, the DSC heat flow reaching a quasi-linear response at $\approx 195 \text{ °C}$.

Table 1. DSC results of the humins/TGPh copolymerization at different catalyst/accelerator ratios

	Hu/Ep- 5C	Hu/Ep- 5A	Hu/Ep- 2.5A + 2.5C	Hu/Ep- 2A + 3C	Hu/Ep- 3A + 2C	Hu/Ep- 1A + 4C	Hu/Ep- 4A + 1C
Reaction T_{max} (interval) (°C)	148 \pm 1 (54-193)	106 \pm 1 (45-182)	142 \pm 1 (38-194)	143 \pm 1 (38-198)	136 \pm 1 (34-190)	142 \pm 1 (42-188)	108 \pm 1 (38-183)
Enthalpy of reaction (J.g⁻¹)	276 \pm 3	294 \pm 3	365 \pm 3	350 \pm 3	333 \pm 3	321 \pm 3	313 \pm 3

4.2.2. Physico-chemical and mechanical properties of bio-based thermosets

Dynamic mechanical analysis was used to investigate the correlation between the three selected formulations on the materials properties. The three systems selected here aim to highlight the influence of the copolymerization initiation step on the viscoelastic behavior of final materials. Even if the overall chemical mechanism of reactions is very complex in the case of humins macromonomer, through these three systems we can observe that the obtained

materials have differences in their thermomechanical behavior, so different copolymers' network structure.

The DMA tool was used in particular to determine materials' stiffness and mechanical damping characteristics. For polymers' applications the stiffness represents the parameter of prime importance. The moduli of polymers show strong dependence on temperature³⁴, such that the effect of temperature on the elastic response (E' - storage modulus) and on the viscous response (E'' - loss modulus) of the three thermoset materials were analyzed. In the Figure 3 are depicted the moduli vs. temperature curves for the three obtained thermosets, in which three regions of viscoelastic behavior are evident: a glassy region followed by a transition from the glassy to rubbery and finally the rubbery plateau.

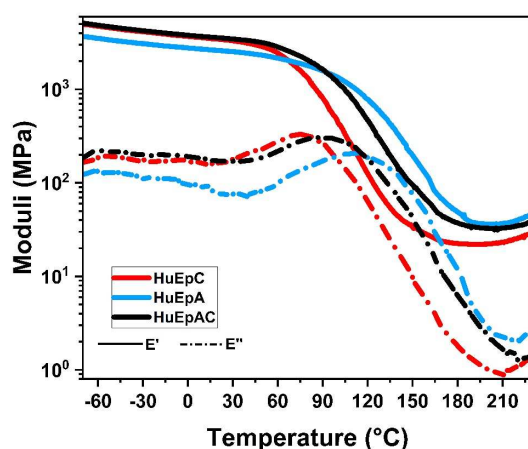


Figure 3. Viscoelastic behavior as a function of temperature for storage (continuous line) and loss (dotted line) moduli as results measured by DMA of the three humins-based thermosets

The storage modulus is continuously decreasing with the temperature between -75 to 200 °C, behavior explained by the increasing of the chains free volume with the thermal expansion. The two materials containing the catalyst (HuEpC and HuEpAC) have similar E' values in the glassy region of ≈ 5 GPa, while for material with the accelerator (HuEpA) the value of E' decreases at ≈ 3.7 GPa. Although the resin only with accelerator has a low value of the storage modulus in the glassy region, the onset of its drop to the rubbery region occurs at higher temperature compared to the thermoset prepared with the BDMA catalyst. The elastic response of the resins in the rubbery region depends highly on the density of the materials crosslinks. The smallest drop interval value between the glassy and rubbery region appears for the system with the accelerator, the HuEpA thermoset (≈ 40 MPa), thus presenting the highest crosslink density. This value is followed by that of HuEpAC resin (35 MPa), the last being the formulation developed only with the catalyst (≈ 26 MPa). The crosslink densities values and the average molecular weight between crosslinks (M_c) of the humins-based resins were also

calculated and given in Table 2. A significant mechanical parameter that should be considered in products' design and development is represented by their brittleness (B). According with studies developed by W. Brostow *et al.*^{35–37} the storage modulus (E') of the materials is inversely proportional to brittleness (B), which means that the humins-based resins with high storage modulus such as HuEpC and HuEpAC, are less fragile compared to HuEpA material.

Since the viscoelastic properties of the thermosets vary with both temperature and time, the study of time dependence or frequency of viscoelasticity was performed for the materials characterization. The viscoelastic curve, called master-curve is using the Time-Temperature Superposition principle.^{38,39} The mechanical properties of the three humins-based resins were analyzed by DMA in the frequency range 10 Hz to 0.1 Hz at a logarithmic increment of 10 steps/decade, under isothermal conditions at different temperatures between $-25\text{ }^{\circ}\text{C}$ to $250\text{ }^{\circ}\text{C}$. The obtained dynamic mechanical data were collected, and the storage moduli plotted as a function of frequency. To obtain the master-curves for each thermoset, each isotherm was shifted (left or right) = $f(\log \text{ frequency})$ axis relative to the reference temperature $T_{ref} = 125\text{ }^{\circ}\text{C}$. Figure 4 shows the storage modulus master curve for each humins-based thermoset materials.

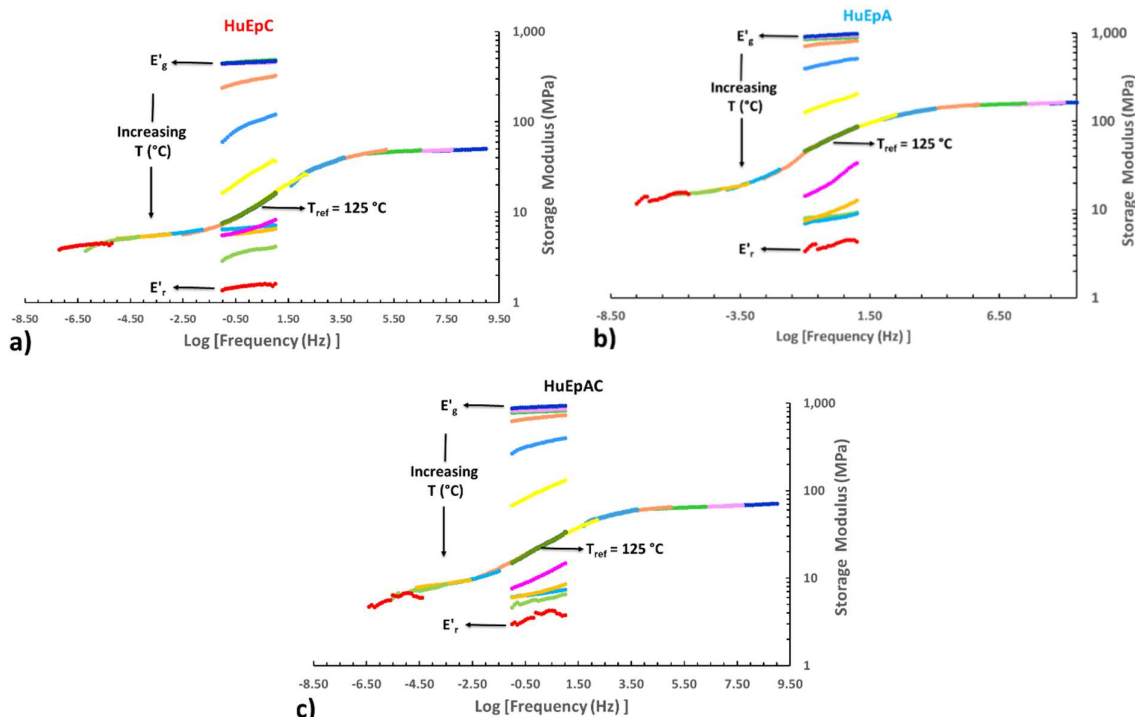


Figure 4. Master curve of storage modulus of humins/epoxy thermosets: a) HuEpC, b) HuEpA, c) HuEpAC obtained after using common shift factor

The storage modulus curves obtained at $T > T_{ref}$ were moved at lower frequencies, and the curves measured at $T < T_{ref}$ were moved at higher frequencies in order to achieve the maximum data overlap. The shifting of the curves was done in this way to ensure that each

curve fits the slope of its immediate neighbor. The master curves for all the three humins-based thermosets were generated in order to understand the effect of crosslink densities of the networks on the viscoelastic properties of the materials. From Figure 4 it can be seen that the viscoelastic transition region of the thermoset resins was shifted to higher frequency scales with the decrease of the crosslink density (Table 2) of the bio-resins.

Another important parameter that generates valuable information regarding the physico-chemical and mechanical properties of the polymers is represented by the glass transition region of the materials. It is known that the glass transition of the materials is not only a value of the transition between the states of thermodynamic equilibrium and is represented by the reversible transition interval from a hard and relatively fragile state into a molten or rubbery state. The glass transition is a dynamic phenomenon being directly dependent on physico-chemical and mechanical factors such as the thermal history of the material, rate of temperature and also the standard/technique used for characterization.⁴⁰ According with ASTM E1640-13 and ASTM D7028-07^{41,42} the glass transition region of the materials can be determined from the DMA results using three different methods like the onset of the storage modulus drop ($T_{g-onset}$), the peak of the maximum of the loss modulus (T_{g-loss}), and the maximum value of the damping factor ($\tan \delta$). Another technique to determine the glass transition phenomenon (T_g) of the materials is the DSC. The glass transition obtained by DSC and the transitions resulting from DMA analysis are used as synonyms because both are trying to model the same molecular phenomenon namely the coordinated chain motions in the network. Meanwhile, the T_{g-DSC} is measured under no mechanical stress being just the effect of the temperature on the chain's mobility, the transitions by DMA are measured under mechanical stress at a given frequency. The obtained values could be quite different depending on the frequency used for mechanical stress.⁴³ The evolutions of the $\tan \delta$ of the humins-based materials in function of the temperature are plotted in Figure 5 and the T_g values obtained by DMA and DSC summarized in Table 2.

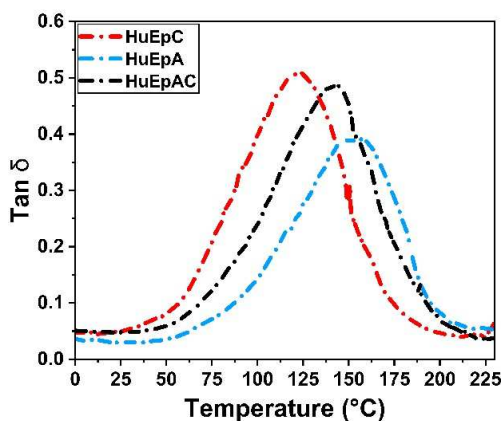


Figure 5. Loss factor ($\tan \delta$) plots as function of temperature determined by DMA for the three thermosets: HuEpC (red line), HuEpA (blue line), HuEpAC (black line)

We can notice that the lowest $\tan \delta$ -maxima value is that of the resin prepared with the catalyst (BDMA), $\tan \delta \approx 122$ °C, followed by that of HuEpAC material ($\tan \delta \approx 144$ °C). The highest $\tan \delta$ value was obtained by the resin prepared with accelerator, $\tan \delta \approx 157$ °C. The temperature range of $\tan \delta$ peak for three thermosets is similar, having the onset at ≈ 15 °C and the end set at around 225 °C. This broad interval of the α relaxation peak (≈ 210 °C) indicates a large distribution of the relaxation times, characteristic for the complex, heterogeneous networks with dangling chains. The $T_{g-onset}$ region obtained from E' and T_{g-loss} from E'' revealed the same trend as the T_g range given by $\tan \delta$ -maxima. So, according with these values the most rigid of the three thermosets is that obtained with the accelerator followed by the resin made with the combination catalyst + accelerator and the last being the thermoset with BDMA. Corroborating these results with that of the DSC analysis of crosslinking we can observe that the accelerator starts a rapid crosslinking, at lower temperature, through a complex mechanism of curing *via* nucleophilic attack on the humins and or TGPh accompanied by structural rearrangements on the humins frame. The obtained thermosets show higher $\tan \delta$ value then the system where the copolymerization follows the catalyst's initiation by a nucleophilic attack on the epoxide ring of TGPh and anionic copolymerization.

Table 2. Calculated and measured parameters for the humins-based thermosets

Sample	Density (g cm ⁻³)	ν (mmol cm ⁻³)	Mc (g/mol)	Glass transition (°C)				Hardness test Shore D
				$\tan \delta$	$T_{g-onset}$ (DMA)	T_{g-loss} (DMA)	T_{g-DSC} (DSC)	
HuEpC	1.1386	2.42	469.07	122	70	77	52	82
HuEpA	1.1284	3.66	307.79	157	107	114	60	87
HuEpAC	1.1389	3.11	364.91	144	86	97	56	85

The DMA results allowed us also to calculate the crosslink density (ν) of the thermosets based on the equation:

$$\nu = \frac{E'}{3RT} \quad (1)$$

where E' is the storage modulus of thermoset in the rubbery plateau region at $T_g + 85$ °C (MPa), R is the gas constant, and T is the absolute temperature (K).⁴⁴ The crosslink density of the material is a parameter directly correlated, proportional with its hardness, moduli, mechanical strength and chemical resistance, while the elongation at break or impact strength have opposite trend.⁴⁵ Also, the average molecular weight between crosslinks (M_c) is a measure of the crosslink density, such that the lower M_c value, the higher the crosslink density. The average molecular weight between crosslinks is given by:

$$M_c = \frac{3\rho RT}{E'} \quad (2)$$

where ρ represents the density of the resin (g cm^{-3}), R is the gas constant, T is absolute temperature (K), and E' is the storage modulus of thermoset in the rubbery plateau (MPa).⁴⁵ In the same time the crosslinking density of a material is related to the amplitude of $\tan \delta$ (Figure 5): higher is the peak amplitude smaller is the crosslink density and the resin is more rigid. As can be seen, in Table 2 the properties resulting from different analyses techniques and the calculated ones are in agreement and have the same tendency. Comparing the mechanical properties of the three bio-based resins developed in this study with those stipulated in literature or industry, it can be said that the humins/TGPh-based resins could compete very well the industrial thermosets produced from fossil resources.^{46–48}

The evolution of the T_{g-DSC} in function of the heating rate was also studied in oxidative atmosphere, the obtained DSC thermograms being presented in Figure 6. The materials present the same trend confirming the results obtained by DMA. The material obtained with the accelerator has the highest T_{g-DSC} , between 56–70 °C (in function of the heating rate), thus being the most rigid of the three resins studied in this work.

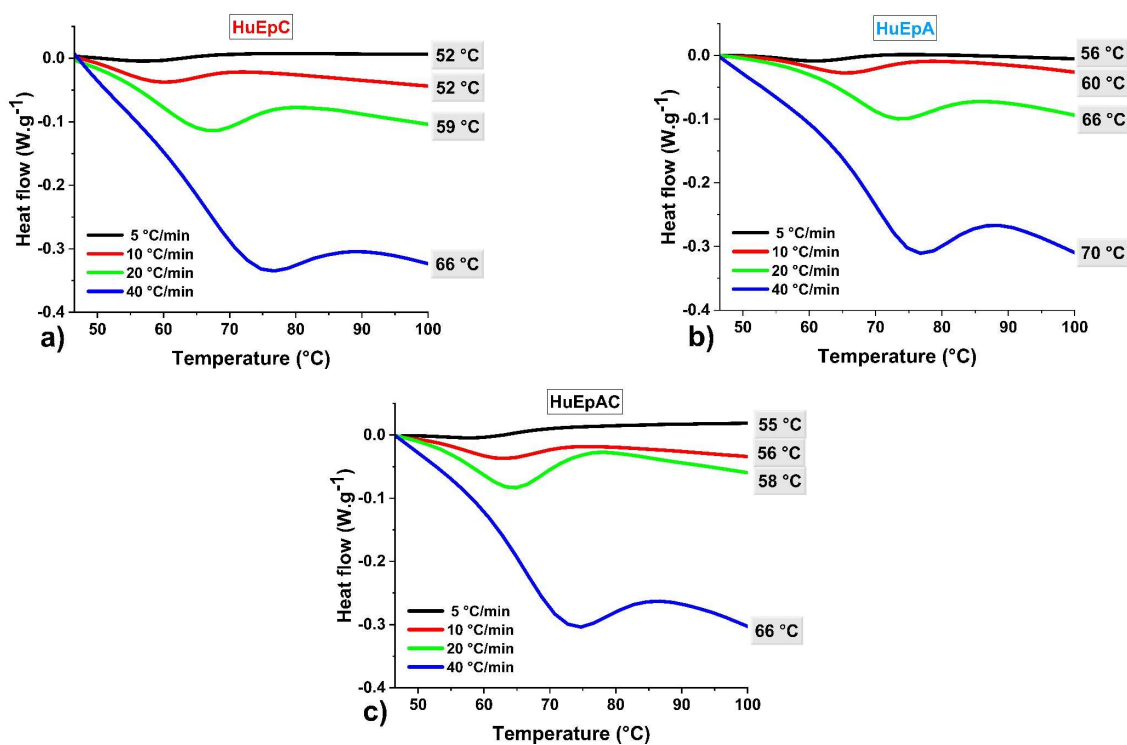


Figure 6. The evolution of the glass transition (T_g) in function of heating rate for a) HuEpC, b) HuEpA and c) HuEpAC obtained by DSC

Moreover, the rigidity of the humins-based thermoset was evaluated by the hardness tests using the Shore D scale. The obtained results are also given in Table 2 and show that the materials' rigidity follow the same trend as the T_g , increasing in the following order: HuEpC < HuEpAC < HuEpA. According with the Shore D results, the hardness of the three thermosets

is characteristic to hard materials, the obtained values being comparable with that of commercial materials (ABS High Impact: 75–85SD, PAN: 85–93SD, PET: 85–95SD, PFA:60–65SD, PTFE: 50–65SD).^{47,49}

4.2.2.1. Thermal stability of thermosets

Thermogravimetric analyses were performed under air and nitrogen atmosphere in order to determine the thermo-oxidative and thermal stability of the three thermoset materials. The TGA thermograms as recorded from continuous heating under air flow are plotted in Figure 7.

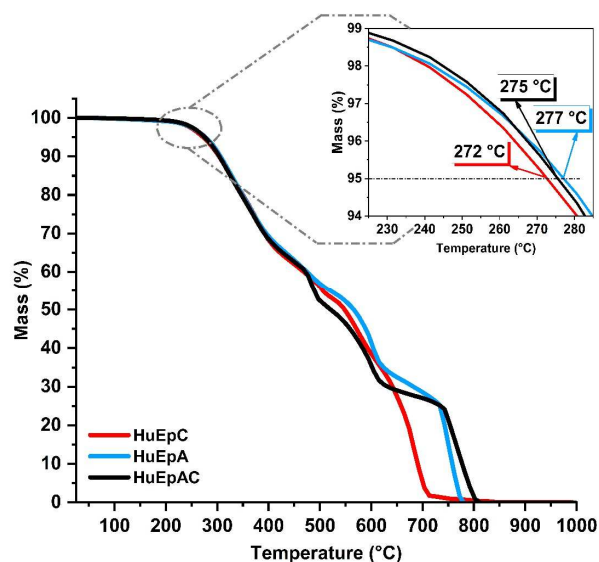


Figure 7. Thermo-oxidative stability of the bio-based humins resins: HuEpC (red line), HuEpA (blue line), HuEpAC (black line); TGA run at $10^{\circ}\text{C min}^{-1}$ under air flow

According with the obtained data, the bio-based thermosets reveal a good thermal stability, the degradation process is accompanied by volatiles release (5% mass loss) at around 280 °C under air. Based on the number of peaks in the DTG thermograms (not presented here) the decomposition process shows the presence of three major stages. This multi-stage decomposition can be explained by the complex profile of humins-based thermosets and also by their heterogeneous structure, as already highlighted by the broad $\tan \delta$ peaks. The first step represents the major thermal decomposition stage for all the three resins, the thermolysis. In this step, the mass loss of the HuEpC resin is approximately 38 wt.% of the initial mass and the end temperature of this degradation occurs at around 450 °C. For the other two resins, with the accelerator, this interval of temperature is larger, ending at around 550 °C, with 45–47 wt.% mass loss. This observation indicates that the thermosets produced in presence of the accelerator are more heterogeneous and more susceptible to thermolysis. In the second step of decomposition the HuEpC resin lost 28 wt.% of mass between 450–620 °C, while the resins

only with the accelerator or combined with the catalyst lost 23 wt.% and 28 wt.% respectively in the range 500–700 °C. The third decomposition is thermal-oxidation and carbonization of the materials.

It is known that the decomposition mechanism and the shape of TGA curves can be influenced by different factors, one of the primary factors being the heating rate of the samples. As the heating rate increases, the decomposition temperature of the sample also increases.⁴⁵ The three bio-based thermosets were investigated under nitrogen flow in four different heating rates between 5–40 °C min⁻¹ in order to analyze the influence of this factor on the thermal stability of the materials. TGA thermograms under nitrogen can be seen in Figure 8 and the results are given in Table 3.

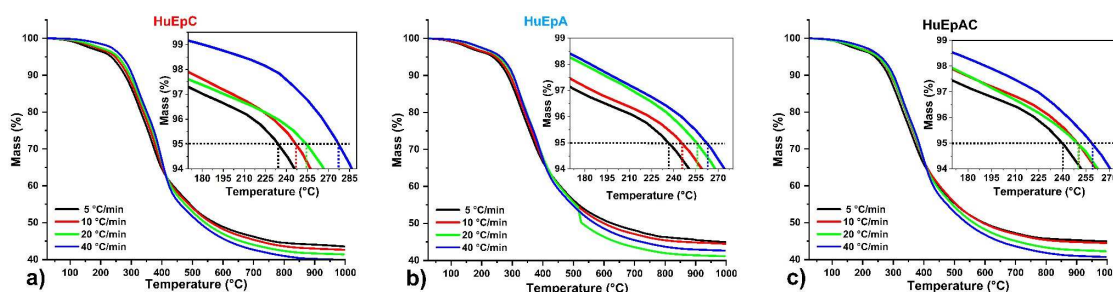


Figure 8. TGA curves at different heating rates under nitrogen flow for the cured humins: a) HuEpC; b) HuEpA; HuEpAC

The thermograms in inert atmosphere show a one stage degradation mechanism and a small shoulder between 150–200 °C which gradually disappears as the heating rate increases. This very small weight loss can be due to the evaporation of moisture or other volatile compounds present in the materials. As expected, by increasing the heating rate the materials start to decompose at higher temperatures.

Table 3. Temperatures of thermal degradation ($T_{5\%}$) of the cured humins bio-based thermosets under inert atmosphere and at different heating rates: a) HuEpC resin; b) HuEpA resin and c) HuEpAC resin

	$T_{5\%}$ (°C) under nitrogen flow			
	5 °C min ⁻¹	10 °C min ⁻¹	20 °C min ⁻¹	40 °C min ⁻¹
HuEpC	232	245	255	270
HuEpA	233	243	255	265
HuEpAC	241	251	250	258

Figure 8 reveals that although the increase of the heating rate improves the thermal stability of the materials at the beginning of degradation, at $T > 450$ °C this factor influences negatively, the thermal stability decreasing. Another fact that show the influence of the analysis parameters on the materials properties is that the heating rate of 5 °C min⁻¹ in nitrogen increase the $T_{5\%}$ temperature of the resins in the following order of HuEpC < HuEpA < HuEpAC, while

at 40 °C min⁻¹ the increase is in the opposite direction. The thermal stabilities of the three humins/epoxy thermosets are improved compared to that of the furan/epoxy bio-resins stipulated in literature ($T_{5\%} = 141\text{--}221$ °C, under air)^{50–52}, the resulting values being comparable with those of commercial epoxy resins.^{53,54}

4.2.2.2. Water absorption analysis

To study the water absorption behavior the three thermosets were immersed in deionized water at 25 °C, and the weight variation was evaluated over time. The evolution of the water sorption is given in Figure 9. The water retention by the thermosets is influenced by numerous factors as the network architecture (mass between crosslinking nodes, crosslinking density, free volume, *etc.*) and by the chemical nature of the components (polar groups).^{55,56} After 24h of immersion in deionized water, the percentage of absorbed water is $\approx 5\text{--}10\%$ (w/w), equivalent with the commercial epoxy values (WA%_{Fiberite 934} = 6.95%, WA%_{Ciba Geigy MY720} = 6.8%).^{57,58}

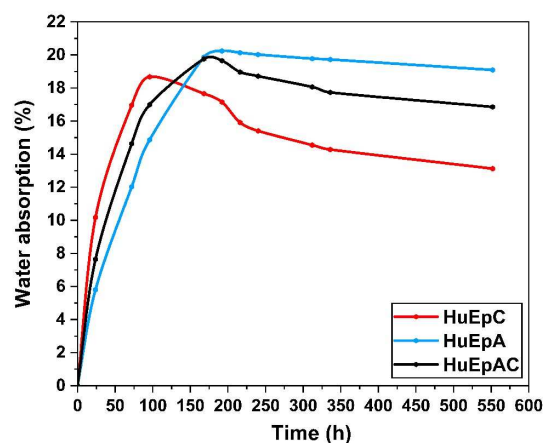


Figure 9. Water absorption % in function of time; Comparison between the three humins-based resins

In Figure 9 it can be observed that the water absorption of the three resins increase in time reaching a maximum point after 96h for HuEpC, 192h for HuEpA and 168h for HuEpAC. The obtained values are again in good accord with the previous results. We can notice that the thermosets prepared with the catalyst, characterized by the lower T_g value and lower degree of crosslinking exhibit the faster water absorption (abrupt slope of the curve). Then, probably the water absorbed molecules block at a certain point the access to the network free volume and the absorption is stop after 75h reaching 19%. The system with the accelerator has a slower kinetic of water absorption with a maximum reached after 170h at around 20%. These values are directly correlated with the materials crosslink densities but also with the number of the free hydroxyl or other polar groups present in the humins-based resins which can increase the water absorption by hydrogen bonding with water. After reaching the maximum absorption value, the water uptake decreases until reached a steady state.

4.2.2.3. Chemical resistance of the bio-based thermosets

Generally, the exposure of polymeric materials to chemical reagents influences and affects the overall properties but especially the mechanical ones. In order to highlight the influence of the chemical reagents on the humins bio-based resins, the three materials were tested in a large variety of solvents like acetone (A), toluene (T), methanol (MeOH), acetonitrile (AcN), dimethylformamide (DMF), dimethyl sulfoxide (DMSO), chloroform (CHCl₃) and tetrahydrofuran (THF) in order to cover a wide range of polar or apolar reagents. Samples in rectangular shape of each type of formulation were immersed in transparent vials with 20 ml solvents and weighed regularly each 24h. The solvents resistance tests were performed for 12 days, because after this time the humins-based materials became stable, gaining a steady state. In Figure 10 can be visualized the appearance of the three resins in different solvents at the end of the experiment (12 days). Considering these results, we can appreciate that the thermosets prepared with the accelerator has the best resistance to the chemical reagents. Again, this finding could be explained by its highest degree of crosslinking, rigidity and stiffness. On the contrast, the thermoset prepared with the catalyst seems the most affected by the polar solvents by small defragmentation in MeOH, being more evident in DMF and DMSO. In the case of the resin with the catalyst + accelerator, a very small decomposition of the material in MeOH and DMSO is observed, in the rest of the solvents being completely resistant. The comparison between these systems is a clear sign that humins/epoxy materials have a different network architecture, chemical bonding and also free functional groups. So, even if the starting comonomers are the same, the nature of the initiator influences drastically the network structure and the overall properties. After 12 days no evolution of the samples occurred.

Figure 11 illustrates the influence of solvents on the weight of bio-based resins, where a positive value implies a weight gain, while a negative value implies a weight reduction. In accordance with the experimental results, it can be observed that the HuEpC resin (red line) present a significative weight loss in MeOH (20.17 wt.%), in DMF (44.95 wt.%), but especially in DMSO (47.77 wt.%). In contrast, the HuEpA resin (blue line) does not lose weight in any of the seven solvents tested, instead this material absorbs small amounts of solvent between 0–0.8% exception the sample immersed in MeOH showing an increase in weight up to 8%.

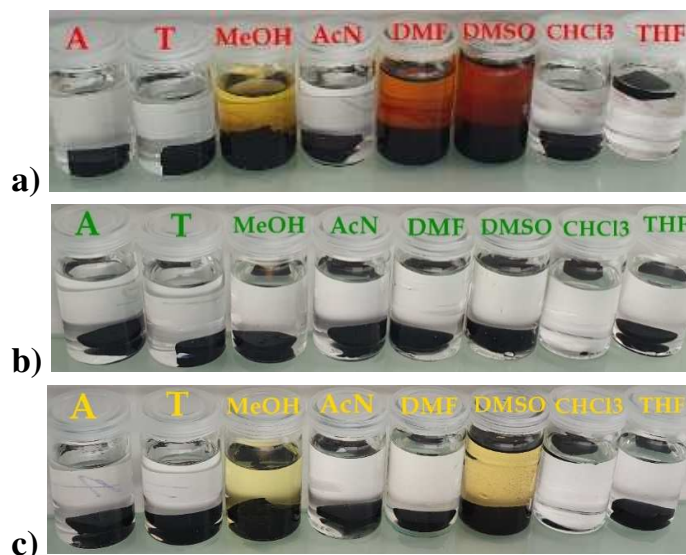


Figure 10. Comparison of chemical stability after immersion in different solvents for 12 days of: a) HuEpC resin, b) HuEpA resin, c) HuEpAC

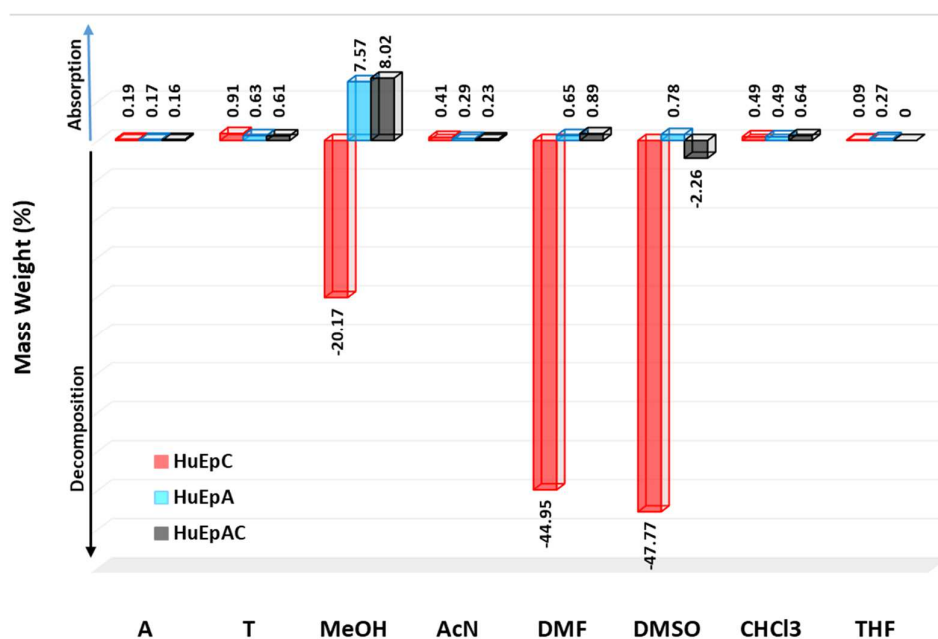


Figure 11. Influence of solvents on the humins/TGPh materials' weight after 288h of immersion at room temperature

4.2.2.4. Bio-based content of Humins/TGPh copolymers

In the last period, a great emphasis is focusing on the development of materials from bio-renewable sources, and on increasing their bio-based content. The bio-based content of a product was defined in 2005 by the US Department of Agriculture⁵⁹ as the amount of bio-based carbon in the material or product as a percentage of the weight (mass) of the total organic carbon in the product. Considering that the structure of humins cannot be precisely defined, so

the reaction mechanism accurately quantified, the bio-based carbon content of the three resins was calculated according to previous studies.^{60,61} Both humins and TGPh are products made from renewable raw materials, so they are 100% bio-based, while BDMA and DMP-30 are 100% petrochemical-based compounds. According to previous studies done on biorefinery humins^{24,62}, it is known that the bio-based carbon of the raw humins is around 54%. Considering the molar mass and the number of carbons in each compound we calculate its carbon percentage. The bio-based carbon content by weight was calculated using the equation:

$$BCC = \frac{\Sigma(W_{100\%} \cdot TC_{100\%})}{\Sigma(W_{100\%} \cdot TC_{100\%}) + \Sigma(W_{0\%} \cdot TC_{0\%})} \cdot 100 \quad (3)$$

where: *BCC* – is the bio-based content of the product expressed as a percentage of the total mass of sample; *W*_{100%} – is the mass of the constituent 100% bio-based, expressed in grams; *TC*_{100%} – is the total carbon of the constituent 100% bio-based, expressed as a percentage of the total molar mass of the constituent; *W*_{0%} – is the mass of the constituent 0% bio-based, expressed in grams; *TC*_{0%} – is the total carbon of the constituent 0% bio-based, expressed as a percentage of the total molar mass of the constituent. The HuEpC and HuEpA systems contains 55 g Humins, 40 g TGPh and 5 g of BDMA or DMP-30, while the HuEpAC system is composed from 55 g Humins, 40 g TGPh, 2.5 g BDMA and 2.5 g DMP-30. Following the calculations, the bio-based carbon content for HuEpC resin is ≈ 93.14%, for HuEpA resin is 94.12% and for the HuEpAC resin is 93.63%.

4.3. Conclusions

In this work, three different thermoset resins were developed by copolymerization of humins with TGPh, a bio-based product obtained from algae or bark tree. Following the calculation of the bio-based carbon content of the humins-based resins considering only the carbon content by weight, it was determined that the *BCC* of the obtained resins is around 94%. The copolymerization's reactivity studies done by DSC reveal a good enthalpy (270–365 J g⁻¹) reaching the maximum reactivity around the temperature of 106–148 °C (depending on the formulation). Also, the physico-chemical and mechanical properties of the cured bio-based resins were investigated using different technics as TGA, DMA, Shore hardness test, water absorption and solvents resistance. It was revealed that the obtained materials present very good mechanical properties with values for the *E'* in glassy region ≈ 3.7–5 GPa. The tan δ -maxima of the three humins-based resins ranges from 122 °C to 154 °C. Also, the thermosets hardness values of 82–85 SD confirms the stiffness of these materials. The thermogravimetric analyses of the materials revealed a very good thermal stability with *T*_{5%} ≈ 272–277 °C. The

bio-resins developed in this work present also a good chemical resistance over time, the HuEpA resin being unaffected in all solvents tested after 12 days of immersion.

In conclusion, following this study, three humins/epoxy-based copolymers thermosets of 95% bio-based resins have been successfully developed, with mechanical performance comparable to those of industrial thermoset materials used in construction or automotive sectors.

4.4. Experimental

4.4.1. Materials

One of the main compounds used in the development of the thermoset resins presented in this study is represented by the industrial polymeric black by-product called Humins produced and supplied by Avantium Chemicals at their Pilot Plant in Geleen, The Netherlands. In order to obtain sustainable thermosets, the humins were copolymerized with triglycidyl ether of phloroglucinol (TGPh) with 7.8 meq/g epoxy content and a repeating unit number (n) between 0.5–1.2, supplied by Specific Polymers (Castries–France). *N,N*-Dimethylbenzylamine (BDMA) and 2,4,6-Tris(dimethylaminomethyl)phenol (DMP-30) purchased from Sigma-Aldrich were used as received to initiate and accelerate the copolymerization and crosslinking between the two bio-compounds.

4.4.1.1. Samples preparation

To design and to develop sustainable thermosets the proper amount of humins (55 wt.%) was weighted and heated on a heating plate to reduce its viscosity. The necessary amount of epoxy comonomer (40 wt.% TGPh) was added and mechanically mixed under temperature with the preheated humins. To obtain the optimal parameters for the copolymerization different amounts of catalyst (BDMA) / accelerator (DMP-30) were analyzed individually or in combination of both. The thermodynamic parameters (time and temperature) of curing but also the reactivity of all the mixtures were analyzed in order to select the optimal formulations for the development of the materials. After the reactivity study, three formulations were selected. The mixture of humins with TGPh was combined with 5 wt.% BDMA or 5 wt.% DMP-30 but also with both (2.5/2.5 wt.%), poured into silicone molds and cured in oven. The materials were crosslinked for 2h at 80 °C and after another 2h at 150 °C. Thereafter, the materials were post-cured at 180 °C for 1h. In order to facilitate the identification of the different formulations, the compounds were noted with the following acronyms: “Hu” for humins, “Ep” for TGPh epoxide, “C” for BDMA catalyst and “A” for DMP-30 accelerator. According to these abbreviations, formulation “HuEpC” correspond to the resin with 55 wt.% humins/ 40 wt.% TGPh / 5 wt.% BDMA, “HuEpA” for the system with 55 wt.% humins/ 40 wt.% TGPh/ 5 wt.%

DMP-30 and “HuEpAC” for the formulation with 55 wt.% humins/ 40 wt.% TGPh / 2.5 wt.% BDMA / 2.5 wt.% DMP-30. The physico-chemical and mechanical properties of the three selected formulations were analyzed and compared.

4.4.2. Experimental techniques

4.4.2.1. Differential Scanning Calorimetry (DSC)

The thermal aspects of copolymerization were analyzed by differential scanning calorimetry, performed with a Mettler-Toledo DSC 3 apparatus equipped with STARe Software. The crosslinking reactions between humins and TGPh were directly performed in 40 μl aluminum pans. Samples of 5–8 mg were reacted under non-isothermal conditions between 25–230 $^{\circ}\text{C}$, under oxidative atmosphere (150 mL min^{-1}) and at a heating rate of 10 $^{\circ}\text{C min}^{-1}$. The DSC studies have been used also to study the completion of chemical conversions or the glass transitions of the thermoset samples prepared in oven. For this, samples of 8–12 mg of cured materials were introduced into 40 μl Al crucibles, and studied over a temperature range from -50 $^{\circ}\text{C}$ to 150 $^{\circ}\text{C}$. The tests were performed at a heating rate of 10 $^{\circ}\text{C min}^{-1}$ under air flow (150 mL min^{-1}).

4.4.2.2. Dynamic mechanical analysis (DMA)

The dynamic mechanical measurements were conducted in a Mettler Toledo DMA 1 apparatus equipped with a three-points bending assembly. The humins-based thermosets were prepared in rectangular shapes of established dimensions (48 length \times 8 width \times 4 thickness mm^3). The DMA tests were performed in the temperature-scanning mode from -70 $^{\circ}\text{C}$ to 225 $^{\circ}\text{C}$, with a constant displacement amplitude of 20 μm and a frequency of 1.0 Hz, at a heating rate of 3 $^{\circ}\text{C min}^{-1}$ under nitrogen atmosphere. By this method, the storage (E') and loss (E'') Young modules but also the damping factor ($\tan \delta = E''/E'$) of the thermosets were determined. According to ASTM E1640-13⁴¹ and ASTM D7028-07⁴², three different values of glass transition (T_g) were determined from DMA measurements such as $T_{g-onset}$ related to the E' drop, T_{g-loss} defined as maximum temperature of E'' and T_{g-peak} corresponding to the maximum temperature of the damping factor $\tan \delta$. The DMA analysis was also used to obtain collections of frequency data as a function of temperature in order to develop the master curves of humins-based resins and to study the effect of frequency on changes caused by temperature on materials. The measurements were performed in the frequency range 10 Hz to 0.1 Hz at a logarithmic increment of 10 steps/decade, under isothermal conditions at different temperatures between -25 $^{\circ}\text{C}$ to 250 $^{\circ}\text{C}$. The maximum force amplitude was 0.1 N and the displacement amplitude was 20 μm .

4.4.2.3. Density of the thermoset resins

The density of the final resins was determined experimentally using the ISO 9427 standard. For five rectangular samples ($50 \times 8 \times 4 \text{ mm}^3$) of each formulation the volume was calculated, and the mass was determined by weighing with a ML3002T Mettler-Toledo precision balance. The density of the samples was calculated as the ratio of the mass to volume.

4.4.2.4. Shore hardness test

A Zwick Roell 3116 Hardness Tester was used to determine the hardness of the humins-based resins, in accordance with ISO 7619-1, ASTM D2240 and ISO 868. The Shore D hardness device was pressed smoothly against the samples with a load force of $50 \text{ N} \pm 0.5 \text{ N}$. The samples hardness value was read after the firm contact between the presser foot and the tested materials.

4.4.2.5. Thermogravimetric analysis (TGA)

To determine the thermal stability of the materials a TGA 2 Mettler-Toledo apparatus was used. The thermal behavior of samples in oxidative atmosphere was analyzed in the temperature range from $25 \text{ }^\circ\text{C}$ to $1000 \text{ }^\circ\text{C}$, at a heating rate of $10 \text{ }^\circ\text{C min}^{-1}$ and an air flow of 150 mL min^{-1} . In order to determine the influence of the heating rate on the thermal stability, the resins were analyzed between $25\text{--}1000 \text{ }^\circ\text{C}$, in nitrogen flow (150 mL min^{-1}), varying the heating rates from $5 \text{ }^\circ\text{C min}^{-1}$ to $40 \text{ }^\circ\text{C min}^{-1}$. For both methods of analysis, samples with weight between $9\text{--}12 \text{ mg}$ were tested in $70 \text{ }\mu\text{l}$ aluminum pans.

4.4.2.6. Water absorption

Water absorption at $25 \text{ }^\circ\text{C}$ of humins-based resins was determined according to ASTM D570 standard test method.⁶³ Five rectangular ($50 \times 8 \times 4 \text{ mm}^3$) samples for each formulation were dried in an oven at $50 \text{ }^\circ\text{C}$ for 24h, after cooled in a desiccator and weighed (t_0). Then, the specimens were immersed in distilled water and maintained at room temperature for 24h. The samples were removed from water after 24h, wiped with a dry towel, weighed and then immediately immersed again in distilled water. The percentage of water absorption was calculated using the next equation:

$$WA\% = \frac{\text{wet weight} - \text{conditioned weight}}{\text{conditioned weight}} \times 100 \quad (4)$$

4.4.2.7. Chemical resistance test

The chemical stability of the prepared thermosets was tested in different solvents as acetone, toluene, methanol, acetonitrile, dimethylformamide, dimethyl sulfoxide, chloroform and tetrahydrofuran. In the first step, the samples, with $15.5 \times 15.5 \times 4.5 \text{ mm}^3$ dimensions were weighed and then immersed in 20 ml of solvent. After 24h, the samples were removed from solvents, wiped with dry clothes, weighed and then immediately immersed in the recipient with

solvent. The samples stability against the solvents was determined visually, but also quantitatively using the following equation:

$$\text{Weight, \%} = \frac{\text{wet weight-conditioned weight}}{\text{conditioned weight}} \times 100 \quad (5)$$

4.4.2.8. Bio-based carbon content

The bio-based carbon content of the materials was determined according with the paper of Pan *et al.*⁶⁰. Humins and triglycidyl ether of phloroglucinol are 100% bio-based. Firstly, the percentage of carbon was determined for each compound, then the bio-based carbon content for the three formulations was calculated based on their mass weight.

Acknowledgements

Funding for this work was received from the European Union's Horizon 2020 Research and Innovation program under Grant Agreement 723268 on a project KaRMA2020.

Notes and references

- (1) Brostow, W.; Lobland, H. E. H. *Materials: Introduction and Applications*; John Wiley and Sons, 2017.
- (2) European commission. *Plastic Waste: Ecological and Human Health Impacts*; 2011. <https://doi.org/KH-31-13-768-EN-N>.
- (3) Geyer, R.; Jambeck, J. R.; Law, K. L. Production, Use, and Fate of All Plastics Ever Made. *Sci. Adv.* **2017**, *3* (7), e1700782. <https://doi.org/10.1126/sciadv.1700782>.
- (4) Ritchie, H.; Roser, M. Plastic Pollution <https://ourworldindata.org/plastic-pollution>.
- (5) Bobade, S. K.; Paluvai, N. R.; Mohanty, S.; Nayak, S. K. Bio-Based Thermosetting Resins for Future Generation: A Review. *Polym. - Plast. Technol. Eng.* **2016**, *55* (17), 1863–1896. <https://doi.org/10.1080/03602559.2016.1185624>.
- (6) Ménard, R.; Negrell, C.; Fache, M.; Ferry, L.; Sonnier, R.; David, G. From a Bio-Based Phosphorus-Containing Epoxy Monomer to Fully Bio-Based Flame-Retardant Thermosets. *RSC Adv.* **2015**, *5* (87), 70856–70867. <https://doi.org/10.1039/c5ra12859e>.
- (7) Li, Y.; Fu, X.; Duan, D.; Liu, X.; Xu, J.; Gao, X. Extraction and Identification of Phlorotannins from the Brown Alga, *Sargassum Fusiforme* (Harvey) Setchell. *Mar. Drugs* **2017**, *15* (2). <https://doi.org/10.3390/md15020049>.
- (8) Arbenz, A.; Avérous, L. Chemical Modification of Tannins to Elaborate Aromatic Biobased Macromolecular Architectures. *Green Chem.* **2015**, *17* (5), 2626–2646. <https://doi.org/10.1039/c5gc00282f>.
- (9) Ornaghi-Junior, H. L.; Zattera, A. J.; Amico, S. C. Dynamic Mechanical Properties and Correlation with Dynamic Fragility of Sisal Reinforced Composites. *Polym. Compos.* **2014**, *36* (1). <https://doi.org/10.1002/pc.22925>.
- (10) Kirke, D. A.; Smyth, T. J.; Rai, D. K.; Kenny, O.; Stengel, D. B. The Chemical and Antioxidant Stability of Isolated Low Molecular Weight Phlorotannins. *Food Chem.* **2017**, *221*, 1104–1112. <https://doi.org/10.1016/j.foodchem.2016.11.050>.
- (11) Park, C.; Cha, H. J.; Hong, S. H.; Kim, G. Y.; Kim, S.; Kim, H. S.; Kim, B. W.; Jeon, Y. J.;

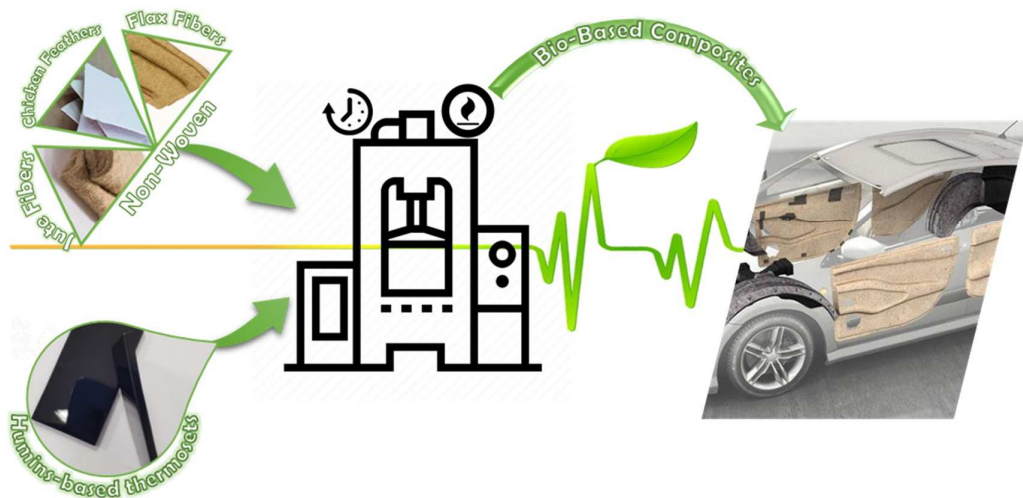
- Choi, Y. H. Protective Effect of Phloroglucinol on Oxidative Stress-Induced DNA Damage and Apoptosis through Activation of the Nrf2/HO-1 Signaling Pathway in HaCaT Human Keratinocytes. *Mar. Drugs* **2019**, *17* (4), 1–16. <https://doi.org/10.3390/md17040225>.
- (12) Ng, F.; Bonnet, L.; David, G.; Caillol, S. Novel Biobased and Food Contact Epoxy Coatings for Glass Toughening Applications. *Prog. Org. Coatings* **2017**, *109*, 1–8. <https://doi.org/10.1016/j.porgcoat.2017.04.008>.
- (13) Peer, M.; Qajar, A.; Rajagopalan, R.; Foley, H. C. Synthesis of Carbon with Bimodal Porosity by Simultaneous Polymerization of Furfuryl Alcohol and Phloroglucinol. *Microporous Mesoporous Mater.* **2014**, *196*, 235–242. <https://doi.org/10.1016/j.micromeso.2014.05.020>.
- (14) Tripathi, P. K.; Gan, L.; Liu, M.; Ma, X.; Zhao, Y.; Zhu, D.; Xu, Z.; Chen, L.; Rao, N. N. One-Pot Assembly of Silica@two Polymeric Shells for Synthesis of Hollow Carbon Porous Nanospheres: Adsorption of Bisphenol A. *Mater. Lett.* **2014**, *120*, 108–110. <https://doi.org/10.1016/j.matlet.2014.01.057>.
- (15) Huang, X.; Li, W.; Li, S.; Wang, C.; Zhang, M.; Sen Luan; Hou, X.; Wang, Q. The Effect of Compressed CO₂ on the Self-Assembly of Surfactants for Facile Preparation of Ordered Mesoporous Carbon Materials. *Soft Matter* **2017**, *13* (41), 7505–7513. <https://doi.org/10.1039/c7sm01839h>.
- (16) Gao, M.; Fu, J.; Wang, M.; Wang, K.; Wang, S.; Wang, Z.; Chen, Z.; Xu, Q. A Self-Template and Self Activation Co-Coupling Green Strategy to Synthesize High Surface Area Ternary-Doped Hollow Carbon Microspheres for High Performance Supercapacitors. *J. Colloid Interface Sci.* **2018**, *524*, 165–176.
- (17) Isikgor, F. H.; Becer, C. R. Lignocellulosic Biomass: A Sustainable Platform for the Production of Bio-Based Chemicals and Polymers. *Polym. Chem.* **2015**, *6* (25), 4497–4559. <https://doi.org/10.1039/c5py00263j>.
- (18) Patil, S. K. R.; Lund, C. R. F. Formation and Growth of Humins via Aldol Addition and Condensation during Acid-Catalyzed Conversion of 5-Hydroxymethylfurfural. *Energy and Fuels* **2011**, *25* (10), 4745–4755. <https://doi.org/10.1021/ef2010157>.
- (19) Van Zandvoort, I.; Wang, Y.; Rasrendra, C. B.; Van Eck, E. R. H.; Bruijninx, P. C. A.; Heeres, H. J.; Weckhuysen, B. M. Formation, Molecular Structure, and Morphology of Humins in Biomass Conversion: Influence of Feedstock and Processing Conditions. *ChemSusChem* **2013**, *6* (9), 1745–1758. <https://doi.org/10.1002/cssc.201300332>.
- (20) Hoang, T. M. C.; Eck, E. R. H. van; Gardeniers, J. G. E.; Lefferts, L.; Seshan, K. Humin Based By-Products from Bioprocessing as Potential Carbonaceous Source for Synthesis Gas Production. *Green Chem.* **2015**, *17*, 959–972. <https://doi.org/10.1039/x0xx00000x>.
- (21) Hu, X.; Lievens, C.; Larcher, A.; Li, C. Z. Reaction Pathways of Glucose during Esterification: Effects of Reaction Parameters on the Formation of Humin Type Polymers. *Bioresour. Technol.* **2011**, *102* (21), 10104–10113. <https://doi.org/10.1016/j.biortech.2011.08.040>.
- (22) Filiciotto, L.; Balu, A. M.; Van der Waal, J. C.; Luque, R. Catalytic Insights into the Production of Biomass-Derived Side Products Methyl Levulinate, Furfural and Humins. *Catal. Today* **2018**, *302*, 2–15. <https://doi.org/10.1016/j.cattod.2017.03.008>.
- (23) Constant, S.; Lancefield, C. S.; Weckhuysen, B. M.; Bruijninx, P. C. A. Quantification and Classification of Carbonyls in Industrial Humins and Lignins by ¹⁹F NMR. *ACS Sustain. Chem. Eng.* **2017**, *5* (1), 965–972. <https://doi.org/10.1021/acssuschemeng.6b02292>.
- (24) Muralidhara, A.; Tosi, P.; Mija, A.; Sbirrazzuoli, N.; Len, C.; Engelen, V.; De Jong, E.; Marlair, G. Insights on Thermal and Fire Hazards of Humins in Support of Their Sustainable Use in Advanced Biorefineries. *ACS Sustain. Chem. Eng.* **2018**, *6* (12), 16692–16701. <https://doi.org/10.1021/acssuschemeng.8b03971>.
- (25) Hoang, T. M. C.; Lefferts, L.; Seshan, K. Valorization of Humin-Based Byproducts from Biomass Processing - A Route to Sustainable Hydrogen. *ChemSusChem* **2013**, *6* (9), 1651–1658. <https://doi.org/10.1002/cssc.201300446>.

- (26) Mija, A.; Jong, E. De; Waal, J. C. Van der; Klink, G. P. M. Van. Humins-Containing Foam. WO 2017/074183 A1, 2017.
- (27) Tosi, P.; van Klink, G. P. M.; Celzard, A.; Fierro, V.; Vincent, L.; de Jong, E.; Mija, A. Auto-Crosslinked Rigid Foams Derived from Biorefinery Byproducts. *ChemSusChem* **2018**, *11* (16), 2797–2809. <https://doi.org/10.1002/cssc.201800778>.
- (28) Mija, A. C.; Waal, J. C. Van Der; Jong, E. De; Klink, G. P. Van. Process for the Modification of Humins. WO2018/062995 A1, 2018.
- (29) Kang, S.; Fu, J.; Deng, Z.; Jiang, S.; Zhong, G.; Xu, Y.; Guo, J.; Zhou, J. Valorization of Biomass Hydrolysis Waste: Activated Carbon from Humins as Exceptional Sorbent for Wastewater Treatment. *Sustain.* **2018**, *10* (6), 16–19. <https://doi.org/10.3390/su10061795>.
- (30) Pin, J. M.; Guigo, N.; Mija, A.; Vincent, L.; Sbirrazzuoli, N.; Van Der Waal, J. C.; De Jong, E. Valorization of Biorefinery Side-Stream Products: Combination of Humins with Polyfurfuryl Alcohol for Composite Elaboration. *ACS Sustain. Chem. Eng.* **2014**, *2* (9), 2182–2190. <https://doi.org/10.1021/sc5003769>.
- (31) Dinu, R.; Mija, A. Cross-Linked Polyfuran Networks with Elastomeric Behaviour Based on Humins Biorefinery by-Products. *Green Chem.* **2019**, *21*, 6277–6289. <https://doi.org/10.1039/c9gc01813a>.
- (32) Montané, X.; Dinu, R.; Mija, A. Synthesis of Resins Using Epoxies and Humins as Building Blocks: A Mechanistic Study Based on in-Situ FT-IR and NMR Spectroscopies. *Molecules* **2019**, *24* (22). <https://doi.org/10.3390/molecules24224110>.
- (33) Cantarutti, C.; Dinu, R.; Mija, A. Biorefinery By-Products and Epoxy Biorenewable Monomers: A Structural Elucidation of Humins and Triglycidyl Ether of Phloroglucinol Crosslinking. *Biomacromolecules* **2019**. <https://doi.org/10.1021/acs.biomac.9b01248>.
- (34) Ebewele, R. *Polymer Science and Technology*; CRC Press LLC, 2000. <https://doi.org/10.1201/9781420057805-7>.
- (35) Brostow, W.; Hagg Lobland, H. E.; Narkis, M. Sliding Wear, Viscoelasticity, and Brittleness of Polymers. *J. Mater. Res.* **2006**, *21* (9), 2422–2428. <https://doi.org/10.1557/jmr.2006.0300>.
- (36) Brostow, W.; Hagg Lobland, H. E. Brittleness of Materials: Implications for Composites and a Relation to Impact Strength. *J. Mater. Sci.* **2010**, *45* (1), 242–250. <https://doi.org/10.1007/s10853-009-3926-5>.
- (37) Brostow, W.; Lobland, H. E. H.; Narkis, M. The Concept of Materials Brittleness and Its Applications. *Polym. Bull.* **2011**, *67* (8), 1697–1707. <https://doi.org/10.1007/s00289-011-0573-1>.
- (38) Menard, K. *Dynamic Mechanical Analysis - A Practical Introduction*, 2nd ed.; CRC Press Taylor & Francis Group, 2008.
- (39) Brostow, W. Reliability and Prediction of Long-Term Performance of Polymer-Based Materials. *Pure Appl. Chem.* **2009**, *81* (3), 417–432. <https://doi.org/10.1351/PAC-CON-08-08-03>.
- (40) Kalogerias, I. M.; Hagg Lobland, H. E. The Nature of the Glassy State: Structure and Glass Transitions. *J. Mater. Educ.* **2012**, *34* (3–4), 69–94.
- (41) ASTM-E1640. Assignment of the Glass Transition Temperature By Dynamic Mechanical Analysis. 2013. <https://doi.org/10.1520/E1640-13>.
- (42) ASTM-D7028. Standard Test Method for Glass Transition Temperature (DMA T_g) of Polymer Matrix Composites by Dynamic Mechanical Analysis (DMA). 2008. <https://doi.org/10.1520/D7028-07E01.2>.
- (43) Fache, M.; Viola, A.; Auvergne, R.; Boutevin, B.; Caillol, S. Biobased Epoxy Thermosets from Vanillin-Derived Oligomers. *Eur. Polym. J.* **2015**, *68*, 526–535. <https://doi.org/10.1016/j.eurpolymj.2015.03.048>.
- (44) Flory, P. J. *Principles of Polymer Chemistry*; Cornell University Press: Ithaca, New York, 1953.

- (45) Ratna, D. *Handbook of Thermoset Resins*; Smithers Rapra, 2009.
- (46) Ma, S.; Liu, X.; Jiang, Y.; Tang, Z.; Zhang, C.; Zhu, J. Bio-Based Epoxy Resin from Itaconic Acid and Its Thermosets Cured with Anhydride and Comonomers. *Green Chem.* **2013**, *15* (1), 245–254. <https://doi.org/10.1039/C2GC36715G>.
- (47) Hardness Shore D <https://omnexus.specialchem.com/polymer-properties/properties/hardness-shore-d>.
- (48) Cambridge University Engineering Department. *Materials Data Book*; 2003.
- (49) Vian, W. D.; Denton, N. L. Hardness Comparison of Polymer Specimens Produced with Different Processes. In *ASEE Annual Conference and Exposition, Conference Proceedings*; 2018; Vol. June.
- (50) Monti, M.; Hoydonckx, H.; Stappers, F.; Camino, G. Thermal and Combustion Behavior of Furan Resin/Silica Nanocomposites. *Eur. Polym. J.* **2015**, *67* (November), 561–569. <https://doi.org/10.1016/j.eurpolymj.2015.02.005>.
- (51) Liu, Y.; Via, B.; Pan, Y.; Cheng, Q.; Guo, H.; Auad, M.; Taylor, S. Preparation and Characterization of Epoxy Resin Cross-Linked with High Wood Pyrolysis Bio-Oil Substitution by Acetone Pretreatment. *Polymers (Basel)*. **2017**, *9* (12), 106. <https://doi.org/10.3390/polym9030106>.
- (52) Nouailhas, H.; Aouf, C.; Guernevé, C. Le; Caillol, S.; Boutevin, B.; Fulcrand-Hoh, H. Synthesis and Properties of Biobased Epoxy Resins. Part 1. Glycidylation of Flavonoids by Epichlorohydrin. *J. Polym. Sci. Part A Polym. Chem.* **2011**, *49*, 2261–2270. <https://doi.org/10.1002/pola>.
- (53) Chairat, A.; Joulia, X.; Floquet, P.; Vergnes, H.; Ablitzer, C.; Fiquet, O.; Brothier, M. Thermal Degradation Kinetics of a Commercial Epoxy Resin-Comparative Analysis of Parameter Estimation Methods. *J. Appl. Polym. Sci.* **2015**, *132* (27). <https://doi.org/10.1002/app.42201>.
- (54) Zhu, J.; Wu, Y.; Zhao, L.; Wei, H. L.; Chu, H. J.; He, J. Study of Thermal Properties of Curing of DGEBA Epoxy Resin with Hexakis-(4-Aminophenoxy)-Cyclotriphosphazene. *Adv. Mater. Res.* **2011**, *284–286*, 365–368. <https://doi.org/10.4028/www.scientific.net/AMR.284-286.365>.
- (55) Chen, Y.; Xi, Z.; Zhao, L. New Bio-Based Polymeric Thermosets Synthesized by Ring-Opening Polymerization of Epoxidized Soybean Oil with a Green Curing Agent. *Eur. Polym. J.* **2016**, *84*, 435–447. <https://doi.org/10.1016/j.eurpolymj.2016.08.038>.
- (56) Li, L.; Yu, Y.; Wu, Q.; Zhan, G.; Li, S. Effect of Chemical Structure on the Water Sorption of Amine-Cured Epoxy Resins. *Corros. Sci.* **2009**, *51* (12), 3000–3006. <https://doi.org/10.1016/j.corsci.2009.08.029>.
- (57) Bouvet, G.; Dang, N.; Cohendoz, S.; Feaugas, X.; Mallarino, S.; Touzain, S. Impact of Polar Groups Concentration and Free Volume on Water Sorption in Model Epoxy Free Films and Coatings. *Prog. Org. Coatings* **2016**, *96*, 32–41. <https://doi.org/10.1016/j.porgcoat.2015.12.011>.
- (58) Zhou, J. M.; Lucas, J. P. Hygrothermal Effects of Epoxy Resin. Part I: The Nature of Water in Epoxy. *Polymer (Guildf)*. **1999**, *40* (20), 5505–5512.
- (59) Norton, G. A.; Devlin, S. L. Determining the Modern Carbon Content of Biobased Products Using Radiocarbon Analysis. *Bioresour. Technol.* **2006**, *97* (16), 2084–2090. <https://doi.org/10.1016/j.biortech.2005.08.017>.
- (60) Pan, X.; Sengupta, P.; Webster, D. C. High Biobased Content Epoxy-Anhydride Thermosets from Epoxidized Sucrose Esters of Fatty Acids. *Biomacromolecules* **2011**, *12* (6), 2416–2428. <https://doi.org/10.1021/bm200549c>.
- (61) NCS-16785. *Bio-Based Content Certification Scheme*; 2016.
- (62) Muralidhara, A.; Bado-Nilles, A.; Marlair, G.; Engelen, V.; Len, C.; Pandard, P. Humins in the Environment: Early Stage Insights on Ecotoxicological Aspects. *Biofuels, Bioprod. Biorefining* **2018**, 1–7. <https://doi.org/10.1002/bbb.1964>.
- (63) ASTM-D570. Water Absorption of Plastics. 1998. <https://doi.org/10.1520/D0570-98>.

Chapter 5

Reprocessable Humins Thermosets and Composites for Sustainable Applications



This chapter is based on Roxana Dinu, Sarah Montes, François Orange and Alice Mija, *“Reprocessable and Sustainable Composites Based on Humins Matrices Reinforced with Chicken Feathers and Vegetal Non-Woven Fibers”*, (in peer review in Green Chemistry).

Abstract

Reduction of polymeric waste together with industrial by-products valorisation are the main objectives of competitive researches. In this perspective, this work reports the preparation of sustainable thermosetting composites having reprocessing ability. The thermosetting matrices were designed by the combination of the humins a biorefinery based product with two epoxide comonomers. The chicken feathers and vegetal non-woven fibers were used for matrices reinforcement. The obtained composites show an increase of T_g region compared with the neat matrices and Shore hardness values (74–85 SD) comparable with those of commercial materials such as epoxy/glass fibers or epoxy/carbon fibers composites. By SEM analysis a proper adhesion and a good compatibility between the matrices and the bio-fillers was observed, without a prior treatment of the fibers. This work reports for the first time the elaboration of reprocessable humins based thermosets. The prepared resins and composites proved their capacity to be mechanically recycled without significant changes in their properties.

5.1. Introduction

One of the main problems of the 21st century remains the environmental concerns caused by the production of plastic materials, both thermosets and thermoplastics, based on fossil and non-renewable raw- materials, which are not biodegradable or recyclable. This leads to a continuous increase of the waste quantities in the landfills.¹ The global plastic production in 2018 was estimated to around 380 million tons.² Since the beginning of the large-scale production and use of synthetic plastics developed around 1950, in these last 70 years were produced about 6.3 billion tons of plastics. Only in 2015 were generated 6300 Mt of plastic waste, of which 9% were recycled, 12% incinerated and 79% were deposited in landfills or in nature.³ With the urgent need to reduce environment burden derived from plastics, new routes of development, recovery and reuse of polymers and materials were investigated, not only for thermoplastics materials but also in the field of thermosets composites, which traditionally were not recyclable. In the case of composites, intense researches were initiated regarding both the development of starting materials from natural, renewable resources or wastes as well as the investigation in their recycling and subsequent reuse. In this paper the development of recyclable thermoset composite materials using industrial by-products such as humins and chicken feathers, or vegetal fibers such as flax and jute is proposed.

Lignocellulosic biomass is an important renewable resource, currently converted into chemical platform molecules. The largest constituents of lignocellulose are the carbohydrates such as cellulose (35–50%), hemicellulose (20–35%) and lignin (10–25%).⁴ Valorization of the lignocellulose biomass in the biorefineries by conversion of carbohydrates into valuable chemical-platform molecules (5-hydroxymethyl furfural, furfural and levulinic acid) also leads to the formation of a dark-colored viscous by-product called humins. According to the previous studies,^{5–9} humins is a complex and heterogeneous product derived from sugar conversion processes, presenting an unknown and variable furan structure that is influenced by the type of feedstock and the processing parameters. Humins are carbon-rich agglomerate particles containing a variety of functional groups such as alcohol, acid, ketone and aldehyde. It has also been shown that this by-product is composed of approximately 50–65 wt.% C, 29–46% wt.% O, and 4–5.5 wt.% H.^{5–9} The complex structure but also the abundance of different functional groups present in humins favors the conversion of this by-product into a potential renewable material for new end-products. This complex product was involved in the development of various categories of materials such as porous carbonaceous materials used as adsorbents, insulation materials or support for solid catalysts,^{10–12} but also as furanic resins and composites for different application sectors such as automotive and construction industries.^{13–16}

Natural fibers have been extensively used as fillers in composites reinforcement in recent years. In general, these fibers are produced from plants, animals or mineral based sources. The major structural component of the vegetal fibers is cellulose, while the animal fibers are constituted by proteins.¹⁷ Natural fibers have an important number of advantages, such as their wide availability at relatively low costs, their ability to be recycled, their bio-renewability and biodegradability, as well as their interesting physical and mechanical properties.¹⁸ Bast fibers, such as flax and jute fibers, are extracted from the stem ribbon and exhibit specific strength and stiffness, flexibility during processing, low self-weight, and resistance to corrosion and fatigue properties.¹⁹ Like any material, besides the multitude of benefits, the plant fibers have some disadvantages such as high moisture absorption, high anisotropy of properties (depending on plant species, age, climate, soil condition, *etc.*), low compatibility with the resins. They are also less homogeneous compared to the glass and carbon fibers.^{17,20} The use of vegetal fibers (*e.g.*, flax, jute, hemp) is more interesting when strength, lightweight, and noise absorption are important, such as in the automotive and construction industries.^{21,22} One of the first uses of vegetal fibers in the automotive industry was made in 1941 by Henry Ford, producing composites from soybean resin reinforced with hemp or flax in order to manufacture exterior body panels.²² Nowadays, the increasing legislation regarding the end of life of vehicles (Directive 2000/53/EC²³, Directive 2002/96/EC²⁴, *etc.*), have led to the use of vegetal fibers in the development of composite materials by most automotive companies.

Another type of natural fibers selected for this work are those from animal-based sources, and in our case chicken feathers. Avian fibers are an important source of protein, becoming a good alternative for replacing the petroleum-based materials. Chicken feathers represent one of the main by-products from the poultry industry, with approximately 9 million tons being generated annually.²⁵ Chicken feathers are mainly composed of keratin ($\approx 91\%$), representing a very rich resource of high protein raw material and are generally deposited in landfills or burned.²⁶ In addition of being a natural product, chicken feathers fibers also have a large number of important advantages which have led to their use in a wide range of applications. Considering the large amount of keratin, their low density (0.8 g/cm^3), their wide availability, recyclability, biodegradability, the both hydrophobic and hydrophilic character (60:40) as well as their physical and mechanical properties,²⁷ chicken feathers are valuable resources with feasible applicability in biomedical field,²⁸ thermoplastics, thermosets or composites for different sectors such as packaging,^{29–31} automotive or construction industries.^{27,32–37}

In the present work, the main part of the thermoset resins' composition used is represented by humins. The bio-based thermosetting resins were obtained by copolymerization

of humins with two epoxy compounds such as resorcinol diglycidyl ether (RDGE), a bio-based epoxide, or trimethylolpropane triglycidyl ether (TMPTE). The crosslinking reaction has been catalysed with the help of N, N-dimethylbenzylamine (BDMA) or 2,4,6-tris(dimethylaminomethyl)phenol (DMP-30). The humins-based thermoset resins were used as matrices in the development of bio-composites. The polymeric matrices were reinforced with four non-woven fabrics made from chicken feathers or vegetal fibers. To select the optimal formulations for composites manufacturing, the thermodynamic parameters of curing, the reactivity of the mixtures but also the ability of the final materials to be recycled were analyzed. Thereafter, the bio-based composites were produced using the two selected resins formulations (one from each epoxy monomer) as matrix and 4 non-woven fabrics as structural elements for reinforcement. The two resins used in this study for the development of bio-composites were selected after determining their recycling behavior. Both resins and composites were recycled using the mechanical method.

The purpose of this work is the development of bio-based composites considering several requirements. Firstly, the valorization of an industrial waste by their use in the development of new materials; the thermoset resins from this work were developed using a significant, maximum possible, amount of industrial by-product (55 wt.% humins). Secondly, the next criterion was the development of eco-friendly materials using natural and renewable raw materials; bio-based composites were produced using untreated chicken feather and vegetal fibers (flax and jute) non-woven as reinforcement. Finally, the study aims to develop composites capable of being recyclable by industrially and economically feasible techniques; in this work, the humins-based bio-composites reinforced with natural fibers have been successfully recycled using thermo-mechanical methods without affecting their properties.

5.2. Results and Discussion

5.2.1. Study of systems reactivity. Selection of optimal thermosetting matrices for the bio-composites development

Firstly, this work focuses on the preparation of bio-based thermoset resins which will act as a matrix in the development of the bio-composites. The DSC tool was used to establish the thermodynamic parameters of copolymerization reactions and crosslinking, and also for the selection of the optimal formulations for bio-composites elaboration.

To develop the bio-based thermosets, humins were reacted with the selected epoxy comonomer (RDGE or TMPTE) using 5% of BDMA or DMP-30 as catalysts. These reactions were thermally induced and analyzed through DSC. The evolution of heat flux vs. temperature

for the four humins-based mixtures is shown in Figure 1, while Table 1 gives the obtained data for the copolymerization reactions.

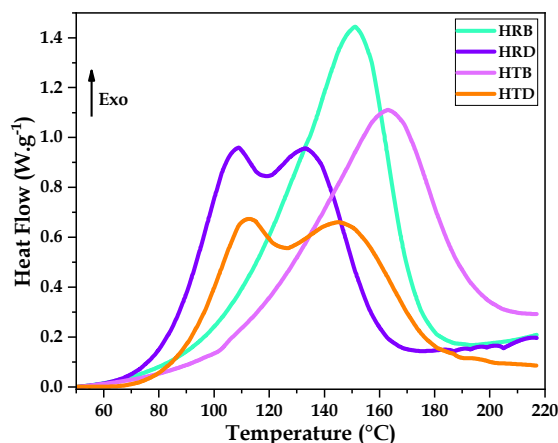


Figure 1. Dynamic DSC curves during heating at $10\text{ }^{\circ}\text{C min}^{-1}$ of thermosetting formulations: HRB (green line), HRD (blue line), HTB (purple line), and HTD (orange line)

The humins/epoxide crosslinking reactions appear as large exotherms events, due to the complex reactivity characteristic for the humins resin. On the Figure 1, it can be observed that the shape of the curves is similar for the formulations with the same catalyst, while the peak intensity and reaction enthalpies are instead both influenced, in these systems, by the epoxy compound. The crosslinking reactions for the systems catalyzed by DMP-30 occur very fast and start at a rather low temperature ($\approx 50\text{--}60\text{ }^{\circ}\text{C}$), with a rapid increase of the curve's slope. The curing of the humins/RDGE mixture catalyzed with BDMA is characterized by a single exothermic peak, in which the heat flow deviation from the baseline occurs at around $55\text{ }^{\circ}\text{C}$, while in the presence of DMP-30 the reaction exhibits a larger exothermic peak with two maxima, and an onset temperature of $53\text{ }^{\circ}\text{C}$. The maximum temperature of curing (T_{max}) of the HRB curing takes place at $151\text{ }^{\circ}\text{C}$ and the completion of curing occurs at around $195\text{ }^{\circ}\text{C}$. In the presence of accelerator (DMP-30) a first reaction peak occurs at $107\text{ }^{\circ}\text{C}$ which can be attributed to the DMP-30 contribution on the main crosslinking reaction. Thereafter, a second exothermal peak with the T_{max} at around $132\text{ }^{\circ}\text{C}$ can be associated to the reaction between the epoxides and the humins -OH functions. In our previous study,³⁸ the chemical mechanism of copolymerization between humins and triglycidyl ether of phloroglucinol (TGPh) activated by different species such as catalyst and/or accelerator (BDMA, DMP-30) was intensively studied by different techniques such as DSC, ATR-FTIR and NMR spectroscopy. Following the analyses, was determined that the humins/TGPh copolymerization implies an anionic mechanism where firstly take place the nucleophilic attack of the catalysts to the epoxy ring, being then followed by the propagation through the TGPh adducts and -OH groups from humins. The results obtained in the current study are in accordance with the previous outcomes.

Table 1. DSC data on copolymerization reaction of analyzed formulations

	HRB	HRD	HTB	HTD
T_{max} , (°C)	151 ± 2	107 ; 132 ± 2	163 ± 2	113 ; 145 ± 2
(reaction interval)	(53 - 195)	(53 - 177)	(66 - 215)	(61 - 210)
ΔH_{cure} (J g ⁻¹)	380 ± 5	290 ± 5	254 ± 5	248 ± 5

For the HTB formulation, the curing appears as an exothermic peak with the onset of crosslinking at 66 °C, reaching the maximum temperature at around 163 °C. In the humins/TMPTE system catalyzed by DMP-30, the reaction is larger, from 61 to 210 °C, presenting two T_{max} : at 113 and 145 °C. The area under the exothermal peaks was integrated in order to evaluate the enthalpy of reaction ΔH_{cure} , J g⁻¹. From Table 1 we can appreciate that the more reactive system is that of humins/RDGE catalyzed by BDMA with an enthalpy of about 380 J g⁻¹ that is 25% higher compared with that obtained for the HRD system (290 J g⁻¹). For the formulations with TMPTE the trend is similar, the reaction enthalpy of HTB system, around 254 J g⁻¹, being higher than that of HTD formulation, 248 J g⁻¹.

Therefore, considering these reactivity results the formulations using BDMA as catalyst were selected as optimal, due to its higher reactivity. The HRB and HTB formulations were selected to produce further the bio-composites with the two natural fillers.

5.2.2. Physico-chemical and mechanical characterization of the humins-based resins and composites

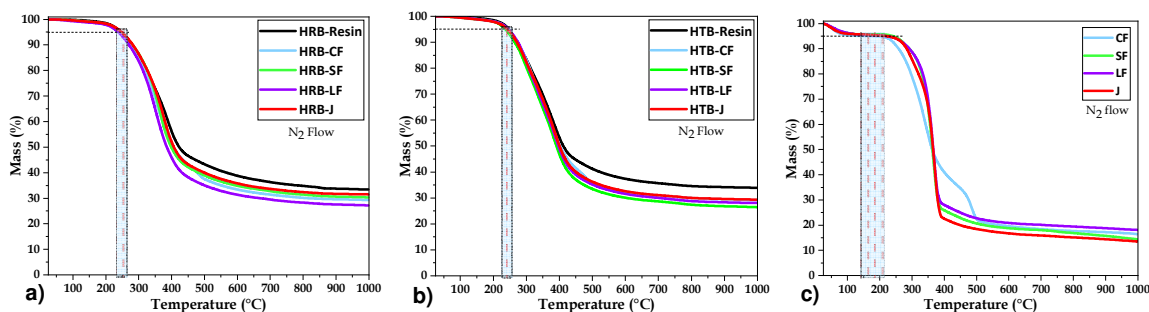
5.2.2.1. Thermal stability studies

Understanding the thermal behavior of developed materials is essential for the evaluation of their potential use in industrial sector applications. The thermal stabilities of the synthesized matrices, of natural reinforcements, and also of the bio-based composites were analyzed. TGA thermograms (Figure 2) and derivative weight loss curves (Figure ES11) were obtained during heating of the samples under inert atmospheres.

The natural fillers were used and analyzed without any preliminary chemical modification or drying treatment. The results of their TGA analyses are shown in Figure 2c. One of the factors responsible for the material thermal stability is their chemical composition. Those of the lignocellulosic fibers are given in Table 2. From these compositions we can observe that a moisture content is present in both, flax or jute, fibers, together with pectins and wax, less thermally stable.

Table 2. Chemical composition and moisture content of the vegetal fibers^{39–42}

Type of fiber	Cellulose (wt.%)	Hemicellulose (wt.%)	Lignin (wt.%)	Pectin (wt.%)	Wax (wt.%)	Moisture content (wt.%)
Flax	64 – 80	17 – 21	2.0 – 2.2	1.8 – 2.3	1.7	8 – 12
Jute	45 – 72	12 – 20	11.8 – 26.0	12.5 – 13.7	0.5	13 – 14

**Figure 2.** TGA thermograms during heating at $10\text{ }^{\circ}\text{C min}^{-1}$, under nitrogen, of (a) HRB thermoset and composites, (b) HTB thermoset and composites, and (c) chicken feathers and vegetal fibers non-woven

From Figure 2c, we can be observed that the thermal degradation of the natural fibers and chicken feathers non-woven occur in three temperature-dependent stages. All fibers present an initial weight decrease (4.1–5.5 wt.%) between 33 °C and 130 °C attributed to the gradual evaporation of absorbed water. Regarding the thermal behavior of the vegetable fibers is already known that their decomposition in nitrogen atmosphere is characterized by a two steps process.^{39,40,43,44} The first decomposition step (200–370 °C) is attributed to the depolymerization of the hemicellulose and the breaking of glycosidic bondings of cellulose, while the main thermal degradation stage (340–370 °C) is due to the degradation of the α -cellulose. Due to its complex structure, the thermal degradation of the lignin take place in large range of temperature (200–500 °C) interposing with that of cellulose and hemicellulose. For the three lignocellulosic non-woven fibers, the second degradation step after de moisture evaporation corresponds to the hemicellulose degradation. As can be seen in Table 2, the mass percentage of hemicellulose and pectin present in flax fiber is lower compared with that in the jute fiber. This fact is correlated with the TGA results (Figure 2c), where the mass loss of the linseed and short flax fibers take place between 200 and 300 °C, being around 8 wt.%, while for the jute fibers (217–316 °C) is ≈ 17 wt.% from the total mass of the sample. The main degradation peak for the flax fibers occurs in the temperature range between 300–410 °C losing the higher amount of its mass (73 wt.% for SF and 69 wt.% for LF). For the jute non-woven, the cellulose decomposition takes place between 315 and 405 °C losing 65 wt.% of the total mass.

In conformity with the DTA thermogram presented in Figure ES11c, the thermal degradation of the chicken feathers non-woven is divided in two main steps. The first degradation step of the CF occurs between 200 and 430 °C reaching a maximum at 340 °C. In this first peak can be observed two small shoulders between 200–300 °C, that according with previous studies^{45,46} are correlated with several different phenomena. In the initial stage (130–280 °C) occurs the breaking of protein bonds and of di-sulfide bridges or the crystalline melting of the protein, while between 250–400 °C occur the forming of the aromatic bonds and cyclic amines. This stage represents the prime thermal degradation of the CF non-woven presenting a percentage in mass loss at around 57.5 wt.%. The second thermal decomposition step of the CF take place in the temperature range 440–530 °C reaching the maximum at 485 °C. This stage is attributed in general to the degradation of the aromatic products formed in the previous step,^{45,46} showing a mass loss of around 20 wt.%. The residual mass left at 700 °C of the natural non-woven varies as follow: J (13.8 wt.%) < SF (15.5 wt.%) < CF (17 wt.%) < LF (18.4 wt.%).

The thermal decompositions of the neat resins were shown in Figure 2 and Figure ES11 showing a single peak of degradation. In Figure ES11 we can observe the presence of a shoulder for HRB resin and two for HTB resin, in the main degradation stage, that can designate the presence of distinct simultaneous degradations that can be due to the structural complexity of the humins resins.^{38,47} The beginning of the degradation stage of the neat resins is located around the temperature of 170 °C, reaching the maximum decomposition rate at 380–390 °C. The main mass loss (up to 650 °C) of the HRB resin is around 65 wt.%, while for the HTB matrix is 63 wt.% of the total mass. In this temperature range, the thermolysis of the polymer structure takes place followed closely by the decomposition of the materials. After 650 °C, a carbon-like structure called “char” is gradually formed, beyond this temperature, the curve becoming flat. The mass percentage of the char left for HRB resin in nitrogen atmosphere is around 38 wt.%, close to that of HTB matrix (36 wt.%).

The influence of the bio-fillers on the thermal stabilities of the humins-based matrices, under inert atmosphere, is displayed in Figure 2a and 2b. The $T_{5\%}$ values of the resins, fibers and composites are compared in Figure 3. From this figure, we can observe that both fillers reduce the thermal stability of the materials by approximately 10–13 °C, from 251 °C to 238–241 °C. This result was expected due to the lower thermal stability of the fillers compared to that of the matrices, as discussed previously and confirmed also by reported studies.^{40,43,48} Dorez *et al.*⁴⁰ investigated the influence of vegetal fibers on the thermal behavior of some bio-composites based on polybutylene succinate (PBS) and natural fibers (cellulose, hemp, flax, sugar cane and bamboo fibers). The authors report that the addition of natural fibers in PBS matrix reduces with around 10–20 °C the temperature stability of the developed bio-composites and influenced the mass residue of the materials. After the temperature of 750 °C in nitrogen

atmosphere, the PBS matrix presented ≈ 0.75 wt.% residual mass, while the bio-composites with natural fibers had a char around 5 and 10 wt.%. A similar result to that of our study, in which the addition of natural fibers decreases the thermal stability of the matrix was found by Manfredi *et al.*⁴³ who studied the thermal properties of jute-reinforced composites using different thermoset matrices such as resol and vinylester matrix. Following the thermogravimetric analyses, they observed that in both matrices, the jute-reinforced composites showed an intermediate thermal behavior between the matrix and the natural fibers.

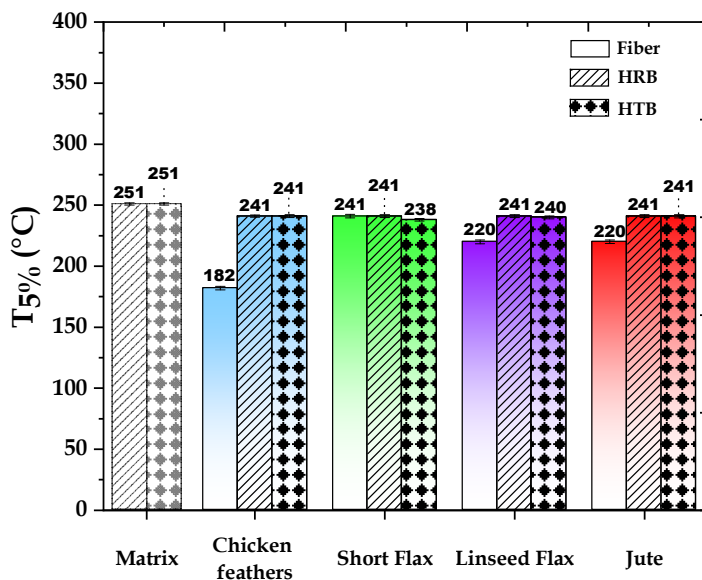


Figure 3. Comparison of the $T_{5\%}$ values of the matrices, fibers and composites obtained by TGA analyses in inert atmosphere

The TGA results of the composites given in Figure 2 and Figure 3 indicate a good thermal stability of the materials, their values combining that of both components the matrices and fibers thermal behavior. In the case of HRB systems, the beginning of degradation of the composites (175–180 °C) is shifted to higher temperature compared with the neat resin (≈ 165 °C) but the thermal curves of the composites return to a quasi linear response at lower temperature than the matrix (500–520 °C for composites, versus 650 °C for HRB resin). The mass loss in the main degradation step for the HRB matrix is around 61.3 wt.%, with the maximal degradation (T_{max}) at ≈ 385 °C. For the HRB-composites, the addition of the natural fibers increases the mass loss as following: HRB–J (64.1 wt.%, $T_{max} = 365$ °C) < HRB–SF (64.7 wt.%, $T_{max} = 365$ °C) < HRB–CF (66.1 wt.%, $T_{max} = 355$ °C) < HRB–LF (68.4 wt.%, $T_{max} = 353$ °C). This maximum rate of degradation is due to the decomposition of the humins-based resin along with the natural fibers present in the composites. On the other hand, the TGA derivatives displayed in Figure ESI1b reveal that the thermal degradation of the HTB systems

take place as a broad and complex event from 176 to 650 °C for HTB resin, and from 160 to 650 °C for HTB composites. The mass loss in this step increases in the following order: HTB–resin (63.4 wt.%, $T_{max} = 381$ °C) < HTB–CF (66.8 wt.%, $T_{max} = 328$ °C) < HTB–J (66.9 wt.%, $T_{max} = 385$ °C) < HTB–LF (67.7 wt.%, $T_{max} = 386$ °C) < HTB–SF (69.3 wt.%, $T_{max} = 385$ °C). It can be observed that although the composites degradation starts at a lower temperature compared with the neat HTB resin, their maximum degradation temperature is increased by 4–5 °C, excepting the HTB composite with CF in which the degradation is divided into two stages. Moreover, the char left after 650 °C of the composites reinforced with natural fibers decreased with around 3–7 wt.% in comparison with that of the neat resins.

The thermal stability of the developed materials was also analyzed by the statistic heat-resistant index (T_s) calculation, this factor representing the temperature of the polymer in the physical heat tolerance limit. The T_s values were determined with the aid of the temperature at 5% ($T_{5\%}$) and 30% ($T_{30\%}$) weight loss of each sample obtained by TGA and calculated by equation:^{49–51}

$$T_s = 0.49[T_{5\%} + 0.6(T_{30\%} - T_{5\%})]$$

The obtained values of T_s both in oxidative and inert atmospheres for studied systems are tabulated in Table 3, observing the same tendency of their thermal stability. These results reveal that the addition of the fillers decreases with around 2–7 °C the T_s values of the composites compared to the neat resins. Following these analyses, it appears that the reinforcement provokes a small decrease of about 10 °C of the thermal properties compared to that of the neat resins. However, the bio- composites exhibit a good thermal stability, loosing 5 wt.% of their mass at temperatures higher than 240 °C.

Table 3. Physico-chemical, thermal, and mechanical properties of bio-based resins and composites

Sample	Density (g/cm ³)	Hardness test ^a (SD)	T_g ^b (°C)	WA ^c (%)	$T_{5\%}$ ^b (°C)		T_s ^b (°C)	
					Air	N ₂	Air	N ₂
HRB	1.24	79	30	12.5	251	251	160	155
HRB-CF	1.15	89	59	21	240	241	147	150
HRB-SF	1.23	81	37	11.7	238	241	147	150
HRB-LF	1.15	83	37	12.7	245	241	149	147
HRB-J	1.20	85	44	15.4	235	241	145	153
HTB	1.19	73	21	12.14	250	251	153	152
HTB-CF	1.02	77	42	21	249	241	151	147
HTB-SF	1.08	74	26	11	240	238	146	144
HTB-LF	0.96	74	28	22.1	240	240	144	147
HTB-J	0.84	75	34	28.3	235	241	145	148

^a STD ± 1 SD; ^b STD ± 0.5 °C; ^c STD ± 2 %.

5.2.2.2. Glass transition and hardness of the bio-based materials

The glass transition (T_g) is a dynamic phenomenon represented by a reversible transition interval, where upon heating, the materials pass from a hard and fragile state into a plastic or rubber state, the polymer chains becoming more mobile. It is known that this phenomenon does not occur suddenly at one unique temperature but rather over a range of temperatures, the T_g being typically defined as the inflection point of the DSC curve.^{52,53}

The obtained data for analyzed samples are summarized in Table 3. Following these analyses, an increase of the T_g values for bio-composites compared with the neat resins was obtained. Also, the nature of the fibers influenced this region regardless the type of the matrix. Both bio-composites systems show an increase of the T_g in the following order: neat resin < matrix-SF < matrix-LF < matrix-J < matrix-CF. The lowest increase in the T_g was generated by reinforcing the humins-based matrices with flax fibers (short or linseed) this transition region increasing with around 5–8 °C. The addition of jute fibers enhances the transition region by 14 °C for both matrices. The highest values were afforded by the reinforcement with CF: around 59 °C for HRB-CF and \approx 42 °C for HTB-CF. In previous studies,^{14,54} we developed humins-based resins with modifiable mechanical properties (from elastomeric to rigid) using aliphatic diglycidyl ethers as comonomers. Following the data obtained by DSC, the T_g of the elastic materials was \approx -8 °C, while that of the rigid one \approx 27 °C. These resins were used as matrix to prepare composites with chicken feathers powder or non-woven mat, and lignin as reinforcement. In the case of resins reinforced with chicken feathers powder or mat, it was observed a decrease of the T_g by approximately 3–10 °C (the filler gives support and elasticity to the polymeric matrix), while in case of the composites reinforced with lignin, the T_g was increased with about 12 °C, giving rigidity to the materials.

Moreover, the resistance of the humins-based resins and composites material to permanent indentation was evaluated by Shore testing. Surface hardness of hard elastomers or thermosets is measured using the Shore D scale. The hardness of the resins and for the bio-composites was analyzed using the type D gauge, the obtained values being displayed in Table 3. These results reveal a good rigidity of materials, in the category of hard materials. Analyzing the surface hardness values obtained for the neat resins and composites, a similar increasing trend was observed for these properties as for the glass transition region. The hardness value for the HRB neat resin is 79SD, while the reinforcement with natural fibers enhances the rigidity of the composites with 2–10SD. In the case of HTB materials, the penetration resistance is slightly lower (73–77SD) compared to HRB resin and composites. The Shore hardness values of the obtained materials in this study were analyzed and compared with the materials already existing on the market, using the MatWeb online database (<http://www.matweb.com/index.aspx>). For example, hardness of the epoxy resins reinforced

with glass fiber obtained by molding is ranged between 75–89SD, while for the epoxy resins reinforced with carbon fiber the surface rigidity is around 85–90SD. According to the Shore D results obtained and compared with the values of commercial products, it can be stated that the composites developed in this study can be suitable for use in industrial sectors, such as the automotive or construction industry.

5.2.2.3. Tensile testing

For a better characterization and for an easier framing in an applicability area, the mechanical properties of the materials were analyzed by tensile tests. The stiffens of the materials known as Young's modulus, the tensile strength and the elongation at break were determined and compared, the experimental data being shown in Figure 4 and Table ESI1.

Although both matrices were developed starting from humins, the difference between the molecular weights, structure and chemical compositions of the epoxy coreactants generate networks with different mechanical properties. From Figure 4a can be observed that the absolute value of tensile stress of the HRB matrix (≈ 1.1 MPa) is three times lower than that of the HTB resin (≈ 3.4 MPa). A similar result was obtained for Young's moduli values, the HTB resin having a double value compared with that of HRB resin: 805 vs. 440 MPa. As shown in the Figure 4b, both matrices are characterized by close values of strain, around 0.6 %. This low value of the elongation at break denotes that the resins developed in this study are rigid materials, as already report by the glass transition regions and Shore hardness results.

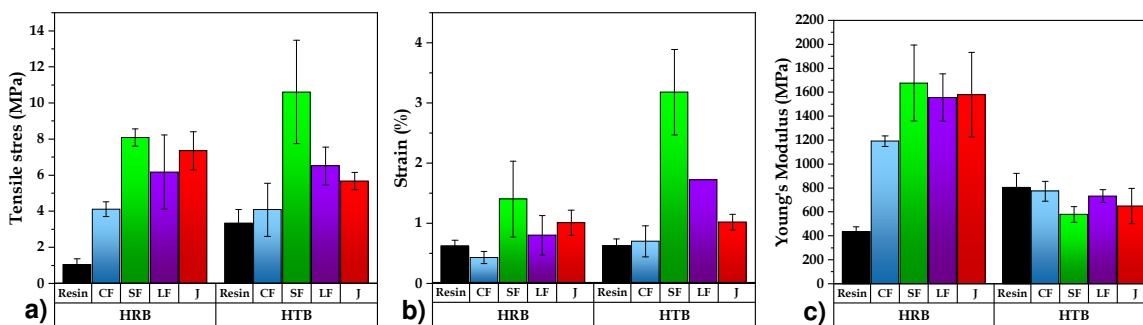


Figure 4. Comparison between the tensile properties of the neat resins and derived composites

According with the reported studies,^{39,55–58} the mechanical properties of the natural fibers reinforced composites are strongly influenced by various factors such as the fibers length, content, orientation or treatment, by matrix nature or by the different techniques to produce the composites. An environmentally-friendly alternative for composites manufacturing was proposed by Fernandes *et al.*⁵⁸. Epoxy matrices were produced from waste vegetable oil (blend of 3/1 of rapeseed/palm oil used 4 days for deep frying) cured with methylhexahydrophthalic anhydride and reinforced with flax and glass fibers. The physico-

chemical and mechanical properties were analyzed and compared with that obtained for DGEBA composites. The authors report that untreated flax fiber reinforced composites led to low properties, instead the treatment of fibers with NaOH and steric acid led to the improvement of the tensile properties of the final composite without affecting other parameters. Boopalan *et al.*⁵⁷ investigate the mechanical properties of the epoxy hybrid composites, in which jute and banana fibers act as reinforcement in DGEBA matrix. The authors conclude that the tensile properties are maximal for 50/50 weight ratio of jute and banana fiber reinforced epoxy hybrid composites, obtaining a tensile strength of around 19 MPa and the Young's modulus around 724 MPa. Comparing the tensile properties of the jute-reinforced composites developed by Boopalan *et al.*⁵⁷ with those developed in our study, we can observe that the tensile strength values of the humins-based composites (5.67 MPa for HTB-J, and 7.35 MPa for HRB-J) are two or three times lower than that of the DGEBA-based composites (16.62 MPa). Although the humins-based composites reveal lower resistance at stress, their stiffness is similar or even two times higher than that of the DGEBA-jute composite presented in Boopalan *et al.*⁵⁷ study.

Table ESI1 summarizes the tensile properties of HRB and HTB resins reinforced with natural fibers. It can be noticed that the standard deviations vary from one sample to another, this phenomenon being common to composites reinforced with mat fibers due to intrinsic inhomogeneity of the non-woven fibers distribution in the samples.^{22,56} From Figure 4 can be observed that the tensile stress and elongation at break values of the bio-composites were improved compared to that of the two resins. Considering the tensile strength, the greatest improvement was given by reinforcing the resins with short flax fiber, the maximum stress value, 8.08 MPa, obtained for HRB-SF composite being about eight times higher than that of the neat resin (1.04 MPa). In the case of HTB-SF composite the increase is three times higher compared with the neat resin: 10.61 vs. 3.34 MPa. For both HRB and HTB based composites, the tensile strength increase takes place in the following order: neat resin < matrix-CF < matrix-LF < matrix-J < matrix-SF.

The stiffness of the materials is displayed in Figure 4c. In the case of the HRB resin, the addition of bio-fillers improves considerably the values of Young's modulus. The addition of chicken feathers in HRB matrix increases the stiffness from 0.44 to 1.2 GPa, while the maximal improvement was exerted by reinforcement with short flax \approx 1.7 GPa. The Young's modulus values for the HRB composites with jute or linseed flax are similar, \approx 1.6 GPa. Although for the HTB matrix the elongation at break and the tensile strength were improved with the addition of the bio-fillers, the Young's modulus decreased in the composites.

It is known that the mechanical properties of the composites are not only influenced by the characteristics of the matrix and fibers, but also by the interface and compatibility between

the two components. According with MatWeb online database (<http://www.matweb.com/index.aspx>), the mechanical properties of the bio-composites studied in this work have been compared with the commercial ones showing similar performances with epoxy/carbon fibers composites or Owens Corning glass fiber reinforced polyurethane. Also, the use of untreated fibers in composites development was considered as the first step for a possible use of the fibers as an effective reinforcement. Further studies will be carried out to evaluate the degree of improvement of the composites properties by applying different physico-chemical treatments on fibers.

5.2.2.4. Moisture absorption behavior

The moisture absorption of the prepared materials was evaluated using the ASTM D570 method. The water uptake evolution of the bio-based materials is displayed in Figure 5. According to reported studies, the water absorption of bio-based materials is influenced by a variety of factors.^{59–61} One of the first defect that can influence the water absorption is generated by the presence of the micro-cracks and pores which can appear in brittle matrices as in some epoxy resins.^{59,62} In Figure 6 are illustrated the morphologies of materials' fractures observed by SEM analysis. The presence of the micro-pores, specific to brittle resins, can be seen. These cracks led to the moisture absorption in the neat resins, the saturation of the HRB resin being reached after 40 hours absorbing around 12.5 wt.%, while HTB resin uptake is \approx 12.14 wt.%. The moisture uptake values are also directly correlated with the number of the free hydroxyl or other polar groups present in the humins-based resins which can increase the water absorption by hydrogen bonding with water.⁶³

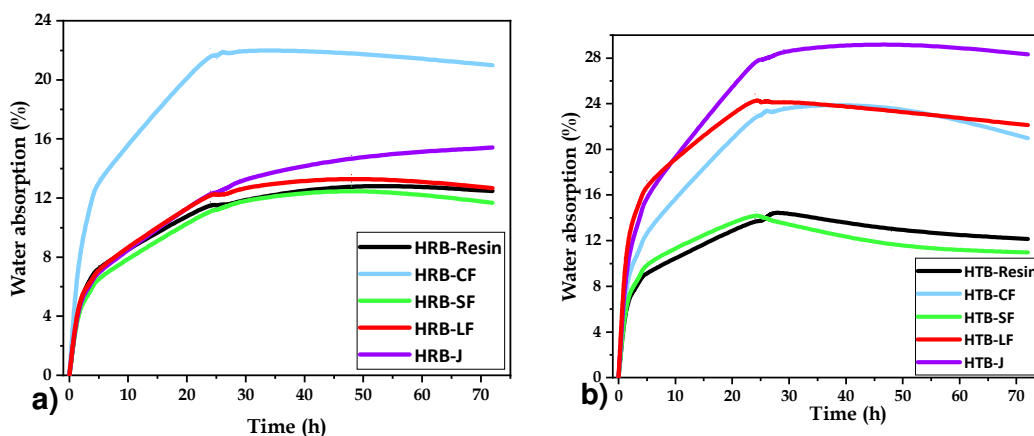


Figure 5. Evolution of water uptake of the resins and their composites (a) HRB and (b) HTB materials

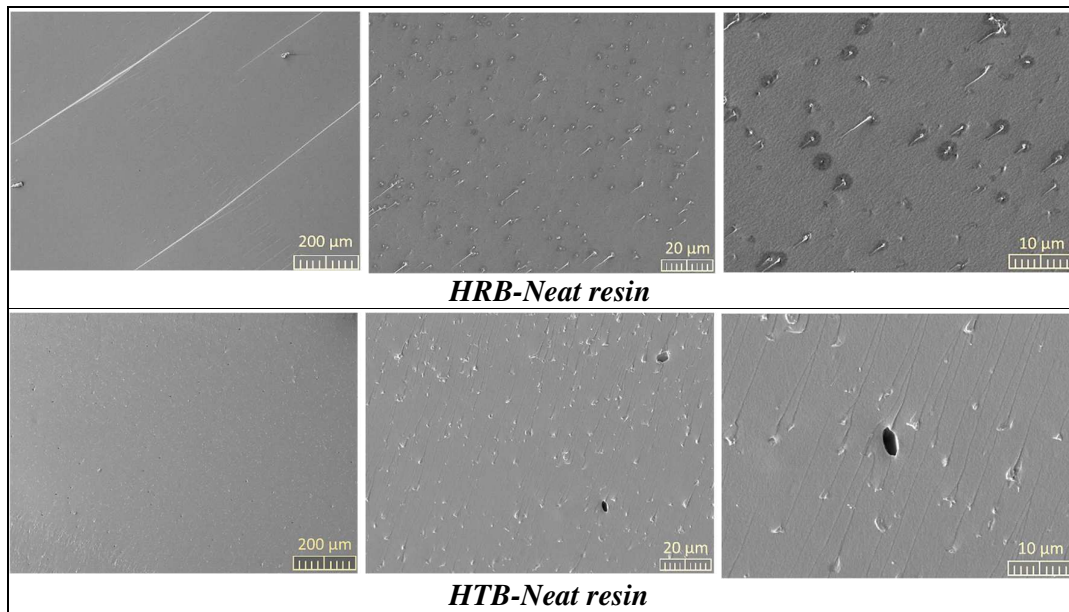


Figure 6. SEM images of the humins-based resins

A factor that influence the moisture behavior of the composites is represented by the fiber's nature. Lignocellulose fibers are highly hydrophilic due to the presence of the -OH groups which permit moisture absorption by hydrogen bonding.⁵⁹ When exposed to water, the fibers from composites swell causing new micro-cracks and increasing the water transport through the fiber-matrix interface.⁶⁴ From Figure 5 we can observe that the amount of absorbed water increases linearly at the beginning, being gradually slowed down with the saturation. For HRB composites, the highest water absorption was obtained with the CF, with a maximum value 21%. For the HRB composites with vegetal fibers an increase of 1–3% in WA was obtained, compared to that of neat resin. In the case of the HTB composites with, the moisture absorption shows a higher increase, in the following order: HTB-J > HTB-LF > HTB-CF > HTB-SF. The difference in WA between the 2 types of resins can be due to several factors. For example, the presence of fibers in the composites can interfere in the cure process of the matrix, leading to a decrease in the matrix crosslinking so facilitating the water penetration in the matrix's network, increasing the water absorption in the composite. Also, a low adhesion between matrix and fibers can influence the moisture uptake of the final composites. Similar WA behavior to that presented in this work was found by Dutta *et al.*⁶⁵ for bio-composites developed with epoxy-modified *Messua ferrea* L. seed oil based polyurethane resins reinforced with alkali-treated jute fibers. The authors report a WA \approx 20–55% in function of the matrix nature or the treatment applied on the fiber surface. Manthey *et al.*⁶⁵ developed new epoxidized hemp oil-based bio-composites reinforced with jute fibers. The moisture absorption results show that the bio-composites followed a linear behavior, whereby the moisture weight gradually reached an equilibrium after a rapid initial phase (15–26%), being competitive with

commercially produced epoxidized soybean oil (ESO) in terms of mechanical performance, dynamic mechanical properties and WA characteristics. According to studies,⁶⁶ the delay or diminution of composites' water absorption can be achieved using adequate coatings or fibers treatment.

5.2.2.5. Fibers/matrix interface investigation by SEM analyses

One of the essential criteria in the composite's development is represented by the effective wetting and compatibility between the fiber reinforcement and the polymer matrix. A proper wettability and compatibility between the two components generate a good adhesion between the fibers and matrix, thus the final properties are optimal. The fracture surfaces of the humins-based composites were examined by SEM to investigate the adhesion between the HRB and HTB matrices with the bio-fillers. Different magnifications were used for a better visualization of the fracture structures, thus obtaining both a representative image of the total behavior of the fiber-matrix and a closer examination of the individual fiber-matrix cohesion. Figure 7 displays the fiber-matrix interface for the HRB based samples, while in Figure 8 shows the adhesion of the natural fibers with HTB matrix.

Analyzing the SEM micrographs, we can observe a good adhesion fillers-matrix, without having a prior treatment of the fibers. In the case of composites with chicken feathers, it is possible to observe a few fibers pull-out, which would indicate a slightly lower compatibility between humins-based resins and CF fiber, compared to the composites with vegetal fibers. This result may be due to the presence of a fat layer on the chicken feathers surface, which could act as a fine barrier decreasing their adhesion to the matrix. Another small defect observed in the SEM pictograms is the presence of small cracks in the polymeric matrix that could lead to the influence of the composites properties. These micro-cracks could be caused by the introduction of air inside the material during manufacturing but can be eliminated by a prior degassing of the mixtures before crosslinking.

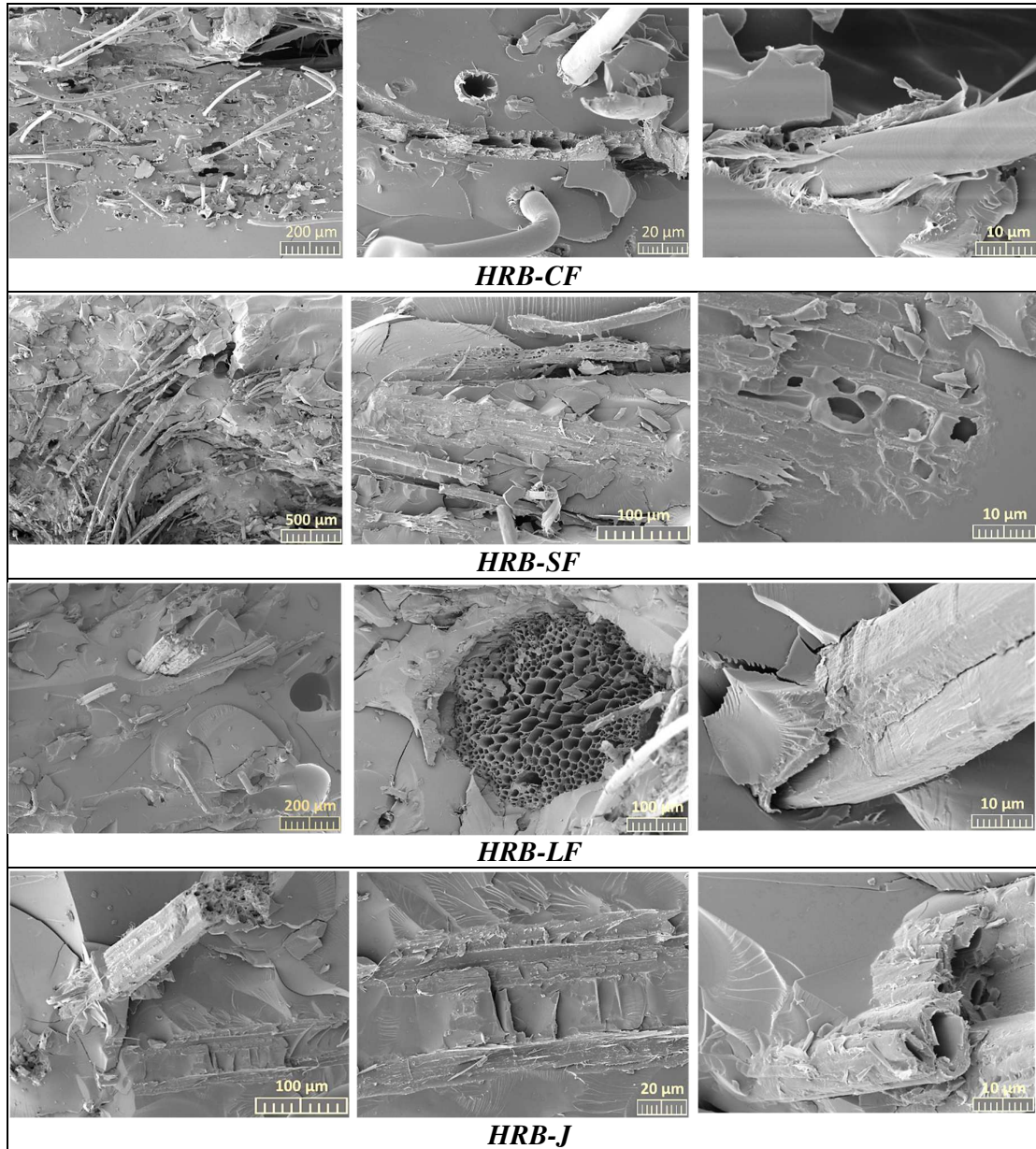


Figure 7. SEM micrographs of fractures' surface of bio-composite developed with HRB matrix and bio-fillers

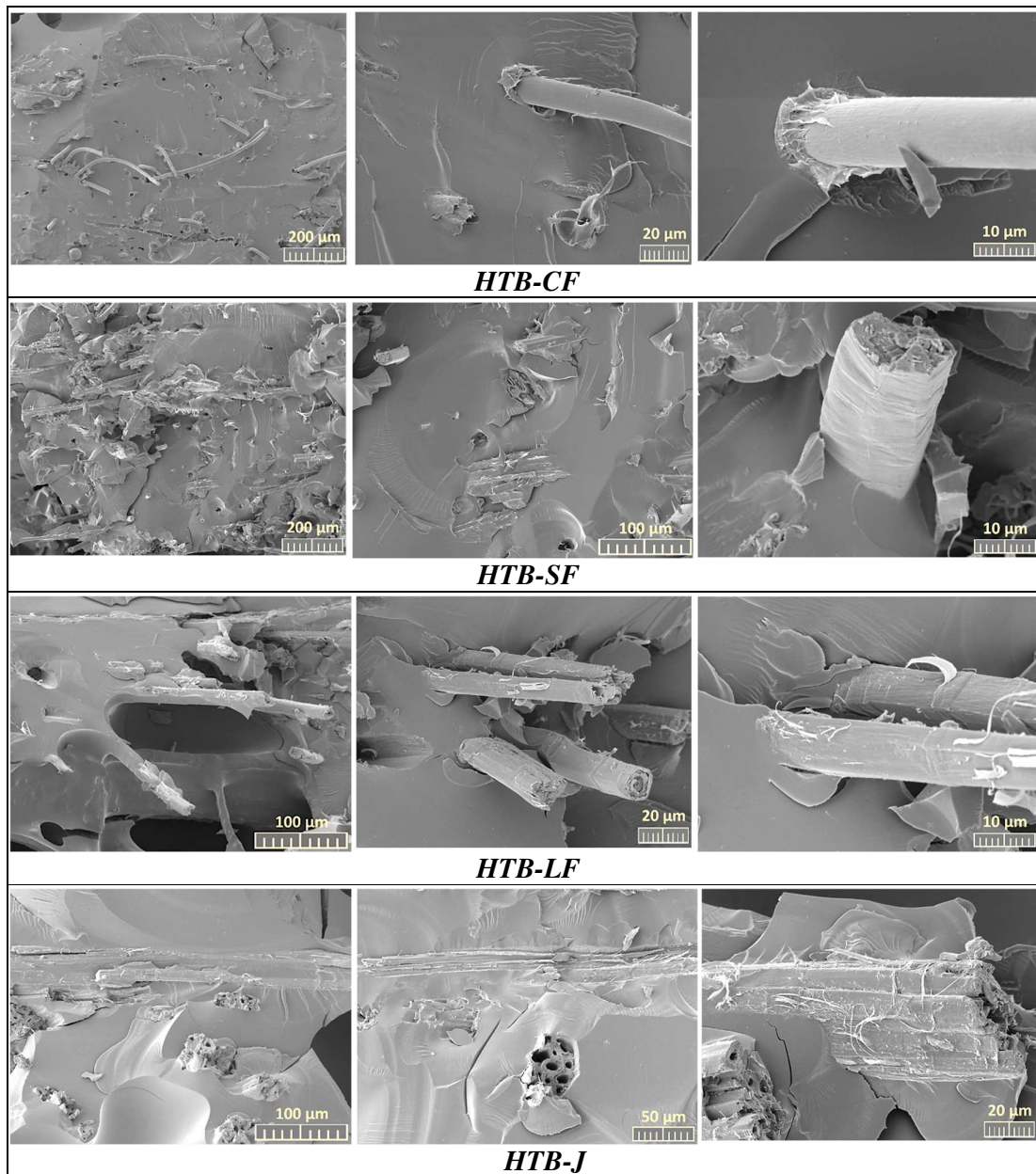


Figure 8. SEM micrographs of the fractures' surface of bio-composite developed with HTB matrix and bio-fillers

In Figure 7 and Figure 8 we can observe an excellent adhesion of vegetal fibers to the humins-based matrices, due to the fibers hydrophilic character which leads to a proper chemical affinity in the case of humins that is an hydrophilic macromonomer. The interfacial delamination between the resin phase and fibers is not present, nor gaps between the two elements. According with the SEM pictograms, the fibers that protrude out of the material's fracture surface are covered with resins, indicating a close contact between the vegetal fibers and polymeric matrices.

Consequently, the reinforcement of the humins-based matrices with untreated natural non-woven fibers led to a proper interaction and adhesion between the compounds, generating composites with optimal properties.

5.2.3. Mechanical recycling of the humins-based composites

The recycling of the thermoset materials at the end of their life cycle is a very difficult challenge because they are crosslinked. Due to this fact, thermoset composites materials cannot be remelted or remolded like thermoplastics materials.⁶⁷

In this study, the humins-based resins but also the composites with chicken feathers and vegetal fibers non-woven were successfully recycled by a thermo-mechanical procedure which is graphically illustrated in Scheme 1. Firstly, the composite materials were mechanically grinded. Then, the ground mixture of matrix and fibers was placed between two metallic plates covered with Kapton film and placed into a hydraulic heated press. To reconstruct the thermoset composite material, the grounded mixture was thermal treated at 175 °C for one hour applying a pressure of 1 bar. The appearances of the resins and composites after the mechanical recycling are shown in Figure 9.



Scheme 1. Schematic representation of the mechanical recycling protocol

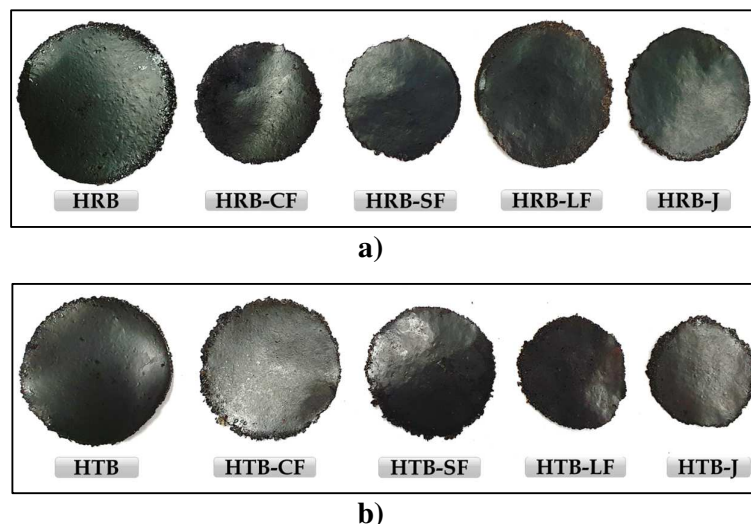


Figure 9. Aspect of (a) HRB resin and composites and (b) HTB resin and composites after the mechanical recycling

In our previous studies,^{38,47} the chemical mechanism of polymerization between humins and epoxy compounds initiated by a tertiary amine has been analyzed and investigated by

different techniques, thus demonstrating that an anionic mechanism is involved in humins-epoxy copolymerization. Following the thermo-mechanical recycling process, the humins-based materials show that they can be thermally remodeled. In our previous studies,³⁸ it was also shown that copolymerization reactions are accompanied by humins structural rearrangements γ -keto cyclization and γ -keto esterification. These structural rearrangements are favored by high temperatures and can be an important factor in increasing and improving the recycling capacity of humins-based thermoset materials. When exposed to heat, humins resins and composites become flexible and can be recycled, while after cooling at room temperature, the materials become rigid. Thereupon, the polymer chains in the humins-based resins and composites can reorganize and reshape into any desired physical form, making them suitable for mechanical recycling.

After the thermo-mechanical recycling, the thermal degradation, the glass transition region of the obtained materials but also the interaction and morphology between fibers-matrix were analyzed in order to study the influence of the recycling on the physico-chemical and mechanical properties of the humins-based materials. According to the literature,⁶⁷⁻⁶⁹ the properties of the recycled materials are slightly reduced compared to the initial ones. Zhang *et al.*⁶⁷ developed self-healing and recyclable polymeric materials based on furan-groups, alternating thermosetting polyketones and bis-maleimide by using the Diels-Alder and Retro-Diels-Alder reaction sequences. Analyzing the physical and mechanical properties of the thermo-mechanically treated materials, they showed that this polymeric system can repeatedly heal or repair itself multiple times, without undergoing major changes in their properties. Badia *et al.*⁶⁹ analyzed the effects of multiple mechanical recycling on the structure and properties of amorphous polylactide (PLA) materials. The five successive cycles of recycling PLA materials have changed their structure and morphology, also influencing its thermal and mechanical properties.

In this study, the thermal stability of recycled materials was analyzed under oxidative atmosphere, the TGA and DTA thermograms being displayed in Figure ESI5. The thermogravimetric curves of the recycled bio-composites reveal similar appearance with the initial ones, presenting two complex main steps of degradation. The thermal degradation onset temperatures of the recycled materials in which the bio-composites lose 5% of their mass are plotted in Table 4 and compared with the values obtained for the virgin ones. We can observe that the recycling influences the thermal stability of materials, but the differences are not so significant. In the case of the recycled HRB matrix, the $T_{5\%}$ is with 6 °C lower than the value obtained for the initial resin, while for the recycled HTB resin the decrease in thermal stability is with around 18 °C. The recycling process of HRB composites decreases the thermal stability

of the bio-materials with around 2–5 °C, while for the HTB-based composites the recycling also reduces the $T_{5\%}$ values of the materials by about 8 °C.

Table 4. Comparison between the $T_{5\%}$, the statistic heat-resistant index (T_s) and the glass transition (T_g) of the initial and recycled materials

Sample	$T_{5\%}$ ^a (°C)	T_s ^a (°C)	T_g ^a (°C)
HRB	251	160	30
Rec-HRB	245	156	28
HRB-CF	240	147	59
Rec-HRB-CF	239	153	51
HRB-SF	238	147	37
Rec-HRB-SF	235	150	24
HRB-LF	245	149	37
Rec-HRB-LF	240	152	24
HRB-J	235	145	44
Rec- HRB-J	233	150	24
HTB	250	153	21
Rec-HTB	232	148	23
HTB-CF	249	151	42
Rec-HTB-CF	241	147	45
HTB-SF	240	146	26
Rec-HTB-SF	232	142	28
HTB-LF	240	144	28
Rec-HTB-LF	232	145	36
HTB-J	235	145	34
Rec-HTB-J	235	148	32

^a STD \pm 0.3 °C.

The mechanical properties of the recycled materials were also evaluated by determining their glass transition (T_g), using the DSC technique, the obtained results being summarized in Table 4. For the HRB-based materials it can be observed that the recycling process leads to the decrease of the transition region, thus generating more flexible materials than the initial ones. For the HRB-CF recycled composite the T_g value decrease with around 8 °C, while for the composites with short and linseed flax the decrease is with \approx 13 °C. The more striking diminution was obtained by the recycling of HRB-J composite leading to a half of the T_g value compared to the initial material (44 °C). For the HTB materials the recycling process gives rigidity to the materials, the transitions regions being increased. The glassy transition region of the recycled HTB composites was increased with around 2–8 °C, the highest being obtained for HTB-LF composite (36 °C).

The recycled materials were analyzed by SEM to investigate the impact of the recycling on the fibers' adhesion to the matrix (Figure ESI6 and Figure ESI7). It can be observed that the morphology and the adhesion between fibers and matrices are affected by the mechanical recycling process. In the recycled composites the fibers are shorter due to mechanical grinding

and their distribution is non-directional but uniform. The fibers-matrix adhesion is lower in the case of recycled materials compared with the virgin ones, observing the appearance of voids and cracks on the filler-matrix interface. Also, it can be observed that the recycled humins-based matrices are less smooth and homogeneous compared with the initial resins.

In conclusion, the recycling process applied to the humins-based resins and composites led to physico-mechanical modifications of the materials. A more detailed investigation on the performances of virgin and recycled materials, on the influence of the chemical treatment of the fibers reinforced in composites, and also the influence of different parameters on the mechanical recycling process will be discussed in a future work.

5.3. Conclusions

New thermoset resins were developed by copolymerizing the humins with epoxy comonomers. The developed humins-based resins were used as matrices in the composites production in which untreated chicken feathers and vegetal non-woven fibers were used as reinforcements. The physico-chemical and mechanical properties of the obtained resins and composites were analyzed and compared, showing that the reinforcement led to an increase of T_g region in the range 26–58 °C. The stiffening of the materials by reinforcement with the bio-fillers was also confirmed by the Shore hardness test, the measured values (74–85SD) being comparable with those of commercial materials such as epoxy/glass fibers or epoxy/carbon fibers composites. The tensile properties of the resins and their composites were determined and compared showing the increasing of the tensile strength and the elongation at break of the composites. The stiffness of the bio-composites was also analyzed. For the HRB materials the addition of the bio-fillers improved the Young's modulus values from 0.44 GPa to 1.2–1.7 GPa, while for the HTB materials was observed an opposite effect, the stiffness of the composites being slightly decreased (from 0.8 GPa to 0.57–0.77 GPa). The matrix/filler interface and the adhesion between the two compounds were analyzed by SEM. It was observed a proper adhesion and a good compatibility between the matrices and the chicken feathers and vegetal fibers non-woven without a prior treatment of the fillers.

Finally, the obtained materials proven their capacity to be mechanically recycled without producing significant changes in their properties.

5.4. Experimental

5.4.1. Materials

The humins were produced and supplied by Avantium Chemicals (Geleen, Netherlands). The resorcinol diglycidyl ether (RDGE), trimethylolpropane triglycidyl ether (TMPTE), N, N-dimethylbenzylamine (BDMA) and 2,4,6-tris(dimethylaminomethyl)phenol (DMP-30) were purchased from Sigma-Aldrich (France) and used as received. The chemical structures of humins, RDGE, TMPTE and initiators are given in Scheme ESI1 and the proposed structure of the humins-epoxy copolymer is presented in Scheme ESI2.

The non-woven fabric with chicken feathers (*CF*) were developed by IBWCh combining 90 wt.% chicken feathers fibers with 10 wt.% bicomponent synthetic fibers, core PET, Type T25 Biko flat 2.2 dtex, semi-matte, used in the production of wet-laid non-woven.⁷⁰

Three non-woven fabrics provided by Dierickx Visschers NV company used in this work for the developments of the bio-composites are made from vegetal fibers such as short flax (*SF*, 400 g/m³), linseed flax (*LF*, 600 g/m³) and jute (*J*, 600 g/m³).

5.4.1.1. Samples preparation

To develop the humins-based thermosetting resins, the required quantity of humins was heated for decreasing its viscosity. The preheated humins samples were then vigorously mixed with the epoxy comonomers RDGE or TMPTE. To initiate the humins/epoxy reactions, two different catalysts such as BDMA and DMP-30 were tested separately, thus obtaining four different type of formulations like humins/RDGE/BDMA, humins/RDGE/DMP-30, humins/TMPTE/BDMA and humins/TMPTE/DMP-30.

Composite panels with non-woven chicken feathers fibers were consolidated from 2 plies of mats, while the composites with vegetal fibers were developed with only one layer of non-woven fabric. The number of non-woven layers used for the composites production was selected in order to reach a thickness of about 0.4 cm.

The non-woven fabrics were cut in accordance with the mold size, then immersed in the uncured thermosetting resin and maintained the needed time to allow the fabric to absorb the proper quantity of resin to reach the saturation. The impregnated non-woven were then laid in a metallic mold and placed in a Carver heated press. The composites processing protocol began by maintaining them at 80 °C for 2 hours and another hour at 140 °C, applying 2 tons pressure. To ensure complete crosslinking of the materials, the bio-composites were post-cured for 1 hour at 180 °C and 2 tons pressure.

The identification of resins and composites was facilitated by coding them according to their composition using the initials of the compounds as acronyms; humins was noted with “H”, RDGE with “R”, TEMPTE with “T”, “B” was used for BDMA and “D” was used for

DMP-30. The non-woven fabrics were abbreviated as following: “CF” for chicken feathers, “SF” for short flax, “LF” for linseed flax and “J” for the non-woven jute fabrics. Therefore, the resin with 55 wt.% humins, 40 wt.% RDGE and 5 wt.% BDMA was noted as “HRB” while its composite with chicken feathers non-woven was abbreviated with “HRB-CF”.

5.4.2. Experimental techniques

5.4.2.1. Differential Scanning Calorimetry (DSC)

Differential scanning calorimetry was firstly used to study the thermal induced copolymerization. Uncured thermosetting resins formulations were analyzed using a Mettler-Toledo DSC 3 apparatus equipped with STARe Software. For each formulation, samples of 5–10 mg were reacted under non-isothermal condition in 40 μl aluminium pans. The thermal aspects of the resins crosslinking were analyzed in the temperature range between 25–230 $^{\circ}\text{C}$, at a heating rate of 10 $^{\circ}\text{C min}^{-1}$.

The reversible transitions of amorphous materials from a molten or rubber state to a hard and relatively fragile state, called the glass transition (T_g), has also been studied by DSC. Samples of 7–12 mg of cured or recycled bio-materials were analyzed applying two heating/cooling cycles from -50 $^{\circ}\text{C}$ to 240 $^{\circ}\text{C}$ at 10 $^{\circ}\text{C min}^{-1}$ heating rate. The T_g values (inflection point) for all the bio-based materials were measured in the second heating analysis.

5.4.2.2. Thermogravimetric analysis (TGA)

Thermogravimetric analysis was used to study the thermal stability of the crosslinked bio-materials. A TGA 2 Mettler-Toledo device was used to analyze the thermal degradation, mass loss and the derivative mass loss of the bio-based materials as a function of temperature. Samples of 10–15 mg were tested in 70 μl aluminium crucibles, using a dynamic heating from 25 to 1000 $^{\circ}\text{C}$ at a heating rate of 10 $^{\circ}\text{C min}^{-1}$. The thermal stability of the materials was analyzed in both oxidative (air) and inert (nitrogen) atmospheres at a debit of 150 mL min^{-1} . The materials degradation temperature was considered as the temperature at which the samples lose 5% of its mass, $T_{5\%}$.

5.4.2.3. Shore hardness test

The hardness of the humins based resins and composites were determined in accordance with ISO 7619-1, ASTM D2240 and ISO 86 using a Zwick Roell 3116 Hardness Tester. The Shore D hardness device was pressed smoothly against the samples with a load force of 50 N \pm 0.5 N. The samples hardness value was read after the firm contact between the presser foot and the tested materials.

5.4.2.4. Tensile test

The mechanical properties of prepared materials, such as Young's modulus, tensile strength and elongation at break were determined by tensile tests using an universal testing machine Instron 3365 (Norwood, MA, USA) controlled by BlueHill Lite software. For each formulation, five rectangular samples with the dimension of $75 \times 10 \times 4 \text{ mm}^3$ were tested applying a crosshead speed of 10 mm min^{-1} . The obtained data were averaged for a better accuracy of the results.

5.4.2.5. Water absorption (WA%)

Another important characteristic analyzed in this study was the percentage of absorbed water of the materials depending on time. The bio-based resins and composites were analyzed using the international standard method ASTM D570. Three rectangular samples ($50 \times 8 \times 4 \text{ mm}^3$) for each formulation were analyzed and the results were averaged in order to avoid the errors. The cured samples were firstly dried in an oven at $50 \text{ }^\circ\text{C}$ for 24h, then cooled in a desiccator and weighed (W_0) using a ML3002T Mettler-Toledo precision balance. After weighing, the samples were immersed in 20 mL deionized water and maintained for 24h at room temperature. Thereafter, the samples were removed, wiped with a dry towel, weighed (W_t) and then immediately immersed again in deionized water. The percentage of water absorption (WA%) was calculated using the following equations:

$$WA\% = \frac{W_t - W_0}{W_0} \times 100$$

5.4.2.6. Evaluation of the resin-fiber interaction by Scanning Electron Microscopy (SEM)

The adhesion between the natural fibers and the humins-based thermoset matrices, but also the morphology of fracture surface of the bio-composites were investigated by scanning electron microscopy (SEM). Fresh fractures of samples of cured materials but also the recycled one were mounted on a SEM stub and coated with platinum prior to observations and afterwards observed using a Tescan Vega 3 XMU SEM at an accelerating voltage of 5 kV.

5.4.2.7. Mechanical recycling of the humins-based resins and composites

In the first step, cured samples of each formulation were mechanically grinded using an electric grinder. Then, the grinded samples were place on Kapton film between two metal plates and placed in a heated press. To find the proper recycling protocol, different parameters like temperature and pressure were modulated and tested. Finally, the resins and composites were mechanically recycled at a temperature of $175 \text{ }^\circ\text{C}$ for 1h and 2 tons pressure.

Acknowledgements

This work was supported by KaRMA2020 project. This project has received funding from the European Union's Horizon 2020 Research and Innovation program under Grant Agreement n° 723268.

CCMA electron microscopy equipment have been funded by the Region Sud - Provence-Alpes-Côte d'Azur, the Conseil Départemental des Alpes Maritimes, and the GIS-IBiSA.

Notes and references

- (1) Brostow, W.; Hagg Lobland, H. E. *Materials: Introduction and Applications*; John Wiley and Sons, 2017.
- (2) Okunola A, A.; Kehinde I, O.; Oluwaseun, A.; Olufiropo E, A. Public and Environmental Health Effects of Plastic Wastes Disposal: A Review. *J. Toxicol. Risk Assess.* **2019**, *5* (2). <https://doi.org/10.23937/2572-4061.1510021>.
- (3) Geyer, R.; Jambeck, J. R.; Law, K. L. Production, Use, and Fate of All Plastics Ever Made. *Sci. Adv.* **2017**, *3* (7), e1700782. <https://doi.org/10.1126/sciadv.1700782>.
- (4) Delidovich, I.; Hausoul, P. J. C.; Deng, L.; Pfützenreuter, R.; Rose, M.; Palkovits, R. Alternative Monomers Based on Lignocellulose and Their Use for Polymer Production. *Chem. Rev.* **2016**, *116* (3), 1540–1599. <https://doi.org/10.1021/acs.chemrev.5b00354>.
- (5) Van Zandvoort, I. *Towards the Valorization of Humin By-Products : Characterization , Solubilization and Catalysis*; 2015. <https://doi.org/10.1111/j.1365-2426.2003.01178.x>.
- (6) Hoang, T. M. C.; Van Eck, E. R. H.; Gardeniers, J. G. E.; Lefferts, L.; Seshan, K. Humin Based By-Products from Bioprocessing as Potential Carbonaceous Source for Synthesis Gas Production. *Green Chem.* **2015**, *17*, 959–972. <https://doi.org/10.1039/x0xx00000x>.
- (7) Hu, X.; Lievens, C.; Larcher, A.; Li, C. Z. Reaction Pathways of Glucose during Esterification: Effects of Reaction Parameters on the Formation of Humin Type Polymers. *Bioresour. Technol.* **2011**, *102* (21), 10104–10113. <https://doi.org/10.1016/j.biortech.2011.08.040>.
- (8) Filiciotto, L.; Balu, A. M.; Van der Waal, J. C.; Luque, R. Catalytic Insights into the Production of Biomass-Derived Side Products Methyl Levulinate, Furfural and Humins. *Catal. Today* **2018**, *302*, 2–15. <https://doi.org/10.1016/j.cattod.2017.03.008>.
- (9) Constant, S.; Lancefield, C. S.; Weckhuysen, B. M.; Bruijninx, P. C. A. Quantification and Classification of Carbonyls in Industrial Humins and Lignins by ¹⁹F NMR. *ACS Sustain. Chem. Eng.* **2017**, *5* (1), 965–972. <https://doi.org/10.1021/acssuschemeng.6b02292>.
- (10) Mija, A.; Jong, E. De; Waal, J. C. Van der; Klink, G. P. M. Van. Humins-Containing Foam. WO 2017/074183 A1, 2017.
- (11) Tosi, P.; Van Klink, G. P. M.; Celzard, A.; Fierro, V.; Vincent, L.; De Jong, E.; Mija, A. Auto-Crosslinked Rigid Foams Derived from Biorefinery Byproducts. *ChemSusChem* **2018**, *11* (16), 2797–2809. <https://doi.org/10.1002/cssc.201800778>.
- (12) Mija, A. C.; Waal, J. C. Van Der; Jong, E. De; Klink, G. P. Van. Process for the Modification of Humins. WO2018/062995 A1, 2018.
- (13) Pin, J. M.; Guigo, N.; Mija, A.; Vincent, L.; Sbirrazzuoli, N.; Van Der Waal, J. C.; De Jong, E. Valorization of Biorefinery Side-Stream Products: Combination of Humins with Polyfurfuryl Alcohol for Composite Elaboration. *ACS Sustain. Chem. Eng.* **2014**, *2* (9), 2182–2190.

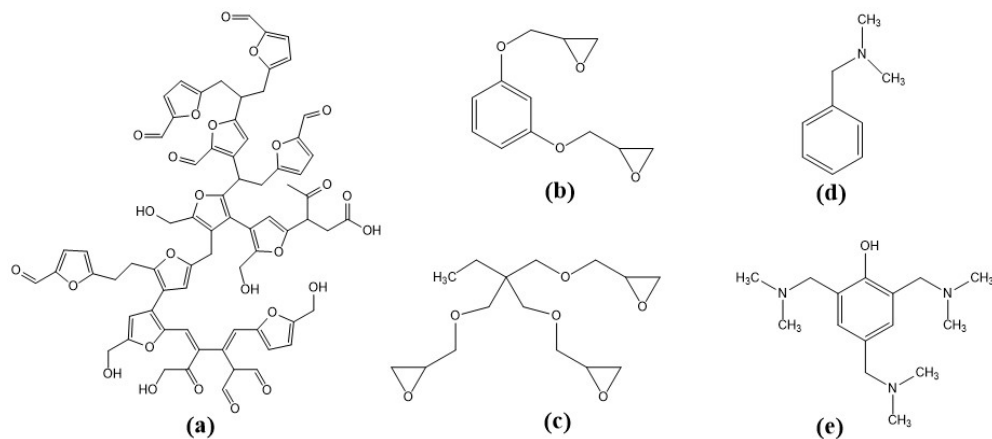
- <https://doi.org/10.1021/sc5003769>.
- (14) Dinu, R.; Mija, A. Cross-Linked Polyfuran Networks with Elastomeric Behaviour Based on Humins Biorefinery by-Products. *Green Chem.* **2019**, *21*, 6277–6289. <https://doi.org/10.1039/c9gc01813a>.
 - (15) Pin, J. M.; Guigo, N.; Vincent, L.; Sbirrazzuoli, N.; Mija, A. Copolymerization as a Strategy to Combine Epoxidized Linseed Oil and Furfuryl Alcohol: The Design of a Fully Bio-Based Thermoset. *ChemSusChem* **2015**, *8* (24), 4149–4161. <https://doi.org/10.1002/cssc.201501259>.
 - (16) Licsandru, E.; Mija, A. From Biorefinery By-Product to Bioresins. Thermosets Based on Humins and Epoxidized Linseed Oil. *Cellul. Chem. Technol.* **2019**, *53* (9–10), 963–969. <https://doi.org/10.35812/CelluloseChemTechnol.2019.53.94>.
 - (17) Gurunathan, T.; Mohanty, S.; Nayak, S. K. A Review of the Recent Developments in Biocomposites Based on Natural Fibres and Their Application Perspectives. *Compos. Part A Appl. Sci. Manuf.* **2015**, *77*, 1–25. <https://doi.org/10.1016/j.compositesa.2015.06.007>.
 - (18) Gholampour, A.; Ozbakkaloglu, T. A Review of Natural Fiber Composites: Properties, Modification and Processing Techniques, Characterization, Applications. *J. Mater. Sci.* **2020**, *55* (3), 829–892. <https://doi.org/10.1007/s10853-019-03990-y>.
 - (19) Wallenberger, F. T.; Weston, N. E. *Natural Fibers, Plastics and Composites*; Springer Science+Business Media: New York, 2004. <https://doi.org/10.1007/978-1-4419-9050-1>.
 - (20) Pereira, P. H. F.; Rosa, M. de F.; Cioffi, M. O. H.; Benini, K. C. C. de C.; Milanese, A. C.; Voorwald, H. J. C.; Mulinari, D. R. Vegetal Fibers in Polymeric Composites: A Review. *Polímeros* **2015**, *25* (1), 9–22. <https://doi.org/10.1590/0104-1428.1722>.
 - (21) Saxena, M.; Pappu, A.; Sharma, A.; Haque, R.; Wankhede, S. Composite Materials from Natural Resources : Recent Trends and Future Potentials. In *Advances in Composite Materials - Analysis of Natural and Man-Made Materials*; Tesinova, P., Ed.; InTech, 2011; pp 121–162.
 - (22) Mohanty, A. K.; Misra, M.; Drzal, L. T. *Natural Fibers, Biopolymers, and Biocomposites*; Taylor & Francis: New York, 2005.
 - (23) *DIRECTIVE 2000/53/EC of the European Parliament and of the Council On End-of Life Vehicles*; 2000; Vol. L 269. <https://doi.org/2004R0726> - v.7 of 05.06.2013.
 - (24) *DIRECTIVE 2002/96/EC of the European Parliament and of the Council on Waste Electrical and Electronic Equipment (WEEE)*; 2003. [https://doi.org/10.1016/S1578-1550\(11\)70052-3](https://doi.org/10.1016/S1578-1550(11)70052-3).
 - (25) Martínez-Hernández, A. L.; Velasco-Santos, C. Keratine Fibers from Chicken Feathers: Structure and Advances in Polymer Composites. In *Keratin: Structure, Properties and Applications*; Dullaart, R., Ed.; 2012; pp 149–211.
 - (26) Martínez-Hernández, A. L.; Velasco-Santos, C.; De-Icaza, M.; Castaño, V. M. Dynamical–Mechanical and Thermal Analysis of Polymeric Composites Reinforced with Keratin Biofibers from Chicken Feathers. *Compos. Part B Eng.* **2007**, *38* (3), 405–410. <https://doi.org/10.1016/j.compositesb.2006.06.013>.
 - (27) Donato, R. K.; Mija, A. Keratin Associations with Synthetic, Biosynthetic and Natural Polymers: An Extensive Review. *Polymers (Basel)*. **2019**, *12* (1), 32. <https://doi.org/10.3390/polym12010032>.
 - (28) Wang, J.; Hao, S.; Luo, T.; Cheng, Z.; Li, W.; Gao, F.; Guo, T.; Gong, Y.; Wang, B. Feather Keratin Hydrogel for Wound Repair: Preparation, Healing Effect and Biocompatibility Evaluation. *Colloids Surfaces B Biointerfaces* **2017**, *149*, 341–350. <https://doi.org/10.1016/j.colsurfb.2016.10.038>.
 - (29) Reddy, N. Non-Food Industrial Applications of Poultry Feathers. *Waste Manag.* **2015**, *45*, 91–107. <https://doi.org/10.1016/j.wasman.2015.05.023>.
 - (30) Shi, Z.; Reddy, N.; Hou, X.; Yang, Y. Tensile Properties of Thermoplastic Feather Films Grafted with Different Methacrylates. *ACS Sustain. Chem. Eng.* **2014**, *2* (7), 1849–1856. <https://doi.org/10.1021/sc500201q>.

- (31) Barone, J. R.; Schmidt, W. F.; Liebner, C. F. E. Thermally Processed Keratin Films. *J. Appl. Polym. Sci.* **2005**, *97* (4), 1644–1651. <https://doi.org/10.1002/app.21901>.
- (32) Colunga-Sánchez, L. M.; Salazar-Cruz, B. A.; Rivera-Armenta, J. L.; Morales-Cepeda, A. B.; Ramos-Gálvan, C. E.; Chávez-Cinco, M. Y. Evaluation of Chicken Feather and Styrene-Butadiene/Chicken Feather Composites as Modifier for Asphalts Binder. *Appl. Sci.* **2019**, *9* (23), 5188. <https://doi.org/10.3390/app9235188>.
- (33) Pourjavaheri, F.; Jones, O. A. H.; Czajka, M.; Martinez-Pardo, I.; Blanch, E. W.; Shanks, R. A. Design and Characterization of Sustainable Bio-Composites from Waste Chicken Feather Keratin and Thermoplastic Polyurethane. *Polym. Compos.* **2018**, *39*, E620–E632. <https://doi.org/10.1002/pc.24794>.
- (34) Aranberri, I.; Montes, S.; Azcune, I.; Rekondo, A.; Grande, H. J. Flexible Biocomposites with Enhanced Interfacial Compatibility Based on Keratin Fibers and Sulfur-Containing Poly(Urea-Urethane)S. *Polymers (Basel)*. **2018**, *10* (10), 1056. <https://doi.org/10.3390/polym10101056>.
- (35) Aranberri, I.; Montes, S.; Azcune, I.; Rekondo, A.; Grande, H. J. Fully Biodegradable Biocomposites with High Chicken Feather Content. *Polymers (Basel)*. **2017**, *9* (11). <https://doi.org/10.3390/polym9110593>.
- (36) Senoz, E.; Stanzione, J. F.; Reno, K. H.; Wool, R. P.; Miller, M. E. N. Pyrolyzed Chicken Feather Fibers for Biobased Composite Reinforcement. *J. Appl. Polym. Sci.* **2013**, *128* (2), 983–989. <https://doi.org/10.1002/app.38163>.
- (37) Amieva, E. J. C.; Velasco-Santos, C.; Martínez-Hernández, A.; Rivera-Armenta, J.; Mendoza-Martínez, A.; Castaño, V. Composites from Chicken Feathers Quill and Recycled Polypropylene. *J. Compos. Mater.* **2015**, *49* (3), 275–283. <https://doi.org/10.1177/0021998313518359>.
- (38) Cantarutti, C.; Dinu, R.; Mija, A. Biorefinery Byproducts and Epoxy Biorenewable Monomers: A Structural Elucidation of Humins and Triglycidyl Ether of Phloroglucinol Cross-Linking. *Biomacromolecules* **2020**, *21* (2), 517–533. <https://doi.org/10.1021/acs.biomac.9b01248>.
- (39) De Rosa, I. M.; Santulli, C.; Sarasini, F. Mechanical and Thermal Characterization of Epoxy Composites Reinforced with Random and Quasi-Unidirectional Untreated Phormium Tenax Leaf Fibers. *Materials and Design*. **2010**, pp 2397–2405. <https://doi.org/10.1016/j.matdes.2009.11.059>.
- (40) Dorez, G.; Taguet, A.; Ferry, L.; Lopez-Cuesta, J. M. Thermal and Fire Behavior of Natural Fibers/PBS Biocomposites. *Polym. Degrad. Stab.* **2013**, *98* (1), 87–95. <https://doi.org/10.1016/j.polymdegradstab.2012.10.026>.
- (41) Li, X.; Tabil, L. G.; Panigrahi, S. Chemical Treatments of Natural Fiber for Use in Natural Fiber-Reinforced Composites: A Review. *J. Polym. Environ.* **2007**, *15* (1), 25–33. <https://doi.org/10.1007/s10924-006-0042-3>.
- (42) Martin, A. R.; Martins, M. A.; da Silva, O. R. R. F.; Mattoso, L. H. C. Studies on the Thermal Properties of Sisal Fiber and Its Constituents. *Thermochim. Acta* **2010**, *506* (1–2), 14–19. <https://doi.org/10.1016/j.tca.2010.04.008>.
- (43) Manfredi, L. B.; Rodríguez, E.; Wladyka-Przybylak, M.; Vázquez, A. Thermal Properties and Fire Resistance of Jute-Reinforced Composites. *Compos. Interfaces* **2010**, *17* (5–7), 663–675. <https://doi.org/10.1163/092764410X513512>.
- (44) Monteiro, S. N.; Calado, V.; Rodriguez, R. J. S.; Margem, F. M. Thermogravimetric Behavior of Natural Fibers Reinforced Polymer Composites—An Overview. *Mater. Sci. Eng. A* **2012**, *557*, 17–28. <https://doi.org/10.1016/j.msea.2012.05.109>.
- (45) Wrześniewska-Tosik, K.; Zajchowski, S.; Bryskiewicz, A.; Ryszkowska, J. Feathers as a Flame-Retardant in Elastic Polyurethane Foam. *Fibres and Textiles in Eastern Europe*. **2014**, pp 119–128.
- (46) Senoz, E.; Wool, R. P.; McChalicher, C. W. J.; Hong, C. K. Physical and Chemical Changes in Feather Keratin during Pyrolysis. *Polym. Degrad. Stab.* **2012**, *97* (3), 297–307.

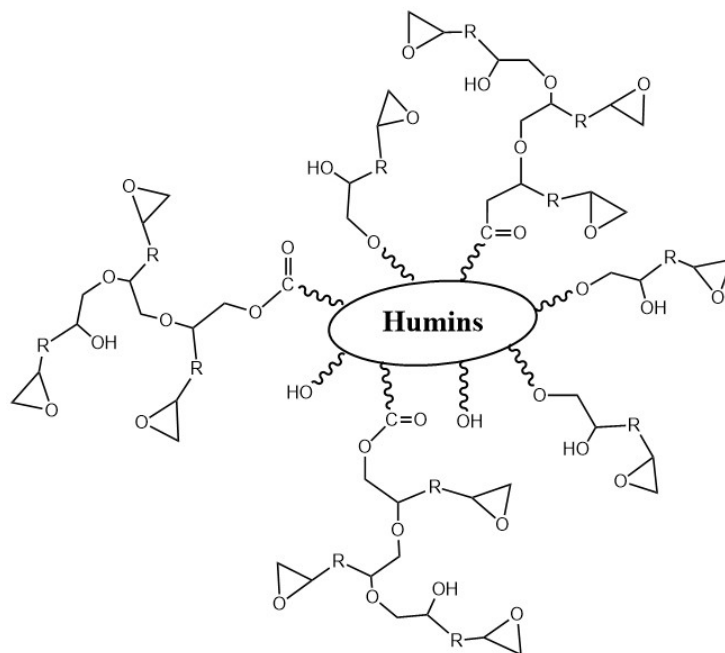
- <https://doi.org/10.1016/j.polymdegradstab.2011.12.018>.
- (47) Montané, X.; Dinu, R.; Mija, A. Synthesis of Resins Using Epoxies and Humins as Building Blocks: A Mechanistic Study Based on in-Situ FT-IR and NMR Spectroscopies. *Molecules* **2019**, *24* (22). <https://doi.org/10.3390/molecules24224110>.
 - (48) Zárate, C. N.; Aranguren, M. I.; Reboredo, M. M. Thermal Degradation of a Phenolic Resin, Vegetable Fibers, and Derived Composites. *J. Appl. Polym. Sci.* **2008**, *107* (5), 2977–2985. <https://doi.org/10.1002/app.27455>.
 - (49) Hafiezal, M. R. M.; Khalina, A.; Zurina, Z. A.; Azaman, M. D. M.; Hanafee, Z. M. Thermal and Flammability Characteristics of Blended Jatropha Bio-Epoxy as Matrix in Carbon Fiber-Reinforced Polymer. *J. Compos. Sci.* **2019**, *3* (1), 6. <https://doi.org/10.3390/jcs3010006>.
 - (50) Aouf, C.; Nouailhas, H.; Fache, M.; Caillol, S.; Boutevin, B.; Fulcrand, H. Multi-Functionalization of Gallic Acid. Synthesis of a Novel Bio-Based Epoxy Resin. *Eur. Polym. J.* **2013**, *49* (6), 1185–1195. <https://doi.org/10.1016/j.eurpolymj.2012.11.025>.
 - (51) Benyahya, S.; Aouf, C.; Caillol, S.; Boutevin, B.; Pascault, J. P.; Fulcrand, H. Functionalized Green Tea Tannins as Phenolic Prepolymers for Bio-Based Epoxy Resins. *Ind. Crops Prod.* **2014**, *53*, 296–307. <https://doi.org/10.1016/j.indcrop.2013.12.045>.
 - (52) Kalogeras, I. M.; Hagg Lobland, H. E. The Nature of the Glassy State: Structure and Glass Transitions. *J. Mater. Educ.* **2012**, *34* (3–4), 69–94.
 - (53) Suchitra, M. Thermal Analysis of Composites Using DSC. In *Advanced Topics in Characterization of Composites*; Kessler, M., Ed.; Trafford Publishing, 2004; pp 11–33.
 - (54) Dinu, R.; Mija, A. Bio-Based Composites from Industrial By-Products and Wastes as Raw Materials. *J. Mater. Sci. Res.* **2020**, *9* (2), 183–199.
 - (55) Fernandes, F. C.; Kirwan, K.; Wilson, P. R.; Coles, S. R. Sustainable Alternative Composites Using Waste Vegetable Oil Based Resins. *J. Polym. Environ.* **2019**, *27* (11), 2464–2477. <https://doi.org/10.1007/s10924-019-01534-8>.
 - (56) Zini, E.; Baiardo, M.; Armelao, L.; Scandola, M. Biodegradable Polyesters Reinforced with Surface-Modified Vegetable Fibers. *Macromol. Biosci.* **2004**, *4* (3), 286–295. <https://doi.org/10.1002/mabi.200300120>.
 - (57) Boopalan, M.; Niranjanaa, M.; Umopathy, M. J. Study on the Mechanical Properties and Thermal Properties of Jute and Banana Fiber Reinforced Epoxy Hybrid Composites. *Compos. Part B Eng.* **2013**, *51*, 54–57. <https://doi.org/10.1016/j.compositesb.2013.02.033>.
 - (58) Marrot, L.; Bourmaud, A.; Bono, P.; Baley, C. Multi-Scale Study of the Adhesion between Flax Fibers and Biobased Thermoset Matrices. *Mater. Des.* **2014**, *62*, 47–56. <https://doi.org/10.1016/j.matdes.2014.04.087>.
 - (59) Moudood, A.; Rahman, A.; Khanlou, H. M.; Hall, W.; Öchsner, A.; Francucci, G. Environmental Effects on the Durability and the Mechanical Performance of Flax Fiber/Bio-Epoxy Composites. *Compos. Part B Eng.* **2019**, *171* (December 2018), 284–293. <https://doi.org/10.1016/j.compositesb.2019.05.032>.
 - (60) Moudood, A.; Rahman, A.; Öchsner, A.; Islam, M.; Francucci, G. Flax Fiber and Its Composites: An Overview of Water and Moisture Absorption Impact on Their Performance. *J. Reinf. Plast. Compos.* **2019**, *38* (7), 323–339. <https://doi.org/10.1177/0731684418818893>.
 - (61) Assarar, M.; Scida, D.; El Mahi, A.; Poilâne, C.; Ayad, R. Influence of Water Ageing on Mechanical Properties and Damage Events of Two Reinforced Composite Materials: Flax-Fibres and Glass-Fibres. *Mater. Des.* **2011**, *32* (2), 788–795. <https://doi.org/10.1016/j.matdes.2010.07.024>.
 - (62) Muñoz, E.; García-Manrique, J. A. Water Absorption Behaviour and Its Effect on the Mechanical Properties of Flax Fibre Reinforced Bioepoxy Composites. *Int. J. Polym. Sci.* **2015**, *2015*, 1–10. <https://doi.org/10.1155/2015/390275>.
 - (63) Capiel, G.; Uicich, J.; Fasce, D.; Montemartini, P. E. Diffusion and Hydrolysis Effects during

- Water Aging on an Epoxy-Anhydride System. *Polym. Degrad. Stab.* **2018**, *153*, 165–171. <https://doi.org/10.1016/j.polymdegradstab.2018.04.030>.
- (64) Dhakal, H. N.; Zhang, Z. Y.; Richardson, M. O. W. Effect of Water Absorption on the Mechanical Properties of Hemp Fibre Reinforced Unsaturated Polyester Composites. *Compos. Sci. Technol.* **2007**, *67* (7–8), 1674–1683. <https://doi.org/10.1016/j.compscitech.2006.06.019>.
- (65) Dutta, S.; Karak, N.; Baruah, S. Jute-Fiber-Reinforced Polyurethane Green Composites Based on Mesua Ferrea L. Seed Oil. *J. Appl. Polym. Sci.* **2010**, *115* (2), 843–850. <https://doi.org/10.1002/app.30357>.
- (66) Ahmad, F.; Choi, H. S.; Park, M. K. A Review: Natural Fiber Composites Selection in View of Mechanical, Light Weight, and Economic Properties. *Macromol. Mater. Eng.* **2015**, *300* (1), 10–24. <https://doi.org/10.1002/mame.201400089>.
- (67) Zhang, Y.; Broekhuis, A. A.; Picchioni, F. Thermally Self-Healing Polymeric Materials: The Next Step to Recycling Thermoset Polymers? *Macromolecules* **2009**, *42* (6), 1906–1912. <https://doi.org/10.1021/ma8027672>.
- (68) Post, W.; Susa, A.; Blaauw, R.; Molenveld, K.; Knoop, R. J. I. A Review on the Potential and Limitations of Recyclable Thermosets for Structural Applications. *Polym. Rev.* **2019**, *0* (0), 1–30. <https://doi.org/10.1080/15583724.2019.1673406>.
- (69) Badia, J. D.; Strömberg, E.; Karlsson, S.; Ribes-Greus, A. Material Valorisation of Amorphous Polylactide. Influence of Thermo-Mechanical Degradation on the Morphology, Segmental Dynamics, Thermal and Mechanical Performance. *Polym. Degrad. Stab.* **2012**, *97* (4), 670–678. <https://doi.org/10.1016/j.polymdegradstab.2011.12.019>.
- (70) Wrześniewska-Tosik, K.; Szadkowski, M.; Marcinkowska, M.; Pałczyńska, M. Chicken Feather-Containing Composite Non-Wovens with Barrier Properties. *Fibres and Textiles in Eastern Europe*. 2012, pp 96–100.

Electronic Supplementary Information (ESI)



Scheme ESI 1. Molecular structure of a) humins, b) RDGE, c) TMPTE, d) BDMA and e) DMP-30



Scheme ESI 2. Proposed structure of the humins-epoxy copolymer

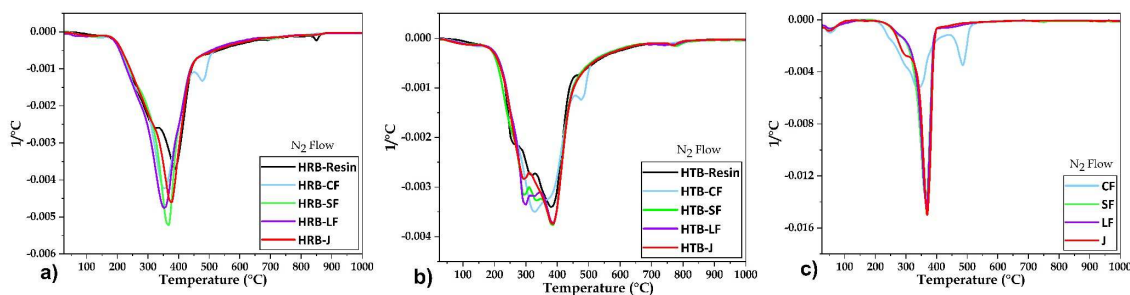


Figure ESI 1. DTA thermograms during heating at $10\text{ }^{\circ}\text{C min}^{-1}$ under nitrogen flow of (a) HRB resin and composites, (b) HTB resin and composites and (c) chicken feathers and vegetal non-woven fibers

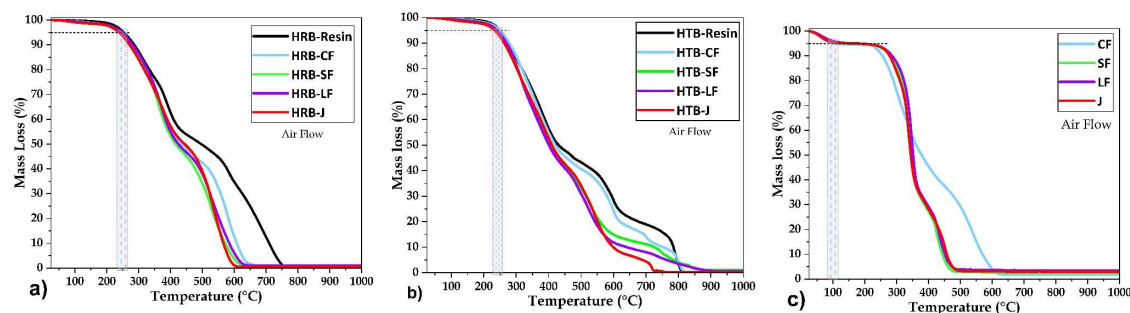


Figure ESI 2. Thermogravimetric curves registered at a heating rate of $10\text{ }^{\circ}\text{C min}^{-1}$ under oxidative atmosphere for (a) HRB resin and composites, (b) HTB resin and composites and (c) chicken feathers and vegetal non-woven fibers

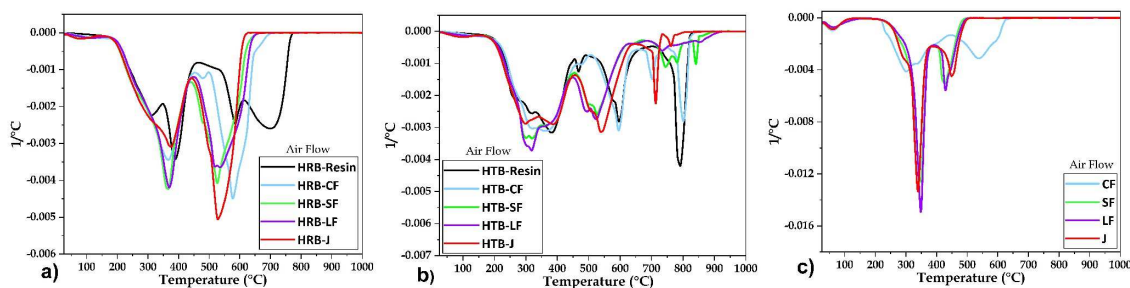


Figure ESI 3. DTA curves at a heating rate of $10\text{ }^{\circ}\text{C min}^{-1}$ under oxidative atmosphere for (a) HRB resin and composites, (b) HTB resin and composites and (c) chicken feathers and vegetal non-woven fibers

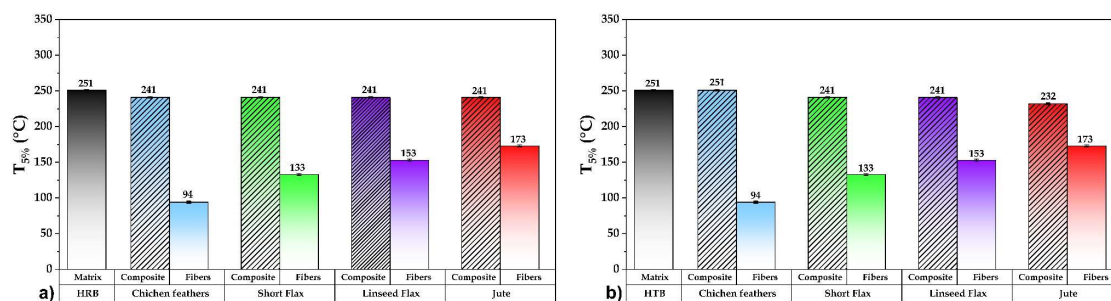


Figure ESI 4. TGA analysis comparison of the $T_{5\%}$ values of the matrices, fibers and composites, in air flow: (a) HRB resin and composites and (b) HTB resin and composites

Table ESI 1. Tensile data for the cured humins-based resins and composites with chicken feather and vegetal non-woven fibers

Formulation	Young's Modulus (MPa)	Maximum Stress (MPa)	Maximum Strain (%)
HRB	436.24 ± 40.49	1.04 ± 0.32	0.62 ± 0.1
HRB-CF	1190.58 ± 44.47	4.11 ± 0.41	0.43 ± 0.1
HRB-SF	1677.46 ± 316.75	8.08 ± 0.48	1.40 ± 0.63
HRB-LF	1556.07 ± 198.65	6.17 ± 2.06	0.8 ± 0.33
HRB-J	1579.41 ± 352.39	7.35 ± 1.05	1.01 ± 0.21
HTB	804.83 ± 118.31	3.34 ± 0.75	0.63 ± 0.11
HTB-CF	773.38 ± 83.37	4.08 ± 1.47	0.70 ± 0.26
HTB-SF	578.97 ± 66.16	10.61 ± 2.87	3.18 ± 0.71
HTB-LF	732.53 ± 53.50	6.51 ± 1.05	1.72 ± 0.00
HTB-J	649.21 ± 147.20	5.67 ± 0.48	1.02 ± 0.13

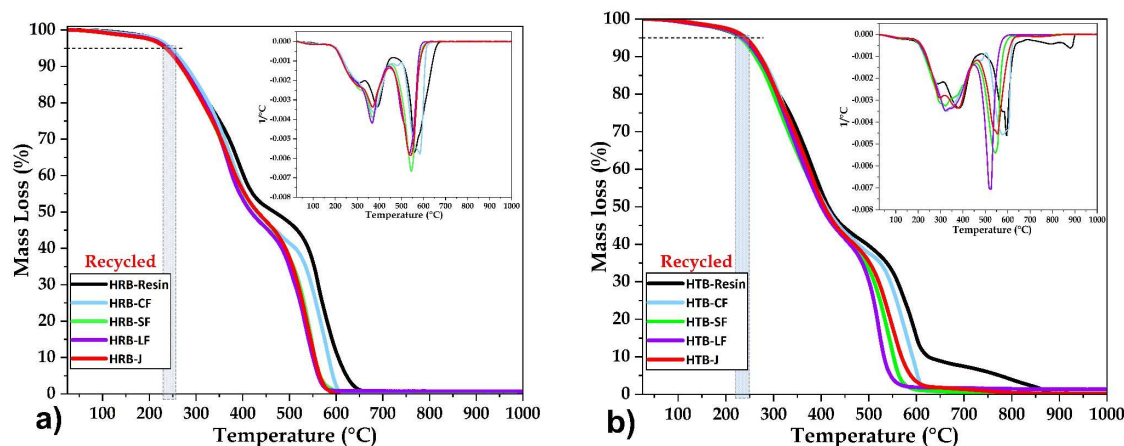


Figure ESI 5. TGA thermograms obtained at a heating rate of $10\text{ }^{\circ}\text{C min}^{-1}$ under oxidative atmosphere for (a) recycled HRB resin and composites and (b) recycled HTB resin and composites

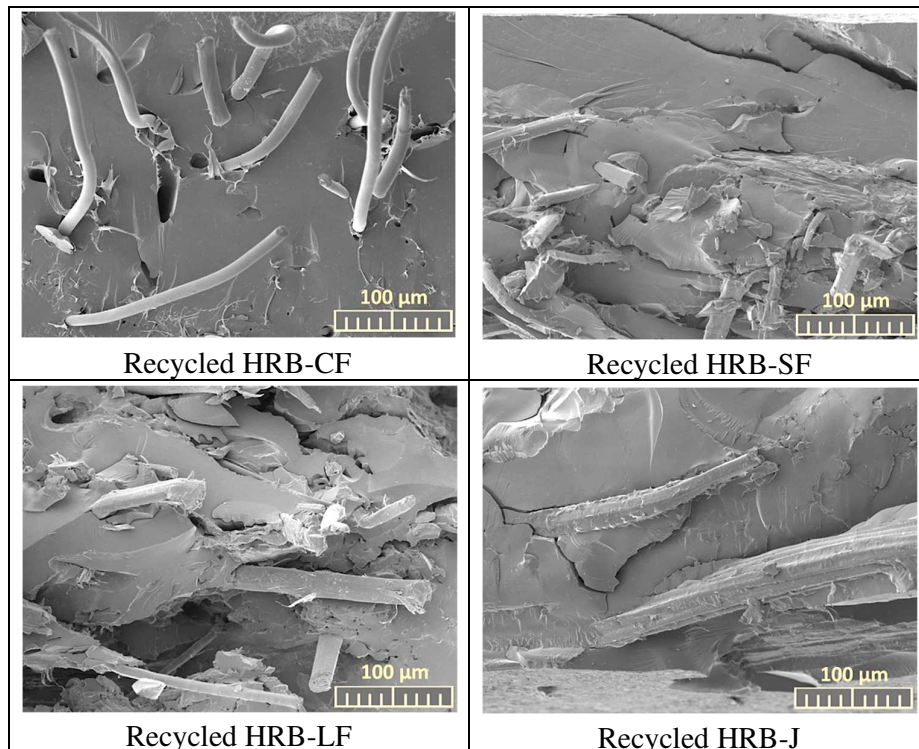


Figure ESI 6. SEM micrographs of the recycled HRB composites

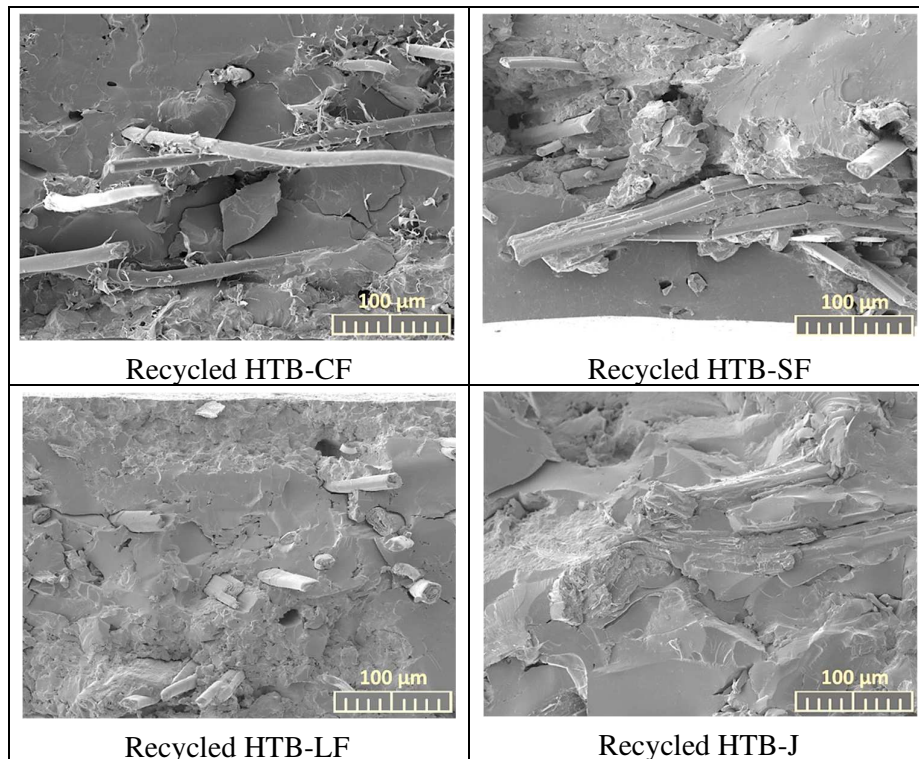


Figure ESI 7. SEM micrographs of the recycled HTB composites

Chapter 6

Design of Sustainable Materials by Cross-linking a Biobased Epoxide with Keratin and Lignin



This chapter is based on Roxana Dinu, Cristina Cantarutti and Alice Mija, "*Design of Sustainable Materials by Cross-linking a Biobased Epoxide with Keratin and Lignin*", ACS Sustainable Chemistry & Engineering, 2020, <https://doi.org/10.1021/acssuschemeng.0c01759> (invited cover page).

Abstract

Awareness of the environmental impact of using polymeric materials obtained from petroleum is causing increased interest in sustainable materials manufacturing. Here, we present the elaboration of fully biobased materials using an aromatic epoxy resin matrix coming from wood biomass and two natural by-products, namely, keratin from chicken feathers and lignin. In situ FTIR kinetic studies show that the two natural fillers increase the conversion of the epoxide during cross-linking. This result, together with DSC studies, proves the chemical interactions between the keratin or lignin and the epoxide network. Up to 30% of these natural components could be reacted and incorporated into the epoxide with a good compatibility. The thermomechanical properties of the elaborated materials are comparable to those of commercial ones.

6.1. Introduction

Growing concerns over the sustainability of polymeric materials from economic and environmental point of view have led to the development of materials based on biorenewable resources. Biomass has shown to be a huge source for the formulation of new polymers and materials with thermomechanical properties comparable to synthetic and petroleum-derived polymers but with a much lower environmental impact.^{1–4} Moreover, in accordance with the circular economy system, which aims at eliminating waste, it is becoming increasingly clear that remanufacturing industrial by-products is an urgent need.^{5,6}

In this perspective, we describe the formulation and the properties of biorenewable composite materials made up of a woody aromatic epoxy resin, *i.e.*, resorcinol diglycidyl ether (RDGE), reinforced with two natural waste products that are chicken feathers (CF) and lignin. RDGE is a diepoxy monomer (Figure 1a) obtained from the glycidylation of resorcinol that is part of the lignocellulosic aromatic fraction.⁷ Regarding the sustainable production from biomass of resorcinol, the literature mentions several ways. Gioia *et al.*⁸ indicate the fermentation and/or chemical process to produce the resorcinol. In this manner, resorcinol can be obtained from catechins by fermentation or from glucose following two ways: *via* an inositol intermediate or *via* a triacetic acid lactone intermediate. Another references indicate the resorcinol synthesis by “Frost method”: the deoxygenation of polyhydroxybenzenes.⁹ Recently, Modjinou *et al.*¹⁰ have reported the synthesis of resorcinol *via* an extraction process after the melting of *Galbanum sagapenum* gum resins.

RDGE's homopolymerization gives polymers (Figure 1b) with high thermomechanical performance.¹¹ RDGE has the big advantage to have a low viscosity (300–500 mPa s), being the most fluidic aromatic epoxide, which is an ideal matrix to embed natural reinforcements.^{7,11} CFs constitute the principal waste from poultry industry with 3.1 million tons per year only in the European Union alone.¹² Nowadays, chicken feathers are mainly dispersed in landfills, incinerated or to a minor extent used to produce low-nutritional-value animal food. Moreover, the increasing consumption of chicken meat will make even more troubling the chicken feather fate issue. CF are mainly constituted by β -keratin that is a filament-forming protein. Its structure is the result of the lateral packing of β -strands held together by intermolecular hydrogen bonds (Figure 1c). Only the central part of the polypeptide chain is involved in this structure, while the terminal part winds around and forms an amorphous matrix in which the fibres are dispersed.¹³ Thanks to their peculiar physical and mechanical properties,¹⁴ chicken feathers have been extensively used as reinforcements for composite materials.¹⁵ Commonly

used matrices are synthetic polymers like polypropylene,^{16,17} polyethylene^{18,19} and the copolymer styrene-butadiene.²⁰

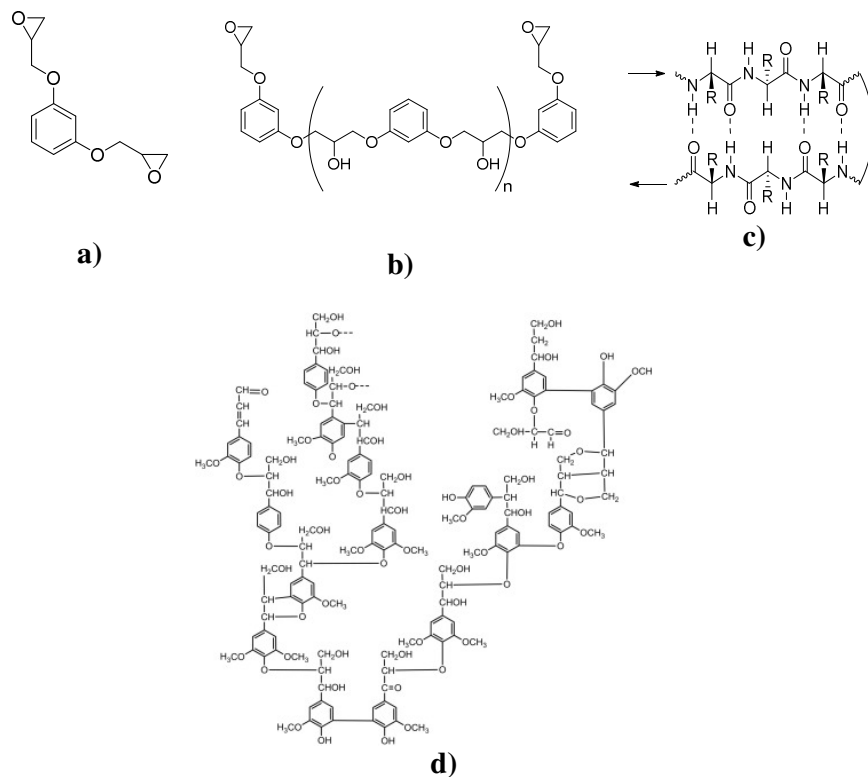


Figure 1. Molecular structure of a) RDGE, b) homopolymerized RDGE, c) chicken feathers keratin, and d) lignin

Keratin from chicken feathers is also incorporated in biodegradable matrices made by polylactic acid and polybutyrate adipate terephthalate, but the fabrication procedure requires high temperatures (170 °C for matrix melting and 200 °C for composite consolidation) because these polymers have high melting points.¹² Concerning epoxy matrices, there are only a few reported examples of chicken feathers composites, all of which based on bisphenol A and bisphenol F diglycidyl ethers (DGEBA and DGEBF).^{21–23} Bisphenol A and F are both petroleum-derived and are known to have toxic effects.²⁴

Lignin comes from the cell wall of plants, especially the woody tissues. It is a phenolic frame network resulting from the dehydrogenative radical polymerization of monolignols, *i.e.*, p-coniferyl, -coumaryl and -sinapyl alcohols, connected through carbon-carbon and ether bonds.²⁵ The functional chemical groups characteristic of lignin are the hydroxyl (phenolic and alcoholic), methoxy, carbonyl and carboxyl (Figure 1d). Lignin is a by-product of chemical pulping processes (sulphite and Kraft process). Organic solvent²⁶ or high-pressure steam treatment are alternative delignification technologies. Twenty billion tons of lignin is produced per year,^{2,27} and most of it is simply burned for energy. Also, lignin has shown to be a suitable

material for composite formulation.²⁸ It has been used as an additive for synthetic polymers like polypropylene²⁹ and polyvinyl chloride³⁰ and for rubber composites.³¹ The main epoxy resin used in combination with lignin has been until now the DGEBA.^{32,33} Zhang *et al.*³⁴ reacted different types of lignin (*e.g.*, raw lignin, demethylated lignin, phenolated lignin and hydroxymethylated lignin) with epichlorohydrin in order to develop new chemical grouting materials as replacements for petroleum-based epoxy precursors. Recently, a lignin-epoxy resin based on glycerol diglycidyl ether has been formulated as wood adhesive.³⁵ Furthermore, lignin-based materials have been produced with epoxidized lignin.^{32,36,37}

6.2. Results and Discussion

6.2.1. Reactivity study

In order to establish the optimal cross-linking parameters and also to analyse the influence of lignin/ keratin on the curing of the epoxy resin, different combinations of uncured mixtures were studied by dynamic DSC. Figure 2 show the obtained heat flow evolutions as a function of the temperature. Surprisingly, the enthalpy of reaction in the initiated systems with the fillers is very close to that of the neat epoxide homopolymerization (Table 1). For both systems, we can observe that the curves' slopes are higher, and the two peaks are narrower than the homopolymerization RDGE peak. This finding is an indication that the two natural products are not inert fillers but chemical co-reactants with the epoxy matrix that are finally chemically linked. Furthermore, a decrease of the reaction temperature interval and of the maximum temperature of reaction was observed for both initiated curing systems in presence of K and L (Table 1). These results could be again the sign that both K and L are participating in the chemical cross-linking reaction rather than being just inert fillers. To further verify this hypothesis, *i.e.*, the chemical reactivity between the RDGE and K or RDGE and L, the two-component mixtures (R_K and R_L) without any catalyst were submitted to thermal curing.

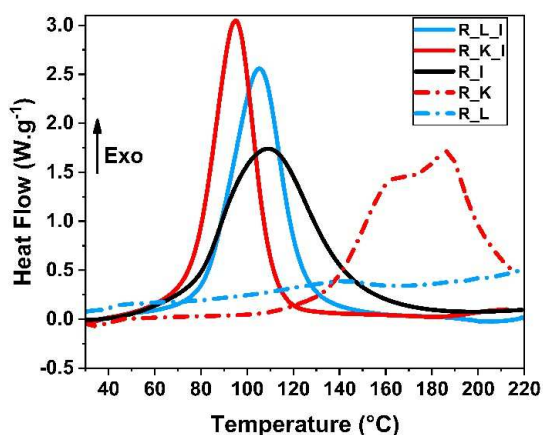


Figure 2. DSC scans registered during heating at $10\text{ }^{\circ}\text{C min}^{-1}$ of RDGE (black solid line), of RDGE with K (red solid line), or L (blue solid line) initiated by the mixture of 5 wt.% BDMA/DMP-30. The dashed lines correspond to uncatalyzed mixtures.

Table 1. Reactivity data of RDGE and RDGE curing systems with keratin and lignin obtained by dynamic DSC.

	R_I	R_K	R_L	R_K_I	R_L_I
Reaction T_{max} (interval) (°C)	110 ± 1 (35–192)	180 ± 1 (116–220)	140 ± 1 (86–175)	101 ± 1 (33–142)	105 ± 1 (33–168)
Enthalpy of reaction ($J g^{-1}$)	414 ± 2	389 ± 2	17 ± 1	418 ± 2	415 ± 2

As shown in Figure 2, the presence of a very small and large exothermic peak at around 140 °C for the RDGE_Lignin mixture can be seen, in contrast to the RDGE_Keratin reaction accompanied by a high exotherm and a complex profile showing two partially overlapped peaks centered at approximately 165 °C and 190 °C. This latter peculiar pattern suggests that the reaction between K and RDGE in the absence of catalysts is characterized by two sequential reactions. In the DSC heating scans of raw materials alone, the absence of any exotherm could be observed (Figure ESI1), results that confirm again that K and L actually react with RDGE.

To follow the molecular structural evolution during curing, attenuated total reflection Fourier transform infrared (ATR-FTIR) spectra were recorded at increasing temperatures going from 30 °C to 200 °C with a heating rate of 10 °C min⁻¹ collecting a spectrum every 10°. The assignment of starting material spectra is reported in the Electronic Supporting Information (Figure ESI2). The same FTIR analysis was done on the neat RDGE as control. During heating of all the samples, the opening of the epoxy moiety is supported by the decrease in RDGE oxirane signal at 901 cm⁻¹, an increase in the band at 1080 cm⁻¹ that reflects alcohol CO stretching, and an increase in the OH stretching band between 3500 and 3600 cm⁻¹ (Figure ESI3a–c). The extent of the polymerization reaction was calculated considering RDGE epoxy conversion (α) determined from the area of the peak at 901 cm⁻¹ (A_{901}) as follows:

$$\alpha = \left(\frac{A_{901}(30\text{ }^{\circ}\text{C}) - A_{901}(T)}{A_{901}(30\text{ }^{\circ}\text{C})} \right) \quad (1)$$

where $A_{901}(30\text{ }^{\circ}\text{C})$ and $A_{901}(T)$ are the epoxy peak areas at 30 °C (taken as reference) and at temperature T, respectively. Before measuring the area of the epoxy peak, the spectra were normalized to RDGE aromatic peak at 1594 cm⁻¹. The conversion-temperature data are reported in Figure 3. The data suggest that the reactivity of the epoxy monomer is higher in the systems comprising K or L than in the neat resin. Moreover, between the two reinforcements, K appear to increase to a larger extent the cross-linking reaction. These results are in agreement with the DSC results. FTIR spectra were recorded also in the absence of the catalysts. When

RDGE is used alone, as the temperature increases, the epoxy signal decreases in intensity, but as the temperature goes back to 30 °C, the epoxy absorbance is recovered (Figure ESI4a).

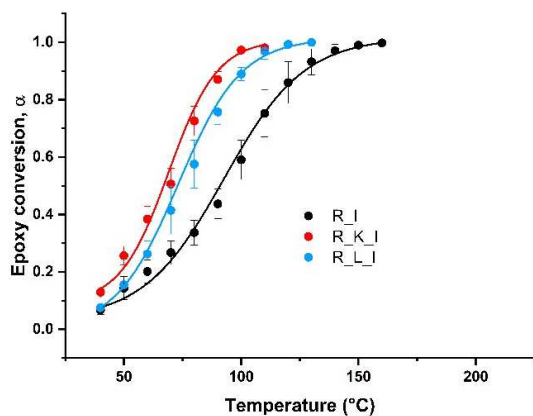


Figure 3. Epoxy conversion (α) as a function of temperature for R_I (black dots), R_K_I (red dots), and R_L_I (blue dots). The data are the average of three independent measurements, and the error is the standard deviation. The lines correspond to the Boltzmann sigmoidal fitting

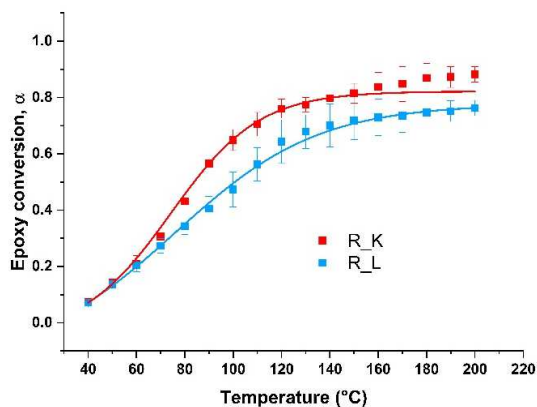
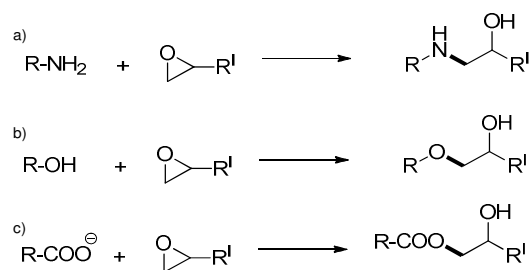


Figure 4. Epoxy conversion (α) as a function of temperature for R_K (red squares) and R_L (blue squares). The data are the average of three independent measurements, and the error is the standard deviation. The lines correspond to the Boltzmann sigmoidal fitting

This means that RDGE alone do not homopolymerize by simply increasing the temperature. The reduction in epoxy signal is likely to reflect intrinsic vibrational effects and density changes, as already reported in literature.^{38,39} When K or L is present, the epoxy peak decreases in intensity as well, but after cooling down to 30 °C, there is no signal recovery (Figure ESI4b and c), meaning that the two fillers are able to open the RDGE's oxirane rings. Again, in agreement with DSC data, K show a higher reactivity (Figure 4). Both keratin and lignin have nucleophilic groups (Nu) that are able to open and react with the epoxy ring. Chicken feathers are mainly constituted by keratin that is a fibrous protein. Polypeptide chains have many reactive functional groups including amine, carboxylate, sulfhydryl, and hydroxyl that can react with epoxies. Sulfhydryl involvement in epoxy ring opening is unlikely since it is engaged in the preservation of keratin structure through the formation of strong disulfide bonds. Amino, carboxylate, and hydroxyl nucleophilic groups can all attack the epoxide electrophilic carbons (Scheme 1).



Scheme 1. Schematic representation of the three principal reaction pathways between proteins and epoxies. The new bonds are depicted in bold

In general, FTIR spectrum of K is dominated by the absorbance of the polypeptide backbone chain, which undergoes complex evolution during temperature increase (Figure ESI5a) due to the rearrangement of the keratin highly ordered structure.⁴⁰ By increasing the temperature in the system R_K_I, in addition to the previously mentioned spectral changes reflecting the epoxy ring opening, two new bands appear and increase in intensity: one at 1115 cm^{-1} and one at 1225 cm^{-1} (Figure ESI4b). These two bands correspond to the stretching of aliphatic ether and carbon-nitrogen bond, respectively, which are formed from K's hydroxyl and amino groups attacking the RDGE epoxy moiety (Scheme 1a and b). Because of the peak superposition, no clear evidences of ester formation can be obtained from the IR spectra (Scheme 1c); therefore, the third cross-linking mechanism appears to occur in a negligible extent. From the comparison of the IR spectra recorded on R_K samples in the presence and in the absence of the BDMA/DMP-30 mixture, it was not possible to determine the actual nature of the second sequential reaction that corresponds to the second peak centered at 190 °C in the DSC curve (Figure 2) recorded only in the absence of the catalysts. Probably, it is a secondary reaction that involves the hydroxyl function formed from epoxy ring opening *e.g.*, a transesterification of protein's carboxylic acid. This secondary reaction does not occur when the catalysts are present because in that case the epoxy ring opening suddenly creates a molecular complex that prevents the accessibility of the new hydroxyl moiety to other keratin reactive functional groups.

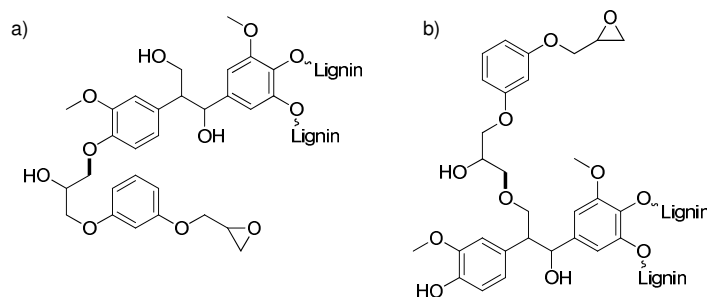
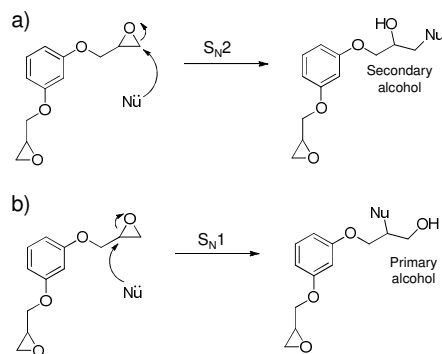


Figure 5. Molecular structures of cross-linked RDGE and lignin through (a) alkyl aryl ether and (b) alkyl ether bonds. The new bonds are depicted in bold

Regarding the system with lignin, during R_L_I heating, a new band at 1209 cm^{-1} appears and grows as the temperature increases (Figure ESI3c). This band corresponds to the aryl alkyl ether bond (Figure 5a) stretching, absent in the lignin spectrum (Figure ESI5b), that can arise only if lignin phenolic functions open the RDGE oxirane ring. Moreover, the peak corresponding to aliphatic ether stretching increases as well suggesting that also the aliphatic alcohols present in lignin structure contribute to the cross-linking reaction (Figure 5b).



Scheme 2. Mechanisms of RDGE epoxy ring opening by nucleophilic attack; Nu represents the nucleophilic groups from keratin and lignin

In both samples, the C-OH stretching band falls above 1075 cm^{-1} indicating the formation of a secondary alcohol rather than a primary one. This implies that the reaction proceeds through an S_N2 mechanism giving the regioisomer coming from the nucleophilic attack on the less substituted epoxy carbon (Scheme 2a). On the other hand, if the mechanism was a S_N1 , a primary alcohol would have been formed (Scheme 2b). The occurrence of the S_N2 mechanism is also consistent with the basic conditions.

6.2.2. Physico-chemical characterization of RDGE-based composites

6.2.2.1. Thermal stability of the obtained materials

The thermochemical stability of the obtained composites was analyzed under oxidative and inert atmospheres and compared with the unfilled epoxy resin. Figure 6 illustrates the thermogravimetric (TGA) and DTA, differential thermal analyses, results as a function of temperature under air flow.

These measurements show the presence of two major steps of thermal decomposition. In the case of composites, a supplementary small decomposition step appears between $200\text{ }^\circ\text{C}$ and $370\text{ }^\circ\text{C}$. This first small step can be attributed to volatilization of adsorbed moisture and to the beginning of the thermal decomposition of the K and L that have both relatively low $T_{5\%}$ values: $\approx 84\text{ }^\circ\text{C}$ for K and $\approx 202\text{ }^\circ\text{C}$ for L (Figure ESI7).^{41–43} This thermal behavior of the two products is reflected in the thermal stability of the generated composites. The temperature's

value of 5% mass loss ($T_{5\%}$) is considered as the material degradation temperature. The RDGE resin loses 5% of its mass at 350 °C, while the composite R_K_I loses it at 255 °C and that with lignin is at 315 °C.

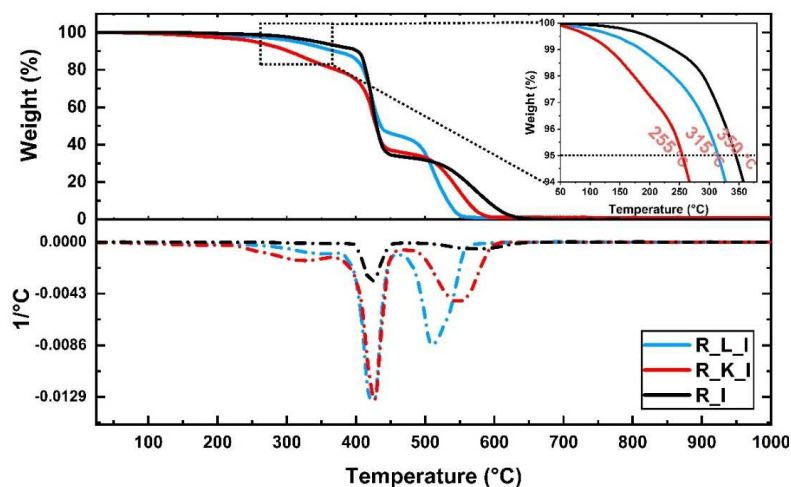


Figure 6. TGA-DTA curves for R_I (black line), R_L_I (blue line), and R_K_I (red line) during heating at 10 °C min⁻¹ under air flow

The second thermal degradation step consists of a sharp decrease in weight and occurs at temperatures between 370 °C and 480 °C. The related process is the thermolysis of the polymeric chain structure. The thermal reaction's intermediary and products residues formed during this degradation process undergo further thermo-oxidative degradations in the last step, which leads to complete decomposition of the materials. All the thermal degradation steps correspond to endothermic peaks in DTA plots that are usually associated with the volatilization of degradation products.⁴⁴ For the R_L_I sample, the presence of a considerable endothermic peak in the DTA plot centered at 510 °C suggests the complete decomposition of the system. The mass loss in this step (480–520 °C temperature range) is \approx 43 wt.%. The epoxy/keratin system presents in this step a better thermal stability than epoxy/lignin material: the complete conversion into carbon of the R_K_I composite (34 wt.% mass loss) occurs at 480–620 °C.

Figure 7 shows the TGA-DTA results of the systems submitted to heating under an inert atmosphere (N₂). According to the DTA curves, the maximum of the first endothermic peak is at approximately 330 °C for both systems, but in this step, R_L_I material loses 13 wt.% of mass while R_K_I loses \approx 25 wt.%. The second and main degradation step occurs for all systems at \approx 500 °C, with a drastic decomposition of 54–57% of their weight. After this point, the systems are thermally stable as the temperature rises, with the remaining residue being around 21% for R_I and R_K_I and 30 wt.% for the R_L_I material. In order to better express the thermal stability of the materials, the statistic heat-resistant index (T_s) value was calculated.

This value was determined from the TGA data and is the temperature at which materials lose 5% ($T_{5\%}$) and 30% ($T_{30\%}$) of their weight. The heat-resistance index represents the temperature of the polymer in the physical heat tolerance limit and was calculated from Eq. (2).^{11,45–47}

$$T_s = 0.49[T_{5\%} + 0.6(T_{30\%} - T_{5\%})] \quad (2)$$

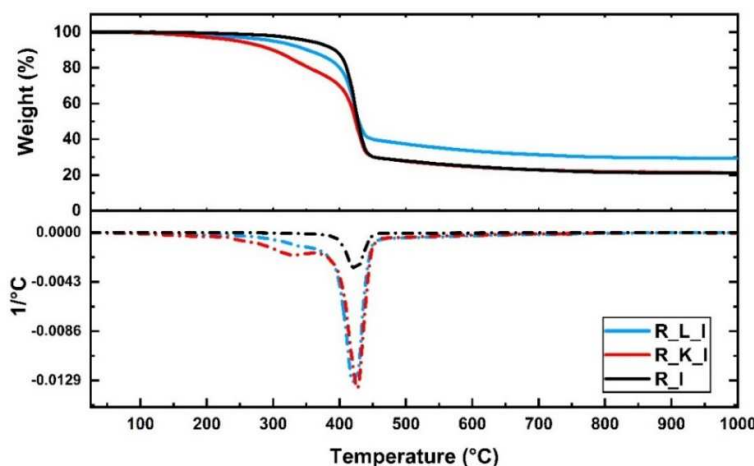


Figure 7. TGA analyses of cured materials under heating at $10^{\circ}\text{C min}^{-1}$ in inert atmosphere

Table 2. Physico-chemical and mechanical properties of the cured biobased materials

Sample	ρ (g/cm^3)	B ($\% \cdot \text{Pa}/10^{10}$)	Hardness test Shore D	$T_{g\text{-DSC}}$ ($^{\circ}\text{C}$)	Young's modulus (MPa)	Tensile strength (MPa)	Elongation at break (%)	$T_{5\%}$ ($^{\circ}\text{C}$)		T_s ($^{\circ}\text{C}$)	
								Air	N_2	Air	N_2
R_I	1.1206	-	89	93	-	-	-	350	350	192	192
R_K_I	1.1433	0.39	92	92	640.98 ± 151.96	4.1 ± 1.4	9.22 ± 2.26	255	245	170	165
R_L_I	1.1787	1.08	92	85	968.87 ± 161.1	14.98 ± 3.31	3.08 ± 1.07	315	300	185	181

The T_s values of the thermoset materials were calculated for the oxidative and inert atmospheres and are summarized in Table 2. The $T_{5\%}$ and T_s values of the RDGE_K_I composite in air/ N_2 were around 8% lower than those of the RDGE_L_I material. We can also notice that both K and L produce a decreasing T_s values compared to the neat resin ($T_s = 192^{\circ}\text{C}$). The thermal stabilities of the systems obtained in this work are comparable to those of commercial epoxy materials (DGEBA = 145°C) or reported in literature ($135\text{--}198^{\circ}\text{C}$).^{48–51}

6.2.2.2. Glass transition determined by DSC

The glass transition of the prepared materials was analyzed by DSC applying a cycle of two heating and cooling steps in the temperature range of $25\text{--}220^{\circ}\text{C}$ at $10^{\circ}\text{C min}^{-1}$. The glass transition regions ($T_{g\text{-DSC}}$) for the RDGE resin material and its composite systems with K or L were measured in the second cooling step and are presented in Figure 8.

The $T_{g\text{-DSC}}$ for R_I resin is $\approx 93^{\circ}\text{C}$, and a similar region was obtained for the composite with K: $T_{g\text{-DSC}} = 92^{\circ}\text{C}$. The presence of the aromatic 3D framework on the lignin structure has

a stronger impact on the α relaxation of the resin, acting as a plasticizer and lowering by ≈ 8 °C the glass transition, $T_{g-DSC} = 85$ °C. These identical or close transition region of three α relaxations reveal the very good chemical and structural compatibility between the RDGE and the K or L. This structural compatibility is also proven by the values of the cross-linking density of the neat and combined RDGE matrix with keratin or lignin. As the cross-linking density of R_I thermoset is around $0.68 \text{ mmol cm}^{-3}$, this value increases in the formulation with lignin to $1.56 \text{ mmol cm}^{-3}$ and, even more, to around $1.95 \text{ mmol cm}^{-3}$ for the R_K_I material. Therefore, more compacted networks are generated by the interaction of RDGE with the keratin compared with the lignin, perhaps due to the higher reactivity of the RDGE with keratin than that with the lignin, as already shown in Figure 3 and 4. If we confront the values of the cross-linking density with the results of systems reactivity, we can observe the same trend, *i.e.*, the higher the reactivity of the formulations, the higher is the cross-linking density of materials: $R_K_I > R_L_I > R_I$.

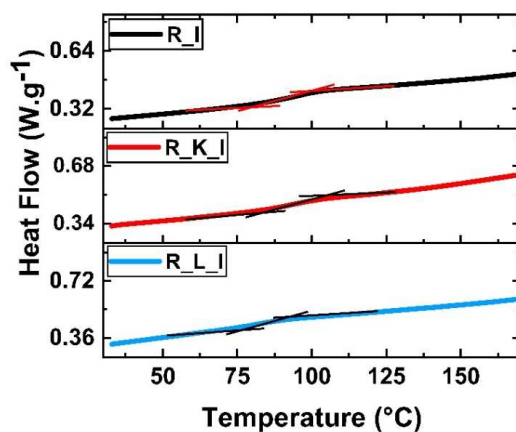


Figure 8. Glass transitions of cross-linked materials obtained at the second cooling ($10 \text{ }^\circ\text{C min}^{-1}$) by DSC

6.2.2.3. Tensile testing

To analyze the potential application field of the obtained materials, the investigation on tensile properties was performed. Young's modulus, tensile strength, and elongation at break of the cured materials were determined by the tensile test technique, with the results being included in Table 2. The obtained values reveal that the two composites are defined by a mechanical behavior. The stiffness of the epoxy/keratin material is around 650 MPa, ≈ 0.67 times lower than the value obtained for the R_L_I material (≈ 970 MPa). Also, the tensile strength of R_K_I resin is lower, while its elongation at break is 3 times higher than the value obtained for the R_L_I material. Even if the cross-linking density of R_K_I resin is higher than that of the R_L_I material, the higher tensile properties of the last one could be attributed to the contribution of aromatic moieties from the lignin 3D structure.

Another significant mechanical parameter considered in the design, research, and development of materials is their brittleness. The quantitative brittleness (B) of the cured materials was analyzed according to studies developed by W. Brostow *et al.*^{52–54} and was calculated using the following equation:

$$B = 1/\varepsilon_b E' \quad (3)$$

where ε_b is the value of elongation at break and E' is the storage modulus obtained by DMA (Figure ESI8). The elongation at break values were determined by tensile tests, while the storage modulus data were collected from DMA analyses using the three-point bending clamp at a frequency of 1.0 Hz. The values used in the calculation of the brittleness were obtained at 25 °C. From the data summarized in Table 2, it can be observed that the elongation at break of R_K_I composite ($\approx 9.22\%$) is higher than that of R_L_I ($\approx 3.08\%$). According to the literature,^{52–54} the materials with high ε_b are fragile, so the lower the brittleness, the higher the dimensional stability of the materials. In compliance with the calculated values, the brittleness of the R_L_I material is around $1.08 \text{ \%}\cdot\text{Pa}/10^{10}$, comparable with the brittleness of commercial polymers like styrene/acrylonitrile copolymer ($1.316 \text{ \%}\cdot\text{Pa}/10^{10}$) or poly(methylmethacrylate) ($0.722 \text{ \%}\cdot\text{Pa}/10^{10}$). In contrast, the brittleness of the composite with keratin is $\approx 0.39 \text{ \%}\cdot\text{Pa}/10^{10}$, a value comparable with that of acrylonitrile/butadiene/styrene copolymer ($0.443 \text{ \%}\cdot\text{Pa}/10^{10}$). So, keratin increases the hardness and the elongation at break of the RDGE resin and produce a material less brittle than the epoxy/lignin composite. These results are in good correlation with the cross-linking density values, with the R_K_I having a higher density than the R_L_I. At the same time, we can highlight that the three materials have very close values of density, so these fillers also have the advantage to reinforce the resin matrix without increasing the materials density, as is the case in classical polymeric composites. With the help of the MatWeb online database (<http://www.matweb.com/index.aspx>), the properties of the developed materials were compared with the commercial ones, thus confirming their performance in the category of epoxy thermoset materials.

6.3. Conclusions

Industrial waste valorization in materials engineering is a challenging way to reduce environmental pollution. We prepared biobased, green composites by combining a biobased diepoxide and keratin or lignin as reinforcements. The two natural co-reactive fillers were successfully reacted and incorporated into the resin and produced fully sustainable materials. The processability of the prepared formulations was easy, and the curing process was fast and efficient. We demonstrated that these two by-products act simultaneously as reinforcements

and cross-linking agents thanks to the abundance of reactive functional groups. The good compatibility between the components lead to materials characterized by very similar α relaxations. The good thermomechanical performances, comparable with those of the commercial resins, could make them as sustainable materials.

6.4. Experimental

6.4.1. Materials

Resorcinol diglycidyl ether (RDGE) was supplied by Sigma-Aldrich. The fractioned Kraft lignin used was supplied by VTT Technical Research Center of Finland. It appears as a brown powder with a weak odor, with pH values between 2.5 and 7 and sulfur content of 1–3%. In order to obtain keratin, the sanitized chicken feathers supplied by Grupo SADA (Madrid, Spain) were pretreated by steam explosion method applying hot steam (160 °C) and pressure (15.5 bar) for 2 minutes. The resulting feathers were ground in a universal cutting mill Fritsch Pulverisette 19, obtaining a wide size distribution. N,N-Dimethylbenzylamine (BDMA) and 2,4,6-Tris(dimethylaminomethyl)phenol (DMP-30) were purchased from Sigma-Aldrich and used as received.

6.4.1.1. Sample preparation

Composite materials were prepared by preheating RDGE at 50 °C in order to decrease its viscosity and promote the incorporation of the fillers. Liquid RDGE (65 wt.%) was then mixed and homogenized by vigorous mechanical mixing with keratin or lignin (30 wt.%) and with a mixture of N,N-Dimethylbenzylamine (BDMA) and 2,4,6-Tris(dimethylaminomethyl)phenol (DMP-30) (2.5 + 2.5 wt.%) as the curing catalyst and accelerator, respectively. In this work, keratin (K) obtained from chicken feathers by the steam explosion process was used. The homogenized mixtures of RDGE_Keratin or RDGE_Lignin were poured in a rectangular metallic mold (150 × 150 × 4 mm³) and cured using a heated press for 30 minutes at 60 °C and for another hour at 80 °C applying 1 MT pressure. In order to obtain completely cured thermosets, the samples were post-cured at 130 °C for 30 min. For better identification, the name of the materials was abbreviated according to their composition. The keratin from chicken feathers was denoted with “K”, lignin was denoted with “L”, and the combination between BDMA and DMP-30 was denoted with “I”. So, the “R_K_I” abbreviation corresponds to the system with 65 wt.% RDGE, 30 wt.% K and 5 wt.% BDMA/DMP-30, while “R_L_I” is the material with 65 wt.% RDGE, 30 wt.% L and 5 wt.% of BDMA/DMP-30.

6.4.2. Experimental techniques

6.4.2.1. Differential Scanning Calorimetry (DSC)

The reactivity study between RDGE and lignin/keratin was performed using a DSC 3 Mettler Toledo apparatus. The instrument was calibrated in three points using standards such as water, indium and zinc and was operated by STARE Software developed by Mettler Toledo. Fresh samples of 4–7 mg were placed in 40 μL aluminum crucibles and analyzed under dynamic conditions over a temperature range of 25–230 $^{\circ}\text{C}$. A heating rate of 10 $^{\circ}\text{C min}^{-1}$ was applied to the samples. The DSC technique was also used to determine the first-order transitions (residual exotherm) or the second-order phase transitions (α relaxations, T_g) of the obtained materials. Cured samples with masses between 6 and 9 mg placed into 40 μl crucibles were submitted to a cycle scan during heating and cooling from 25 $^{\circ}\text{C}$ to 220 $^{\circ}\text{C}$ at 10 $^{\circ}\text{C min}^{-1}$ rate under 150 mL min^{-1} air flow.

6.4.2.2. Attenuated Total Reflection Fourier Transform Infrared (ATR-FTIR) spectroscopy

IR spectra of all the starting materials were acquired at 30 $^{\circ}\text{C}$ accumulating 32 scans with 4 cm^{-1} resolution going from 4000 cm^{-1} to 600 cm^{-1} . A temperature ramp going from 30 $^{\circ}\text{C}$ to 200 $^{\circ}\text{C}$ with an increment of 10 $^{\circ}\text{C min}^{-1}$ was accomplished by recording a spectrum every 10 $^{\circ}\text{C}$ to highlight the structural evolutions occurring during the heating of the different systems. The same studies were done both with and without the catalysts and for the starting materials alone to assess their structural evolution with the temperature. The spectra of the blends were normalized with respect to the aromatic C=C peak of RDGE monomer.

6.4.2.3. Thermogravimetric analysis (TGA)

The TGA technique was used to determine the thermal stability of the materials. The mass loss and its derivatives as a function of temperature were analyzed in oxidative and inert atmospheres (150 mL min^{-1}) using a TGA 2 Mettler-Toledo apparatus. Samples of 8–10 mg placed into 70 μL alumina pans were tested over a temperature range of 25 $^{\circ}\text{C}$ to 1000 $^{\circ}\text{C}$ at a heating rate of 10 $^{\circ}\text{C min}^{-1}$. Each formulation was analyzed three times for average calculation.

6.4.2.4. Tensile testing

The effort response of the materials when a traction force was applied was analyzed by a universal testing machine Instron, Norwood, MA, USA model 3365, controlled by BlueHill Lite software (Instron, Norwood, MA, USA). The crosshead speed applied to the rectangular samples with dimensions of 75 \times 10 \times 4 mm^3 (length \times width \times thickness) was 10 mm min^{-1} . The tensile properties such as Young's modulus, tensile strength, and elongation at break for the final biobased thermosets were determined. In order to avoid errors, 10 samples for each formulation were tested.

6.4.2.5. Shore hardness test

The hardness of the developed materials was determined using a Zwick Roell 3116 Hardness Tester in accordance with standards as ISO 868, ISO 7619-1 and ASTM D2240. The measurements were performed using the Shore D Hardness scale, which is intended for measuring the hardness of hard rubbers, semirigid plastics, and hard plastics. The hardness values were determined by measuring the depth of penetration of a specific indenter.

6.4.2.6. Density of materials

According to the ISO 9427 standard, the densities of the cured materials were experimentally determined. In the first stage, the volume of the samples was calculated, and then their mass was determined using an ML3002T Mettler-Toledo precision balance. Material density values were obtained by calculating the ratio between mass and volume. For a high data accuracy, the final density values were obtained by analyzing five rectangular samples ($50 \times 8 \times 4 \text{ mm}^3$) for each formulation.

6.4.2.7. Dynamic mechanical analysis (DMA)

DMA measurements were performed using a Mettler-Toledo DMA 1 equipped with a three-point bending assembly at an oscillatory frequency of 1.0 Hz and an amplitude of 20 μm . The analyzed samples had rectangular dimensions of $48 \times 8 \times 4 \text{ mm}^3$ (length \times width \times thickness). Each resin formulation was analyzed three times, and the values were averaged. The DMA was performed in the temperature-scanning mode with a constant displacement amplitude and frequency. The temperature ramp covered a range from -150 to $180 \text{ }^\circ\text{C}$ at a heating rate of $3 \text{ }^\circ\text{C min}^{-1}$ under a nitrogen atmosphere.

Cross-linking density was calculated by the Equation (4):

$$\nu = \frac{E'}{3RT} \quad (4)$$

where E' is the storage modulus of the thermoset in the rubbery plateau region at $T_g + 80 \text{ }^\circ\text{C}$, R is the gas constant, and T is the absolute temperature in Kelvin.

Notes and references

- (1) Morris, D. J.; Ahmed, I. *The Carbohydrate Economy: Making Chemicals and Industrial Materials from Plant Matter*; Institute for Local Self-Reliance, 1992.
- (2) Wool, R.; Sun, X. S. *Bio-Based Polymers and Composites*, 1st Editio.; Elsevier, 2005.
- (3) Gandini, A. Furans in Polymer Chemistry. *Prog. Polym. Sci.* **1997**, *22* (6), 1203–1379. [https://doi.org/10.1016/S0079-6700\(97\)00004-X](https://doi.org/10.1016/S0079-6700(97)00004-X).
- (4) Khot, S. N.; Lascala, J. J.; Can, E.; Morye, S. S.; Williams, G. I.; Palmese, G. R.; Kusefoglu, S. H.; Wool, R. P. Development and Application of Triglyceride-Based Polymers and Composites. *J. Appl. Polym. Sci.* **2001**, *82* (3), 703–723. <https://doi.org/10.1002/app.1897>.
- (5) Datta, J.; Kopczyńska, P. From Polymer Waste to Potential Main Industrial Products: Actual State of Recycling and Recovering. *Crit. Rev. Environ. Sci. Technol.* **2016**, *46* (10), 905–946. <https://doi.org/10.1080/10643389.2016.1180227>.
- (6) Yusuf, M. Agro-Industrial Waste Materials and Their Recycled Value-Added Applications: Review. In *Handbook of Ecomaterials*; Martínez, L. M. T., Kharissova, O. V., Kharisov, B. I., Eds.; Springer International Publishing: Cham, 2017; pp 1–11. https://doi.org/10.1007/978-3-319-48281-1_48-1.
- (7) Durairaj, R. B. *Resorcinol: Chemistry, Technology and Applications*; Springer Science & Business Media, 2005. <https://doi.org/10.1007/b982897>.
- (8) Gioia, C.; Banella, M. B.; Vannini, M.; Celli, A.; Colonna, M.; Caretti, D. Resorcinol: A Potentially Bio-Based Building Block for the Preparation of Sustainable Polyesters. *Eur. Polym. J.* **2015**, *73*, 38–49. <https://doi.org/10.1016/j.eurpolymj.2015.09.030>.
- (9) Hansen, C. A.; Frost, J. W. Deoxygenation of Polyhydroxybenzenes: An Alternative Strategy for the Benzene-Free Synthesis of Aromatic Chemicals. *J. Am. Chem. Soc.* **2002**, *124* (21), 5926–5927. <https://doi.org/10.1021/ja0176346>.
- (10) Modjinou, T.; Versace, D. L.; Abbad-Andaloussi, S.; Langlois, V.; Renard, E. Enhancement of Biological Properties of Photoinduced Biobased Networks by Post-Functionalization with Antibacterial Molecule. *ACS Sustain. Chem. Eng.* **2019**, *7* (2), 2500–2507. <https://doi.org/10.1021/acssuschemeng.8b05402>.
- (11) Nouailhas, H.; Aouf, C.; Le Guerneve, C.; Caillol, S.; Boutevin, B.; Fulcrand, H. Synthesis and Properties of Biobased Epoxy Resins. Part 1. Glycidylation of Flavonoids by Epichlorohydrin. *J. Polym. Sci. Part A Polym. Chem.* **2011**, *49* (10), 2261–2270. <https://doi.org/10.1002/pola.24659>.
- (12) Aranberri, I.; Montes, S.; Azcune, I.; Rekondo, A.; Grande, H. J. Fully Biodegradable Biocomposites with High Chicken Feather Content. *Polymers (Basel)*. **2017**, *9* (11). <https://doi.org/10.3390/polym9110593>.
- (13) Wang, B.; Yang, W.; McKittrick, J.; Meyers, M. A. Keratin: Structure, Mechanical Properties, Occurrence in Biological Organisms, and Efforts at Bioinspiration. *Prog. Mater. Sci.* **2016**, *76*, 229–318. <https://doi.org/10.1016/j.pmatsci.2015.06.001>.
- (14) Zhan, M.; Wool, R. P. Mechanical Properties of Chicken Feather Fibers. *Polym. Compos.* **2011**, *32* (6), 937–944. <https://doi.org/10.1002/pc.21112>.
- (15) Lucio, D. S. V.; Rivera-Armenta, J. L.; Rivas-Orta, V.; Díaz-Zavala, N. P.; Páramo-García, U.; Rivas, N. V. G.; Cinco, M. Y. C. Manufacturing of Composites from Chicken Feathers and Polyvinyl Chloride (PVC). In *Handbook of Composites from Renewable Materials*; John Wiley & Sons, Inc.: Hoboken, NJ, USA, 2017; Vol. 1–8, pp 159–174. <https://doi.org/10.1002/9781119441632.ch25>.
- (16) Amieva, E. J. C.; Velasco-Santos, C.; Martínez-Hernández, A.; Rivera-Armenta, J.; Mendoza-Martínez, A.; Castaño, V. Composites from Chicken Feathers Quill and Recycled Polypropylene. *J. Compos. Mater.* **2015**, *49* (3), 275–283.

- <https://doi.org/10.1177/0021998313518359>.
- (17) Reddy, N.; Yang, Y. Light-Weight Polypropylene Composites Reinforced with Whole Chicken Feathers. *J. Appl. Polym. Sci.* **2010**, *116*, NA-NA. <https://doi.org/10.1002/app.31931>.
 - (18) Barone, J. R.; Schmidt, W. F. Polyethylene Reinforced with Keratin Fibers Obtained from Chicken Feathers. *Compos. Sci. Technol.* **2005**, *65* (2), 173–181. <https://doi.org/10.1016/j.compscitech.2004.06.011>.
 - (19) Oladele, I. O.; Okoro, A. M.; Omotoyinbo, J. A.; Khoathane, M. C. Evaluation of the Mechanical Properties of Chemically Modified Chicken Feather Fibres Reinforced High Density Polyethylene Composites. *J. Taibah Univ. Sci.* **2018**, *12* (1), 56–63. <https://doi.org/10.1080/16583655.2018.1451103>.
 - (20) Mendez-Hernandez, M. L.; Salazar-Cruz, B. A.; Rivera-Armenta, J. L.; Estrada-Moreno, I. A.; Chavez-Cinco, M. Y. Preparation and Characterization of Composites from Copolymer Styrene-Butadiene and Chicken Feathers. *Polímeros* **2018**, *28* (4), 368–372. <https://doi.org/10.1590/0104-1428.08217>.
 - (21) Zhan, M.; Wool, R. P.; Xiao, J. Q. Electrical Properties of Chicken Feather Fiber Reinforced Epoxy Composites. *Compos. Part A Appl. Sci. Manuf.* **2011**, *42* (3), 229–233. <https://doi.org/10.1016/j.compositesa.2010.11.007>.
 - (22) Srivatsav, V.; Ravishankar, C.; Ramakarishna, M.; Jyothi, Y.; Bhanuparakash, T. N. Mechanical and Thermal Properties of Chicken Feather Reinforced Epoxy Composite. In *AIP Conference Proceedings*; 2018; Vol. 1992, p 040034. <https://doi.org/10.1063/1.5047999>.
 - (23) Verma, A.; Negi, P.; Singh, V. K. Experimental Analysis on Carbon Residuum Transformed Epoxy Resin: Chicken Feather Fiber Hybrid Composite. *Polym. Compos.* **2019**, *40* (7), 2690–2699. <https://doi.org/10.1002/pc.25067>.
 - (24) Moreman, J.; Lee, O.; Trznadel, M.; David, A.; Kudoh, T.; Tyler, C. R. Acute Toxicity, Teratogenic, and Estrogenic Effects of Bisphenol A and Its Alternative Replacements Bisphenol S, Bisphenol F, and Bisphenol AF in Zebrafish Embryo-Larvae. *Environ. Sci. Technol.* **2017**, *51* (21), 12796–12805. <https://doi.org/10.1021/acs.est.7b03283>.
 - (25) Constant, S.; Wienk, H. L. J.; Frissen, A. E.; Peinder, P. De; Boelens, R.; Van Es, D. S.; Grisel, R. J. H.; Weckhuysen, B. M.; Huijgen, W. J. J.; Gosselink, R. J. A.; Bruijninx, P. C. A. New Insights into the Structure and Composition of Technical Lignins: A Comparative Characterisation Study. *Green Chem.* **2016**, *18* (9), 2651–2665. <https://doi.org/10.1039/C5GC03043A>.
 - (26) Cruz, J. M.; Domínguez, J. M.; Domínguez, H.; Parajó, J. C. Solvent Extraction of Hemicellulosic Wood Hydrolysates: A Procedure Useful for Obtaining Both Detoxified Fermentation Media and Polyphenols with Antioxidant Activity. *Food Chem.* **1999**, *67* (2), 147–153. [https://doi.org/10.1016/S0308-8146\(99\)00106-5](https://doi.org/10.1016/S0308-8146(99)00106-5).
 - (27) Lora, J. H.; Glasser, W. G. Recent Industrial Applications of Lignin: A Sustainable Alternative to Nonrenewable Materials. *J. Polym. Environ.* **2002**, *10* (1–2), 39–48. <https://doi.org/10.1023/A:1021070006895>.
 - (28) Faruk, O.; Sain, M. *Lignin in Polymer Composites*, 1st Editio.; Elsevier, 2016.
 - (29) Dias, O. A. T.; Negrão, D. R.; Silva, R. C.; Funari, C. S.; Cesarino, I.; Leao, A. L. Studies of Lignin as Reinforcement for Plastics Composites. *Mol. Cryst. Liq. Cryst.* **2016**, *628* (1), 72–78. <https://doi.org/10.1080/15421406.2015.1137677>.
 - (30) Ping, Q.; Xiao, J.; Zhao, J. The Preparation and Property of Organic Solvent Lignin and PVC Composite Materials. *Adv. Mater. Res.* **2011**, *236–238*, 1195–1198. <https://doi.org/10.4028/www.scientific.net/AMR.236-238.1195>.
 - (31) Ikeda, Y.; Phakkeeree, T.; Junkong, P.; Yokohama, H.; Phinyocheep, P.; Kitano, R.; Kato, A. Reinforcing Biofiller “Lignin” for High Performance Green Natural Rubber Nanocomposites. *RSC Adv.* **2017**, *7* (9), 5222–5231. <https://doi.org/10.1039/c6ra26359c>.
 - (32) Sun, J.; Wang, C.; Yeo, J. C. C.; Yuan, D.; Li, H.; Stubbs, L. P.; He, C. Lignin Epoxy

- Composites: Preparation, Morphology, and Mechanical Properties. *Macromol. Mater. Eng.* **2016**, *301* (3), 328–336. <https://doi.org/10.1002/mame.201500310>.
- (33) Yin, Q.; Yang, W.; Sun, C.; Di, M. Preparation and Properties of Lignin-Epoxy Resin Composite. *BioResources* **2012**, *7* (4), 5737–5748. <https://doi.org/10.15376/biores.7.4.5737-5748>.
- (34) Zhang, Y.; Pang, H.; Wei, D.; Li, J.; Li, S.; Lin, X.; Wang, F.; Liao, B. Preparation and Characterization of Chemical Grouting Derived from Lignin Epoxy Resin. *Eur. Polym. J.* **2019**, *118* (May), 290–305. <https://doi.org/10.1016/j.eurpolymj.2019.05.003>.
- (35) Li, R. J.; Gutierrez, J.; Chung, Y. L.; Frank, C. W.; Billington, S. L.; Sattely, E. S. A Lignin-Epoxy Resin Derived from Biomass as an Alternative to Formaldehyde-Based Wood Adhesives. *Green Chem.* **2018**, *20* (7), 1459–1466. <https://doi.org/10.1039/C7GC03026F>.
- (36) Malutan, T.; Nicu, R.; Popa, V. I. Lignin Modification by Epoxidation. *BioResources* **2008**, *3* (4), 1371–1376. <https://doi.org/10.15376/biores.3.4.1371-13767>.
- (37) Ferdosian, F.; Yuan, Z.; Anderson, M.; Xu, C. Sustainable Lignin-Based Epoxy Resins Cured with Aromatic and Aliphatic Amine Curing Agents: Curing Kinetics and Thermal Properties. *Thermochim. Acta* **2015**, *618*, 48–55. <https://doi.org/10.1016/j.tca.2015.09.012>.
- (38) Duemichen, E.; Javdanitehran, M.; Erdmann, M.; Trappe, V.; Sturm, H.; Braun, U.; Ziegmann, G. Analyzing the Network Formation and Curing Kinetics of Epoxy Resins by in Situ Near-Infrared Measurements with Variable Heating Rates. *Thermochim. Acta* **2015**, *616*, 49–60. <https://doi.org/10.1016/j.tca.2015.08.008>.
- (39) Hagemann, H.; Snyder, R. G.; Peacock, A. J.; Mandelkern, L. Quantitative Infrared Methods for the Measurement of Crystallinity and Its Temperature Dependence. Polyethylene. *Macromolecules* **1989**, *22* (9), 3600–3606. <https://doi.org/10.1021/ma00199a017>.
- (40) Serrano, V.; Liu, W.; Franzen, S. An Infrared Spectroscopic Study of the Conformational Transition of Elastin-like Polypeptides. *Biophys. J.* **2007**, *93* (7), 2429–2435. <https://doi.org/10.1529/biophysj.106.100594>.
- (41) Hirose, S.; Hatakeyama, T.; Hatakeyama, H. Novel Epoxy Resins Derived from Biomass Components. *Procedia Chem.* **2012**, *4*, 26–33. <https://doi.org/10.1016/j.proche.2012.06.004>.
- (42) Väisänen, T.; Das, O.; Tomppo, L. A Review on New Bio-Based Constituents for Natural Fiber-Polymer Composites. *J. Clean. Prod.* **2017**, *149*, 582–596. <https://doi.org/10.1016/j.jclepro.2017.02.132>.
- (43) Senoz, E.; Wool, R. P.; McChalicher, C. W. J.; Hong, C. K. Physical and Chemical Changes in Feather Keratin during Pyrolysis. *Polym. Degrad. Stab.* **2012**, *97* (3), 297–307. <https://doi.org/10.1016/j.polymdegradstab.2011.12.018>.
- (44) Kandola, B. K.; Krishnan, L.; Deli, D.; Luangtriratana, P.; Ebdon, J. R. Fire and Mechanical Properties of a Novel Free-Radically Cured Phenolic Resin Based on a Methacrylate-Functional Novolac and of Its Blends with an Unsaturated Polyester Resin. *RSC Adv.* **2015**, *5* (43), 33772–33785. <https://doi.org/10.1039/c5ra01813g>.
- (45) Hafiezal, M. R. M.; Khalina, A.; Zurina, Z. A.; Azaman, M. D. M.; Hanafee, Z. M. Thermal and Flammability Characteristics of Blended Jatropha Bio-Epoxy as Matrix in Carbon Fiber-Reinforced Polymer. *J. Compos. Sci.* **2019**, *3* (1), 6. <https://doi.org/10.3390/jcs3010006>.
- (46) Benyahya, S.; Aouf, C.; Caillol, S.; Boutevin, B.; Pascault, J. P.; Fulcrand, H. Functionalized Green Tea Tannins as Phenolic Prepolymers for Bio-Based Epoxy Resins. *Ind. Crops Prod.* **2014**, *53*, 296–307. <https://doi.org/10.1016/j.indcrop.2013.12.045>.
- (47) Aouf, C.; Nouailhas, H.; Fache, M.; Caillol, S.; Boutevin, B.; Fulcrand, H. Multi-Functionalization of Gallic Acid. Synthesis of a Novel Bio-Based Epoxy Resin. *Eur. Polym. J.* **2013**, *49* (6), 1185–1195. <https://doi.org/10.1016/j.eurpolymj.2012.11.025>.
- (48) François, C.; Pourchet, S.; Boni, G.; Rautiainen, S.; Samec, J.; Fournier, L.; Robert, C.; Thomas, C. M.; Fontaine, S.; Gaillard, Y.; Placet, V.; Plasseraud, L. Design and Synthesis of Biobased Epoxy Thermosets from Biorenewable Resources. *Comptes Rendus Chim.* **2017**, *20* (11–12),

- 1006–1016. <https://doi.org/10.1016/j.crci.2017.10.005>.
- (49) Chairat, A.; Joulia, X.; Floquet, P.; Vergnes, H.; Ablitzer, C.; Fiquet, O.; Brothier, M. Thermal Degradation Kinetics of a Commercial Epoxy Resin-Comparative Analysis of Parameter Estimation Methods. *J. Appl. Polym. Sci.* **2015**, *132* (27). <https://doi.org/10.1002/app.42201>.
- (50) Fache, M.; Boutevin, B.; Caillol, S. Epoxy Thermosets from Model Mixtures of the Lignin-to-Vanillin Process. *Green Chem.* **2016**, *18* (3), 712–725. <https://doi.org/10.1039/c5gc01070e>.
- (51) Nisha, S. S.; Nikzad, M.; Al Kobaisi, M.; Truong, V. K.; Sbarski, I. The Role of Ionic-Liquid Extracted Lignin Micro/Nanoparticles for Functionalisation of an Epoxy-Based Composite Matrix. *Compos. Sci. Technol.* **2019**, *174* (July 2018), 11–19. <https://doi.org/10.1016/j.compscitech.2019.02.009>.
- (52) Brostow, W.; Hagg Lobland, H. E.; Narkis, M. Sliding Wear, Viscoelasticity, and Brittleness of Polymers. *J. Mater. Res.* **2006**, *21* (9), 2422–2428. <https://doi.org/10.1557/jmr.2006.0300>.
- (53) Brostow, W.; Hagg Lobland, H. E. Brittleness of Materials: Implications for Composites and a Relation to Impact Strength. *J. Mater. Sci.* **2010**, *45* (1), 242–250. <https://doi.org/10.1007/s10853-009-3926-5>.
- (54) Brostow, W.; Hagg Lobland, H. E.; Narkis, M. The Concept of Materials Brittleness and Its Applications. *Polym. Bull.* **2011**, *67* (8), 1697–1707. <https://doi.org/10.1007/s00289-011-0573-1>.

Electronic Supplementary Information (ESI)

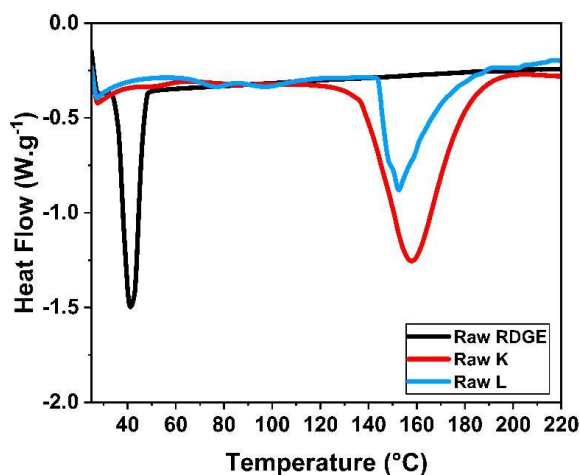


Figure ESI 1. DSC thermograms during heating of RDGE, K and L at $10^{\circ}\text{C min}^{-1}$

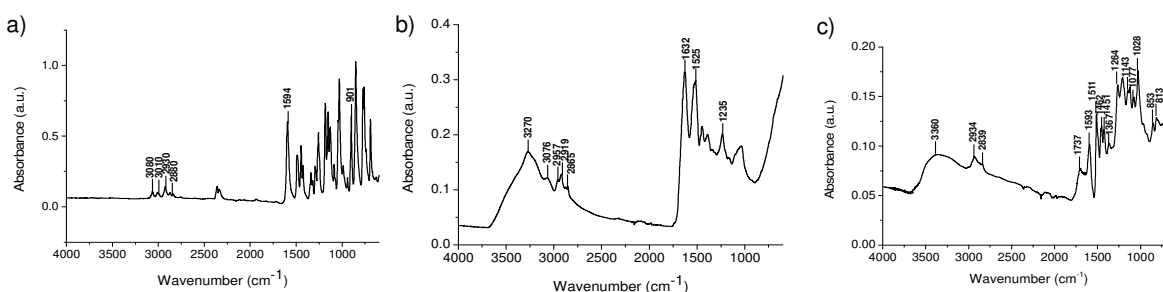


Figure ESI 2. FTIR spectra of a) RDGE, b) K and c) lignin at 30°C

RDGE spectrum (Figure ESI2a). The aromatic and the glycidyl methylene CH stretching give rise to the peaks just above and below 3000 cm^{-1} , respectively. The strong absorption at 1594 cm^{-1} is due to the aromatic carbon-carbon double bonds. The peak at 901 cm^{-1} corresponds to the asymmetric stretching of the epoxy ring. There is no clear evidence of RDGE homo-polymerization product in the starting material because in the FTIR spectrum a hydroxyl band around 3500 cm^{-1} cannot be distinguished.

K spectrum (Figure ESI2b). The chicken feathers (CF) spectrum shows the characteristic features of proteins. The NH stretching vibration gives rise to two bands at 3270 and 3076 cm^{-1} (amide A and B bands), the amide I band that arises mainly from the carbonyl stretching vibration with contributions from the out-of-phase CN stretching vibration can be found at 1632 cm^{-1} a value compatible with a β -sheet secondary structure, the amide II is the out-of-phase combination of the NH in plane bending and the CN stretching vibration and is located at 1525 cm^{-1} and the band at 1235 cm^{-1} is the amide III band that corresponds to the in-phase combination of the NH bending and the CN stretching vibration. The amide A band

presents a shoulder around 3500 cm^{-1} that is due to OH stretching of serine residues of which CF keratin is reported to be particularly rich.

Lignin spectrum (Figure ESI2c). A large band between 3600 and 3000 cm^{-1} is related to hydroxyl stretching. The bands at 2934 and 2840 cm^{-1} are related to sp^3 CH coming predominantly from the aromatic methoxyl groups and also from methyl and methylene side chains. The band that extends between 1800 and 1600 cm^{-1} is related to carbonyls/carboxyls. The peaks at 1593 and 1511 cm^{-1} arise from the vibrations of the aromatic skeleton. CH bending is responsible for the peaks at 1462 and 1451 cm^{-1} . The region below 1400 cm^{-1} is complex to analyse because the contribution of various vibrations overlaps. The band at 1367 cm^{-1} is assigned to CO bond vibration in phenolic OH and aliphatic CH in methyl groups bending, the peak at 1209 cm^{-1} is related to aryl alkyl ether CO stretching, while the peaks at 1077 and 1028 cm^{-1} reflect CO deformation in alcohols. In this region, there are some characteristic bands specific to different monolignol units. For example, for the guaiacyl unit is possible to observe the ring breathing at 1263 cm^{-1} , the aromatic C-H in-plane deformation at 1143 cm^{-1} , the aliphatic ether aromatic CH in-plane deformation at 1028 cm^{-1} and the aromatic CH out-of-plane deformation at 853 and 813 cm^{-1} . The typical bands of syringyl at 1326 and 843 cm^{-1} could not be clearly found.

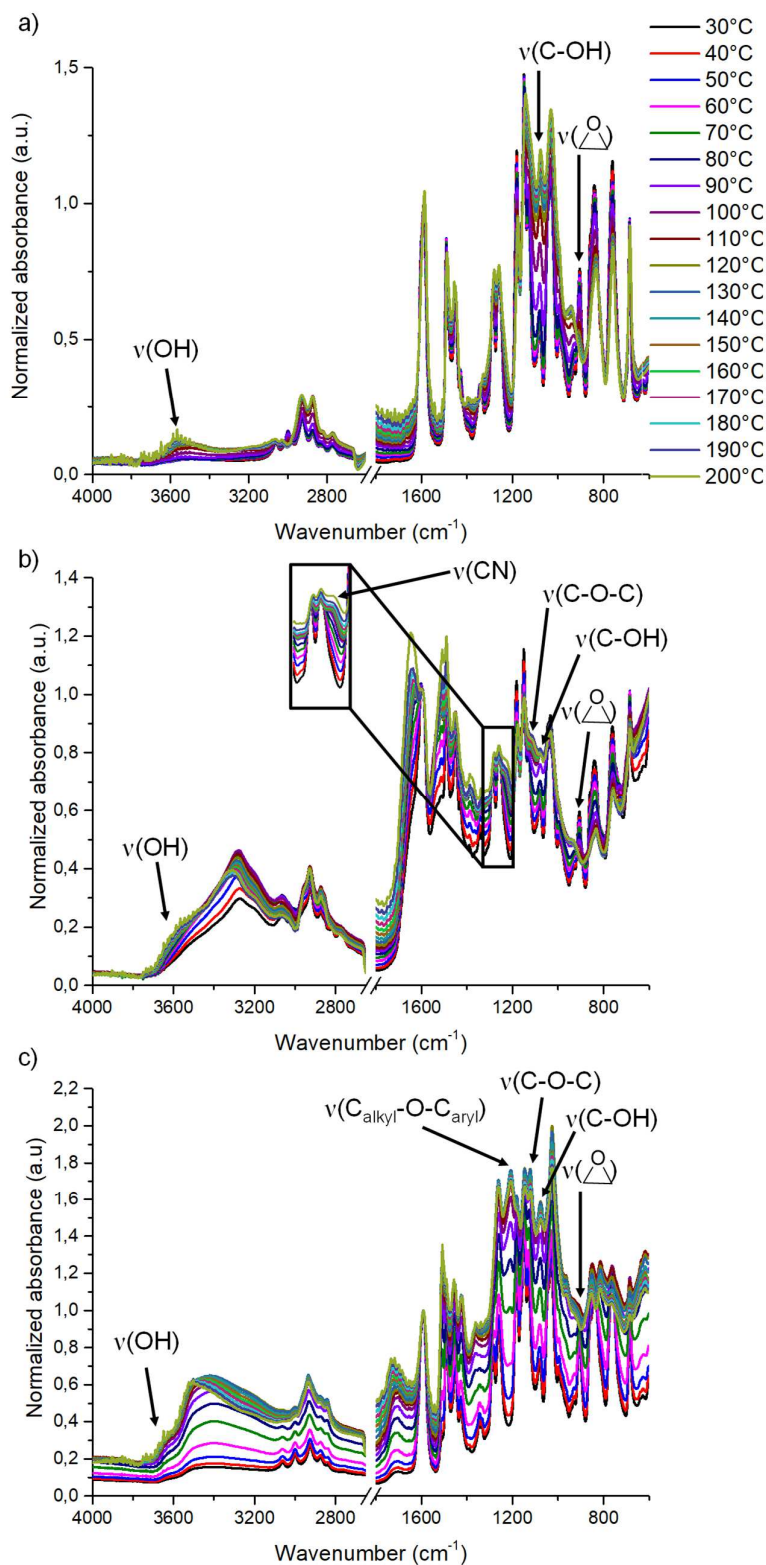


Figure ESI 3. FTIR spectra during curing of a) R_I; b) R_K_I and c) R_L_I. For the temperature-colour correspondence in the spectra see the legend in panel a)

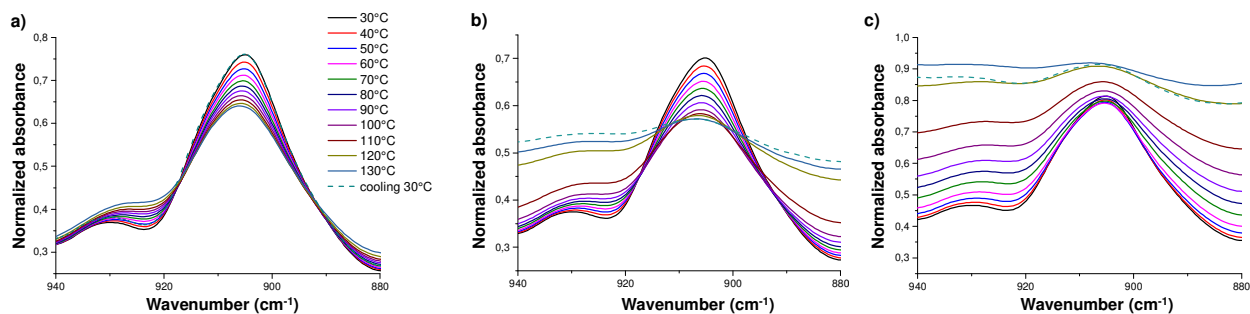


Figure ESI 4. RDGE epoxy signal in FTIR spectra at increasing temperatures (solid lines) and after cooling down at 30 °C (dashed lines) for a) RDGE; b) R_K and c) R_L. For the colour-temperature correspondence see the legend in panel a)

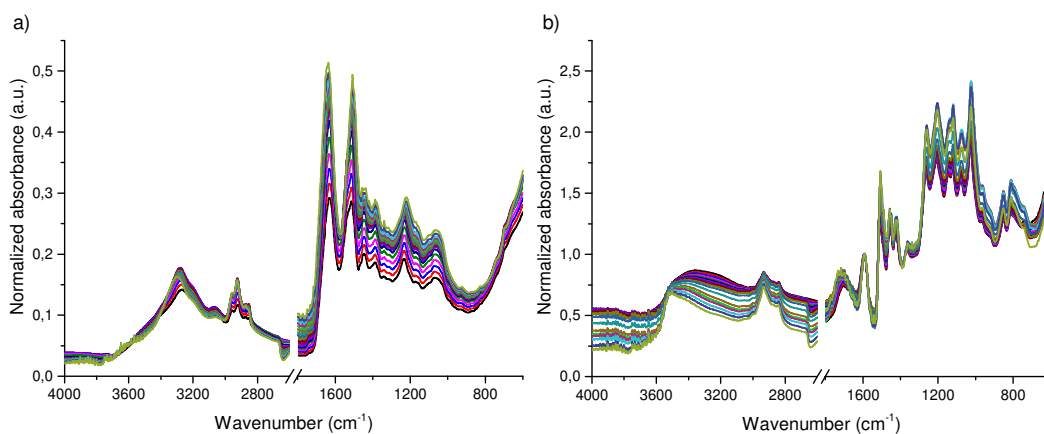


Figure ESI 5. Temperature evolution of FTIR spectrum of a) K and b) lignin. For the temperature-color correspondence see the legend in Figure ESI3a

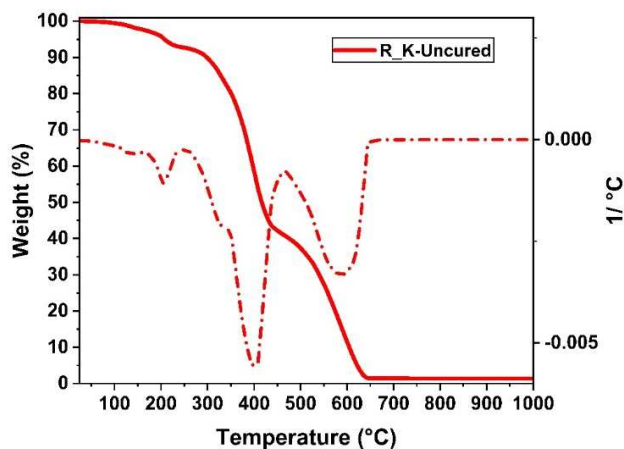


Figure ESI 6. TGA-DTA curves for uncured mixture between RDGE and K chicken feathers without initiator, at 10 °C min⁻¹ under air flow

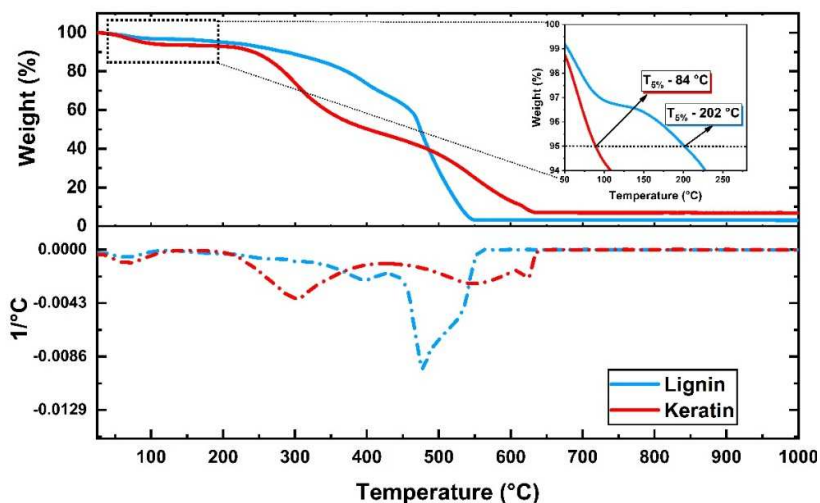


Figure ESI 7. TGA-DTA curves for raw lignin (blue line) and raw keratin (red line) at $10^{\circ}\text{C min}^{-1}$ under air flow

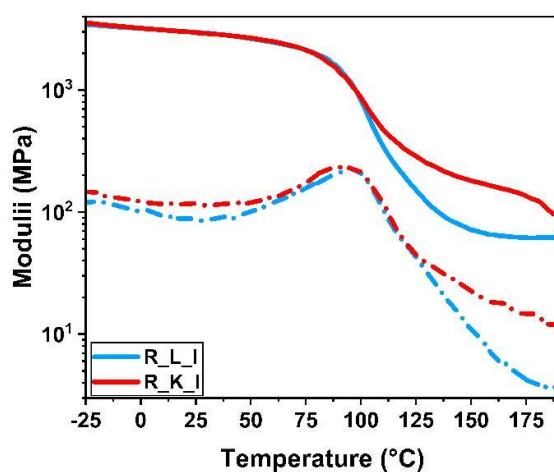


Figure ESI 8. Comparison of the storage and loss modulus according to temperature between the R_L_I (blue line) and R_K_I (red line) composites

The viscoelastic behavior curves of the developed materials revealed the presence of three different region as glassy region, rubbery plateau and the transition between the two phases. From Figure ESI 8 it can be observed that the shape of storage modulus curve in glassy region is almost identical for both materials, the E' values of the cured systems at room temperature being ≈ 3 GPa. After 100°C , the storage modulus curves of the two materials start to don't have any more the same behavior. It can observe that the E' value in rubbery region of the R_K_I (120 MPa) is double compared with that of the composite with lignin. Also, the drop interval value between the glassy and rubbery region for the material with keratin is smaller than in the system with lignin, which means a higher crosslink density for the R_L_I .

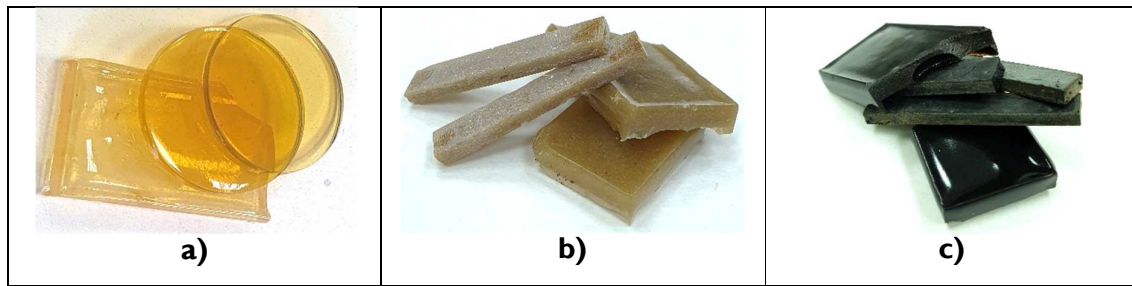


Figure ESI 9. Physical appearance of the bio-based materials: a) R_I; b) R_K_I and c) R_L_I

Conclusions and Perspectives

The main purpose of this thesis research aims investigating and designing new sustainable valorisation of humins, chicken feathers and lignin or some vegetal fibers, to innovate green products for industrial areas. A first challenge of this work was represented by the use of industrial humins, which have a complex and unknown chemical structure, as raw material in the development of materials with good performances. Also, the brittleness nature of furanic materials is a major factor limiting their used in the development of materials with optimal properties for industries areas such as construction or automotive. In the second chapter of this thesis, the industrial humins were combined with different aliphatic diglycidyl ethers in order to develop new bio-based resins with modulated properties. Firstly, the effect of formulations compositions on the systems' reactivity but also the optimal parameters of curing were intensely investigated. By varying the composition of the copolymerisation mixtures, three types of resins with different mechanical properties and a high humins content have been successfully developed. Investigating the physico-chemical and mechanical properties of the crosslinked humins-based materials was found that the length of the aliphatic chains of the diglycidyl ether comonomers influenced these properties obtaining resins with rigid or elastic behaviour. The tensile testing of the humins-based materials confirmed the rigid character of a resin, obtaining an elongation at break of about 7%, while the elastic ones showed an elongation of about 60% and a tensile strength value comparable to that of butyl rubbers or of silicone elastomers. The use of humins in large quantities, the development of materials through cost competitive processes, but especially the tailoring of furanic materials with elastomeric behaviour (not mentioned in the specialized literature), make these resins feasible products for the industrial sector.

The desire to develop environmentally friendly materials but also to valorise and use other resources from industrial wastes, has led our research to a new stage. The three humins-based resins developed previously were used as polymeric matrices for the development of bio-composites. As reinforcing materials were used two types of chicken feathers, such as powder and non-woven mat which are food industry waste, and also lignin from biorefinery. The composites properties were investigated for an in-deep understanding of the effect and behaviour of the filler on the matrix depending on its nature, but also on its form. All the bio-fillers, *i.e.* the chicken feathers powder & non-woven mat and lignin, have led to a significant improvement of the humins-based composites properties. Moreover, based on SEM analyses we proved a very good interaction between the bio-fillers and humins-based resins without prior application of any chemical or physical treatment on the composites' components.

Other thesis studies propose the humins combination with a bio-based triepoxide comonomer in order to design fully bio-based thermoset resins. Following the calculation of the bio-based carbon content (*BCC*) of the obtained thermosets it was determined that the *BCC* is about 94%. Furthermore, by studying the stability of the material, we found that are extremely stable losing about 5% of their mass at 280 °C. Also, by analysing the mechanical properties high values of the storage modulus were measured, of ≈ 4 GPa at room temperature, as well as high values of the glass transition region of the materials (≈ 120 – 150 °C). The high stiffness of the synthesized resins was confirmed by Shore hardness test (82–85 SD), proving that these materials could be candidates for the automotive and construction industry. Moreover, according with the solvent test, the humins-based resins revealed a good chemical resistance over time, being unaffected in all solvents tested after 12 days of immersion, thus confirming their ability to be used in the industrial production of out-door hard materials.

In order to fulfil the concept of circular economy, three different strategies such as reuse, recycling and remodelling were considered. For this purpose, humins-based resins were used as matrices in composite's development in which as reinforcement were used recycled natural fibers such as chicken feathers and vegetable fibers non-woven. The physico-chemical and mechanical properties of these bio-composites were investigated showing comparable performances with the commercial materials such as epoxy/glass fibers and epoxy/carbon fibers composites. Also, the interaction between compounds was investigated revealing a good interaction matrix/filler without any prior physical or chemical treatment of the fillers or matrix. Moreover, these materials showed that can be mechanically recycled without producing substantial decreasing in their properties.

The last attempt to valorise the industrial wastes studied in this thesis was the development of thermosetting materials by copolymerization of an aromatic epoxy compound from wood biomass, the resorcinol diglycidyl ether, with two natural side-products such as keratin (from chicken feathers) and lignin. The thermoset materials were developed using about 30% by weight of the natural by-product and by using compression molding method, the crosslinking of the materials taking place at low temperatures. Following the DSC and FTIR analyses during crosslinking of the materials, we observed the presence of the chemical interactions between the keratin and lignin with the epoxide network. Also, the physical and mechanical tests showed that the addition of the natural side-products improved the properties of the final materials. Therefore, considering these factors, we can confirm successfully development of new green bio-based materials in which the natural by-product play double role such as comonomer in the reaction, and as filler in the composites structure.

In conclusion, this thesis work proposes some valorisation ways for the chicken feather and humins, but also for other by-products. Some of the materials designed in this thesis were

also passed from the laboratory scale to the pilot level, thus confirming the truthfulness of the new routes for the valorisation of these by-products at the industrial level.

Based on the studies developed in this thesis, we demonstrated that both the humins and chicken feathers have a real potential in the development of industrial materials. This work represents a first step towards a tangible valorisation pathway of these by-products. The parameters and processing protocols of the bio-based materials will be analysed and improved at pilot scale to be feasible for an upscaling at industrial level. In future studies, the effect of treated vegetable fibers on the physico-chemical and mechanical properties of the humins-based composites will be investigated. Also, properties such as fire resistance, resistance at impact, at compression or at different environmental factors could be investigated in order to develop feasible composite materials for fabrication of automotive component parts. Another perspective for humins and chicken feathers valorisation is the development of porous materials. Intense studies are underway, in which porous materials based on humins and chicken feathers powder have been designed. So far, we observed that depending on the formulations' composition the properties of the foams can be modulated from elastic to rigid, and the chicken feathers powder and the processing parameters are responsible for the pore size and distribution in the designed foams. Elaborated studies on the physico-chemical and mechanical properties will be carried out in future studies. Likewise, the substances absorption and retention capacity of the porous materials will be analysed for their potential valorisation as wastewater treatment and supports for solid catalysts. On the other hand, the soundproofing and thermal insulation foams abilities, as well as the flame retardant properties and their behaviour to different environmental factors, will be investigated in order to use these bio-materials in the development of insulating materials for construction sector.

Scientific contributions

Publications

Dinu, R.; Mija, A. *Cross-Linked Polyfuran Networks with Elastomeric Behaviour Based on Humins Biorefinery by-Products*, *Green Chemistry*, **2019**, 21, 6277–6289. <https://doi.org/10.1039/c9gc01813a>.

Montané, X.; **Dinu, R.;** Mija, A. *Synthesis of Resins Using Epoxies and Humins as Building Blocks: A Mechanistic Study Based on in-Situ FT-IR and NMR Spectroscopies*, *Molecules* **2019**, 24 (22), 4110 <https://doi.org/10.3390/molecules24224110>.

Cantarutti, C.; **Dinu, R.;** Mija, A. *Biorefinery By-Products and Epoxy Biorenewable Monomers: A Structural Elucidation of Humins and Triglycidyl Ether of Phloroglucinol Crosslinking*, *Biomacromolecules*, **2020**, 21(2), 517-533. <https://doi.org/10.1021/acs.biomac.9b01248>.

Dinu, R.; Mija, A. *Sustainable Thermosets Obtained by Copolymerization of Humins with Triglycidyl Ether of Phloroglucinol*, *Journal of Materials Science Research*, **2020**, 9(2), 1-17, <https://doi.org/10.5539/jmsr.v9n2p1>

Dinu, R.; Mija, A. *Bio-Based Composites from Industrial By-products and Wastes as Raw Materials*, *Journal of Materials Science Research*, **2020**, 9(2), 29-45, <https://doi.org/10.5539/jmsr.v9n2p29>

Dinu, R.; Cantarutti, C.; Mija, A. *Design of Sustainable materials by Cross-linking a Biobased Epoxide with Keratin and Lignin*, *ACS Sustainable Chemistry & Engineering*, **2020**, <https://doi.org/10.1021/acssuschemeng.0c01759>

Dinu, R.; Montes, S.; Orange, F.; Mija, A. *Reprocessable Humins Thermosets and Composites for Sustainable Applications*, **2020** (in peer review in *Green Chemistry*)

Cover pages

Dinu, R.; Mija, A. *Cross-Linked Polyfuran Networks with Elastomeric Behaviour Based on Humins Biorefinery by-Products*, *Green Chemistry*, 2019, 21, invited back cover page.

Dinu, R.; Cantarutti, C.; Mija, A. *Design of Sustainable materials by Crosslinking a Bio-based Epoxide with Keratin and with Lignin*, *ACS Sustainable Chemistry & Engineering*, **2020**, <https://doi.org/10.1021/acssuschemeng.0c01759>, supplementary cover page

Oral presentations

Dinu, R.; Mija, A. *Industrial Feather Waste Valorisation for Sustainable KeRatin-based Materials*, International Conference Circular Economy for Textiles and Plastics “Rethinking the value chain of textiles and plastics”, Brugge, Belgium, November 2018

Dinu, R.; Mija, A. *Industrial Feather Waste Valorisation for Sustainable KeRatin-based Materials*, Spring 2019 ACS National Meeting, Orlando, Florida, March 2019

Dinu, R.; Peuvrel-Disdier, E.; Orange, F.; Mija, A. *Industrial Wastes as Raw Materials for Bio-based composites*, EUROMAT, Stockholm, Sweden, September 2019

